Electrochemical Society

GLC Anodes Are CUSTOM MADE

for

Hooker Chemical Corporation

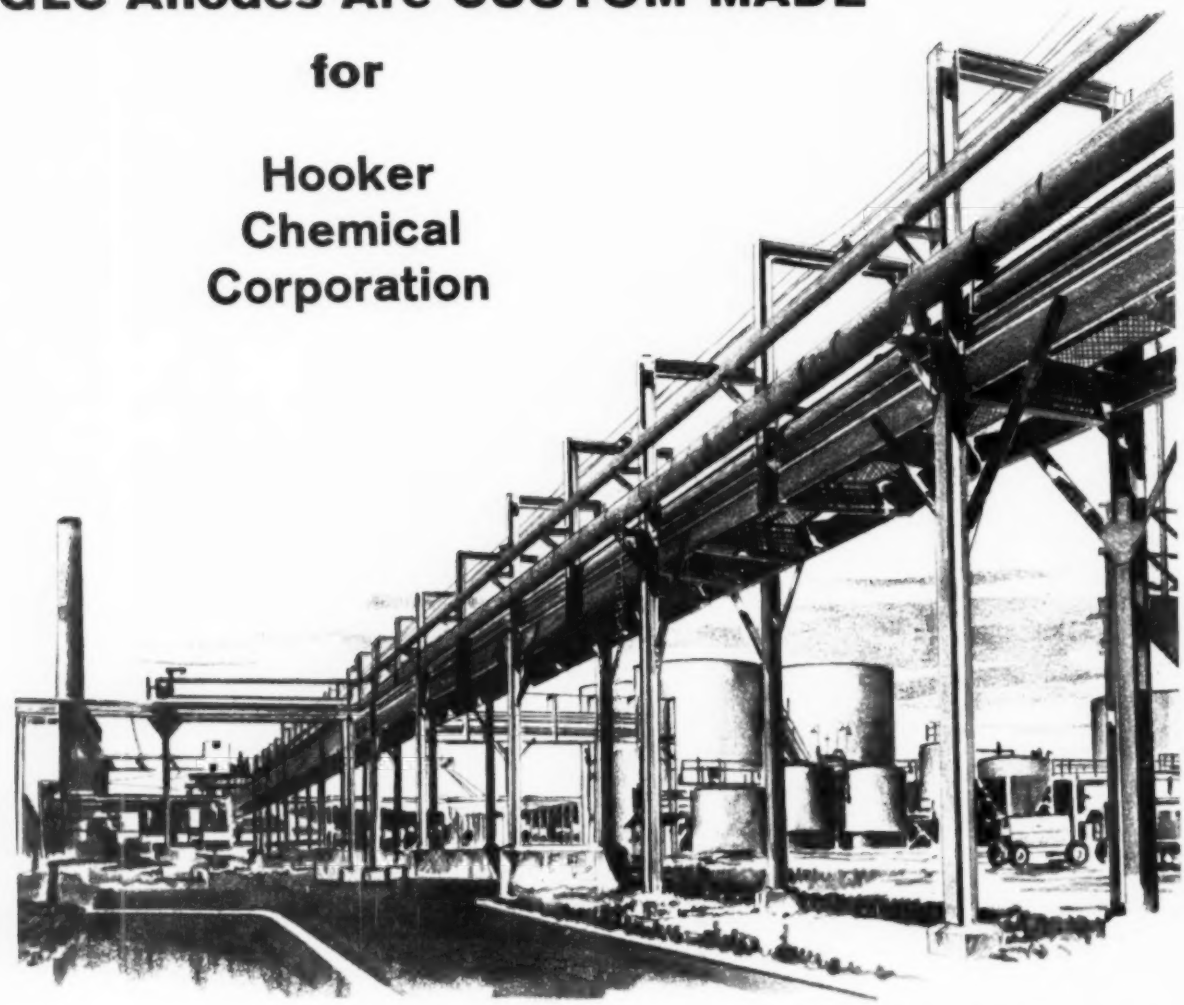

The Hooker Chlor-Alkali Plant at Montague, Mich.

Longer anode life, longer diaphragm life, reduced power consumption and reduced labor costs are the goals of the GLC program of technical exchanges between our engineers and those of our chlor-alkali customers.

GLC anodes now in use are achieving greater records of performance than ever before.

And as a result of our continuing technical exchange program, GLC customers can look forward to still better anode performance in the future.

Are your chlor-alkali operations experiencing the cost-saving advantages of GLC anodes, custom made to your special requirements?

PRODUCTS ELECTRODE GLC DIVISION YOU CAN TRUST ®

GREAT LAKES CARBON CORPORATION

18 EAST 48TH STREET, NEW YORK 17, N.Y. OFFICES IN PRINCIPAL CITIES

EDITORIAL STAFF

C. L. Faust, Chairman, Publication Committee

Cecil V. King, Editor

Norman Hackerman, Technical Editor

Ruth G. Sterns, Managing Editor

U. B. Thomas, News Editor

H. W. Salzberg, Book Review Editor

Natalie Michalski, Assistant Editor

DIVISIONAL EDITORS

W. C. Vosburgh, Battery

Milton Stern, Corrosion, I

R. T. Foley, Corrosion, II

T. D. Callinan, Electric Insulation

Seymour Senderoff, Electrodeposition

H. C. Froelich, Electronics, I

Ephraim Banks, Electronics, II

Ernest Paskell, Electronics—Semiconductors

Sherlock Swann, Jr., Electro-Organic, I

Stanley Wawzonek, Electro-Organic, II

John M. Blocher, Jr., Electrothermics and Metallurgy, I

J. H. Westbrook, Electrothermics and Metallurgy, II

N. J. Johnson, Industrial Electrolytic

C. W. Tobias, Theoretical Electrochemistry, I

A. J. deBethune, Theoretical Electrochemistry, II

ADVERTISING OFFICE

ECS

1860 Broadway, New York 23, N. Y.

ECS OFFICERS

R. A. Schaefer, President
Electric Storage Battery Co., Yardley, Pa.

Henry B. Linford, Vice-President
Columbia University, New York, N. Y.

F. L. LaQue, Vice-President
International Nickel Co., Inc., New York, N. Y.

W. J. Hamer, Vice-President
National Bureau of Standards, Washington, D. C.

Lyle I. Gilbertson, Treasurer
Air Reduction Co., Murray Hill, N. J.

I. E. Campbell, Secretary
National Steel Corp., Weirton, W. Va.

Robert K. Shannon, Executive Secretary
National Headquarters, The ECS, 1860 Broadway, New York 23, N. Y.

Manuscripts submitted to the Journal should be sent, in triplicate, to the Editorial Office at 1860 Broadway, New York 23, N. Y. They should conform to the revised Instructions to Authors, published on pp. 23C-24C of this issue. Manuscripts so submitted become the property of The Electrochemical Society and may not be published elsewhere, in whole or in part, unless permission is requested of and granted by the Editor.

Inquiries re positive microfilm copies for volumes should be addressed to University Microfilms, Inc., 313 N. First St., Ann Arbor, Mich.

The Electrochemical Society does not maintain a supply of reprints of papers appearing in its Journal. A photoprint copy of any particular paper, however, may be obtained by corresponding directly with the Engineering Societies Library, 29 W. 39 St., New York 18, N. Y.

Journal of the Electrochemical Society

JANUARY 1961 **VOL. 108 • NO. 1**

CONTENTS

Editorial

Clarity Begins at Home. *F. A. Lowenheim* 3C

Technical Papers

Investigation of the Electrochemical Characteristics of Organic Compounds, VI. Aromatic Hydroxy, Aromatic Amine, and Aminophenol Compounds. *R. Glicksman* 1

The Oxidation of Tin, I. The Kinetics of Oxidation of Pure Tin and the Effects of Temperature and Oxygen Pressure. *W. E. Boggs, R. H. Kachik, and G. E. Pellissier* 6

The Oxidation of Tin, II. The Morphology and Mode of Growth of Oxide Films on Pure Tin. *W. E. Boggs, P. S. Trozzo, and G. E. Pellissier* 13

The Oxidation and Corrosion of Zirconium and Its Alloys, V. Mechanism of Oxide Film Growth and Breakdown on Zirconium and Zircaloy-2. *B. Cox* 24

A Study of the Formation of Anodic Oxide Films on Uranium, I. An Optical Reflectivity Method for Determining the Kinetics of Film Growth. *A. E. Stebbens and L. L. Shreir* 30

Electrochemical Behavior of the Magnesium Anode. *J. L. Robinson and P. F. King* 36

Cyclic Photogalvanic Silver Halide Cells. *S. Zaromb, M. E. Lasser, and F. Kalhammer* 42

The A-C Properties of Tantalum Solid Electrolytic Capacitors. *D. A. McLean* 48

The Chemistry of Cable-Oil Deterioration. *G. Feick, W. F. Olds, and E. D. Eich* 56

Electrodeposition of Cobalt-Molybdenum Alloys. *A. Krohn and T. M. Brown* 60

Electrodeposition of Nickel-Cobalt Alloys from the Pyrophosphate Bath. *V. Sree and T. L. Rama Char* 64

Electrolysis in Anhydrous Ether. *I. E. Gillet* 71

The Elastic Modulus and Internal Friction of Electrodeposited Copper. *H. J. Read and A. H. Graham* 73

The Significance of the Temperature Dependence of Fluorescence Intensity. *C. H. Haake* 78

Growth from the Vapor of Large Single Crystals of Lead Selenide of Controlled Composition. *A. C. Prior* 82

Preparation of High-Purity Vanadium Metal by the Iodide Refining Process. *O. N. Carlson and C. V. Owen* 88

Thermodynamic Properties of Molten Mixtures of Cerium Chloride and Calcium Chloride. *S. Senderoff, G. W. Mellors, and R. I. Bretz* 93

Transient Strain-Induced Electrode Potentials. *K. Nobe, E. Baum, and W. F. Seyer* 97

Technical Notes

Electrical Conduction in Thin Films of Silver Telluride. *W. M. Kane and C. Wood* 101

Polarization Measurements Made with a Luggin-Haber Capillary Magnitude of *IR*-Drop Corrections in Electrode. *S. Barnartt* 102

Electrolytic Polish for Lead Telluride. *P. H. Schmidt* 104

Digital Programming Unit for Automatic Temperature Control during Pyrosynthesis of Inorganic Compounds. *N. L. Hozak, J. S. Cook, and D. R. Mason* 105

Preparation of Nickel Polyhedra by Reduction in Fused Salt Systems. *R. A. Lefever* 107

Brief Communications

Twin Structures in Silver Dendrites. *J. W. Faust, Jr., and H. F. John* 109

Ferroelectric Properties of the System $(NH_2CH_2COOH)_3 \cdot H_3(SO_4, PO_3F)$. *T. G. Dunne and M. L. Wang* 111

Feature Section

Henry B. Linford—The Acheson Medalist. *L. I. Gilbertson* 7C

The Education of Electrochemists. *H. B. Linford* 8C

Current Affairs 11C-22C

Published monthly by The Electrochemical Society, Inc., from Manchester, N. H., **Executive Offices, Editorial Office** and **Circulation Dept.,** and **Advertising Office** at 1860 Broadway, New York 23, N. Y., combining the JOURNAL and TRANSACTIONS OF THE ELECTROCHEMICAL SOCIETY. Statements and opinions given in articles and papers in the JOURNAL OF THE ELECTROCHEMICAL SOCIETY are those of the contributors, and The Electrochemical Society assumes no responsibility for them. Subscription to members as part of membership service; subscription to nonmembers $24.00. Single copies $1.70 to members, $2.25 to nonmembers.

Copyright 1961 by The Electrochemical Society, Inc.

Entered as second-class matter at the Post Office at Manchester, N. H., under the act of August 24, 1912.

One of a series.

Why we eliminated the earth's magnetic field... almost

In an isolated laboratory in southwestern Ohio, GM Research scientists have reduced the earth's magnetic field to one ten-thousandth of its usual strength. This is about as weak as the interplanetary field detected by the Pioneer V solar satellite.

Why neutralize the earth's field? To perform with precision one of the more fundamental experiments in magnetism — measuring the Einstein-DeHaas effect. The measurement is simple in concept, experimentally difficult because of the tiny forces involved. It is made by suspending a ferromagnetic rod in a nearly field-free environment . . . magnetizing the rod . . . then measuring the effect (how much the rod rotates) when this known magnetization is reversed.

The beauty of the experiment is that the resulting values can be related directly to the motions of electrons in the rod. The values indicate the large portion of magnetization due to the *spin* of electrons . . . and the slight, but theoretically important, remaining portion due to *orbital* motion of electrons.

These measured values are helping scientists form a better understanding of the perplexing phenomenon — ferromagnetism. Currently being pursued in cooperation with the Charles F. Kettering Foundation, this long-standing project is one of the ventures in basic research of the General Motors Research Laboratories.

General Motors Research Laboratories

Warren, Michigan

Gyromagnetic Ratios

	a	***b***
Iron	*1.92*	*1.90*
Cobalt	*1.85*	*1.83*
Nickel	*1.84*	*1.83*
Supermalloy	*1.91*	*1.91*

Comparison of (a) gyromagnetic ratios measured in the new Kettering Magnetics Laboratory with (b) corresponding ferromagnetic resonance measurements. These ratios would equal 2 if magnetization were due only to electron spin, or 1 if due only to orbital electron motion.

System of Helmholtz coils used to neutralize earth's magnetic field.

Editorial

Clarity Begins at Home

FOR centuries, preachers of all faiths have been inveighing against sin, but modern man does not seem noticeably nearer saintliness than his ancestors. The preaching fraternity, of course, can always argue that things would be a lot worse if it were not for their efforts. It is with somewhat the same mixture of resignation and hope that one approaches the subject of this editorial.

We continue to be amazed that a competent scientist will spend a year or more of his time, and considerable serious thought, on initiating and carrying through a piece of research; and then, when it comes time to communicate the results of his work to his fellow-scientists at a national meeting of this or another society, will jot down a note or two on the back of a piece of scratch-paper, throw together a few illegible slides, and mumble, hem, and haw his way through an over-long presentation which is about as interesting to the audience as the reading of a laundry list. It has been said before, of course; but it has to be said again and yet again: the work is not finished until it is communicated; and presentation at national meetings of scientific societies is one of the recognized ways of communicating.

Many speakers at our meetings, of course, are much better than the—unfortunately not hypothetical—one just described; many are very good indeed. And the whole point is that these superior speakers owe their success not to any overwhelming natural oratorical abilities—very few scientists have the talents of a Churchill—but to the facts that they respect the art of communication and they take pains to do a good job.

This is not the place to detail the elements of good oral communication; but it might be inquired, What concrete steps, more efficient than exhortations like this one, can be taken to encourage better presentations—and, thus, better national meetings? One of our sister societies has tackled the problem by giving awards for excellence in presentation; selected referees in the audience score each speaker on various aspects of his performance, and these scores are used as the basis for determining the recipients of the awards. Speakers know they are being rated; natural vanity does the rest, with the result that this society enjoys the reputation of having much better than average oral presentations at its national meetings.

Our own Society may wish to consider some such system. It won't be a panacea; but, to this inveterate attender of our meetings, anything which might improve the level of communication seems worth trying. For the scientist may also adopt the three Biblical virtues, with a slight twist: Faith, in the orderliness of the universe and the methods of scientific investigation; Hope, that his own contribution, though small, may be significant; and, in his communications, Clarity. And the greatest of these ....

—F. A. LOWENHEIM[1]

[1] Metal and Thermit Corp., Rahway, N. J.

FUTURE MEETINGS OF
The Electrochemical Society

Indianapolis, Ind., April 30, May 1, 2, 3, and 4, 1961
Headquarters at the Claypool Hotel
Sessions probably will be scheduled on
Electric Insulation, Electronics (including Luminescence and Semiconductors), Electrothermics and Metallurgy, Industrial Electrolytics (including a Symposium on Fuel Cells), and Theoretical Electrochemistry (including a Symposium on Instrumentation)

★ ★ ★

Detroit, Mich., October 1, 2, 3, 4, and 5, 1961
Headquarters at the Statler Hotel
Sessions probably will be scheduled on
Batteries, Corrosion, Electrodeposition (including symposia on Addition Agents and on Electrodeposited Magnetic Films), Electronics (Semiconductors), Electro-Organics, and Electrothermics and Metallurgy

★ ★ ★

Los Angeles, Calif., May 6, 7, 8, 9, and 10, 1962
Headquarters at the Statler Hilton Hotel

★ ★ ★

Boston, Mass., September 16, 17, 18, 19, and 20, 1962
Headquarters at the Statler Hilton Hotel

Papers are now being solicited for the meeting to be held in Detroit, Mich., October 1-5, 1961. Triplicate copies of each abstract (*not exceeding 75 words in length*) are due at Society Headquarters, 1860 Broadway, New York 23, N. Y., *not later than May 15, 1961* in order to be included in the program. *Please indicate on abstract for which Division's symposium the paper is to be scheduled, and underline the name of the author who will present the paper.* No paper will be placed on the program unless one of the authors, or a qualified person designated by the authors, has agreed to present it in person. Complete manuscripts should be sent in triplicate to the Managing Editor of the JOURNAL at 1860 Broadway, New York 23, N.Y.

Presentation of a paper at a technical meeting of the Society does not guarantee publication in the JOURNAL. However, all papers so presented become the property of The Electrochemical Society, and may not be published elsewhere, either in whole or in part, unless permission for release is requested of and granted by the Editor. Papers already published elsewhere, or submitted for publication elsewhere, are not acceptable for oral presentation except on invitation by a Divisional program Chairman.

A GIANT RADIO HIGHWAY IS PERFECTED FOR TELEPHONY

A radio relay system operating at 6 billion cycles per second and able to transmit 11,000 voices on a single beam of microwaves—several times as many as any previous system—has been developed at Bell Laboratories. Utilizing the assigned frequency band with unprecedented efficiency, this new, heavy-traffic system was made possible by the development and application of new technology by Bell Laboratories engineers and scientists.

For example, they arranged for the waves in adjacent channels to be polarized 90 degrees apart, thus cutting down interference between channels and permitting the transmission of many more telephone conversations in the same frequency space. They developed ferrite isolators to suppress interfering wave reflections in the waveguide circuits; and a new traveling wave tube that has ten times the power handling capacity of previous amplifiers and provides uniform and almost distortionless amplification of FM signals. They devised and applied a new high-speed diode switching system which instantly switches service to a protection channel when trouble threatens.

To transmit and receive the waves, the engineers applied their invention, the horn-reflector antenna. Elsewhere, this versatile antenna type is brilliantly aiding space communication research in the reception of radio signals from satellites. For radio relay, a single horn-reflector antenna can efficiently handle both polarizations of the 6000 megacycle waves of the new system; at the same time it can handle 4000 and 11,000 megacycle waves used for existing radio relay systems. Thus it enables all three systems to share economically the same radio towers and routes.

Produced by the Bell System's manufacturing unit, Western Electric, the new system is now in operation between Denver and Salt Lake City, and will gradually be extended from coast to coast. This new advance in radio technology is another example of how Bell Telephone Laboratories works to improve your Bell communication services.

BELL TELEPHONE LABORATORIES

World center of communications research and development

SARGENT-SLOMIN ANALYZERS
are standard equipment in prominent laboratories

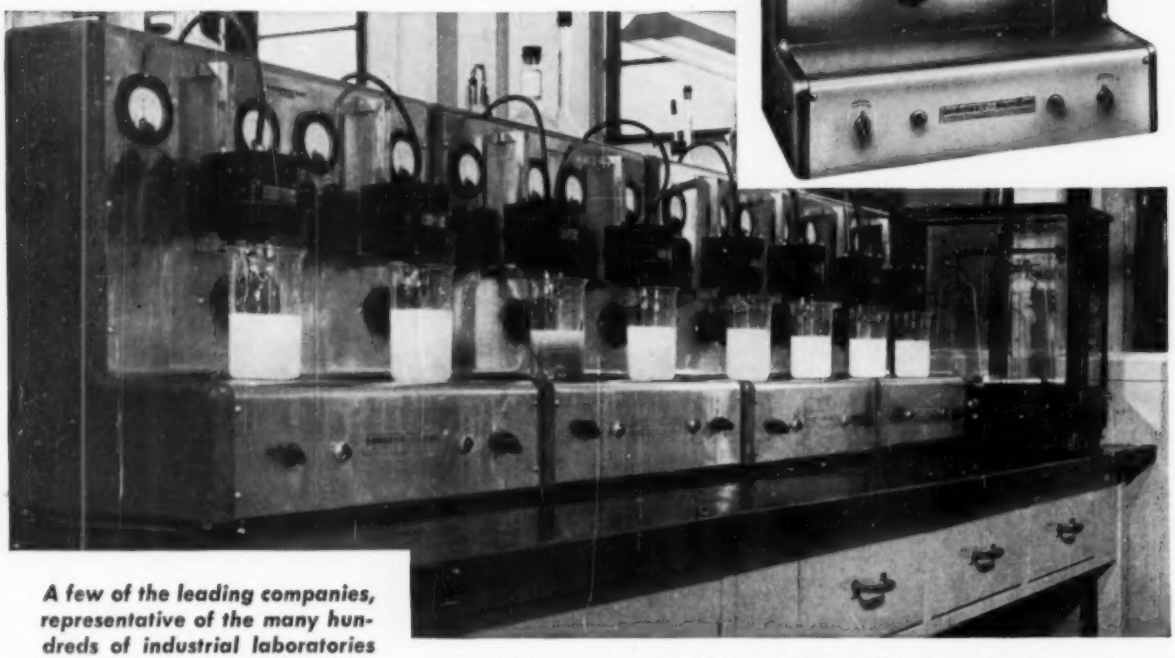

Photo Courtesy INTERNATIONAL HARVESTER COMPANY, Melrose Park, Illinois

A few of the leading companies, representative of the many hundreds of industrial laboratories using the Sargent - Slomin and Heavy Duty Analyzers for control analyses . . .

AMPCO METAL, Inc.
ANDERSON LABORATORIES
CALERA MINING COMPANY
EUREKA WILLIAMS COMPANY
THE FEDERAL METAL CO.
FORD MOTOR COMPANY
THE GLIDDEN COMPANY—Chemical, Metal and Pigment Division
HOT POINT CO.
HOWARD FOUNDRY COMPANY
INTERNATIONAL HARVESTER COMPANY
KENNAMETAL Inc.
McQUAY - NORRIS MANUFACTURING CO.
NATIONAL LEAD COMPANY, Fredericktown, Missouri
PIASECKI HELICOPTER CORPORATION
REVERE COPPER & BRASS INCORPORATED
THE RIVER SMELTING & REFINING COMPANY
SILAS MASON COMPANY
THE STUDEBAKER CORPORATION
THOMPSON PRODUCTS, INC.

Sargent-Slomin Electrolytic Analyzers are recommended for such electro analytical determinations as: Copper in—ores, brass, iron, aluminum and its alloys, magnesium and its alloys, bronze, white metals, silver solders, nickel and zinc die castings. Lead in—brass, aluminum and its alloys, bronze, zinc and zinc die castings. Assay of electrolytical copper, nickel and other metals.

Sargent analyzers are completely line operated, employing self-contained rectifying and filter circuits. Deposition voltage is adjusted by means of autotransformers, with meters indicating volts and amperes and controls on the panel. An easily replaceable fuse guards against circuit overload. Maximum D.C. current capacity is 5 to 15 amperes; maximum D.C. voltage available, 10 volts.

Sargent-Slomin Analyzers stir through a rotating chuck operated from a capacitor type induction motor, having a fixed speed of 550 r.p.m. with 60 cycle A.C. current or 460 r.p.m. with 50 cycle A.C. current. Motors are sealed against corrosive fumes and are mounted on cast metal brackets, sliding on ½" square stainless steel rods, permitting vertical adjustment of electrode position over a distance of 4". Pre-lubricated ball-bearings support the rotating shaft. All analyzers accommodate electrodes having shaft diameters no greater than 0.059 inch. Stainless steel spring tension chucks permit quick, easy insertion of electrodes and maintain proper electrical contact. Special Sargent high efficiency electrodes are available for these analyzers. Illustrated above is one model of the five types of Sargent-Slomin and Heavy Duty Analyzers.

S-29465 ELECTROLYTIC ANALYZER—Motor stirred, Two Position, 5 Ampere. With two adjustable heaters, pilot lights and control knobs. For operation from 115 volt, 50 or 60 cycle A.C. circuits.....**$590.00**

SARGENT *SCIENTIFIC LABORATORY INSTRUMENTS • APPARATUS • SUPPLIES • CHEMICALS*

E. H. SARGENT & CO., 4647 W. FOSTER, CHICAGO 30, ILLINOIS
DETROIT 4, MICH. • DALLAS 35, TEXAS • BIRMINGHAM 4, ALA. • SPRINGFIELD, N.J.

Investigation of the Electrochemical Characteristics of Organic Compounds

VI. Aromatic Hydroxy, Aromatic Amine, and Aminophenol Compounds

R. Glicksman

Semiconductor and Materials Division, Radio Corporation of America, Somerville, New Jersey

ABSTRACT

A study of the electrochemical characteristics of aromatic hydroxy, aromatic amine, and aminophenol compounds in basic electrolyte shows that the anode potential of these compounds depends on the aromaticity of the compound, as well as the type and position of substituted groups on the aromatic ring. The effect of these factors on the anode potential is interpreted in terms of the electron density distribution in the molecule. The use of these compounds as anode materials in primary cells also is considered.

A knowledge of the relative stability or ease of oxidation of organic compounds is desirable for many purposes. Because most organic compounds cannot be oxidized reversibly, they exhibit no thermodynamic oxidation potentials and their potentials cannot be determined by standard methods. Two potentiometric methods for studying organic oxidation and reduction reactions involve the "apparent oxidation potential" (1) and the "critical oxidation potential" (2). Procedures for obtaining these values are lengthy, however, and the results can be considered only approximate because theoretical objections to both can be raised. Polarographic methods, which are simpler and less time consuming, also have been applied to the study of the oxidation of organic compounds (3, 4). A comparison of the polarographic half-wave potentials with the earlier measurements of the "apparent" and "critical oxidation potentials" indicates fairly good agreement (4).

As part of a general investigation of the electrochemical characteristics of organic compounds, a study of organic reducing agents is being made by the same electrochemical method used to investigate the electrochemical characteristics of various organic oxidizing agents (5, 6).

Apparatus and Technique

A technique, previously described in the literature (7), has been modified slightly and used to measure the operating potential during current flow of the various organic reducing agents. The apparatus used in this study is shown in Fig. 1. In this technique, a 0.5 g sample of the organic anode material mixed with 0.05 g of Shawinigan acetylene black is discharged at a constant current drain of 0.005 amp/g, in a large volume of electrolyte. The change in anode potential with time is measured with an L&N type K potentiometer using a saturated calomel reference electrode. The measured potentials are corrected for the *IR* drop associated with the apparatus and electrolyte by means of an oscillographic technique.

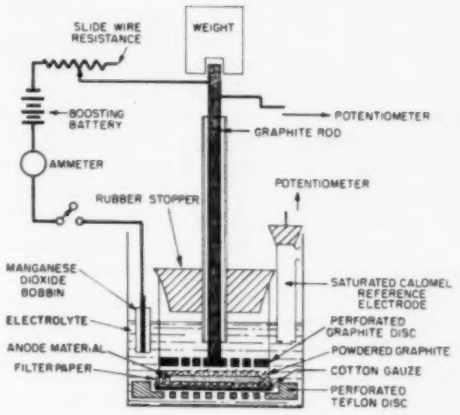

Fig. 1. Apparatus used for anode half-cell potential studies

All half-cell potential data reported are referred to the normal hydrogen electrode and include a liquid junction potential. For most of the measurements, an aqueous 1.44*M* NaOH solution ($a_{OH^-} = 1$)[1] was used as the electrolyte, and a manganese dioxide bobbin wrapped in cheese cloth served as the cathode. A manganese dioxide cathode also was employed with the acidic NH_4Cl-$ZnCl_2$-H_2O and weakly basic $MgBr_2$-H_2O electrolytes to study the effect of *p*H on potential.

Experimental Data and Discussion of Results

Effect of substituted groups and their position in the molecule on the anode potential of aromatic hydroxy and aromatic amine compounds.—Figure 2 shows half-cell potential discharge curves of phenol, pyrocatechol, and pyrogallol obtained when these compounds are discharged at a rate of 0.005 amp/g in 1.44*M* NaOH solution. These data illustrate the effect on the anode potential of the substitution of additional hydroxyl groups on the ortho position of mono- and di-hydroxybenzene. Both the ease of oxidation and the anode potential increase with an

[1] Calculated from the data given by Latimer (8).

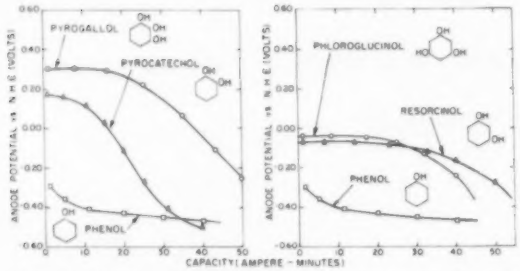

Fig. 2. Effect of additional hydroxyl groups on the anode potential of aromatic hydroxy compounds discharged at a rate of 0.005 amp/g in 1.44M NaOH.

increased number of hydroxyl groups on the benzene nucleus. This same effect is observed for the addition of hydroxyl groups to the meta position of mono- and di-hydroxy benzene, as evidenced by the half-cell potential discharge data for phenol, resorcinol, and phloroglucinol shown in Fig. 2.

The product first formed on the oxidation of a phenol is not definitely known, but is probably either ortho or para dihydroxybenzene. These two compounds actually have been obtained from phenol by electrolytic oxidation and by oxidation with peroxysulfuric acid. Because these dihydroxy compounds are oxidized even more easily than phenol itself, the oxidation generally proceeds further and yields other products (9). The relative difficulty of oxidizing phenol is apparent from the markedly lower anode potential of this compound as compared with the potentials of the di- and tri-hydroxybenzene compounds.

The addition of a meta hydroxyl group to the benzene ring of resorcinol raises the anode potential by 0.03 v, while the potential of pyrocatechol is raised 0.13 v by the addition of an ortho hydroxyl group to the ring. The influence of this electron repelling group is essentially to increase the electron density in the vicinity of the oxidizable hydroxyl groups, which decreases their affinity for electrons and results in a compound having a higher anode potential. The same effect in terms of "critical oxidation potentials" has been illustrated by Fieser for aromatic hydroxy compounds (2). Similarly in the aliphatic series, the accumulation of hydroxyl groups renders a molecule (glycerol, for example) more susceptible to oxidation.

Figure 3 presents half-cell potential discharge curves of aniline, ortho phenylenediamine, and 1,2,4-benzenetriamino dihydrochloride obtained when these compounds are discharged at the rate of 0.005 amp/g in 1.44*M* NaOH solution. These data illustrate the effect on the anode potential of mono- and diaminobenzene of the substitution of additional amino groups to the benzene ring. As with the aromatic hydroxy compounds, the ease of oxidation (and the anode potential) increases with an increased number of amino groups on the benzene nucleus. The effect produced on the anode potential of o-phenylenediamine by the addition of an amino group to the benzene ring is considerable, as evidenced by the fact that 1,2,4-benzenetriamino dihydrochloride operates at a potential 0.2 v higher than the phenylenediamine compound.

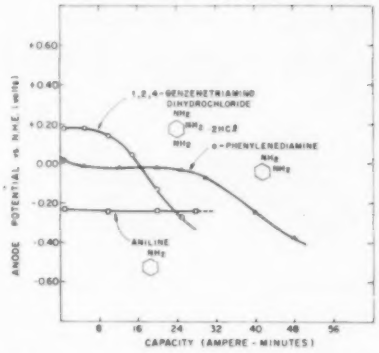

Fig. 3. Effect of additional amino groups on the anode potential of aromatic amine compounds discharged at a rate of 0.005 amp/g in 1.44M NaOH.

Under varying conditions aniline can be converted into a host of oxidation products, including azobenzene, azoxybenzene, nitrobenzene, quinone, aniline black and many products resulting from secondary processes of condensation. Most of the reaction products can be derived through an initial abstraction of one amino hydrogen atom with the formation of a transient free radical sensitive to further attack either at the nitrogen atom or at the para position of the nucleus (10). On the other hand, the aromatic diamines first are oxidized to the quinone-diimine. This compound is then hydrolyzed rapidly in aqueous solution and forms the corresponding quinone compound.

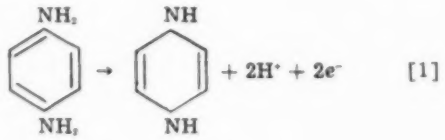

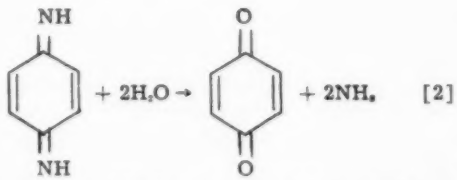

The relative difficulty of oxidizing aniline is apparent from the lower anode potential of this compound as compared with the potentials of the di- and tri-aminobenzene compounds.

A comparison of the half-cell potential discharge curves of the three isomeric dihydroxybenzenes and phenylenediamines is shown in Fig. 4. The ortho and para isomers are oxidized more easily than the meta isomer because they can lose two hydrogen atoms from oxygen (or nitrogen) to give the corresponding stable quinoid compounds. For pyrocatechol the reaction is as follows:

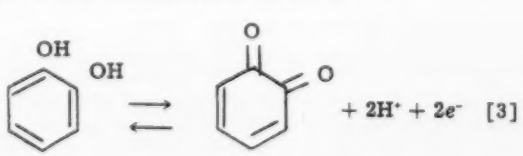

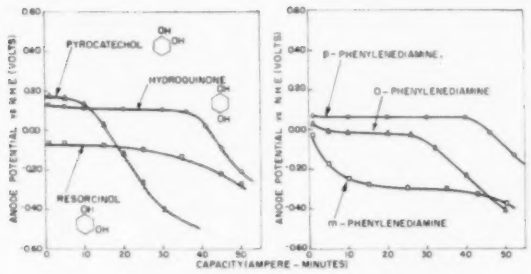

Fig. 4. Half-cell potential discharge curves of the three isomeric dihydroxybenzene and phenylenediamine compounds discharged at a rate of 0.005 amp/g in 1.44M NaOH.

This type of oxidation is not possible for the meta isomer because no stable structure can be written for meta quinone. It is first necessary to oxidize a nuclear carbon-hydrogen bond in an ortho or para position. The product is then capable of producing a quinone (11).

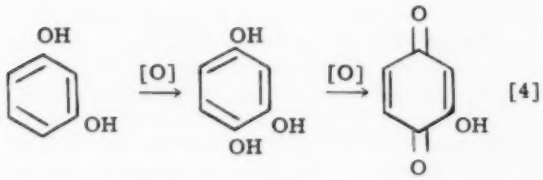

[4]

Resorcinol, the most resistant of the dihydroxybenzenes to oxidation, has a potential which is approximately 0.2 v less anodic than its ortho and para isomers, while meta phenylenediamine has a potential which is approximately 0.25-0.35 v less anodic than its ortho and para isomers. Polarographic half-wave potential measurements of the phenylenediamine isomers agree with these results (4).

Compared to their corresponding aromatic dihydroxy compounds, the ortho and para phenylenediamine compounds operate at potentials 0.05-0.15 v lower while m-phenylenediamine operates at an anode potential approximately 0.2 v lower than resorcinol. This same effect in terms of "critical oxidation potentials" has been illustrated by Fieser for aromatic hydroxy and amino compounds (2).

Figure 5 gives half-cell discharge curves of various substituted hydroquinone and p-phenylenediamine compounds discharged at a rate of 0.005 amp/g in 1.44*M* NaOH solution. These data illustrate the effect of substituted groups, other than hydroxyl or amino, on the anode potential of aromatic dihydroxy and diamino compounds. The introduction into the molecule of electron repelling groups such as $-CH_3$ raises the potential, while the addition of an electron attracting -Cl group lowers the potential of the parent compound. The addition of more than one electron attracting or electron repelling group to hydroquinone or p-phenylenediamine affects the potential still further, as shown by the discharge curves of dichlorohydroquinone, 1,4-diamino-2,6-dichlorobenzene, and trimethylhydroquinone. As with the addition of a hydroxyl or amino group, added methyl and chloro groups are believed to alter the electron density in the vicinity of the oxidizable hydroxyl and amino groups. For example, electron attracting groups such as -Cl decrease the electron density near the oxidizable -OH or $-NH_2$ group, increase its affinity for electrons, and render it a weaker reducing agent. Thus the effect of added groups on the anode potential of aromatic hydroxy and aromatic amine compounds is the reverse of their effect on the cathode potential of organic oxidizing agents such as the aromatic nitro and quinone compounds.

Effect of aromaticity on the anode potential of aromatic hydroxy and aromatic amine compounds. —Previous work shows that the cathode potential of aromatic nitro compounds increases with increasing ring aromaticity (12) in the following order: 1-nitronaphthalene, nitrobenzene, and 2-nitropyridine. These results were attributed to a lower electron density in the vicinity of the reducible nitro group for the more strongly aromatic pyridine compound. Conversely, the anode potential of aromatic hydroxy and aromatic amine compounds would be expected to be greatest for the more weakly aromatic compounds such as naphthol and naphthylamine, which have comparatively high electron densities in the vicinity of their oxidizable groups. This high electron density decreases the affinity of the hydroxyl or amino group for electrons and renders the compound a stronger reducing agent. This effect has been demonstrated for aromatic hydroxy compounds by Fieser (2) with the "critical potentials" of various phenols, naphthols, and anthrols.

Figure 6 presents half-cell discharge curves of 1,4-naphthalenediol and hydroquinone which show

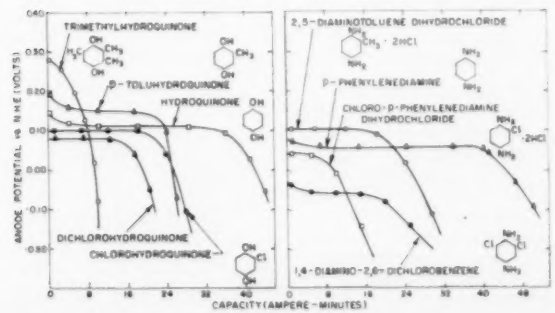

Fig. 5. Effect of substituted groups on the anode potential of hydroquinone and p-phenylenediamine discharged at a rate of 0.005 amp/g in 1.44M NaOH.

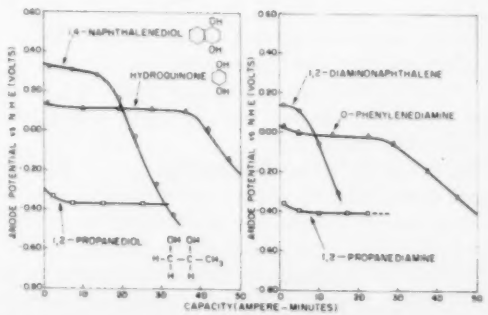

Fig. 6. Effect of aromaticity on the anode potential of aromatic dihydroxy and aromatic diamine compounds discharged at a rate of 0.005 amp/g in 1.44M NaOH.

the effect of aromaticity on the anode potential of organic dihydroxy compounds. The more weakly aromatic naphthalenediol compound operates at a potential 0.2 v more anodic than hydroquinone, a result in agreement with standard potential measurements.[3] For reactions such as the oxidation of 1,4-naphthalenediol and hydroquinone, where changes in ring structure occur, not only must the aromaticity and free energy of the reactants be considered, but also the aromaticity and free energy of the products. In the final analysis, the potential of this particular system will be governed by the change in aromaticity, or more correctly, by the change in free energy, in going from the hydroquinone to the quinone form. The half-cell potential discharge curves for 1,2-diaminonaphthalene and o-phenylenediamine also presented in Fig. 6 show that the same effect holds for aromatic amine compounds. The more weakly aromatic diaminonaphthalene compound operates at a potential about 0.1 v more anodic than o-phenylenediamine.

For comparison the half-cell potential discharge curves of 1,2-propanediol and 1,2-propanediamine also are included in Fig. 6. These alkyl compounds are considerably weaker reducing agents than the aromatic dihydroxy and diamino compounds.

Effect of pH on the anode potential of aromatic hydroxy and aromatic amine compounds.—Equation [3] shows that hydrogen ions take part in the oxidation of aromatic hydroxy compounds such as pyrocatechol and, consequently, the electrode potentials of these compounds should be pH dependent. In accord with theory, polarographic data for the pyrocatechol-o-benzoquinone system (14) show that the half-wave potentials of pyrocatechol vary linearly with pH in the acidic and weakly basic pH ranges. The curve has a slope of −0.058 in close agreement with the theoretical value of −0.0591. The half-wave potential of hydroquinone also has been found to decrease linearly with increasing pH in the range of pH 1 to 8 (9).

Similarly, hydrogen ions take part in the oxidation of aromatic amine compounds such as p-phenylenediamine, and the electrode potentials of these compounds also should be pH dependent. Polarographic data for ortho and para phenylenediamine obtained with a rotating platinum electrode (15) indicate that the oxidation of these compounds is a 2 electron process in buffer media, corresponding to the diamine-diimine redox system. Further, the data indicate a decrease in the half-wave potential of these compounds with increasing pH in agreement with theory. However, the slope of the $E_{1/2}$ *vs.* pH curve was not linear, but had a number of inflections over the pH range 1-10.

Figure 7 gives half-cell potential discharge curves of hydroquinone and p-phenylenediamine obtained when these compounds are discharged at a rate of 0.005 amp/g in three electrolytes having different pH values. In general, the ease of oxidation increases with increasing pH, and little if any capacity

[3] Conversely, the cathode potential of p-benzoquinone has been found to be 0.2-0.3 v higher than that of 1, 4-naphthoquinone when measured at the same current density in a 250 g/l $MgBr_2 \cdot 6H_2O$ electrolyte (13).

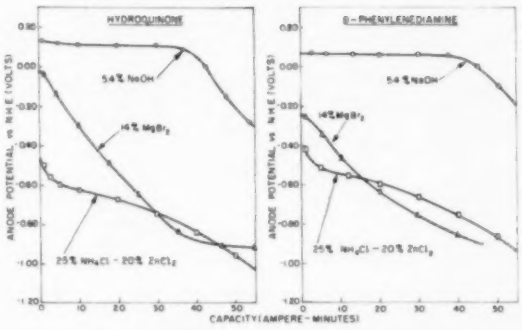

Fig. 7. Effect of pH on the anode potential of hydroquinone and p-phenylenediamine discharged at a rate of 0.005 amp/g in various aqueous electrolytes.

is obtained from these compounds in the $MgBr_2$ (pH = 8-9) and NH_4Cl-ZnCl (pH = 4-5) electrolytes.

In addition to the effect of pH on potential, the pH of the medium often changes the nature of the molecule being oxidized. For phenylenediamine, the ease of oxidation is increased greatly in alkaline solution and decreased in acid solution because the electron donating power of an amino group is much greater than that of an ammonium ion. Similarly in alkaline solution, the ease of oxidation of aromatic hydroxy compounds increases greatly because the electron donating power of the oxide ion is much greater than that of a hydroxyl group.

Coulombic capacities of the aromatic hydroxy and aromatic amine compounds.—Table I lists theoretical capacities and electrode efficiencies of various aromatic hydroxy and aromatic amine compounds calculated from the half-cell discharge data shown in Fig. 1-6. The theoretical capacities were com-

Table I. Theoretical capacities and electrode efficiencies of various aromatic hydroxy, aromatic amine, and aminophenol compounds

Anode material	Capacity, amp-min/g		Efficiency, %
	Theoretical	Experimental	
Zinc	49.2	44.3	90
Magnesium (AZ10 alloy)	132	53-86	40-65
Hydroquinone	29.2	39.5	135
Trimethylhydroquinone	21.2	4.6	21.7
Toluhydroquinone	25.9	23.7	91.5
Chlorohydroquinone	22.2	23.4	105
Dichlorohydroquinone	18.0	18.2	101
Pyrocatechol	29.2	10.4	35.6
1, 4-Naphthalenediol	20.1	15.6	77.6
Pyrogallol	25.5	22.1	86.7
Phloroglucinol	25.5	27.2	107
p-Phenylenediamine	29.8	44.6	150
2, 5-Diaminotoluene dihydrochloride	16.5	21.7	132
Chloro-p-phenylenediamine dihydrochloride	14.9	10.1	67.8
1, 4-Diamino-2, 6-dichlorobenzene	18.2	22.5	124
o-Phenylenediamine	29.8	30.3	102
1, 2-Diaminonaphthalene	20.4	5.8	28.4
1, 2, 4-Benzenetriamino dihydrochloride	16.4	11.0	67.1
o-Aminophenol	29.5	19.8	67.1
p-Aminophenol	29.5	20.9	70.8
4-Amino-3-methylphenol	26.1	21.8	83.5

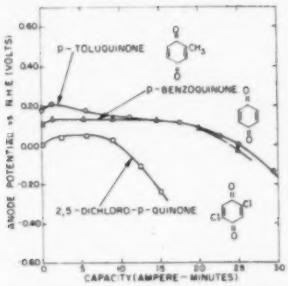

Fig. 8. Anodic half-cell potential discharge curves of various quinone compounds discharged at a rate of 0.005 amp/g in 1.44M NaOH.

puted by means of Faraday's law, with the assumption that oxidation takes place to the quinone and quinoneimine stage with a corresponding 2 electron change. Experimental capacities were measured on the basis of a 0.05 v drop in potential from the flat portion of the half-cell potential discharge curve for the end potential. Also included in Table I are comparable data for conventional zinc and magnesium anodes when discharged in NH_4Cl-$ZnCl_2$ and $MgBr_2$ electrolytes, respectively.

With the exception of pyrocatechol and trimethylhydroquinone, two of the more active reducing agents, the electrode efficiencies of the aromatic hydroxy compounds are usually very high, ranging from 78 to 107%. For hydroquinone, electrode efficiencies of 135% are obtained if a 2 electron change is assumed. The efficiencies in excess of 100% are believed to be caused by a continued oxidation of the products of the initial oxidation reaction. This has been verified experimentally by the fact that p-benzoquinone, p-chlorobenzoquinone, and p-toluquinone give 10-20 amp-min of capacity when discharged at a rate of 0.005 amp/g in 1.44*M* NaOH, as shown by the half-cell discharge data in Fig. 8. This is also in agreement with the fact that p-benzoquinone itself is oxidized easily in alkaline solution and yields maleic and meso-tartaric acids (16). It is interesting to note that these quinone compounds operate at anode potentials close to that of their corresponding hydroquinone compounds. This suggests that some air oxidation of the hydroquinone to the quinone compounds may have taken place.

Similarly, with the exception of chloro-p-phenylenediamine dihydrochloride, the electrode efficiencies of the p-phenylenediamine derivatives are considerably in excess of 100%, ranging from 124 to 150%. These high efficiencies also can be attributed to the continued oxidation of the quinone compounds, formed by the hydrolysis of the primary oxidation products, i.e. the quinonediimine compounds.

On the basis of theoretical and experimental data, the aromatic hydroxy and aromatic amine compounds do not provide as high a coulombic capacity as do the inorganic anode materials. Moreover, the anode potentials of the more strongly reducing aromatic hydroxy and aromatic amine compounds range from +0.1 to +0.3 v, values considerably lower than the anode potentials of 1.3 v for magnesium in aqueous magnesium bromide solution, and 0.7 and 1.3 v for zinc in acidic and strongly alkaline solutions respectively.

Aminophenol compounds as anode materials.— The aminophenols are both aryl amines and phenols and give the characteristic reactions of both classes of substances. Like the dihydric phenols and the diamines, they are oxidized readily in alkaline solution.

The oxidation of p-aminophenol may be represented by the following equation:

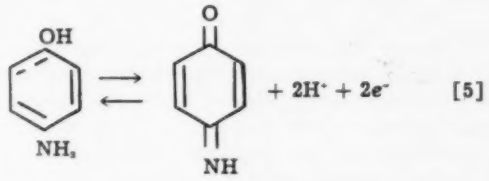

[5]

Like the p-benzoquinone-hydroquinone system, the quinoneimine-aminophenol couple forms a reversible oxidation-reduction system. Quinoneimine, however, is very unstable and readily hydrolyzes to quinone.

Figure 9 shows half-cell potential discharge curves of the three isomeric aminophenol compounds and various substituted p-aminophenol compounds discharged at a rate of 0.005 amp/g in 1.44*M* NaOH solution. As in the case of the aromatic dihydroxy and diamine compounds, the ortho and para isomers are oxidized more easily than the meta isomer, having anode potentials of from +0.12 to +0.14 v. These values are comparable to those of the aromatic dihydroxy compounds and are 0.05-0.15 v higher than the anode potentials of the phenylenediamine compounds.

The effect of electron attracting and electron repelling groups on the anode potential of p-aminophenol closely parallels their effect on the anode potentials of hydroquinone and p-phenylenediamine, and can be explained by the same theory used to explain these effects for those compounds.

Table I shows that the aminophenol compounds operate at efficiencies of 67-84%. These electrode efficiencies are less than those attained for compar-

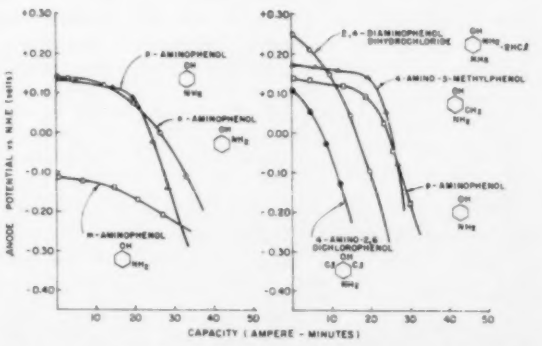

Fig. 9. Half-cell potential discharge curves of the three isomeric aminophenol compounds and various substituted p-aminophenol compounds discharged at a rate of 0.005 amp/g in 1.44M NaOH.

able aromatic dihydroxy and diamine compounds under similar conditions of discharge.

Summary

The effect of added groups, aromaticity, and electrolyte pH on the anode potential of aromatic hydroxy, aromatic amine, and aminophenol compounds is the reverse of their effect on the cathode potential of organic oxidizing agents such as the aromatic nitro and quinone compounds. The anode potentials of the former compounds are raised by the substitution of electron repelling groups in the molecule and lowered by the addition of electron attracting groups to the molecule. Higher anode potentials are obtained also in more basic electrolytes and with the more weakly aromatic compounds. The effect of these factors on the anode potential can be explained readily on the basis of the electron density distribution in the molecule.

Because of the lower theoretical and observed coulombic capacities of these organic reducing agents, they are not as suitable as magnesium or zinc for use as anode materials in galvanic cells.

Acknowledgment

The author wishes to acknowledge support of this work by the Power Sources Division of the U. S. Army Signal Research and Development Laboratory under Contract No. DA-36-039-sc-78048.

Manuscript received June 8, 1960. This paper was prepared for delivery before the Columbus Meeting, Oct. 18-22, 1959.

Any discussion of this paper will appear in a Discussion Section to be published in the December 1961 JOURNAL.

REFERENCES

1. J. B. Conant, *Chem. Revs.*, **3**, 1 (1926).
2. L. F. Fieser, *J. Am. Chem. Soc.*, **52**, 5204 (1930).
3. P. J. Elving and V. F. Gaylor, *Anal. Chem.*, **25**, 1078 (1953).
4. S. S. Lord, Jr., and L. B. Rogers, *ibid.*, **26**, 284 (1954).
5. R. Glicksman and C. K. Morehouse, *This Journal*, **105**, 299 (1958).
6. R. Glicksman and C. K. Morehouse, *ibid.*, **106**, 288 (1959).
7. R. Glicksman and C. K. Morehouse, *ibid.*, **103**, 94 (1956).
8. W. M. Latimer, "Oxidation Potentials," p. 354, Prentice-Hall, Inc., New York (1952).
9. V. F. Gaylor, P. J. Elving, and A. L. Conrad, *Anal. Chem.*, **25**, 1078 (1953).
10. L. F. Fieser and M. F. Fieser, "Organic Chemistry," 3rd ed., p. 605, Reinhold Publishing Corp., New York (1956).
11. C. R. Noller, "Chemistry of Organic Compounds," p. 506, W. B. Saunders Co., Philadelphia (1951).
12. R. Glicksman and C. K. Morehouse, *This Journal*, **107**, 717 (1960).
13. R. Glicksman and C. K. Morehouse, *ibid.*, **106**, 741 (1959).
14. C. M. Wheeler, Jr., and R. P. Vigneault, *J. Am. Chem. Soc.*, **74**, 5232 (1952).
15. R. E. Parker and R. N. Adams, *Anal. Chem.*, **28**, 828 (1956).
16. H. J. Lucas, "Organic Chemistry," p. 415, American Book Co., New York (1935).

The Oxidation of Tin

I. The Kinetics of Oxidation of Pure Tin and the Effects of Temperature and Oxygen Pressure

W. E. Boggs, R. H. Kachik, and G. E. Pellissier

Applied Research Laboratory, United States Steel Corporation, Monroeville, Pennsylvania

ABSTRACT

By means of a vacuum microbalance, the rates of oxidation of pure tin have been determined over a temperature range of 150°-220°C, and for several different pressures of oxygen in the range of 10^{-5} mm to 500 mm Hg. For oxygen pressures of 1 mm and above, the oxidation appears to proceed with time in three stages: (*a*) initially, the rate is low, but it increases to a maximum; (*b*) it then decreases and follows a direct logarithmic relationship; and (*c*) finally, for long times and thick films, the rate becomes erratic, either increasing rapidly or leveling off. Below an oxygen pressure of 1 mm, the oxidation rate increases continuously with time, and the rate-determining step in the kinetic process appears to be the dissociation of oxygen.

Filming and aging treatments in which oxide films are formed on tin plate, either electrochemically or naturally, have been used extensively in the tinplate industry to improve the lacquerability, solderability, resistance to discoloration in storage, and corrosion resistance to certain food products such as condensed milk. In spite of this wide-spread practical use of tin-oxide films, the tin-oxygen system largely has been ignored as a subject for scientific investigation. Only a few papers concerning the kinetics of oxidation of tin, particularly in relation to the microstructure and composition of the tin oxides, have appeared in the literature of the past 40 years.

Tammann and Köster (1) investigated the oxidation of tin in air, observing that the rate of oxide-film thickening obeyed a logarithmic relationship. Kenworthy (2), on the other hand, reported that the

weight increase of tin specimens exposed to air was a linear function of time over a period of two years. Katz (3), however, also observed logarithmic tin-oxide growth in air at room temperature.

Published information concerning the composition of the oxide film formed on tin was as incomplete and confused as the kinetic information. Kutzelnigg (4) obtained stannic reactions from the oxide films removed from tin with 10% ferric chloride solution. Steinheil (5) observed the electron-diffraction patterns of both stannous and stannic oxide in oxide films removed by melting the tin base. Jenkins (6) found that stannous oxide films were formed on tin just above its melting point (231.9°C), but that stannic oxide was formed at higher temperatures. Hart (7) heated a spot on a specimen of tin foil and then determined the composition of the oxide film with respect to the hottest spot by means of electron diffraction. He found that stannic oxide was formed at the center; this was surrounded by a region of stannous oxide which was surrounded in turn by an area of amorphous oxide. He also reported that the oxide film formed on tin, heated in air for 15 min at less than about 130°C, was amorphous.

The most recent papers on the oxidation of tin are those of Britton and Bright (8) on the reaction of tin and tin alloys with wet and dry air, and the concurrent study of the structure of the tin-oxide films by Trillat, Tertian, and Britton (9). These investigators reported that the oxidation of tin at 180° and 210°C followed a parabolic rate law, whereas below 180°C the reaction followed a logarithmic rate law. They were unable to obtain electron diffraction patterns from films formed below 170°C and therefore reported that the oxide film was amorphous below this temperature. Above 170°C, crystalline stannous oxide was found.

Luner (10) of this Laboratory has published the results of his independent study of the kinetics of tin oxidation in pure oxygen. He found that the oxidation process obeyed a logarithmic rate equation in the temperature (168°-211°C) and oxygen-pressure (4-10 mm Hg) range studied. The oxide was identified as α-SnO.

Because of the conflicting and incomplete nature of the published literature about the oxidation of tin, and because of the practical importance of oxide films to manufacturers and users of tin plate, the authors of this paper made a thorough study of the oxidation kinetics and the morphology and mode of growth of tin-oxide films. They studied the kinetics of oxidation by means of a vacuum microbalance system in which the conditions of temperature, pressure, and gas composition could be controlled closely. At the same time they studied, by means of electron microscopy and electron diffraction, the microstructure, mode of growth, and identification of the crystalline oxide films formed during various time intervals in the kinetic investigation.

The program was divided into four major areas: (i) effect of temperature at constant oxygen pressure (pure, dry oxygen) on the microstructure of the oxide film and on the kinetics of oxidation; (ii) effect of oxygen pressure (pure, dry oxygen) at constant temperature; (iii) influence of various impurities in the tin on the oxidation process; and (iiii) effect of impurities in the oxygen on the oxidation process.

Investigations of the effect of temperature and oxygen pressure are now essentially complete. The results are presented in three parts. The first part, the subject of this paper, deals with a factual presentation of the kinetic data accumulated during the investigation of the effects of temperature and oxygen pressure. The second part, the subject of the following paper, is confined to a presentation of the microstructure information obtained by electron-microscopic examination of the oxide films formed during various time intervals in the kinetic investigation. The third part, the subject of the final paper in this series, gives the theoretical interpretation of the data associating the observed kinetics of the oxidation of pure tin foil with the morphology of the oxide films thus formed.

Experimental Procedure

The design of the vacuum microbalance has been described in detail in the literature (11). The particular balance used in this study was built by Andrew of the Westinghouse Electric Corporation Research Laboratory, according to an original design by Gulbransen of the same laboratory. It has a sensitivity of 0.10 μg/0.001 mm deflection of the beam end. The maximum load is 1 g.

The balance is completely enclosed in an evacuated glass envelope. The tin-foil specimen is hung from one end of the beam, and a gold-foil tare hung from the other end, by means of 0.002-in. diameter Nichrome wires. The specimen and tare are enclosed in separate Pyrex glass tubes connected to the glass-balance envelope. Both tubes, or legs, are heated in the furnace to minimize the errors introduced by so-called "thermomolecular effects" (12). The furnace tubes are wound noninductively to minimize the interaction between the heating coil and the induced currents in the sample, since this interaction would lead to measuring errors as the power input to the furnace varied.

The effectiveness of the two-leg balance, and of heating both legs, in minimizing balance errors arising from the thermomolecular effects, was investigated in the following manner. The position of the beam was determined first in vacuum (10^{-6} mm) and then at oxygen pressures of 10^{-3}, 10^{-2}, 10^{-1}, 1, 10, and 100 mm Hg, with a dummy specimen suspended in one leg and the usual gold tare in the other. Both legs were heated to 190°C. The apparent weight changes were small at 100 and 10 mm; they increased to a maximum at 10^{-1} mm, and then decreased. During the oxidation experiments at 100 and 10 mm, the error was found to be so consistent and reversible that suitable corrections to the individual readings could be obtained from the initial and final beam readings in vacuum. However, at oxygen pressures of 1 mm and below, the error was so large and erratic that no suitable corrections could be made. At pressures higher than 400 mm, the bal-

ance is no longer stable. Therefore, all weight measurements of samples oxidized at oxygen pressures below 10 mm and above 400 mm were made after evacuation to 10^{-7} mm or better. The position of the balance beam in vacuum was recorded at the beginning and the end of each oxidation run. The true weight change resulting from oxidation can be calculated from the difference between these two readings. This procedure is, of course, time-consuming because it requires a different sample to obtain each point of a plot of weight increase versus time of oxidation. It does have the advantage, however, of providing specimens (that have been oxidized for progressively longer intervals, corresponding to each point of the oxidation rate curves) for structural studies of the oxide films by means of electron microscopy and electron diffraction. Thus the morphology and mode of growth of the oxide films may be correlated with the kinetics of oxidation.

The tin foil used in this study was obtained from A. D. MacKay Company and had a claimed purity of 99.999%. The grain size of this material was approximately 0.6 mm average grain diameter (4 grains/mm^2). Since the supplier prepares this foil by rolling the initially 99.999% pure sheet tin between copper platens, it was suspected that the surface of the tin foil might be contaminated with copper. Fortunately, any surface treatment (such as electropolishing) given the foil to obtain a smooth surface prior to oxidation should tend to remove metallic surface contamination. To investigate this situation, spectrochemical and microchemical analyses were made of the tin foil in the as-received condition and after electropolishing. Results of these analyses are given in Table I. Note that the major contaminant in the as-received material was, in fact, copper, and that electropolishing did materially reduce this copper contamination. Nevertheless, the final purity of the tin foil used in these experiments was about 99.994%.

After preliminary experiments, electropolishing was chosen as the most promising of the possible methods of surface preparation. Distorted, flowed, or smeared metal and surface contaminants are readily removed, and the resulting surface should have a specific area very nearly equal to the geometric area; also, any oxide originally present on the surface should be removed. The electropolishing procedure used for smoothing the tin foil specimens in this investigation was essentially that proposed by Jacquet (13) many years ago. The solution recommended by Jacquet consisting of 194 ml of concentrated perchloric acid (70-72% aqueous solution, sp gr 1.61) and 806 ml of acetic anhydride (98%) was considered to be rather hazardous, and so it was modified by substituting glacial acetic acid for the acetic anhydride. This solution is safer, it can be mixed at room temperature, and it provides a satisfactorily polished surface on the tin foil.

The optimum electropolishing conditions, such as time and voltage, were determined by light and electron microscope examinations of electropolished surfaces of the tin specimens. A Zeiss Interference Microscope was used to evaluate the degree of smoothness of the electropolished surfaces. A typical microinterferogram of the final surface is shown in Fig. 1. The interference fringes of the microinterferogram are similar to the contour lines of a topographic map. A smooth surface is indicated by straight, parallel interference fringes of uniform spacing.

After the electropolishing, all specimens used in the oxidation study were annealed in the microbalance system for 1 hr at 200°C and a pressure of 10^{-7} mm, or less, to stabilize the microstructure of the tin and to relieve any stresses accidentally introduced in the foil during preparation and handling. Specimens then were oxidized, without delay or exposure to the atmosphere.

To evaluate surface cleanliness and smoothness after this vacuum-annealing treatment, a few control specimens were taken out of the vacuum microbalance and examined by means of the interference microscope and the electron microscope. The interferograms showed about the same degree of surface smoothness as was observed after electropolishing; some additional slight surface irregularities apparently were introduced by the annealing, perhaps because of localized evaporation or migration of tin ("thermal etching"), especially at grain boundaries

Table I. Purity of tin foil used in the oxidation study

Element	Spectrochemical analysis		Microchemical analysis	
	As-received, %	After electropolish, %	As-received, %	After electropolish, %
Copper	0.012	0.001	0.012	0.003
Lead	<0.001	<0.001	0.0003	0.0003
Iron	0.001	0.001	0.0023	0.0018
Arsenic	0.004	0.001		
Antimony	<0.001 IA*	<0.001 IA		
Zinc	ND**	ND		
Nickel	ND	ND		
Silver	ND	ND		
Cadmium	ND	ND		
Cobalt	ND	ND		
Bismuth	<0.001 IA	<0.001 IA		

* IA, if any. ** ND, none detected.

Fig. 1. Microinterferogram of electropolished tin-foil surface in the condition selected for oxidation experiments. Magnification 110X before reduction for publication.

("thermal grooving"). Annealing produced only slight grain growth.

Coulometric reduction measurements on electropolished tin specimens indicated the presence of a film which would be only about 20Å thick if it is assumed to be continuous and to consist of crystalline α-SnO. However, no evidence of such a film could be obtained by transmission or reflection electron diffraction after the tin was annealed in vacuum at 200°C for 1 hr, although crystalline oxide could be detected by these techniques after very short exposures to oxygen at 10 mm at the same temperature. Examination of conventional plastic replicas of the annealed tin surface, by means of electron microscopy, revealed that the surface was still smooth, except for grain boundaries; neither electron microscopy nor electron diffraction studies of these replicas yielded evidence of the presence of any oxide after annealing. In an effort to detect any slight structural detail in the surface that might not have been revealed by the conventional plastic replica because of insufficient contrast, electropolished and annealed tin specimen surfaces were preshadowed with chromium and then replicated with plastic. Electron microscope examination of these preshadowed replicas did not provide any indication of surface roughening or oxidation.

High-purity (Matheson "extra dry" grade) oxygen was condensed in a liquid nitrogen trap and then was allowed to evaporate into the balance system until the pressure reached the desired level. It is believed that this system of purification practically eliminated the impurities present in the tank gas, with the exception of nitrogen and perhaps argon; any remaining small amounts of the inert gases cannot affect the oxidation experiments significantly. At pressures of 0.1 mm and above, depletion of oxygen in the balance system (volume of 8 liters) by oxidation of the specimen, is insignificant. Normally, no special effort was made to maintain absolutely constant pressure during an oxidation experiment.

A liquid nitrogen trap was used to prevent contamination of the sample by diffusion-pump oil and stopcock grease. Since there were no grease or wax seals between the balance cold trap and the microbalance proper, the glass-balance envelope had to be opened and resealed with a glass-blowing torch to insert and remove the specimens. A small flow of dry nitrogen was maintained through the vacuum system during the period in which it was open to the atmosphere to minimize contamination of the balance system with dust and water vapor.

Results and Discussion

Effect of Temperature at Constant Pressure

Figure 2 shows a linear plot of the weight-change data during oxidation vs. the time of oxidation for seven different temperatures, at a constant oxygen pressure (10 mm Hg). These curves show that the rate of oxidation initially is low, that it increases rapidly to a maximum, and then gradually decreases with time. Evans (14) and Tylecote (15) attribute an initial "sigmoid curl," a so-called induction period

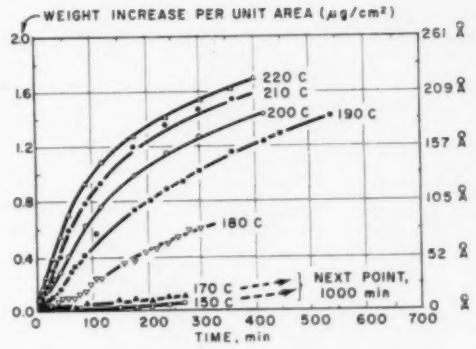

Fig. 2. Influence of temperature on the oxidation of tin at an oxygen pressure of 10 mm Hg (linear plot).

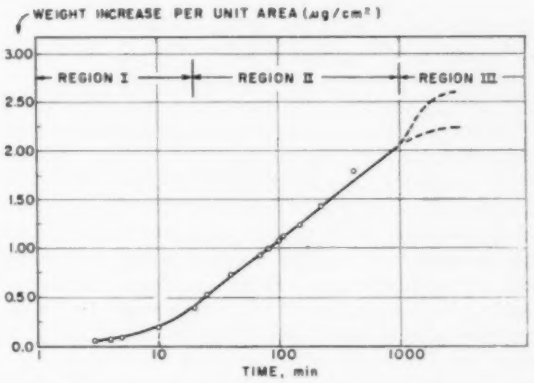

Fig. 3. Oxidation of pure tin at an oxygen pressure of 10 mm Hg and 220°C (log time plot).

in which the rate of oxidation is increasing, to the nucleation and lateral spreading of oxide over the surface to form a continuous film. There is no sharp change in curvature where the sigmoid curl ends, but a gradual merging into the period of decreasing rate. The initial region of rapidly increasing oxidation is more clearly evident in a semilogarithmic plot of typical data, in which the expanded time scale at the beginning of oxidation tends to emphasize this feature of the kinetics, as shown by Region I of the curve of Fig. 3.

In the following stage of oxidation, Region II of the curve of Fig. 3, where the rate is decreasing, the data clearly conform to a direct logarithmic relationship of the form

$$W = k \log (at + 1)$$

where W is the weight of oxygen reacted at time t, k is the logarithmic rate constant, and a is a constant associated with the displacement of the logarithmic portion of the curve to longer times at lower temperatures, Fig. 4.

Subsequently, the oxidation rate changes in a rather erratic manner, either increasing rapidly, or leveling off, as indicated by Region III of the curve of Fig. 3. It is possible that at this stage of oxidation the film has grown so thick that the strains, generated by the specific volume difference between the tin substrate and the oxide, are sufficient to

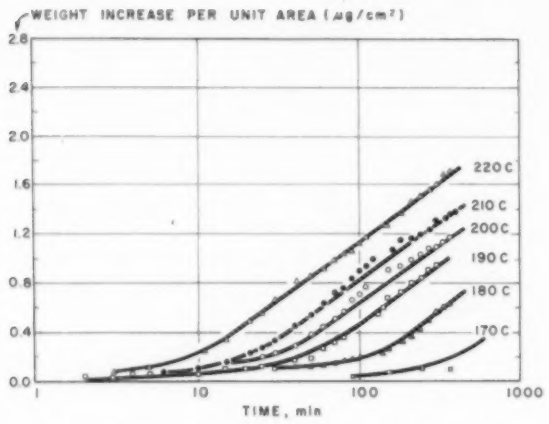

Fig. 4. Influence of temperature on the oxidation of tin at an oxygen pressure of 10 mm Hg (log time plot).

cause rupture of the film. Available information on the specific volumes of β-tin and α-SnO indicates that the oxide occupies about 20% greater volume than the tin. The cracks thus formed may permit direct access of gaseous oxygen to the tin; this would increase the over-all oxidation rate until such time as the cracks were plugged with more oxide and the rate decreases, as has been suggested frequently in the literature on oxidation to explain such kinetic phenomena. Microscopic evidence which tends to confirm this supposition will be presented in a later paper.

Figure 4 shows that the curves relating weight change to the logarithm of time at different temperatures, in the region of logarithmic behavior (Region II), are nearly parallel; this indicates that the logarithmic rate constant is essentially independent of temperature. The length of the "induction period" (Region I), however, is clearly governed by the temperature. It is generally the practice when logarithmic behavior is observed in oxidation studies to plot w against log $(t + t_o)$, where t_o is proportional to $1/a$, and to adjust t_o in such a way as to make *all* of the data when replotted, particularly those obtained in the "induction period," conform to a logarithmic relationship. Since the length of the induction period is a function of temperature, this treatment obviously changes the slopes of the curves and forces temperature dependence on the logarithmic rate constant. Because of this, calculating an energy of activation for oxidation on the basis of the new values of the logarithmic rate constant is not justified. Evans (14) and Tylecote (15) have pointed out that lateral growth of oxide patches may occur in the early stage of oxidation, that is, during the induction period. Certainly if this type of growth occurs, the kinetic data obtained during the early period of oxidation should not be expected to conform to a logarithmic relationship; in fact, effort to force such a fit tends to obscure important clues as to the operation of some different growth mechanisms during the initial period of oxidation, as contrasted to that which occurs in the true logarithmic region. More specifically, for the oxidation of tin, information obtained concurrently, in an electron microscope study in this laboratory on the morphology and manner of growth of tin oxide films, has shown that the films do in fact start to form by lateral spreading of oxide patches from nucleation or growth centers. This information is presented in a following paper.

Several mechanisms have been proposed to account for the logarithmic rate of oxide growth that is frequently observed when metals are oxidized below about 350°C. These include the concepts of (*a*) penetration of the oxide film by oxygen only at leakage points, which tend to close because of compressive stresses accompanying the oxidation (14); (*b*) expanding diffusion blocks occurring during the film growth (14); (*c*) electron tunneling effect (16); (*d*) continuous recrystallization of the oxide film (17); (*e*) space-charge effects within the oxide film (18); and (*f*) the extension of chemisorption phenomena (19). In any given instance of logarithmic oxidation behavior, it seems rather pointless, if not unreasonable, to select a particular mechanism of oxidation to explain such behavior on the basis of kinetic data alone, particularly if it is possible to obtain supplementary and more direct information about the manner in which the films form, thicken, and change in character during the oxidation. There appears to be enough latitude in the accuracy of the kinetic data, and in its treatment, to preclude a sound, meaningful, and unambiguous interpretation of oxidation mechanism from kinetics alone. In two following papers on the oxidation of tin, the powerful assistance that can be provided by microstructural examination of the oxide films, conducted in conjunction with the kinetic experiments, will be demonstrated.

Effect of Oxygen Pressure on the Oxidation Kinetics

The effect of oxygen pressure at 190°C has been investigated from 10^{-8} mm to 500 mm Hg. At 1.0 mm and above, the major portion of the data fit the direct logarithmic rate law discussed above. Increasing pressure causes a displacement of the curves to the left on the time axis, Fig. 5, but the curves tend to converge at long times. Below 1.0 mm the oxidation rate increases continuously with time, Fig. 6. The effect of oxygen pressure on the oxidation rate is also illustrated in Fig. 7, where the weight increase

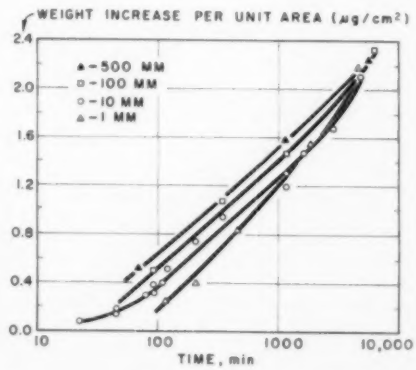

Fig. 5. Influence of oxygen pressure on the oxidation of tin at pressures of 1 mm Hg and above (log time plot).

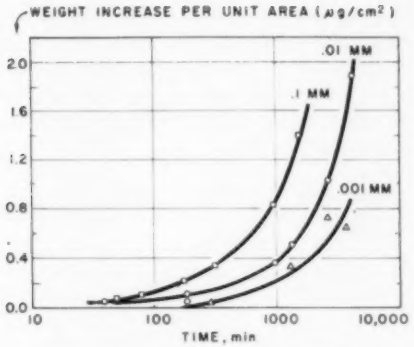

Fig. 6. Influence of oxygen pressure on the oxidation of tin at pressures less than 1 mm Hg (log time plot).

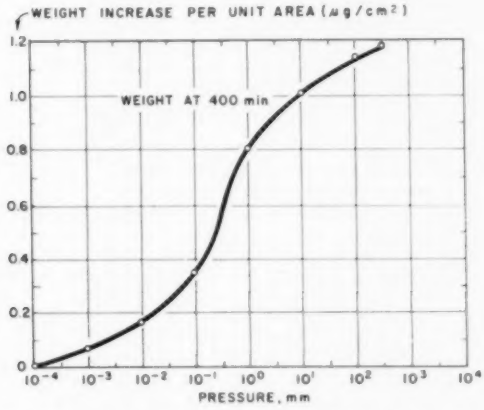

Fig. 7. Effect of oxygen pressure on the oxidation of tin at 190°C (log pressure plot).

of the foil after 400 min is plotted as a function of the log of the oxygen pressure. The result is a sigmoid curve indicating an increasing effect of pressure to about 0.5 mm and then a decreasing effect.

When the initial oxidation rate is plotted as a function of the square root of oxygen pressure, a linear relationship is observed for pressures of 10^{-3}, 10^{-2}, and 10^{-1} mm, Fig. 8. This suggests that the dissociation of oxygen is rate controlling at these low pressures. Further evidence that the dissociation of

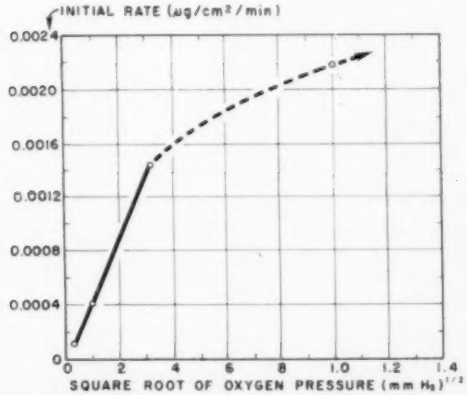

Fig. 8. Effect of oxygen pressure on the initial oxidation rate at 190°C.

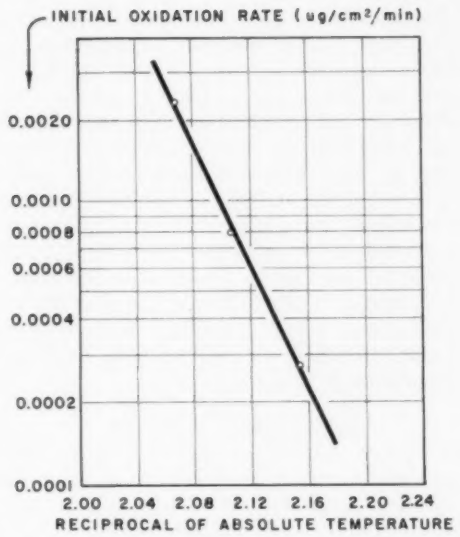

Fig. 9. Plot of the log of the initial rate of oxidation of tin at an oxygen pressure of 10^{-2} mm Hg vs. the reciprocal of the absolute temperature.

oxygen is the slow step in the oxidation of tin at low pressures is obtained when the logarithms of the initial rates of oxidation (20) at 10^{-3} mm oxygen pressure and temperatures of 210°C, 200°C, and 190°C are plotted against the reciprocals of the absolute temperatures, Fig. 9. The slope of this Arrhenius plot corresponds to an activation energy of 53 kcal/½ mole, or 106 kcal/mole of oxygen. This value is reasonably close to the published value for the dissociation energy of the oxygen molecule of 117.96 kcal/mole (21).

The over-all effect of oxygen pressure at constant temperature is shown in Fig. 10, where the log of the weight gain is plotted *vs.* the log of the time. For pressures of 10 and 100 mm, there appears to be a break in the curves around 1000 to 1400 min, with a slight increase in oxidation rate. This might be caused by breakup of the oxide film, which allows oxygen in the gas phase to come into direct contact

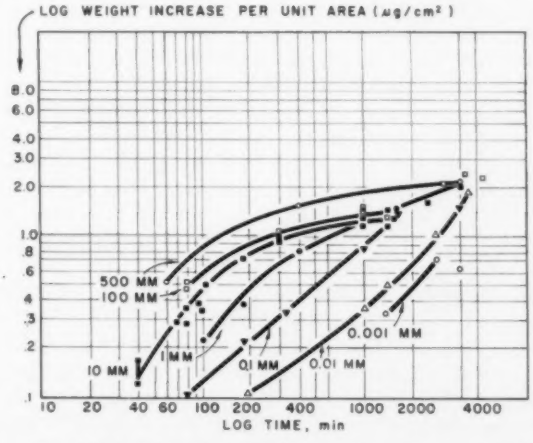

Fig. 10. Log log plot for the oxidation of tin at 190°C showing the effect of oxygen pressure.

with the underlying metal; the result is an increased reaction rate. Curves obtained at pressures of 500 mm to 1 mm are concave to the log-time axis, whereas the curves obtained at 0.1 mm and 0.01 mm are convex to the log-time axis. At an initial pressure of 0.001 mm the data are scattered, probably because, at this pressure, depletion of oxygen from the system by the oxidation reaction is becoming serious. The decrease in pressure is also measurable, but not serious, for an initial pressure of 0.01 mm; but at 0.1 mm and above there is a considerable excess of oxygen in the 8-liter vacuum system. It is interesting to note that the weight of oxygen reacted approaches the same value at around 4000 to 5000 min, regardless of the pressure.

Summary and Conclusions

The kinetics of the oxidation of 99.994% pure polycrystalline tin foil has been investigated over a temperature range of 150°-220°C and an oxygen pressure range of 10^{-3} mm to 500 mm Hg.

At oxygen pressures of 1.0 mm and above, the rate of oxidation initially is low; it then increases to a maximum and gradually decreases with time. After long times, the data become erratic and the rate may increase. The initial sigmoid curl of the rate curve is attributed to nucleation and lateral spreading of the oxide over the surface to form a continuous film. In the period of decreasing rate, the data conform to the direct logarithmic rate law, for which there are many different explanations in the literature. The final period, in which the rate becomes erratic, could be attributed to rupture of the oxide film; strains generated by the specific volume difference between the tin substrate and the oxide might cause cracking which permits direct access of gaseous oxygen to the tin substrate.

At oxygen pressures of less than 1.0 mm, the oxidation rate increases continuously with time, at least over the period studied; this indicates that the oxide film is discontinuous or spongy and provides no barrier between the gaseous oxygen and the underlying metal. The rate of dissociation of oxygen exerts a major influence on the rate of oxidation in the low-pressure region.

Manuscript received May 11, 1960. This paper was prepared for delivery before the Houston Meeting, Oct. 9-13, 1960.

Any discussion of this paper will appear in a Discussion Section to be published in the December 1961 JOURNAL.

REFERENCES

1. G. Tammann and W. Köster, *Z. anorg. u. allgem. Chem.*, **123**, 196 (1922).
2. L. Kenworthy, *Trans. Faraday Soc.*, **31**, 1331 (1938).
3. W. Katz, *Stahl u. Eisen*, **76**, 1672 (1956).
4. A. Kutzelnigg, *Z. anorg. Chem.*, **202**, 418 (1931).
5. A. Steinheil, *Ann Phys.*, **19**, 495 (1934).
6. R. D. Jenkins, *Proc. Phys. Soc.*, **47**, 107 (1935).
7. R. K. Hart, *ibid.*, **65B**, 955 (1952).
8. S. C. Britton and K. Bright, *Metallurgia*, **56**, 163 (1957).
9. J. J. Trillat, L. Tertian, and S. C. Britton, *Métaux Corrosion Industries*, **32**, 475 (1957).
10. C. Luner, *J. Metals*, **11**, 71 (1959).
11. E. A. Gulbransen, *Trans. Electrochem. Soc.*, **81**, 327 (1942).
12. T. N. Rhodin, *Adv. in Catalysis*, **5**, 39-117 (1953).
13. P. A. Jacquet, Bulletin No. 90, International Tin Research and Development Council (1939).
14. U. R. Evans, *Rev. Pure Appl. Chem.*, **5**, 1 (1955).
15. R. F. Tylecote, *J. Inst. Met*, **81**, 681 (1953).
16. N. Cabrera and N. F. Mott, *Repts. Progr. Phys.*, **12**, 163 (1949).
17. N. F. Mott, *Trans. Faraday Soc.*, **36**, 472 (1940).
18. H. H. Uhlig, *Acta Met.*, **4**, 541 (1956).
19. P. T. Landsberg, *J. Chem. Phys.*, **23**, 1079 (1955).
20. W. W. Smeltzer, The Oxidation of Iron in Carbon Dioxide—Carbon Monoxide Atmospheres, to be published.
21. T. L. Cottrell, "The Strength of Chemical Bonds," Butterworths Scientific Publications, London (1954).

The Oxidation of Tin

II. The Morphology and Mode of Growth of Oxide Films on Pure Tin

W. E. Boggs, P. S. Trozzo, and G. E. Pellissier

Applied Research Laboratory, United States Steel Corporation, Monroeville, Pennsylvania

ABSTRACT

Oxide films formed during the study of the kinetics of oxidation of pure tin, under different conditions of time, temperature, and oxygen pressure, have been examined by means of electron microscopy and electron diffraction. Under all the conditions investigated, the oxide nucleates at numerous sites on the tin surface and spreads laterally, until the surface is essentially completely covered with oxide.

For oxygen pressures of 1 mm Hg and above, at all temperatures investigated, the oxide nuclei develop into microscopic, wheel-shaped "growth centers" about 1 micron in diameter. Segments of the rims of some of these growth centers grow outward as spikes or spines, generally in a spiral pattern and rapidly develop into oxide platelets. The platelets from adjacent growth centers extend laterally until they mutually impinge. This occurs as the oxidation rate reaches a maximum.

Cavities have been found at the oxide-metal interface. They extend nearly through the oxide film, but are closed near the oxide-oxygen interface by a thin membrane of oxide. These cavities are first detected at the junctions of growth lamellae within the oxide platelets and enlarge with time, as the oxidation rate decreases in a logarithmic manner, until they reduce the area of contact between the oxide and metal by as much as one-third.

At oxygen pressures below 1 mm, the oxide grows in a dendritic manner. The dendrites spread laterally but evidently do not cover the tin surface in a compact layer, since the oxidation rate increases continually during the period of time investigated. The main direction of growth of these dendrites from various centers appears to be the same within the area of a given tin grain in the substrate, but is different for adjacent areas corresponding to tin grains of generally different orientations. The electron diffraction results show that only one crystalline oxide, alpha-SnO, is formed under all of the oxidation conditions investigated.

A previous paper (1) that presented information on the kinetics of the oxidation of pure tin foil showed that for oxygen pressures of 1 mm Hg and above, the rate curves have a sigmoidal shape. The oxidation rate increases with time to a maximum and then begins to decrease in conformance with a direct logarithmic rate law. At pressures below 1 mm, the oxidation rate increases continuously with time, and the kinetic data indicate that (at least initially) the dissociation of molecular oxygen is the rate-controlling step in the oxidation process. At higher pressures, the more usual rate-controlling processes, such as diffusion, appear to be operative. As was noted in the earlier paper, however, it is difficult, or perhaps impossible, to deduce valid mechanisms from kinetic data alone, particularly when the data conform to an ambiguous rate law such as the direct logarithmic rate law.

It appeared that direct information on the microstructure and mode of growth of the tin-oxide films formed in the kinetic studies would be very helpful; therefore, the present investigation was made, with the use of electron microscopy and electron diffraction to examine the films. The objectives of the investigation were to determine (*a*) the location and nature of the first detectable oxide that forms on the metal substrate, (*b*) the manner in which the oxide grows, (*c*) changes in structure that occur with time of oxidation, and (*d*) effects of temperature and pressure on the oxide's morphology and mode of growth. It was reasoned that this information could be obtained by interrupting the course of oxidation in the microbalance at several intervals, removing the specimen from the balance, and examining the oxide film at various stages of its formation and growth; in other words, it was proposed to conduct a "time-lapse" structural study. The oxidized specimens are, of course, too thick and opaque to be examined by transmission-electron microscopy; therefore, either the contour of the oxidized metal surface must be replicated *in situ* with a thin film of plastic or carbon that is transparent to electrons, or the oxide itself must be removed from the metal substrate by a kind of extraction-replica technique whereby the oxide, in place on the substrate, is coated and fixed with a thin plastic film, which is then separated in some manner from the substrate. The latter technique was preferred because it would permit direct observation of the oxide and thus provide electron images of better contrast and resolution than usually are obtained from conventional surface replicas; furthermore, it seemed likely that more

structural detail would be revealed throughout the thickness of the oxide film than could be obtained from surface replication. Although the extraction-replica technique was used predominantly in the present studies, surface replicas of the top and bottom surfaces of the stripped oxide films did provide extremely useful supplementary information.

The most difficult step in applying an extraction-replica technique to the removal of oxide films from most metal surfaces is the stripping of the plastic replicating film to which oxide from the substrate is attached. Dry mechanical stripping generally results in distortion and tearing of the thin replica. Chemical or electrochemical stripping methods, in which the oxide and supporting plastic film is undermined and separated by dissolution of the surface layer of the metal substrate, introduce the uncertainty of chemical reaction with the oxide and consequent alteration of its structure. Fortunately, in the case of tin, it is possible to remove the metal substrate by amalgamation, without any attack on or alteration of the oxide.

The study of the structure of oxide films is, of course, not new. Bardolle and Benard (2) investigated with the light microscope the structure of the oxide films formed on iron under various conditions and the effect of the crystallographic orientation of the iron substrate on the structure and orientation of the oxide. Harris, Ball, and Gwathmey (3) studied with the electron microscope the structure of oxide films formed on selected crystalline faces of copper single crystals. Gulbransen and his co-workers (4-8) have used electron diffraction and electron microscopy to investigate the oxide films formed during kinetic studies of the oxidation of iron, several of its alloys, and other metals. Kofstad (9) and Hurlen (10) used electron diffraction and electron microscopy, in conjunction with kinetic measurements, in their study of the mechanism of oxidation of titanium and titanium alloys.

Trillat, Tertian, and Britton (11) used electron diffraction to identify films formed in an investigation of the oxidation of tin by Britton and Bright (12); their attempts to study the microstructure of the oxide films with the electron microscope were not successful because of difficulty with the single-stage replication technique used for stripping and supporting the oxide film. A thick layer of Formvar was used to support the oxide during stripping; then this layer was partially dissolved to make it thin enough for transmitting electrons in the electron microscope. In this procedure, the oxide films were deformed and broken up. The two-layer plastic replication technique used in the present investigation overcomes this difficulty and provides, completely intact, undistorted oxide films for electron microscope examination.

As will be evident from this and the following paper, the electron microscope can be an extremely valuable tool in oxidation studies; by supplementing kinetic studies with structural information, it is possible to formulate or select realistic oxidation mechanisms for various conditions of temperature and pressure.

The electron microscope and diffraction studies reported here cover the oxidation of two series of tin-foil specimens: one series at an oxygen pressure of 10 mm Hg and at temperatures of 75°-220°C, and the other at oxygen pressures of 10^{-4} to 500 mm Hg and at a temperature of 190°C.

Experimental Techniques

The preparation of the tin specimens prior to oxidation and the oxidation experiments in the microbalance were described in the previous paper (1). Discussed here are the procedures used for removing the oxide films from the tin substrate and the technique for replicating the top and bottom surfaces of the stripped oxide films, in preparation for electron microscopy and electron diffraction studies.

Removal of oxide films from the tin substrate.— After a tin-foil specimen has been oxidized at a selected pressure and temperature, and for a given time, it is removed from the vacuum microbalance and immediately coated with a solution of 0.35% Formvar in p-dioxane; when this coating dries it forms a thin plastic film, tightly adherent to the oxide, which "fixes" and supports the oxide film during subsequent stripping and handling, in preparation for electron microscopy and diffraction. This Formvar film is reinforced with a much thicker layer of Parlodion, applied as a solution in amyl acetate; 200-mesh, ⅛-in. diameter stainless-steel support screens are pressed into the Parlodion backing layer while it is still wet. This heavy backing film, with metal support screens, is needed to prevent damage to the Formvar film carrying the oxide during stripping and subsequent handling; the areas of film supported on screens ultimately are cut out of the large plastic film and serve as specimen holders for insertion in the electron microscope or diffraction unit.

Figure 1A is a schematic cross-sectional diagram showing the composite of plastic films and support screen on the oxide film. The oxide and the supporting films are separated from the tin substrate by amalgamation (12). This is accomplished by first cutting the edges of the specimen to expose tin and then placing the specimen in a shallow pool of mercury so that the tin base is amalgamated and the oxide and support float off on top of the pool of

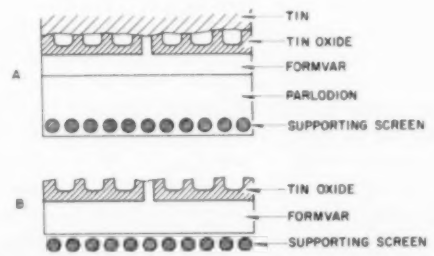

Fig. 1. Schematic diagram showing: A, tin oxide before tin removal and, B, isolated tin oxide in Formvar and the supporting screen.

mercury. The extraction replica is lifted from the mercury-tin amalgam and washed very carefully with fresh, clean, triple-distilled mercury to remove most of the amalgam adhering to the oxide. Solution of the parlodion by leaching with amyl acetate (13) leaves the tin-oxide film on the Formvar substrate, supported by a screen, as is shown in Fig. 1B. This two-layer technique provides an extraction replica that is entirely suitable for electron-microscopic and -diffraction examination, to obtain information concerning the size, shape, and distribution of the oxide as well as information about its crystallographic and chemical identity. Unfortunately, the cleaning steps are not always completely successful; therefore a background of undissolved parlodion and/or fine particles of tin sometimes appears in the electron micrographs. This contamination may be recognized by the fact that it appears not only in areas free of oxide but also on or behind the oxide particles.

Each of the tin samples oxidized in the microbalance was treated as described above. Representative plastic films containing the oxide were carefully examined and photographed with the electron microscope. In addition, transmission electron-diffraction studies were made, and certain preselected oxide particles, or groups of particles, were isolated and examined by selected-area diffraction.

Replication of top and bottom surfaces of oxide films.—In addition to the examination of the oxide itself by transmission electron microscopy, replicas of the top and bottom surfaces of the oxide films were prepared to permit a better understanding of certain microstructural features observed; in particular, such topographical studies of the two surfaces permit less equivocal interpretation of small areas of different electron transparency within the film. In the replication of the top surface of the oxide, the oxidized tin specimen is cemented to a glass microscope slide and an impression of the oxide surface is made by means of the conventional negative Formvar-replication technique. The procedure is similar to that illustrated in Fig. 1, except that instead of the tin being amalgamated and the oxide extracted, the plastic layers and embedded screens are stripped from the oxide, so that the Formvar film contains an impression or replica of the contour of the top surface of the oxide (gas-oxide interface).

To make an impression of the bottom surface of the oxide (oxide-metal interface) a two-stage, parlodion-carbon replication technique is used. First, the oxide is coated with a thick solution of parlodion, Fig. 2A. The parlodion and oxide are then stripped by amalgamation of the tin, and carbon is evaporated onto the underside of the oxide (oxide-metal interface). One-eighth-inch squares of this plastic-oxide-carbon film sandwich are placed on the specimen screens with the carbon side down, Fig. 2B; the screens are inserted in a special holder and immersed in amyl acetate so that the parlodion is exposed to the solvent. The parlodion dissolves, and some of the oxide is washed away, leaving a carbon replica of the underside of the oxide film in some areas and a carbon-stannous oxide composite film in other areas, Fig. 2C.

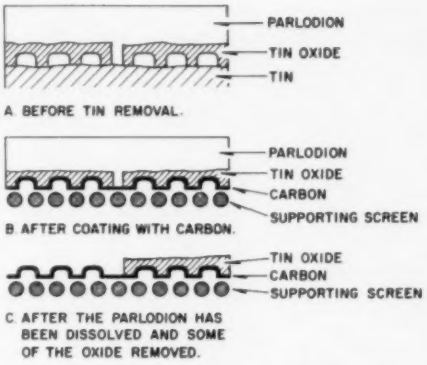

Fig. 2. Schematic diagram showing the technique for replicating the bottom surface of tin oxide.

So that some estimate of the height and depth of the topographical features of these carbon replicas could be obtained, the replicas were charged with a dilute water suspension of monodisperse latex spheres of known diameter (14,15); after drying, the replicas were shadow-cast with chromium at a preselected low angle. By comparing the lengths of the shadows cast by the spheres and by the various topographical features of the replica in the resulting electron micrographs, quantitative estimates of the height and depth of these features could be made.

Estimation of the thickness of oxide films.—It is possible to estimate the average thickness of the oxide film, from the known weight increase during oxidation in the microbalance, the density of the tin oxide, and the area of tin substrate covered by the oxide as obtained from areal analysis measurements of the electron micrographs. Although such calculations were made, an independent and more direct method of determining oxide film thickness was desirable, because of some uncertainty about the actual density of the oxide, and particularly if this method would permit measurement of the thickness of individual platelets or patches of oxide. Thus, the Formvar films bearing the stripped oxide were charged with latex spheres and shadowed with chromium, as described above. The determinations made by the two methods on identical films were in fair agreement, but there was some doubt that the oxide platelets were standing entirely in relief on the plastic supporting film, to create a shadow of proper length upon shadow-casting. To insure that the oxide platelets or patches would stand completely above the replica surface, modifications of the simple replicating system, such as preshadowing and two-stage replication, were attempted. They were not successful, and, in fact, the results indicated that the oxide was situated on and not in the surface of the simple plastic film or replica.

Identification of the crystal structure of the oxide.—The same oxide-bearing plastic films that were prepared for electron microscopy were utilized to obtain transmission electron diffraction patterns.

This technique was preferred over the reflection technique that might have been applied to the oxide in place on the tin substrate, because it is believed to be more sensitive and reliable. In some instances, transmission electron diffraction patterns were prepared by means of the selected-area diffraction attachment of the RCA EMU-2D electron microscope.

Results and Discussion

Oxidation at Constant Pressure (10 mm)

Because of the manner in which the tin-foil surfaces were prepared for the oxidation studies, that is, by electropolishing and vacuum-annealing there was a possibility of formation of some oxide prior to the controlled oxidation. In an investigation to determine whether oxide did in fact form, plastic films were stripped from the tin-foil surfaces, after vacuum annealing but before exposure to oxygen, in the same manner as for the oxidized specimens. Examination of these films by electron microscopy and electron diffraction yielded no indication of crystalline oxide. The electron micrographs revealed an essentially clean surface that was smooth except at the tin grain boundaries, where steps or grooves were formed by the vacuum annealing. In an attempt to increase the sensitivity of detection of surface irregularities, or of any areas of solid oxide film, the surface of the annealed tin foil was preshadowed with chromium, prior to replication of the surface with the thin plastic film. This technique failed to reveal any additional structural detail. Thus, it was not possible to obtain any structural evidence of the existence of an oxide film prior to the start of oxidation in the microbalance.

Initial stage of oxidation: "growth centers."— Soon after the introduction of oxygen at a pressure of 10 mm Hg into the microbalance system, oxide nuclei, or more correctly "growth centers" (the actual nuclei are, of course, too small to detect microscopically), appeared on the tin surface, Fig. 3. These growth centers appear to grow to a certain size, about 1μ in diameter, before large platelets begin to grow from them. The density per unit area of these growth centers is in the same range as the density per unit area of etch pits formed on electropolished and vacuum-annealed tin foil, approximately 2×10^8 growth centers or etch pits per square centimeter. This observation suggests that the oxide growth centers may be associated with dislocations in the metal. It should be noted that there is a high probability of oxide nucleation at grain boundaries, as shown in Fig. 4. This may be due to the higher concentration of dislocations at grain boundaries, or simply to the presence of a step or thermal groove at the boundaries.

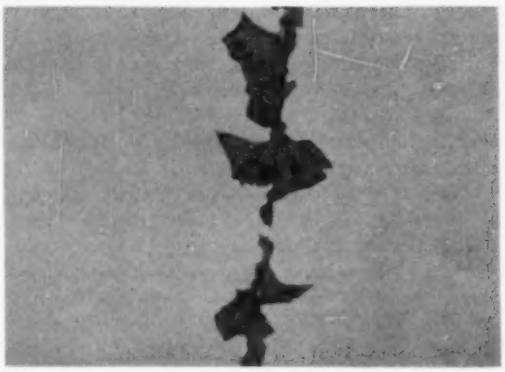

Fig. 4. Electron micrograph of α-SnO crystals growing along a tin grain boundary after exposure to oxygen at 10 mm and 190°C for 20 min. Magnification 15,000X before reduction for publication.

Typical growth centers in various stages of development are shown in Fig. 5. A central "hub" appears first, and from it "spokes" begin to radiate outward in a manner suggestive of spiral growth, Fig. 5A. After these spokes have grown outward to about 0.25 μ, the space between the tips begins to fill in to form a rim about 1.0-1.5 μ in diameter. As the rim fills in, it continues to thicken without much increase in diameter, but the space inside the

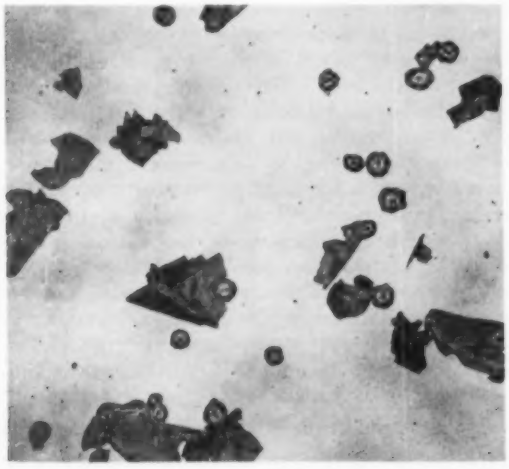

Fig. 3. Electron micrograph of stannous oxide formed at an oxygen pressure of 1 mm Hg and 190°C for 100 min, showing growth centers and platelets forming from them. Magnification 7000X before reduction for publication.

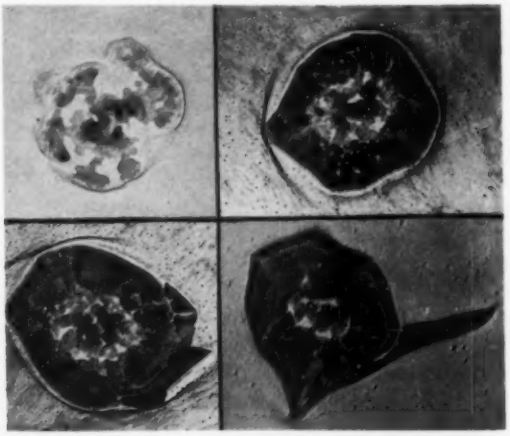

Fig. 5. High-magnification electron micrographs of growth centers in different stages of development, showing details of structure. Magnifications: (A) (top left) 55,000X; (B), (C), (D) 36,000X before reduction for publication.

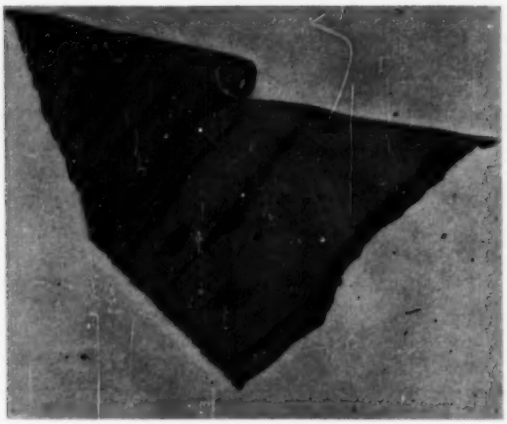

Fig. 6. Electron micrograph of stannous oxide formed at an oxygen pressure of 10 mm and 220°C for 15 min, showing the growth of a large oxide plate from a growth center. Magnification 20,000X before reduction for publication.

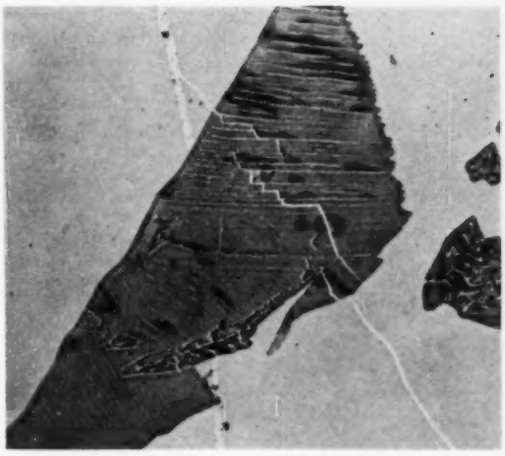

Fig. 7. Electron micrograph of α-SnO crystal formed at an oxygen pressure of 10 mm and 220°C for 15 min, showing laminar growth of crystal, mechanical fracture, and embryonic cavities. Magnification 15,000X before reduction for publication.

rim, between the spokes, seldom fills in completely, Fig. 5B. In most instances, some segment (or segments) next begins to grow out as a spike or finger from the original structure, Fig. 5C. These spikes then start to spread laterally, Fig. 5D, forming large single-crystal platelets of oxide, which eventually surround the original growth center and impinge on platelets developing from neighboring growth centers. It is interesting, and perhaps significant, that these stannous oxide growth centers resemble the blisters on cathode-sputtered copper films reported by Henschke (16), although they are much smaller.

Development of platelets: lateral growth.—The lateral development of a crystalline platelet of oxide from a growth center is shown in Fig. 6. From the morphology of this platelet, it is evident that three relatively straight spines or spikes grew outward from the spiral center at angles of approximately 0°, 108°, and 180°, respectively. Concurrently, parallel, lath-shaped crystallites, suggestive of dendritic growth lamellae, extended from each spine at an oblique angle (60° for the two 180° spines), as indicated by the parallel striations (lamellae boundaries) that terminate at the individual angular facets that make up the serrated, advancing growth front of the platelet. Because the lengths of the growth lamellae decrease uniformly with distance along the growing spine, and in view of the protruding spine tips, it seems clear that the lamellae growth lagged that of the spines, and that the lamellae must have grown from the spines. This is perhaps more clearly shown in the micrograph of Fig. 7 of a similar platelet that was fractured after removal in a plastic film from the tin substrate; the fracture path and the microscopic separations indicate planes of weakness between the lamellae.

Analysis of a selected-area electron-diffraction pattern of the platelet of Fig. 6, demonstrated that the platelet is a single crystal of α-SnO, oriented with its basal (100) plane parallel to the tin surface. It is surmised that the type of platelet growth described is related to the crystallographic orientation of the tin substrate, and that it occurs for a relatively broad range of angular orientation, since it appeared to predominate for the many tin crystals of presumably random orientation in the several polycrystalline tin foils examined.

Each platelet spreading laterally from its growth center eventually encounters one or more other platelets spreading from neighboring growth centers, as is shown in Fig. 8. This mutual impingement interferes with lateral growth and would be expected to bring about a reduction in oxidation rate. Some growth centers are slow to form platelets and become enveloped by rapidly advancing platelets from adjacent growth centers.

The fraction of the area of the tin substrate that was covered by oxide in a given time under standardized conditions (190° or 220°C and 10 mm O_2) was estimated by an area analysis of a number of electron micrographs of each stripped plastic film,

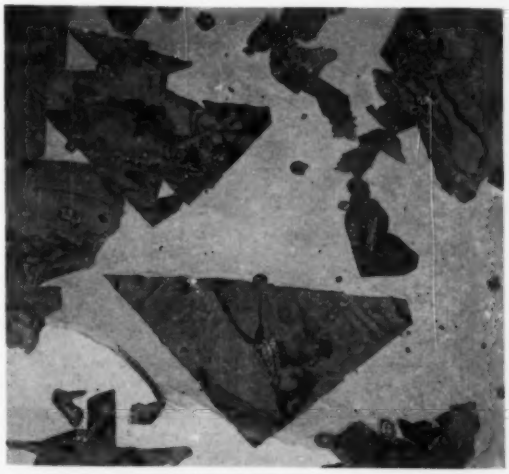

Fig. 8. Electron micrograph of α-SnO platelets formed at an oxygen pressure of 10 mm and 190°C for 95 min, showing impingement of neighboring platelets. Magnification 7,000X before reduction for publication.

Table I. Areal analysis of micrographs for 190°C oxidation

Time, min	Equiv. film thickness, Å	Area ratio oxide/total	Area of sample, cm²	Area covered by oxide, cm²	Change in weight per unit total area, μg/cm²	Calculated oxide thickness corrected for area of oxide, Å	Point No. on curve of Fig. 10
20	14	0.044	11.88	0.52	0.11	329	1
60	33	0.219	12.03	2.63	0.25	149	2
70	44	0.208	12.65	2.63	0.34	213	3
80	47	0.284	13.16	3.74	0.36	166	4
90	50	0.481	12.60	6.06	0.38	103	5
100	61	0.842	11.97	10.08	0.47	73	6
300	120	0.957	12.60	12.06	0.92	125	7
600	156	0.971	12.60	12.23	1.19	161	8
1400	195	0.993	12.04	11.96	1.49	196	9
4000	273	1.000	12.32	12.32	2.09	273	10

Table II. Areal analysis of micrographs for 220°C oxidation

Time, min	Equiv. film thickness, Å	Area ratio oxide/total	Area of sample, cm²	Area covered by oxide, cm²	Change in weight per unit total area, μg/cm²	Calculated oxide thickness corrected for area of oxide, Å
5	15	0.093	11.62	1.081	0.118	166
10	31	0.159	11.48	1.825	0.238	196
20	69	0.691	11.62	8.029	0.530	100
30	81	0.930	11.48	10.676	0.616	87
40	103	0.945	11.76	11.113	0.785	109
75	132	0.970	12.10	11.737	1.008	136
100	138	0.994	12.96	12.882	1.055	139
200	186	0.998	12.42	12.395	1.420	186
300	210	0.998	12.26	12.235	1.604	210

Tables I and II. As is shown in Fig. 9, in which the weight increase resulting from oxidation is plotted as a function of the fraction of area covered, the weight increase is an approximately linear function of the fraction of total area covered by oxide, until the coverage reaches about 80%. At this stage of oxidation, there is almost complete impingement and interference among oxide platelets spreading from adjacent growth centers, and only small interstices remain unoxidized. Beyond 80% coverage, the weight begins to increase sharply with coverage. Comparison of this curve with the corresponding logarithmic plot of the data, Fig. 10, shows that the foot of the logarithmic curve (the region of nonconformance to the direct logarithmic rate law) corresponds to less than 80% coverage of the metal by the oxide film. The fact that the foot of the logarithmic curve also corresponds to the period of increasing rate (as shown in linear plots of the data) was discussed in a previous paper (1). Thus, it is evident that the initial period of increasing rate is a result of nucleation and lateral growth of the crystalline oxide film, as suggested by Evans (17) and Tylecote (18). The practice of forcing the kinetic data to fit a logarithmic relation, particularly in the early stage of oxidation, by adjustment of the constants in the logarithmic rate equation, clearly is not justified in this instance since it masks the significance of the initial rate data.

Region of logarithmic rate of growth: cavities.— As the coverage of the metal by the oxide film ap-

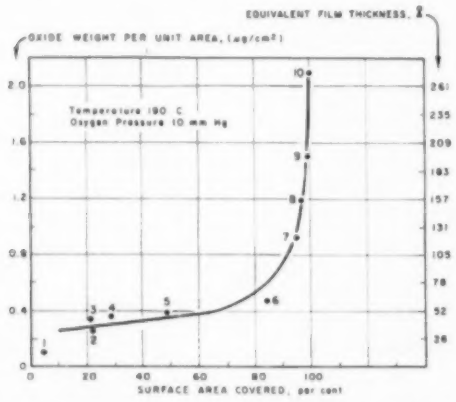
EQUIVALENT FILM THICKNESS, Å
OXIDE WEIGHT PER UNIT AREA, (μg/cm²)
Temperature 190 C
Oxygen Pressure 10 mm Hg
SURFACE AREA COVERED, per cent

Fig. 9. Increase in weight per unit area as a function of area covered by oxide at 190°C.

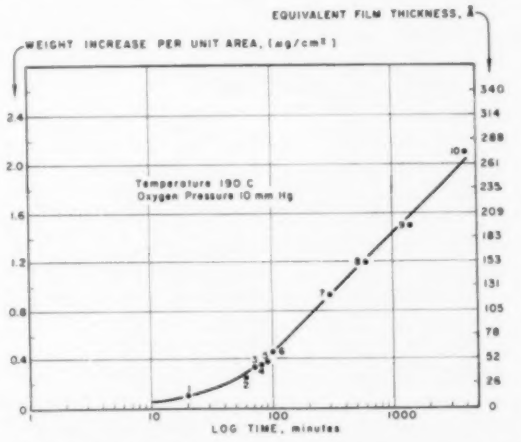
EQUIVALENT FILM THICKNESS, Å
WEIGHT INCREASE PER UNIT AREA, (μg/cm²)
Temperature 190 C
Oxygen Pressure 10 mm Hg
LOG TIME, minutes

Fig. 10. Log-time plot of total weight-change per unit area of oxidized samples used for the areal analysis in Fig. 9.

proaches completion and the data begins to conform to the direct logarithmic rate law, holes or thin places begin to appear along the edges of the growth lamellae within individual oxide platelets, Fig. 11. As the film thickens, these thin places grow and coalesce, as is shown in a series of micrographs of progressively thicker stannous oxide films, Fig. 11 through 14, until after 1000 min (10 mm O_2 and 220°C), about 30% of the area of the film is comprised of these thin places or cavities.

It is certain from the following considerations that these holes or cavities in the oxide films form during the oxidation process and are not a spurious effect of subsequent manipulation of the films in preparation for electron microscopy and diffraction. Thermodynamic calculations indicate that the mercury used in removing the tin substrate by amalgamation should not react with the tin-oxide film. Experimental verification that the α-SnO film is not soluble in, and does not react with, the mercury was obtained when part of an oxide film was examined immediately upon stripping, but the remainder of the film was allowed to remain in contact with mercury for five days before examination. No significant difference in structure could be found between these two sections of film. Inasmuch as the cavities occur in rows or lines that appear to be related to crystallographic planes in the various oxide platelets or grains, it is unlikely that they are the result of straining or buckling of the film. Furthermore, cracks or tears that sometimes occur in the oxide film during handling are considerably different in appearance, Fig. 7.

The thin areas in the oxide platelets develop and grow as the rate of oxidation is decreasing exponentially (direct logarithmic rate law). If holes or breaks that would permit direct contact between the oxygen and the metal were developing in the

Fig. 11. Electron micrograph of stannous oxide formed at an oxygen pressure of 10 mm and 220°C for 160 min, showing almost complete coverage and the beginnings of visible cavities between growth lamellae. Magnification 15,000X before reduction for publication.

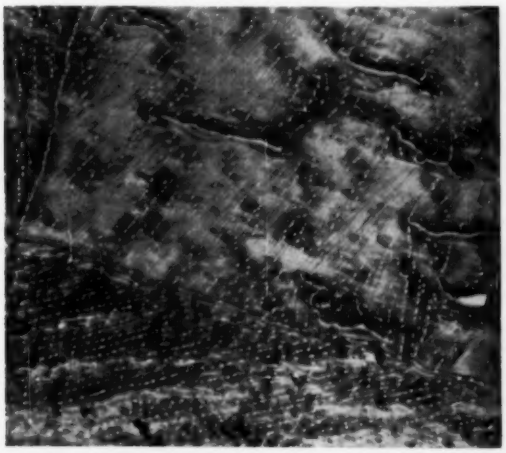

Fig. 12. Electron micrograph of stannous oxide formed at an oxygen pressure of 10 mm and 220°C for 380 min, showing growth of cavities as the film thickens. Magnification 15,000X before reduction for publication.

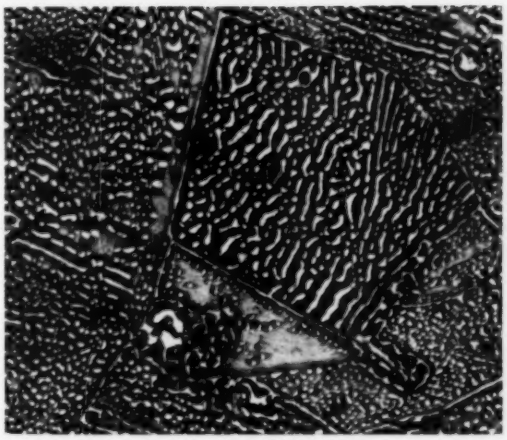

Fig. 13. Electron micrograph of stannous oxide formed at an oxygen pressure of 10 mm and 220°C for 700 min, showing growth of cavities as the film thickens. Magnification 15,000X before reduction for publication.

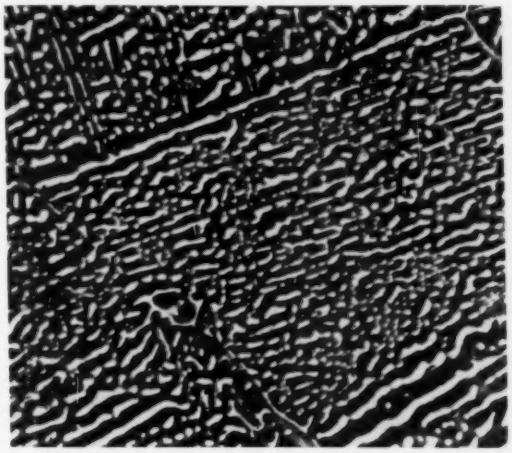

Fig. 14. Electron micrograph of stannous oxide formed at an oxygen pressure of 10 mm and 220°C for 1000 min, showing development of very large cavities involving 30% of the total area of the film. Magnification 15,000X before reduction for publication.

film, the oxidation rate would be expected to increase (19). Just such an increase in oxidation rate, caused by cracking of the film, was reported in a recent paper on the oxidation of niobium (20) and was observed in the last stage of oxidation of tin in the present investigation. Since no increase in rate was observed during the formation of the thin regions of the oxide platelets, it was reasoned that these regions must consist of blisters or cavities in the oxide film that are covered with a thin skin of oxide, which prevents direct access of the oxygen atmosphere to the metal at the base of the cavities.

Evans (17) has derived one version of the direct logarithmic rate law from the assumption that cavities develop at the oxide-metal interface; these act as diffusion barriers and thus alter the normal diffusion kinetics. Replication of the top (oxygen-oxide interface) and bottom (oxide-metal interface) surfaces of the oxide film, Fig. 15 and 16, respectively, makes it possible to examine the topography of each of these surfaces separately in the electron microscope. Through a fortunate accident, one segment of oxide film adhered to the carbon replica but was displaced only slightly from its original position. It was thereby possible to examine both the oxide itself and the corresponding replica of its under-surface, Fig. 16. The dark areas in Fig. 16 are patches of oxide still adhering to the carbon replica. It is apparent that the ridges in the carbon replica correspond to the light areas in the oxide crystal. Thus, the light areas observed in the α-SnO crystals are in fact voids in the oxide film. The smoothness of the replica of the top surface of the oxide film, Fig. 15, demonstrates that these voids do not extend completely through the oxide film, but are covered by a thin skin of oxide at the oxide-oxygen interface. Replicas of the metal surface from which the oxide has been removed have a contour similar to that of the under-surface of the oxide film, but the topographic relief is much less. Thus, the thin places in the oxide film, which increase in size as the film thickens, are actually cavities or voids in the oxide film and contain no solid phase. Figure 17 shows a schematic diagram of the cross section of the oxide film after the cavities have developed.

Fig. 15. Electron micrograph of replica of top surface of an oxide film similar to that shown in Figure 14. Magnification 20,000X before reduction for publication.

Fig. 16. Electron micrograph of chromium-shadowed carbon replica of undersurface of an oxide film similar to that shown in Fig. 14, showing both an oxide platelet and the replica of its undersurface. Magnification 20,000X before reduction for publication.

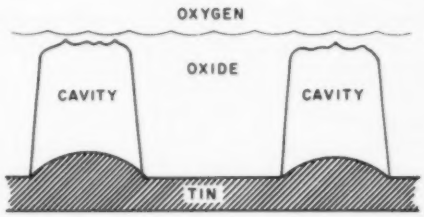

Fig. 17. Schematic diagram of the cross section of the oxide film after the development of large cavities at the oxide-metal interface.

Comparison of shadows of 2640Å-diameter monodisperse latex spheres with the shadows of carbon ridges such as are shown in Fig. 16 indicate that the voids may extend as much as 800Å into the oxide film. However, the average thickness of the oxide film calculated from the uptake of oxygen, as measured by the microbalance, and from the published density of stannous oxide, is only about 300Å. Obviously, the oxide film is much less dense than bulk stannous oxide. In the region of incomplete coverage by the oxide, where cavities were nonexistent or very minute, the agreement between the measured oxide thickness and the calculated thickness was better. For one of the specimens oxidized at 190°C and 10 mm oxygen for 100 min, a thickness value of 114Å was obtained by the shadowing technique, whereas the thickness calculated from the oxygen uptake and corrected for the area covered was 88Å.

Thick-film region: cracking.—A sample of tin foil was oxidized at an oxygen pressure of 10 mm and a temperature of 220°C for 6990 min. The resulting oxide film, Fig. 18, contained fewer voids and appeared to be fragmented and recrystallized. Apparently the oxide skin covering the voids became

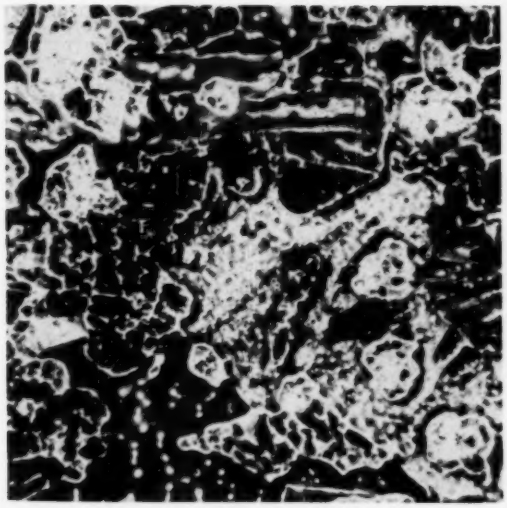

Fig. 18. Electron micrograph of α-SnO film at an oxygen pressure of 10 mm and 220°C for 6990 min, showing fragmentation of the oxide film and a reduction in the number of cavities. Magnification 10,000X before reduction for publication.

so strained that it ruptured, allowing gaseous oxygen to come into contact with the metal exposed at the base of the cavities. This caused an increase in the observed oxidation rate. Oxide then began to grow in the cavities, plugging them. Since the specific volume of stannous oxide is about 20% greater than the specific volume of the metal, the growth of a plug exerts a force on the walls of a cavity. The oxide surrounding the cavity is subjected to an increasing stress and eventually cracks again, admitting oxygen to react directly with the metal substrate. The cycle of alternate opening and healing of cracks repeats itself, causing fragmentation of the oxide film.

Crystalline structure of the oxide.—By means of transmission electron diffraction patterns, the oxide was identified as α-SnO (tetragonal crystal structure), for all conditions of oxidation investigated. A typical diffraction pattern is given in Table III. Even for very short oxidation intervals, in which the weight-gain of the specimen was so slight that it could not be detected with the microbalance, crystalline oxide was observed by electron microscopy and detected by electron diffraction. It has been reported in the literature that the oxide film formed on tin at temperatures below 170°C (12) or 130°C (21) is amorphous because no diffraction patterns were obtained from specimens oxidized at lower temperatures. In this study, an attempt is being made to find some low-temperature limit for the formation of crystalline alpha-stannous oxide. Up to the present time, it has been possible to identify crystalline α-SnO, formed by the oxidation of tin, down to temperatures as low as 75°C. The electron diffraction pattern obtained from the oxide formed at 75°C is given in Table IV. Very long times of exposure to oxygen are required to form enough crystalline oxide at such low temperatures to permit detection. At 75°C, an interval of about 49,000 min (811 hr) was required to form sufficient oxide to be detectable by transmission electron diffraction. Apparently, the minimum temperatures for the formation of crystalline tin oxide reported in the literature are the result of too short an exposure to oxygen, rather than the formation of amorphous oxide.

Table III. Electron diffraction patterns obtained from oxide films grown on pure tin at 220°C and an oxygen pressure of 10 mm

Observed patterns			ASTM x-ray powder data file			
No. 1 d, Å	No. 2 d, Å	I/I_1	α-SnO d, Å	I/I_1	SnO_2 d, Å	I/I_1
4.9	4.85	10	4.85	10	—	—
4.17	4.13	10	—	—	—	—
3.78	3.74	10	—	—	—	—
3.00	2.972	100	2.989	100	—	—
2.70	2.672	100	2.688	37	2.644	81
2.437	2.413	10	2.418	14	—	—
2.360	2.338	20	—	—	2.369	24
2.050	2.031	10	2.039	<1	—	—
1.912	1.893	80	1.901	13	—	—
1.807	1.790	50	1.797	27	—	—
1.784	1.767	50	—	—	1.765	63
1.706	1.690	10	—	—	1.675	63
1.613	1.597	100	1.604	25	1.593	8
1.499	1.485	30	1.494	11	1.498	13
1.393	1.380	10*	1.382	3	—	—
1.354	1.340	40	1.344	5	1.322	7
1.305	1.292	30	—	—	—	—
1.232	1.220	40	1.225	4	1.215	11
1.217	1.205	10	1.209	3	—	—
1.206	1.195	40	1.202	4	1.184	3
1.179	1.168	50*	1.170	8	—	—
1.16	1.150	10	1.152	1	1.155	8
1.126	1.115	10	—	—	1.117	3
1.115	1.104	10	1.103	4	—	—
1.083	1.072	30	1.077	6	1.081	8
1.058	1.047	10	—	—	1.059	3
1.037	1.027	90	1.030	4	—	—
1.024	1.014	10	1.020	3	—	—
1.005	0.996	10	0.997	1	—	—
0.992	0.983	10	0.985	1	—	—
0.969	0.960	10	0.967	<1	—	—
0.946	0.937	10	0.937	3	—	—
0.912	0.902	70	0.906	4	0.908	8
0.886	0.878	20	0.882	5	0.881	6

* = Two lines.

Table IV. Electron diffraction pattern obtained from oxide film formed on pure tin at 75°C at an oxygen pressure of 10 mm

Observed pattern, d, Å	ASTM x-ray powder data	
	d, Å	I/I_1
2.70	2.688	37
1.90	1.901	13
1.34	1.344	5
1.20	1.202	4
0.95	0.9507	3
0.90	0.9056	4
0.85	0.8503	4

Effect of Oxygen Pressure at Constant Temperature (190°C)

It was mentioned in the previous discussion (1) that the dissociation of molecular oxygen is believed to be rate controlling at pressures below about 0.1 mm Hg. The oxide formed at these low oxygen

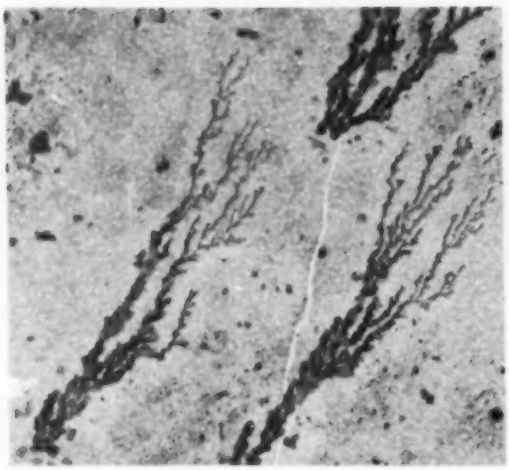

Fig. 19. Electron micrograph of dendritic oxide formed at an oxygen pressure of 10^{-4} mm and 190°C for 1000 min. Magnification 15,000X before reduction for publication.

pressures is shown by electron microscopy to consist mainly of fine dendrites or filaments, which appear to have a preferred orientation with respect to some crystallographic direction in the tin substrate, that is, the oxide filaments tend to grow principally along some one direction in the surface of a given tin grain, which in general is different from that for the adjacent, differently oriented tin grains. An example of this type of growth is shown in Fig. 19. This oxide formed on tin that was exposed to an oxygen pressure of 10^{-4} mm for 1000 min. The microbalance was not sensitive enough to detect the weight change corresponding to the formation of these dendrites. To explain this type of oxide growth, it is reasonable to assume that crystalline oxide grows from a film of oxygen, adsorbed or chemisorbed on the tin surface. The oxide presumably nucleates at certain sites, such as dislocations, and then grows laterally along some preferred crystallographic direction of the tin crystal. The areas adjacent to the oxide filaments become depleted in oxygen, as the oxygen in the sorbed film is incorporated into the crystal lattice of the oxide filaments, so that further growth of oxide must be outward toward the areas that are richer in oxygen. At the higher oxygen pressures, oxygen in the adsorbed layer is replenished as fast as it is consumed by crystal growth, and thus the dendrites fill in to form platelets.

For the study of the effect of oxygen pressure on the microstructure of the tin oxide, a series of samples was oxidized to the same equivalent thickness (the theoretical thickness of a uniform film of oxide of the given weight) at different pressures and at 190°C. Electron micrographs were made of each oxide film showing the detailed morphology of selected oxide clusters.

In all of these micrographs, certain structures appear that evidently are the growth centers for the oxide. The morphology of these growth centers appears to change with oxygen pressure. However, such centers can be recognized at all pressures. At an oxygen pressure of 10^{-2} mm and above, the shape

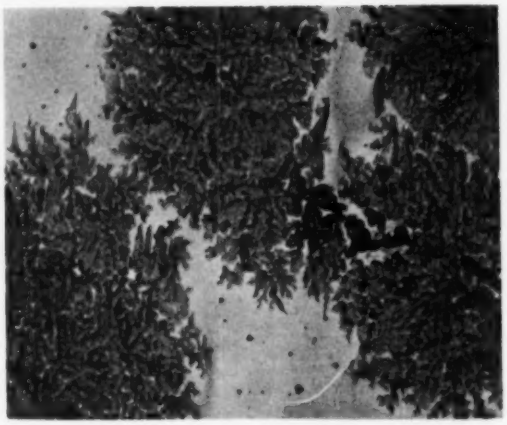

Fig. 20. Electron micrograph of dendritic oxide clusters formed at an oxygen pressure of 10^{-3} mm and 190°C for 1350 min. Magnification 15,000X before reduction for publication.

of these growth centers is suggestive of a spiral growth mechanism.

Figure 20 is an electron micrograph of oxide grown at an oxygen pressure of 10^{-3} mm to an equivalent film thickness of 43Å. The oxide consists mainly of clusters of oriented dendritic crystals. A few dense platelets of oxide, presumably filled-out dendrites, are growing at an angle to the basic tree-like structures. At a pressure of 10^{-2} mm, the fine dendritic oxide structure (46Å) predominates, but more of the larger, dense crystals appear. The clusters of dendritic oxide particles appear to be less well oriented than at 10^{-3} mm and have assumed a circular or spherulitic shape, Fig. 21, suggestive of a spiral growth mechanism. Figure 22 is an electron micrograph of oxide grown in oxygen at 0.1 mm to an equivalent thickness of 44Å. This oxide consists of acicular platelets, formed by growth of lamellae from spikes in a manner similar to that observed in oxide formed at 10 mm pressure. The influence of the orientation of the tin substrate on the growth direction of the oxide is evident.

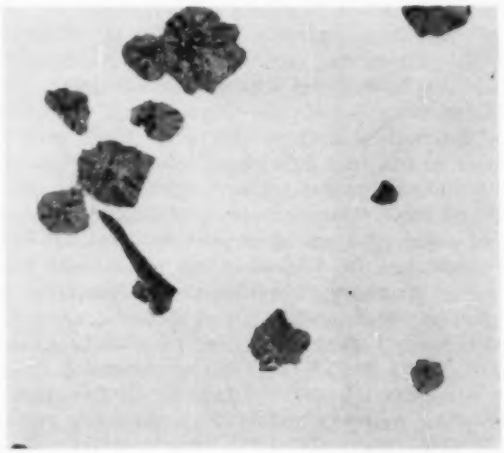

Fig. 21. Electron micrograph of oxide growth centers formed at an oxygen pressure of 10^{-2} mm and 190°C for 190 min, showing spherulitic shape. Magnification 15,000X before reduction for publication.

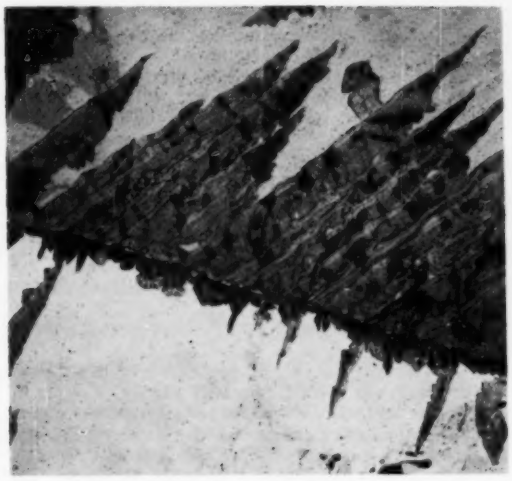

Fig. 22. Electron micrograph of acicular platelets formed at an oxygen pressure of 0.1 mm and 190°C for 330 min. Magnification 7,000X before reduction for publication.

Figure 23 is an electron micrograph of an oxide film grown to an equivalent thickness of 41Å at an oxygen pressure of 1 mm. A number of rosette-shaped growth centers are observed, and the preferred orientation of the oxide platelets is less evident than that for oxidation at a pressure of 0.1 mm. The fine, dendritic structures characteristic of oxidation at the lower oxygen pressures are no longer present. As a result of oxidation at a pressure of 10 mm or 100 mm, large platelets form from wheel-like growth centers; oxide grown under the latter pressure, to an equivalent film thickness of 47Å, is shown in Fig. 24. Regardless of the oxygen pressure, the density of growth centers appears to be about $2 \times 10^6/cm^2$.

Summary

Electron microscopic and electron diffraction techniques have been used in conjunction with the study of the kinetics of oxidation of pure tin to investigate the morphology, mode of growth, and crystalline identity of oxide films. Extraction replication techniques were used that made possible the removal and direct examination of intact oxide films. In addition, methods were devised for the separate replication of the top and bottom surfaces of the oxide film. Also, the relatively unaltered surface of the metal was examined after removal of the oxide film. Use of these latter techniques made it possible to show not only differences in contour between the top and bottom surfaces of the oxide, but also topographic differences between the bottom surface of the oxide and the surface of the metal after oxidation.

When pure oxygen comes into contact with the tin at pressures of at least 1 mm Hg, "wheel-shaped" or "rosette-like" growth centers, 1.0-1.5 μ in diameter, develop at certain sites on the surface of the metal. As the oxidation proceeds, certain rim segments of some of these growth centers begin to develop spike-like projections or spines growing parallel to the metal surface. These spines develop into the large crystalline platelets of oxide that spread out and eventually impinge and cover the entire surface of the metal. Comparison of an areal analysis of the micrographs with plots of the kinetic data shows that the "foot" of the logarithmic curves (that is, the region of nonconformance to the logarithmic rate law) corresponds to the region of development of the growth centers and the lateral spreading of the oxide platelets before formation of a continuous crystalline oxide film.

As the coverage of the metal by the oxide film approaches completion and the kinetic data begin to conform to the direct logarithmic rate law, cavities begin to develop within the individual oxide platelets. These cavities grow and coalesce as the oxidation proceeds until a large fraction of the oxide film consists of voids. Replicas of the top and bottom surfaces of the oxide show that the cavities are based at the oxide-metal interface and are covered by a thin skin of oxide at the gas-oxide interface. Thus, the growth of these cavities reduces the area of oxide in contact with the metal. This reduction in area amounts to as much as one-third of the total area after oxidation for 1000 min at an oxygen pressure of 10 mm and a temperature of 220°C.

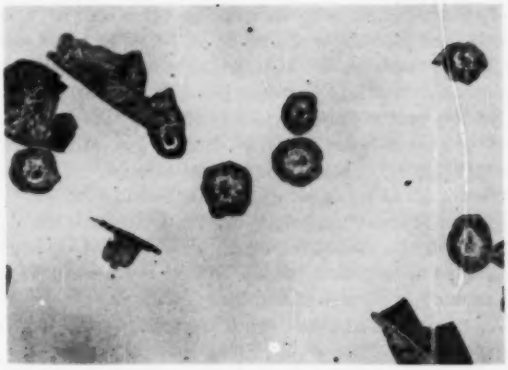

Fig. 23. Electron micrograph of stannous oxide formed at an oxygen pressure of 1 mm and 190°C for 180 min, showing growth centers. Magnification 15,000X before reduction for publication.

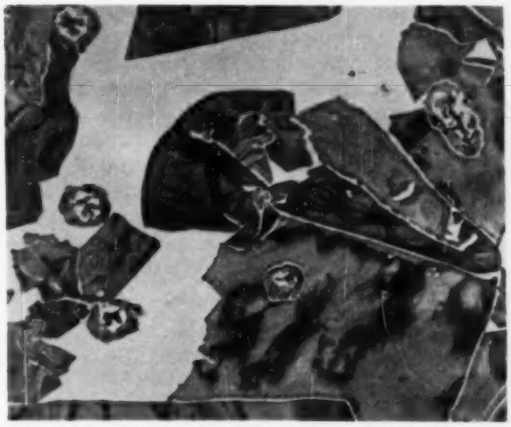

Fig. 24. Electron micrograph of stannous oxide formed at an oxygen pressure of 100 mm and 190°C for 60 min, showing growth centers and platelets. Magnification 15,000X before reduction for publication.

The oxidation experiments in this study were conducted at temperatures of 75°-220°C and under oxygen pressures of 10^{-4} mm Hg to 500 mm Hg. Electron diffraction patterns permitted positive identification of the oxide as α-SnO for all temperatures and pressures of oxidation studied. At the lower temperatures, extremely long oxygen exposures were required to develop sufficient oxide for identification. There was, however, no indication of any change in the structure of the oxide (that is, crystalline to amorphous) at the lowest temperatures, as previously reported in the literature.

At pressures of less than 0.1 mm, a change in the morphology of the oxide films was found, although the crystalline structure remained the same (α-SnO). The oxide formed at these low pressures consists mainly of fine, dendritic crystals or filaments that appear to have a preferred orientation with respect to some crystallographic direction of the tin grains of the substrate. The microstructure of the oxide growth centers changes at low pressures. Instead of the clearly defined wheel-like structures observed at oxygen pressures of 1 mm and above, the growth centers assume the shape of spherulites.

The use of the morphological information obtained by electron microscopy, in conjunction with the kinetic data on the oxidation of tin obtained with a vacuum microbalance, has made possible the development of a comprehensive and realistic mechanism of oxidation of pure tin. The theoretical interpretation of this mechanism is the subject of a following paper.

Manuscript received May 11, 1960. This paper was prepared for delivery before the Houston Meeting, Oct. 9-13, 1960.

Any discussion of this paper will appear in a Discussion Section to be published in the December 1961 JOURNAL.

REFERENCES

1. W. E. Boggs, R. H. Kachik, and G. E. Pellissier, *This Journal*, **108**, 6 (1961).
2. J. Bardolle and J. Bénard, *Compt. rend.*, **232**, 2217 (1951); *Rev. Metall.*, **49**, 613 (1952); *Proc. Int. Symp. Reactivity of Solids*, Göthenburg, 263 (1952).
3. W. W. Harris, F. L. Ball, and A. T. Gwathmey, *Acta Met.*, **5**, 574 (1957).
4. R. T. Phelps, E. A. Gulbransen, and J. W. Hickman, *Ind. & Eng. Chem.*, **18**, 391 (1946).
5. E. A. Gulbransen and R. Rulsa, *This Journal*, **99**, 360 (1952).
6. E. A. Gulbransen and W. R. McMillan, *ibid.*, **99**, 393 (1952).
7. E. A. Gulbransen and K. F. Andrew, *ibid.*, **106**, 511 (1959).
8. E. A. Gulbransen, W. R. McMillan, and K. F. Andrew, *Trans. AIME*, **200**, 1027 (1954).
9. Per Kofstad, Investigation of the Mechanism of Oxidation of Titanium and Titanium Alloys at High Temperatures, A.R.D.C. report, Central Institute for Industrial Research, Blindern, Oslo, Norway, April 1957.
10. T. Hurlen, H. Kjollesdal, J. Marlseli, and N. Norman, U.S.A.F. Final Technical Report A.F. 61 (514)-892, April (1958).
11. J. J. Trillat, L. Tertian, and S. C. Britton, *Métaux Corr. Ind.*, **32**, 475 (1957).
12. S. C. Britton and K. Bright, *Metallurgia*, **56**, 163 (1957).
13. M. S. Jaffe, Proc. Electron Microscope Soc. of America meeting at Toronto, Sept. 1948.
14. R. C. Backus and R. C. Williams, *J. Appl. Phys.*, **20**, 224 (1949).
15. E. B. Bradford and J. W. Vandershoff, *ibid.*, **26**, 864 (1955).
16. E. B. Henschke, *ibid.*, **29**, 1495 (1958).
17. U. R. Evans, *Rev. Pure Appl. Chem.*, **5**, 1 (1955).
18. R. F. Tylecote, *J. Inst. Met*, **81**, 681 (1953).
19. U. R. Evans, Pittsburgh International Conference on Surface Reactions, p. 73, 1948. [N. B. Pilling and R. E. Bedworth, *J. Inst. Met.*, **29**, 529 (1923)].
20. J. V. Cathcart, J. J. Campbell, and G. P. Smith, *This Journal*, **105**, 442 (1958).
21. R. K. Hart, *Proc. Roy. Soc.*, **65B**, 955 (1952).

The Oxidation and Corrosion of Zirconium and its Alloys

V. Mechanism of Oxide Film Growth and Breakdown on Zirconium and Zircaloy-2

B. Cox

Chemistry Division, Atomic Energy Research Establishment, Harwell, Berkshire, England

ABSTRACT

Theories of the mechanism of film growth and breakdown on zirconium and zircaloy-2 are discussed in the light of recent evidence obtained at A.E.R.E. and a further explanation of the observed phenomena is offered. Additional experiments which are necessary to obtain confirmatory information are considered.

The corrosion kinetics of zirconium and zircaloy-2, an alloy of superior corrosion resistance developed in the U.S.A., at temperatures of 250°-450°C in water or steam are fairly well established and take the form shown in Fig. 1 (1). An initial period of corrosion, in which the rate law ($\log w = n \log t + k$) is of higher order (exponent $n \cong 0.3$) than parabolic (exponent $n \cong 0.5$), is superseded by a period of linear oxidation. This linear oxidation continues indefinitely, and the point at which the change takes place has been described as the breakaway or transition point (1). Although several explanations of the mechanism of corrosion and the effect of alloying elements and impurities have been proposed, the basic features of the corrosion of zirconium alloys remain unexplained. Thus, the initial rate of film growth is neither a true parabolic nor a true cubic rate law, and, since the parabolic rate law for thick

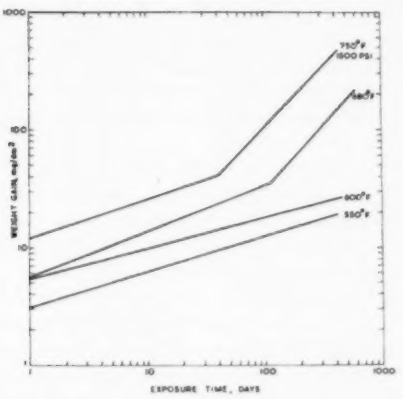

Fig. 1. Weight gain-time curves for the corrosion of zircaloy-2 in high-temperature and steam (from WAPD-TM-97), 750°, 680°, and 550°F specimens annealed below 800°C, 600°F specimens as hot rolled.

films is the only one with a sound theoretical basis, the film growth cannot be a simple diffusion controlled process. Nevertheless, this assumption is generally made, and a considerable proportion of the experimental data, particularly for gaseous oxidation, has been published in a form which presupposes that the rate law ought to be parabolic. Hence the validity of much of the data on activation energies and diffusion coefficients so deduced is doubtful.

Similarly, the nature of the breakaway process, which involves the transformation of the oxide from a protective to a nonprotective state, remains to be elucidated, and the explanations offered fall short in so far as the failure of the oxide is considered either purely in terms of a uniform coating, excluding any localized effects, or as being entirely the result of local factors, ignoring the effect of the intervening uniform oxide film. Recent evidence, which we have obtained (2, 3), suggests that, in the initial period at least, two mechanisms of film growth are operating simultaneously and that in considering the breakaway process each alloy must be considered individually.

Previous experimental work on the oxidation of zirconium in oxygen (4-10) has resulted in some disagreement as to whether a parabolic rate law or a cubic rate law best fits the data. Taking into account the duration of the various experiments, it seems likely that there is a steady transition from an exponent close to 0.5, at short exposure times, to an exponent of about 0.3, after long exposures. Data on the oxidation of zirconium in air (11, 13) show the same effect; at very short oxidation times, however, there is some evidence for a logarithmic oxidation rate followed by a parabolic or cubic rate law (12).

The occurrence of a transition in the oxidation rate (Fig. 1) is a feature of the oxidation of zirconium and its alloys in water and steam, which is not observed during the gaseous oxidation of zirconium. A similar transition in the gaseous oxidation curves of zirconium alloys is observed (11, 14-16). The linear posttransition rate law is usually represented as a line with slope unity on the log/log plot passing through the transition point. Experimental variations from a slope of unity reported in the open literature are generally small (1, 15-21).

While the line through the breakaway point with slope unity does represent a linear rate law, this is only one possible linear rate and is in fact the rate obtained by extrapolating the line joining the origin and the transition point on a normal plot (Fig. 2). The effect of varying the posttransition linear corrosion rate on the resulting log/log plot is shown in Fig. 3. The posttransition weight gain data published so far have been for limited periods, due to the subsequent spalling of the oxide. Under these conditions, the resulting curves would give slopes differing significantly from unity on the log/log plot if the data did not fit the linear rate which passes through the origin and the transition point. The curvature of the posttransition plots other than this one would not be obvious in circumstances

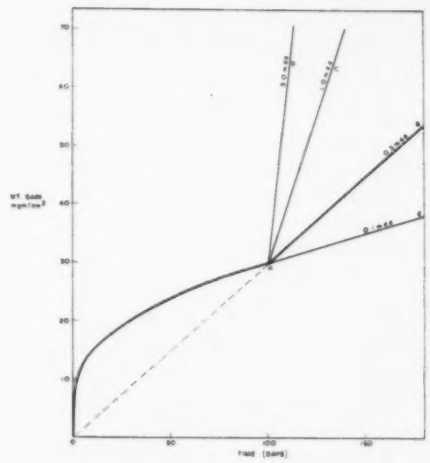

Fig. 2. Postbreakaway corrosion rates illustrating their relation to the prebreakaway rate. Curves represent corrosion of hypothetical Zr alloy specimens. Weight gains found in practice follow heavy line OAB. AB can be obtained by joining the breakaway point, A, to the origin and extending the line. Lines AC, AD, and AE represent other possible linear postbreakaway rates not observed in practice.

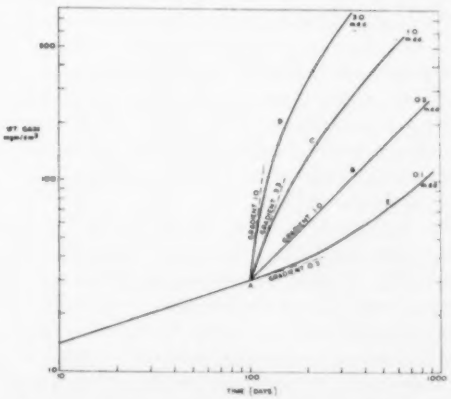

Fig. 3. Effect of varying linear corrosion rate on the log weight gain/log time plot for postbreakaway corrosion. Log/log plot of corrosion curves shown in Fig. 2.

where the duration of observation after transition was short. Hence, if a straight line of slope unity is obtained on a log/log plot of the posttransition weight gain data, this must represent the linear rate which passes through the origin and the transition point. Other linear rates would result in this slope of unity only after periods of time long compared with the time to transition. In these circumstances the curvature of the line immediately after transition should be obvious.

Since experimental data (obtained over relatively short periods) appear to give a close approximation to a slope of unity on the log/log plot, the posttransition corrosion rate would not appear to be a property of a particular billet or alloy. It appears that the posttransition corrosion rate of a particular specimen is determined by the time taken for the transition in kinetics to occur and the weight gain at which it occurs.

During the initial period of oxidation, the growth of the protective film is reported to occur by oxygen ion diffusion via anion vacancies (22). Only the parabolic rate law of Wagner can be derived satisfactorily on the basis of a single diffusion mechanism (24). In practice this law is not obeyed, and a rate law closer to cubic than parabolic is found for long oxidation times. The breakaway weight gain at 300-350°C is about 30 mg/dm^2 and, since little solution of oxygen in the metal takes place at these temperatures, these oxide films fall in the range of thickness to which the Mott thin film law is applicable. Cabrera and Mott (25) estimated that this parabolic rate law applies to oxide films up to limiting thickness of 2×10^{-4} cm (32.5 mg/dm^2 for zirconium alloys); therefore prior to the transition point, the growth of the oxide film may be controlled by the electric field set up, rather than by a simple diffusion process. The Mott parabolic law for thin films, however, ignores the effect of space charge in the oxide, and it seems more likely that Uhlig's extension of this idea (26), which takes into account the effect of changing charge and results in a logarithmic rate law, would apply to zirconium oxidation.

At high temperatures, where breakaway weight gains up to 100 mg/dm^2 are observed, the diffusion controlled parabolic rate law is more likely to apply. However, it should be remembered that a significant part of this weight gain is probably oxygen dissolved in the metal, and the net film thickness may therefore be little greater than at lower temperatures. This dissolution of oxygen in the metal may affect radically the mechanism of film growth and breakdown at these temperatures.

The nature of the breakaway process suggests that, at a critical film thickness, cracking of the film occurs due to stresses set up in it during growth. These stresses may result from the high Pilling-Bedworth ratio of 1.56 (1). It has also been suggested that a phase transformation from tetragonal (or cubic) to monoclinic, with an accompanying volume change, might result in cracking of the oxide (23), nucleation of this transformation being the effect of inclusions in the metal. These inclusions have been equated with hydride precipitates in some instances, and precipitation, at the metal-oxide interface, of hydride originating from hydrogen released in the corrosion process has been suggested as a possible mechanism for the breakdown of the oxide film (1).

To date, however, no satisfactory comprehensive explanation of film growth and failure in zirconium alloys has been suggested and, as Thomas (1) points out, the proposed mechanisms have tended to consider only one aspect of the film growth, *i.e.*, either solely diffusion through a uniform film, or solely the effect of inclusions. A full explanation of the mechanism of film growth and failure should take into account both the diffusion aspect of the process and the effect of precipitated phases in the metal and inhomogeneities in the oxide, *i.e.*, grain boundaries, dislocations, etc.

Experimental

Oxidation of zirconium and zircaloy-2 specimens has been at 300°C either in steam at 1 atm pressure or in aqueous solution in small titanium autoclaves of the same design as those used for irradiation experiments (39). The solutions used were 0.04M Na_2SO_4/0.02M H_2SO_4 and an overpressure of 200 psi. Oxygen was added to the cold autoclave.

Specimens were disks ½ in. in diameter x 0.040 in. thick with a 9/64 in. diameter center hole for supporting the specimen. They were prepared by abrading to 4/0 emery, followed by an attack polish on an alumina lap moistened with dilute HF/HNO_3 solution. In some instances specimens subsequently were etched cathodically with argon ions at low pressure. Electron microscope replicas were prepared by a two-stage Formvar-carbon method and were viewed on a Philips EM.100 electron microscope.

Results

Previous observations of the growth of oxide films on zirconium and zircaloy-2 by weight gain measurements and by observation of the interference colors exhibited by thin films (3) have shown that film thicknesses estimated by these two methods agree well in the initial stages of film growth. However, the interference color film appeared to reach a limiting thickness and did not continue to follow the sequence of colors established from anodization (3). A logarithmic plot of the interference color film growth gave a reasonable straight line, and the weight gain plot followed this up to a thickness of about 2000-2500Å (3.2-4.1 mg/dm^2). Further observations showed that the region in which the weight gain and interference color estimates of film thickness diverge corresponds to the region in which darkening of the oxide film and disappearance of the interference colors takes place. This darkening was observed to take place uniformly on zircaloy-2, within the resolution of the optical microscope, whereas the darkening of the film on arc-melted zirconium was found to be nonuniform.

Darkening of the oxide film on arc-melted zirconium was found to occur first at grain boundaries; this darkening was shown to consist of more rapid oxidation at these points, producing ridges of thicker

oxide along grain boundaries (3). As the degree of thickening varied widely from site to site it was ascribed to diffusion along selected grain boundaries in the oxide, and not to the effect of accumulated impurity atoms, which would be expected to be present equally at all grain boundaries. Thus, the growth of the dark film on arc-melted zirconium appears to result from the transport of reactive species along easy diffusion paths in the film provided by the grain boundaries. In the earlier study of arc-melted zirconium a close correlation was found between the onset of inhomogeneous dark film growth and the cracking and failure of the oxide film. Zircaloy-2 passed through this region satisfactorily and formed a uniform dark film which did not fail during the period of study (3). Observation of zircaloy-2 specimens, corroded for long periods in aqueous solution (Fig. 8), has shown that failure of the oxide occurred not by cracking of the film nucleated at a few points but by a progressive increase of nuclei, which do not spread individually, but eventually coalesce (Fig. 4). The nuclei themselves have features similar to those found previously (2) when examined under the electron microscope (Fig. 5), apart from the absence of cracking outward from them. The increase in the number of nuclei until coalescence takes place is similar to the situation reported by Cathcart during the failure of oxide films on niobium (36), although the scale of the whole phenomenon in the case of zircaloy-2 is very much larger than for niobium.

Careful polishing of a zircaloy-2 specimen in the early stages of breakaway to the point where the oxide film (and the hemispherical pits present under the nuclei) had just been removed failed to reveal any precipitated phase in the metal-oxide interface, although evidence for the uniform distribution of a small amount of hydride throughout the specimen

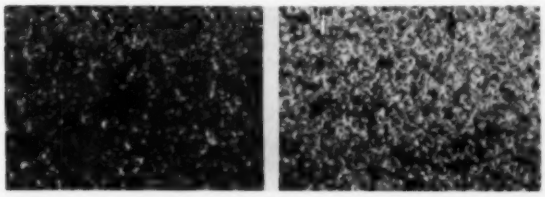

Fig. 4. Increasing numbers of white oxide nuclei forming during breakdown of the oxide film of zircaloy-2. Magnification 50X before reduction for publication.

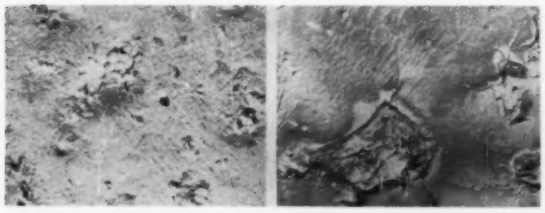

Fig. 5. Breakaway oxide nuclei in zircaloy-2 (billet 142): (a))left) early stage of breakdown of nuclei; shadowing effects suggest that cracking is taking place at tops of "pimples;" (b) (right) later stage of failure with isolated oxide nodules clearly visible. Magnification 4000 times before reduction for publication.

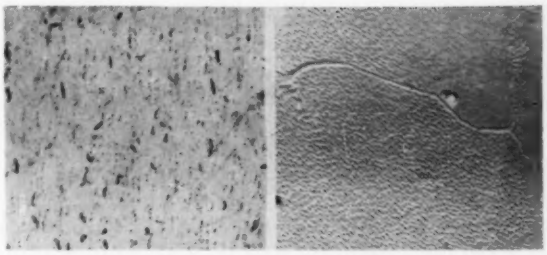

Fig. 6. Micrographs of zircaloy-2 after breakaway: (a) hydride revealed as etch pits by attack polishing; magnification 250 times before reduction for publication; (b) (right) electron micrograph of metal surface immediately below the oxide film after cathodic vacuum etching. (Z303). Magnification 10,000X before reduction for publication.

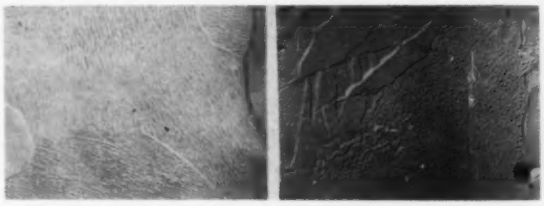

Fig. 7. Electron micrographs of cathodically etched specimens from two zircaloy-2 billets showing that intermetallic particles are not revealed by this method of preparation; (a) (left) billet Z8006; magnification 4000X before reduction for publication; (b) (right) billet Z303; magnification 8000X before reduction for publication.

was obtained (Fig. 6). Subsequent cathodic etching of the same specimen did not reveal any evidence of the presence of a precipitate within the grains (Fig. 6). It is interesting to note that the intermetallic particles reported to be present (1) do not show up as a result of the cathodic etching either of the postbreakaway specimen or of uncorroded specimens of zircaloy-2 (Fig. 7). The etch patterns produced by cathodic etching are invariably uniform over the whole grain and are similar to etch figures found by other investigators (37).

Discussion

In the light of the evidence obtained in this study and the previous one on arc-melted zirconium (3), the following mechanism for oxide film growth and breakdown is proposed. The growth of the thin interference color film has been found experimentally to obey a logarithmic growth law (3), and it is probable, therefore, that this is an example of the applicability of Uhlig's thin film growth law to a case of metal oxidation. The initial oxidation of hafnium (34) and titanium (27-30) has been found also to obey a logarithmic law at temperatures below 350°C.

It is suggested that, in the case of zircaloy-2, the uniform thickening of the oxide film, during the period where the interference colors are disappearing, results from the presence of sufficient easy diffusion paths within the film to prevent preferential oxidation along grain boundaries. The provision of these paths is thought to be due to the presence of a fine intermetallic precipitate (containing iron, chromium, and nickel), which is distributed uniformly within the grains. The oxidation of these particles

results in inhomogeneous regions in the overlying oxide, and, since the proportion of the surface area which is supplied with reactant via these paths is probably very small, the actual diffusion rates along these routes must be several orders of magnitude greater than the diffusion rate through the bulk oxide. This would be in agreement with estimates of the relative rates of grain boundary and bulk diffusion in metals (38). The fact that a uniform film, with only small over-all variations in thickness, results from this process is due to lateral diffusion of reactant away from the relatively narrow diffusion path, which provides the easy route. The degree of uniformity which results will depend on the size and distribution of the intermetallic particles. Evidence for the occurrence of (Fe, Ni)O in thin oxide films on zircaloy-2 was obtained by electron diffraction (32).

Thus the prebreakaway film growth on zircaloy-2 appears to be the result of transport of reactive species by at least two processes occurring simultaneously. A third process, the dissolution of oxygen in the underlying metal, can be shown to be insignificant at 300°C by extrapolation of Pemsler's data (33).

The transport of reactive species along easy diffusion paths provided by grain boundaries and regions of inhomogeneity in the oxide film is a special case of the Evans law describing the effect of blisters and pores on the oxidation rate (31). Hence, the growth of the dark oxide film on zircaloy-2 would be expected to follow a logarithmic law, and the over-all rate of film growth, as shown by weight gain measurements, might be described therefore by the sum of two logarithmic rate laws. Figure 8 compares the experimental film growth for two batches of zircaloy-2 (35) and one of crystal-bar zirconium with the theoretical film growth, calculated from the sum of two such logarithmic rate laws. The derivation of these is shown in Fig. 9 where the interference film growth law is that obtained experimentally (3). It is assumed that the average rate of growth of the uniform interference color film does not vary from batch to batch. The second logarithmic law or "leakage rate" (Fig. 9), representing the material transported via easy diffusion paths, is obtained for each billet by plotting

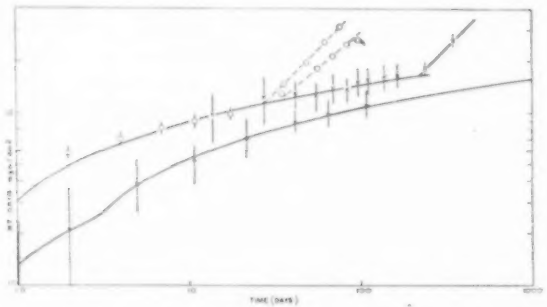

Fig. 8. Correlation between experimental data and corrosion curves calculated as the sum of two logarithmic laws. Zircaloy-2: X billet 142, + billet Z303; zirconium: O crystal bar.

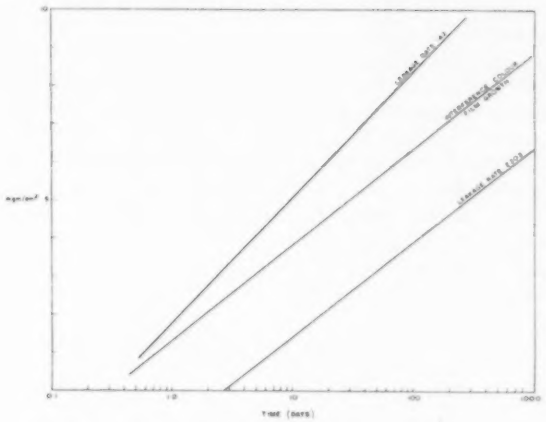

Fig. 9. Logarithmic rate laws used for estimating weight gain-time curves in Fig. 8. The interference color film growth rate is that found for arc-melted Zr (3); observations of Z303 specimens corroded in aqueous solution indicated substantially the same initial growth rate. Data for zircaloy-2 quoted in (3) appear to show an anomalously high initial formation rate.

the difference between the first logarithmic curve and the experimental data at two arbitrary points on a log/linear scale and inserting a straight line through them.

In order to fit the theoretical curve to the experimental data for crystal bar zirconium, it is necessary to assume a more rapid growth law for the interference color oxide than that obtained experimentally for arc-melted zirconium and zircaloy-2. Variations in film growth rate with grain orientation are prominent in zirconium alloys, and, since the crystal-bar zirconium employed was almost single crystal in form (as far as individual specimens were concerned), the more rapid initial oxidation rate probably results from the large grain size and the ensuing sampling error.

If the initial oxide is growing at a rate determined by Uhlig's logarithmic growth law, then the failure to observe higher order interference colors at grain boundaries prior to the formation of the dark film (3) is explicable. In the initial stages the transport of ions and electrons through the film (by such a mechanism) is controlled by the electric field set up, rather than by the diffusion coefficients of the oxide. On attaining a sufficient film thickness, diffusion becomes a contender for the transport of reactive species. At this point, however, diffusion via easy paths is likely to manifest itself before bulk diffusion can become significant. Thus the second logarithmic rate, which is a measure of this diffusion via easy paths, need not pass through the origin, since transport in the early stages is governed by the electric field in the oxide. The magnitude of this second logarithmic rate is expected to vary more widely from billet to billet than the logarithmic rate, which describes the growth of the interference color oxide, as it will be a function of the impurity content of the material and the distribution of intermetallic particles.

The mechanism by which the subsequent failure of the film occurs remains to be explained. The in-

ability to detect precipitated phases in the metal-oxide interface after breakaway has occurred may be evidence against the suggestion that precipitation of hydride, resulting from the corrosion reaction at the interface causes nucleation of breakaway; alternatively it may indicate merely the unsuitability of the experimental procedure. The appearance of the nucleation sites is contrary to that to be expected if failure was due to mechanical stresses in the oxide resulting from the increasing thickness. Were this the case, cracking would be expected along lines of high stress as was found in previous studies (2, 3).

Consideration of the nature of the breakaway process suggests that the mechanism involved in the formation of the dark film and in the failure of the oxide on arc-melted zirconium (3) may be responsible for the failure of the oxide film on zircaloy-2. We have suggested that the transition from an interference color film to a dark film in zircaloy-2 is facilitated by the even distribution of the alloying elements as intermetallic precipitates. These precipitates provide regions of inhomogeneity in the oxide film, along which diffusion is rapid, and hence counterbalance the effect of diffusion along grain boundaries. If they are sufficiently close together and sufficiently small in size, then lateral diffusion will smooth out the effect of rapid transport along these paths and a uniform film will result. However, while the resulting film appears to be uniform within the limits of resolution of the optical microscope, on a smaller scale there may still be differences in the growth rate of the film on different areas. Over the long periods involved before the breakaway of zircaloy-2 these differences could still be large enough to result in localized stresses, which would result in failure in a manner analogous to the grain boundary failure in arc-melted zirconium.

On the basis of this mechanism for the breakaway of zircaloy-2 each of the nuclei observed would correspond to the site of an intermetallic particle, since (even allowing for lateral diffusion) the greatest oxide film thickness would still occur at this point. Variations in the time to breakaway would then be related to the size and distribution of the intermetallic particles; a schematic representation of the effect of such variations in distribution is given in Fig. 10. It is obvious that confirmation of this hypothesis must await the positive location and identification of the intermetallic particles and the following of their behavior throughout the corrosion process. Attack polishing of zircaloy-2 specimens often results in a scatter of very fine markings, which are said to be the intermetallic precipitate. Electron microscopy shows these to be etch pits (39), and, while they may mark the sites of intermetallic particles, no positive identification of such particles in zircaloy-2 has been reported. It is unfortunate that no particles are observed in specimens after cathodic etching; a uniform etch pattern is found over the whole grain. However, suggestions have been made that the etch patterns so obtained may be produced by migration of material on the surface rather than by removal of material, and it is possible that fine precipitates could be covered up by this mechanism.

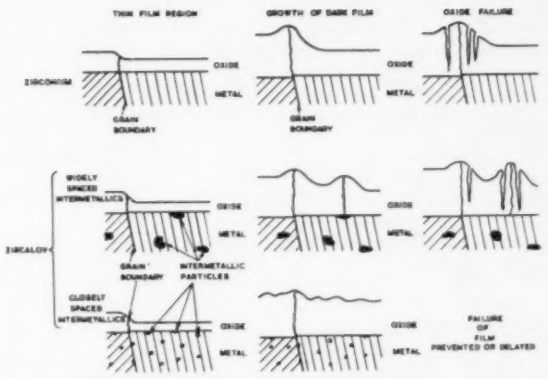

Fig. 10. Diagrammatic representation of film growth and failure in Zr alloys.

Conclusion

It is suggested that the prebreakaway corrosion kinetics of zirconium alloys can be explained on the basis of two logarithmic growth rates. The first, which applies to the growth of the interference color film, may be identical with Uhlig's suggested logarithmic rate law. The second logarithmic growth rate comes into operation only when the film has already grown to several thousand angstrom's, and is a true diffusion process, but along preferred paths only. These preferred paths are provided by the misorientation in the oxide at grain boundaries and inhomogeneous regions in the film due to impurities or alloying elements originally in the metal. The distribution of these inhomogeneous regions determines the subsequent behavior of the material. On this basis the early failure of arc-melted zirconium is explained, and a hypothesis is proposed to explain the breakaway of zircaloy-2 at temperature below 400°C. It is suggested that the latter occurs when stresses produced by residual small-scale variations in growth rate (resulting from incomplete smoothing of the growth due to the second oxidation process) lead to the nucleation of failure in the oxide. As these sites are small and scattered in nature, a progressive increase in the number of nuclei is produced rather than cracking propagating from them. At higher temperatures, where diffusion of oxygen into the metal becomes significant, the proposed mechanism may require modification.

Acknowledgments

The author would like to thank Mr. R. Harwood for the preparation of specimens, Mr. D. Armstrong for cathodic etching, and Mrs. B. W. Jenkins for the preparation of replicas. He is grateful to Dr. J. K. Dawson for discussion on the subject.

Manuscript received Oct. 26, 1959.

Any discussion of this paper will appear in a Discussion Section to be published in the December 1961 JOURNAL.

REFERENCES

1. B. Lustman and F. Kerze, "Metallurgy of Zirconium," McGraw Hill Book Co., New York (1955).
2. B. Cox, Part II, A.E.R.E.-R 2873 (1959).
3. B. Cox, Part III, A.E.R.E.-R 2874 (1959).
4. E. A. Gulbransen and K. F. Andrew, *Trans. Am. Inst. Mining Met. Engrs.*, **185**, 515 (1949).

5. E. A. Gulbransen and K. F. Andrew, *J. (and Trans.) Electrochem. Soc.*, **96**, 364 (1949).
6. J. Belle and M. W. Mallett, *This Journal*, **101**, 339 (1954).
7. D. E. Thomas and J. Chirigos, WAPD-98, (1953).
8. E. A. Gulbransen and K. F. Andrew, *J. Metals*, **209**, 394 (1957).
9. R. G. Charles, S. Barnett, and E. A. Gulbransen, *Trans. Met. Soc. AIME*, **212**, 101 (1958).
10. E. A. Gulbransen and K. F. Andrew, *This Journal*, **104**, 709 (1957).
11. L. F. Kendall, HW 39190 (1955).
12. I. I. Korobkov, D. V. Ignatov, A. I. Yestvukhin, and V. S. Yemelyanov, 2nd Int. Conf. on the Peaceful Uses of Atomic Energy, 1958, Geneva, P/2054.
13. D. J. McAdam, Jr., and G. W. Geil, *J. Research Natl. Bur. Standards*, **28**, 593 (1942).
14. M. W. Mallett and W. M. Albrecht, *This Journal*, **102**, 407 (1955).
15. E. A. Gulbransen and K. F. Andrew, *Corrosion*, **14**, 32t (1958).
16. D. E. Thomas and S. Kass, *This Journal*, **104**, 261 (1957).
17. D. E. Thomas and S. Kass, *ibid.*, **103**, 478 (1956).
18. D. S. Kneppel, NMI-1119 (1954).
19. O. Flint, A.E.R.E. M/R 2646 (1958).
20. R. S. Ambartsumyan, A. A. Kiselev, R. V. Grebennikov, V. A. Myshkin, L. J. Tsuprun, and A. V. Nikulina, 2nd Inst. Conf. on the Peaceful Uses of Atomic Energy, 1958, Geneva, P/2044.
21. F. H. Krenz, G. J. Biefer, and N. A. Graham, 2nd Int. Conf. on the Peaceful Uses of Atomic Energy, 1958, Geneva, P/194.
22. J. Chirigos and D. E. Thomas, TID-5084 (1952).
23. C. M. Schwartz, D. A. Vaughan, and G. G. Cocks, BMI-793, (1952).
24. O. Kubaschewski and B. E. Hopkins, "Oxidation of Metals and Alloys," Butterworths, London (1953).
25. N. Cabrera and N. F. Mott, *Repts. Progr. Phys.*, **12**, 163 (1948).
26. H. H. Uhlig, *Acta Met.*, **4**, 541 (1956).
27. W. M. Albrecht, NP-6415 (1957).
28. P. Kofstad, WADC-TN-57-231.
29. P. Kofstad and K. Hauffe, *Werk u. Korr.*, **1**, 642 (1956).
30. E. A. Gulbransen and K. F. Andrew, *Trans. Am. Inst. Mining Met. Engrs.*, **185**, 741 (1949).
31. U. R. Evans, *Trans. Electrochem. Soc.*, **91**, 547 (1947).
32. B. Cox, Part IV, A.E.R.E.-R 2875 (1959).
33. J. P. Pemsler, *This Journal*, **105**, 315 (1958).
34. W. W. Smeltzer and M. T. Simnad, *Acta Met.*, **5**, 328 (1957).
35. B. Cox and K. Alcock, A.E.R.E. C/M 353 (1958).
36. W. V. Cathcart, J. J. Campbell, and G. P. Smith, *This Journal*, **105**, 442 (1958).
37. Bierlein and Mastel, *Met. Prog.*, **72**, P71 (1957).
38. D. Mclean, "Grain boundaries in Metals," Oxford (1957).
39. K. Alcock and B. Cox, Part I, A.E.R.E. C/R 2826 (1959).

A Study of the Formation of Anodic Oxide Films on Uranium

I. An Optical Reflectivity Method for Determining the Kinetics of Film Growth

A. E. Stebbens and L. L. Shreir

Battersea College of Technology, London, England

ABSTRACT

An optical reflectivity method is described which has been used for investigating film growth during the anodic oxidation of uranium, and which may have a wider application in the field of anodic oxidation provided the optical constants of the film can be determined. In the present study, multiple-beam interferometry and polarized light methods have been used to measure the optical constants of uranium and the anodically formed film. Using the former method a value of 1.94 has been obtained for the refractive index of the oxide.

The anodic oxidation of metals such as tantalum, niobium, aluminum, and zirconium, which form stable dielectric oxide films when anodically polarized in a variety of aqueous electrolytes has been investigated in detail in recent years. With uranium, however, Flint, *et al.* (1) have shown that anodic oxidation is possible only in nonaqueous electrolytes and have used ammoniated ethylene glycol at temperatures in the range −40° to 0°C since all aqueous electrolytes studied by these workers caused pitting.

The present investigation represents a study of the conditions of formation of anodic films, their chemical and physical properties, and the kinetics of film formation. During this study several techniques were developed for studying film growth, and the present paper is confined to a description of these methods.

The method for determining film thickness, kinetically, is based on the measurement of the intensity of monochromatic light reflected from the metal surface during anodic oxidation. No assumptions have been made as to the chemical and physical nature of the oxide film since the refractive index has been determined directly by polarized light and multiple-beam interferometry techniques (2). The latter method, which has not been used previously for anodic oxides owing to the absence of a suitable reference plane defining the oxide/metal interface, has been applied successfully in the present work as the anodic film on uranium was found to be solu-

ble readily in dilute acids, so that a sharp oxide step could be obtained.

Experimental Procedure

Specimen mounting and pretreatment.—The uranium (99.75% purity) used in this study was supplied by the U.K.A.E.A. in the form of disks 1 in. in diameter and 0.125 in. thick, which had been cut from a cast rod and had a polycrystalline α uranium structure. Metal of higher purity (99.9%) became available later and was used for certain aspects of the work.

In order to anodize a known area of the specimen, and to facilitate surface preparation, the disks of uranium were mounted in Araldite Casting Resin 103 (CIBA) (A.R.L. Ltd.). To ensure adhesion of resin to the metal the disks were electropolished before mounting, and mounting was carried out at 80°C to reduce the extent of the reaction between resin and metal. This procedure was necessary to avoid cracks forming at the resin/metal interface which would allow electrolyte to enter and cause pitting. An electrical contact to the back of the disk was provided first by vigorously rubbing an acidified solution of copper sulfate on the uranium, and then soldering a lead to the copper deposit so formed. (The electrical resistance of a contact formed by this method was found to be negligible.) A glass tube was passed over the lead and attached to the mount by means of melted polyethylene; this prevented the lead coming into contact with the electrolyte and provided a support for the mounted specimen.

Specimens which had been abraded with emery paper and then anodized in ammoniated ethylene glycol were observed to give long induction periods before the voltage commenced to rise owing to gas evolution rather than film thickening. This effect, which was due possibly to both disturbance of the surface material and the presence of surface impurities, was not observed when abrasion with emery was followed by adequate electropolishing: in addition this technique gave flat, highly reflecting surfaces which were essential for the optical studies.

After first grinding on 0 grade emery, specimens were electropolished in a solution containing 40% by vol. H_2SO_4 and 20% by vol. H_3PO_4.

A platinum cathode was used, and the current density for optimum polishing was 0.6 amp/cm^2. The surface of the uranium was brushed gently during the polishing to remove reaction products and prevent staining. (3)

Electrolyte.—Although this procedure of mounting and surface preparation enabled reasonably reproducible results to be obtained in ammoniated glycol at room temperature, control of the water content of this electrolyte was difficult owing to its hygroscopic nature. In addition, there was some evidence that localized corrosion occurred during anodizing. For these reasons other electrolytes were investigated (detailed results will be considered in a future paper), and it was established that aqueous ammonia solution, over a wide range of concentration, enabled uranium to be anodized reproducibly to high voltages with the formation of bright interference colors comparable with those obtained with tantalum. The investigation of techniques was carried out, therefore, using this electrolyte.

Power supply.—Guntherschultze and Betz (4) showed that during the anodic polarization of aluminum in boric acid the current density, i, obeys the relationship

$$i = A \exp BF \qquad [1]$$

where F is the field in the oxide and A and B are constants. This has been confirmed by Charlesby (5, 6). To investigate the validity of this expression for uranium it was convenient to be able to polarize the specimen either at constant current or at constant voltage.

If the above relationship is obeyed and the conduction mechanism remains unchanged with increasing film thickness, the rate of film formation should be constant at constant current, even when the efficiency is less than 100%, since both the ion current and electron current depend only on the field in the oxide.

At constant current $A \exp BF$ is constant so that $F = V/\delta$ is constant, where V is the potential across the oxide and δ is the film thickness. Since the thickness is proportional to the charge it follows that

$$V \propto \delta \propto t$$

The linear relationships between V, δ, and t can be investigated readily and any change in film properties ascertained from discontinuities in the curves.

To avoid an initial current surge, formation at a predetermined constant current should precede anodizing at constant voltage. At constant voltage the film continues to form but as the field in the oxide decreases, the current decays. Charlesby (5) has shown that the product, $i\,t$, changes only slowly with time and has verified Eq. [1] for aluminum by measuring the decrease in the film capacitance.

A suitable power unit was designed (7) which could supply either constant current, variable from 0 to 50 ma and with a maximum potential of 350 v, or constant voltage, variable between 0 to 350 v, with a maximum current of 50 ma.

The increase in cell voltage at constant current was followed by means of an automatic pen recorder (Elliott, 5 ma moving coil) which, when the power unit was switched to a preselected constant voltage, recorded the decay of current with time. The measured cell voltage was corrected for the voltage drop across the electrolyte and for the potential of the polarized cathode.

The output of the power unit was not affected by changes in mains voltage of up to 12%, and the level of ripple on the d-c output was less than 7 mv under all conditions. The output impedance of the constant current supply could be varied by application of positive feedback and made negative (−50 kohm) if required. It was possible, therefore, to cancel out the resistance of any measuring instrument connected in parallel with the anodizing cell and thus achieve an infinite output impedance

(>300 Mohms, i.e., effectively perfect output regulation) at all voltages and currents.

Determination of Film Thickness

Several methods have been described in the literature which may be applied to the measurement of anodic film thickness up to several thousand angstroms; these include gravimetric methods (8), capacitance measurements (9), film stripping (10), electrometric reduction (11), and numerous optical techniques (12-14).

Gravimetric methods do not, in general, permit accurate measurement of thin films and require a knowledge of film density which, for the anodic oxide on uranium, is not known. Similarly capacitance measurements could not be used since the dielectric constant of the oxide has not been determined and the power factor of the oxide films formed on the less pure uranium is low. However, by using values of film thickness derived from the optical method to be described both the film density and dielectric constant could be estimated.

It was considered that any method which involved periodic removal of the anode from the electrolyte also would be unsatisfactory for kinetics studies. Any interruption of polarization during anodizing was found to cause anomalies in the voltage-time plot, and this effect was even more marked when specimens were removed from the electrolyte, dried to examine interference colors, and then returned to the anodizing cell. In the method developed in the present work the intensity of monochromatic light reflected normally from the surface of the specimen was measured during anodizing, thus providing a continuous method of estimating film growth.

The apparatus is shown diagramatically in Fig. 1. Light from a high-pressure mercury arc, 1, was rendered converging by the condensing lens, 2, and, after passing through Kodak 'Q' (ultraviolet) and 808 (mercury yellow) filters, was brought to a focus on a small mirror, 3, mounted inside the main tube, 4, at 45°. It then was reflected as a diverging beam through the plano-convex lens, 5, which also formed the front of the anodizing cell, 6, and after reflection from the specimen, 7, (placed behind the lens), was transmitted again through the lens and passed down the tube as a parallel beam to fall on the photoelectric cell, 8. The maximum deviation from normal incidence on the specimen using this arrangement was about 5°. A second tube, 9, contained a filter, a 45° white diffuser, and another photoelectric cell, 10, and light was transmitted to this tube from the mercury lamp via a variable shutter, 11. The two photocells, which had a linear response over the range of intensities used and did not suffer from fatigue, were connected in opposition, and the shutter then was used to back off any photo current caused by extraneous light entering the main tube. The stability of the light source was ensured by using a constant voltage transformer (a 4% fluctuation of mains voltage resulted in an intensity change of less than 1%).

The anodizing cell (Fig. 1) was constructed of polyethylene and contained a centrifugal pump which maintained a rapid, controlled flow of electrolyte upward and around the specimen which was supported in front of the lens by the lead-in tube. This agitation removed any adherent gas bubbles from the specimen and minimized concentration effects. It was possible to examine the surface of the specimen obliquely during the course of the experiment. A thin platinum wire ring formed the cathode.

The high-pressure mercury lamp, which was necessary to obtain sufficient reflected intensity from the specimen, had a considerable output in the ultraviolet. Although it was considered that this would be filtered effectively by the thick condensing lenses and the 808 yellow filter, which absorbs in the u.v. range, an ultraviolet filter was introduced as an additional precaution. It was observed, however, that the latter had no significant influence on the results.

Intensity-Time Curves for Tantalum and Aluminum

To show whether this apparatus would function satisfactorily, intensity-time curves at constant current were obtained using tantalum and aluminum anodes.

The curve for tantalum is shown in Fig. 2, where the periodic changes in intensity clearly locate the maxima and minima of interference, and the con-

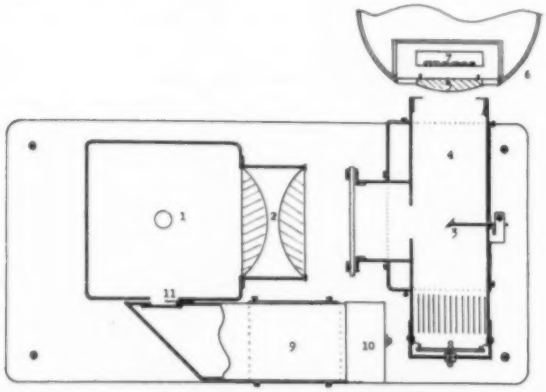

Fig. 1. Apparatus for measuring reflected intensity (plan view).

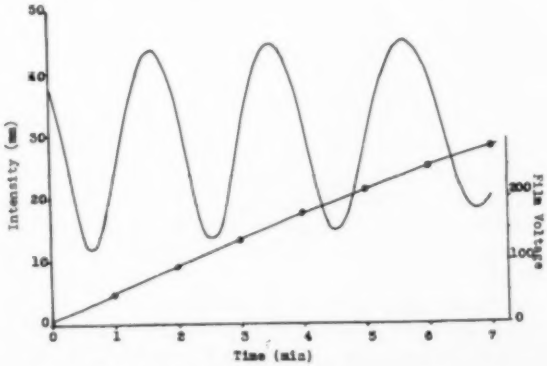

Fig. 2. Reflected intensity-time and corresponding voltage-time curve for tantalum.

stancy of amplitude indicates that no absorption occurs in the oxide layer.

The condition for the destructive interference of light reflected normally at the electrolyte-oxide and metal-oxide interfaces is given by

$$2nd + \phi = (p + \tfrac{1}{2})\lambda$$

where d is the film thickness, ϕ the residual phase change, and p (an integer) the order of interference. For maximum intensity

$$2nd + \phi = p\lambda \qquad [2]$$

Hence the minima and maxima of reflected intensity are given by

$2nd + \phi = m\lambda$ where $m = \frac{1}{2}, \frac{3}{2}, \frac{5}{2}$, for the minima and 1, 2, 3, for the maxima.

At a given thickness

$$V_m/d_m = F = \frac{1}{R} \qquad [3]$$

where, since [1] is obeyed by tantalum, R can be taken as the growth rate in Å/v at the current density used.

From [2] and [3] $m = \dfrac{2nRV_m}{\lambda} + \dfrac{\phi}{\lambda}$

so that plotting m against V_m gives a straight line of slope $2nR/\lambda$.

As λ is the wave length of mercury yellow, which was taken as 5780 Å, R can be calculated providing the refractive index, n, is known.

Assuming a value for the refractive index of Ta_2O_5 of 2.42, the growth rate at 2 ma/cm² was found to be 15.0 Å/v compared with 14.95 Å/v obtained by Vermilyea using gravimetric and optical methods (8).

Aluminum, unlike tantalum, does not give pronounced interference colors during anodizing owing to the low refractive index of the oxide and the high reflectivity of the metal substrate, resulting in shallow and rather sharp absorption bands. Using the reflectivity apparatus, however, with maximum galvanometer sensitivity, periodic changes in intensity were observed readily. There was no visible absorption in the oxide, and, assuming the refractive index to be 1.77, a value for the growth rate of 12 Å/v was obtained, which compares favorably with 12.5 and 11.8 Å/v quoted in the literature (15, 16).

This method therefore appears capable of considerable accuracy when only the maxima and minima of interference are used for calculating the growth rate.

Optical Measurements

To obtain quantitative data for the normal reflectivity of film coated uranium the refractive index (n) and absorption index (k) of uranium and the anodic oxide were required. These determinations were made using a polarizing spectrometer fitted with a Babinet Compensator.

After electropolishing and drying the specimen, it was transferred rapidly to the spectrometer and, since the results were found to be consistent over the time of measurement, it was apparent that no further oxidation was occurring. It is probable, however, that a thin film of oxide is present on the metal surface and, if it is assumed to be approximately 50Å thick, it can be shown that the error in the calculated values of n and k will be about 10%. This accuracy is considered to be sufficient for the purpose of the optical calculation. The values obtained for uranium were: $n = 1.50$, $k = 1.87$.

When uranium of purity 99.75% was anodized to a high voltage (200 v) a brown absorbing layer was formed, which eliminated the reflection of the metal, and a very rapid phase change was observed in passing the polarizing angle. From the film voltage and estimated refractive index the approximate film thickness was obtained so that the attenuation of the incident light after its double passage through the oxide could be calculated. This calculation confirmed the belief that the brown oxide layer was completely absorbing and justified the assumption that it could be regarded as a bulk sample of oxide. The following values were obtained for the anodic oxide: $n' = 1.88$, $k' = 0.278$.

The expression for the reflected amplitude at normal incidence of light reflected from a film covered metal immersed in a dielectric (12) is given by:

$$\frac{A_r}{A_i} = \frac{k_0 e^{i\phi_0} + k_1 e^{i\phi_1} \cdot e^{-2\gamma\delta}}{1 + k_0 k_1 e^{i(\phi_0 + \phi_1)} \cdot e^{-2\gamma\delta}} \qquad [4]$$

where $k_0 e^{i\phi_0}$ and $k_1 e^{i\phi_1}$ are the reflection coefficients at the electrolyte/oxide interface and the oxide/metal interface, respectively; γ, the propagation constant, is given by $\gamma = \alpha + i\beta$ where $\alpha = \dfrac{2\pi k'}{\lambda}$ and $\beta = \dfrac{2\pi n'}{\lambda}$; λ is the wave length of the light used and δ the film thickness.

The experimental values of the four constants n, k, n', and k', and the refractive index of the electrolyte then were substituted in [4]. Since the expression for reflected intensity becomes very complicated analytically, numerical values were obtained by a graphical method. The final intensity curve took the form shown in Fig. 3, where intensity is plotted against film thickness. It can be seen that the amplitude of oscillation decreases steadily with increasing film thickness. The second curve shows that the

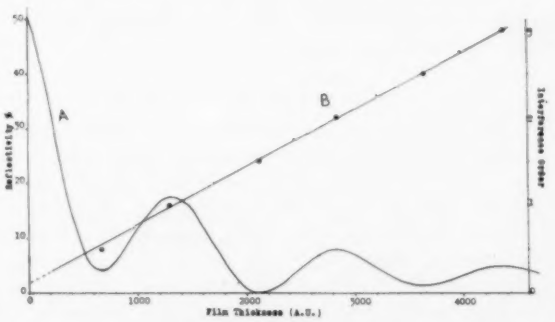

Fig. 3. A, Theoretical reflectivity thickness curve for the system U/U_xO_y/ammonia; B, relationship between maxima and minima of reflected intensity (order of interference) and film thickness.

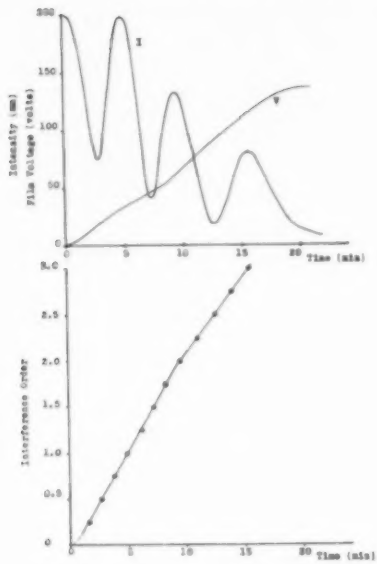

Fig. 4. Variation of intensity (I), voltage (V) and order of interference with time for uranium (99.5% purity).

maxima and minima of interference lie on a straight line.

An experimental intensity curve, obtained by anodizing uranium (99.75%) at constant current in 10*N* ammonia solution took the form shown in Fig. 4. Unlike the calculated curve (Fig. 3) the film appears to remain transparent over the first 1½ orders of interference, and then rapidly becomes absorbing, suggesting that the properties of the film change suddenly during growth. The optical growth rate, measured by the maxima and minima of interference, appeared to be constant up to 2 orders, after which the efficiency decreased, with visible gas evolution. The quantity of gas evolved was small in the 10*N* ammonia and was not evident at all in less concentrated solutions. By switching off the polarizing current it could be readily established that the gas had no effect on the intensity measurement.

Anodizing high-purity uranium under similar conditions gave the result shown in Fig. 5. In this case the intensity remained fairly constant over 4½ orders and a linear growth rate was obtained.

These results, which will be considered in a subsequent paper, show clearly the influence of metal purity on anodic oxidation.

Multiple-Beam Interferometry

The formation of a transparent oxide film on high-purity uranium, which was quite free from inclusions, enabled multiple-beam interferometry to be used for determining the refractive index. This provided an alternative method which could be used to check the value of the refractive index obtained for the absorbing oxide.

The anodic film on uranium was found to be soluble in dilute acids, so that by dissolving the film from part of an anodized specimen sharp oxide steps could be formed. Dilute sulfuric acid (5% by vol.) was painted in lines on an anodized specimen

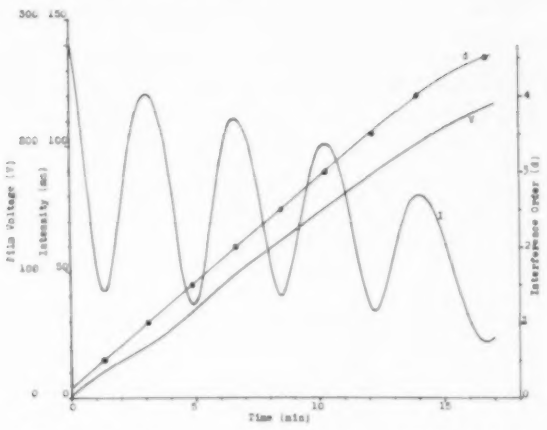

Fig. 5. Variation of intensity (I), voltage (V) and interference order (d) with time. High-purity uranium.

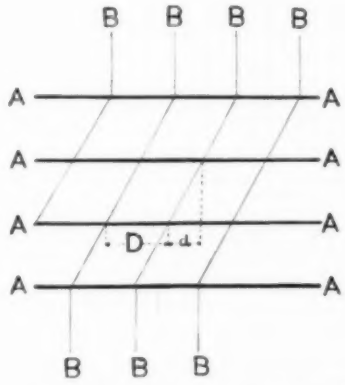

Fig. 6. Multiple beam fringe system

and by controlling the time of acid treatment it was found that a shallow wedge of oxide, rather than a sharp step, could be obtained. When this was examined under the microscope in monochromatic light, dark fringes corresponding to interference minima in the oxide were found to run along the length of the wedge. An interference system then was set up under the microscope as follows: monochromatic light from a pinhole source was collimated and reflected normally on to the specimen by a half-silvered mirror fixed at 45° under the objective lens and a small (2 x 5 mm) partially silvered glass flat was placed on top of the specimen and suitably clamped in position. In this way a second series of fringes were formed in conjunction with the surface of the oxide, which crossed the line of the wedge at right angles. In passing over the wedge these fringes become displaced laterally, as shown in Fig. 6, where BB and AA represent fringes in air and in the oxide, respectively. By measuring the points of intersection of the two systems, the lateral displacement of an air fringe in passing from one order in the oxide to the next could be measured. The physical thickness of oxide between successive minima is $d = \lambda/2n$ where λ is the wave length of the light used; also the ratio d/D gives the value of $2d/\lambda$ so that n can be determined:

$$d/D = 2d/\lambda = 1/n$$

Owing to the small physical dimensions of the fringe system the experimental scatter was quite large, but by taking measurements over a number of fringes and several orders of interference a mean value of $n = 1.95$ was obtained. It should be noted that this method is independent of attack of the uranium substrate by the acid. A direct measurement of step height was, however, carried out and gave the value $n = 1.93$, which is in good agreement with the previous value.

The value of n for the transparent oxide therefore did not differ greatly from that of 1.88 obtained for the absorbing oxide using polarized light measurements.

Discussion

A consideration of the literature shows that in determining film thickness assumptions have been made regarding the values of the physical constants, *e.g.*, the dielectric constant (4) in capacity measurements, density in gravimetric methods, etc. As the physical constants of the anodic oxide are not usually available, the appropriate value of the bulk oxide has been used which, in view of the fact that the anodic oxides are usually amorphous and only crystallize when heated or subjected to a strong electrical field, is seldom justified. Vermilyea (17) has, however, measured the physical thickness after flaking the oxide from the metal surface, but this is of limited application as usually the oxide is adherent to the substrate.

In optical studies of film growth errors arise in several ways. In comparing the interference colors of two dissimilar systems, *e.g.*, the color of the oxide with those of an air film, it is assumed that the subjective color match indicates equal film thickness (1). This will be the case only if the optical properties of all components of the systems are similar; this condition is seldom realized in practice. A knowledge of the refractive index is necessary to convert the optical growth rate to the actual growth rate and frequently the value for the bulk oxide has been used, although refractive index, like density, may be dependent on film structure. It should be observed that the measurement of the refractive index of a thin film on a metal substrate is difficult as the underlying metal surface cannot be exposed for depth measurement.

It has been found that the anodic oxide film on uranium is unusual as it is readily soluble in dilute acids so that oxide steps could be obtained. (It is of interest to observe in this connection that thermally prepared UO_2 is practically insoluble, indicating that the chemical and physical properties of the anodic and bulk oxide cannot be assumed to be the same.) The multiple-beam interferometry experiments described enable the refractive index to be determined directly and, in principle, the variation of the refractive index with film thickness can be measured at each interference order. Owing to experimental scatter, the refractive index has been assumed to remain practically constant with thickness, but it is apparent that any change in the properties of the film during growth may introduce errors into the determination. It is necessary to emphasize, however, that the refractive index of the thick brown absorbing oxide was found to differ from that of the transparent oxide by only 3%. This was confirmed by experiment, as the optical growth rate (Fig. 5) remained constant over four orders of interference, and a similar result was obtained under most experimental conditions.

The relationship between reflected intensity and film thickness was found to vary with the purity of the metal used and did not agree quantitatively with the calculated relationship which was determined using the optical constants. As a result, only the maxima and minima of interference could be located with precision, and more approximate interpolation has to be used when required. The theoretical curve was of value, however, as when compared with the experimental curve it was evident from the latter that a transparent film was formed for some time and then became absorbing suddenly; this feature was not evident from visual inspection.

Tantalum (Fig. 2) and aluminum have served to demonstrate the form of curve to be expected from systems which are simpler than uranium and show that a high degree of precision can be obtained, and a determination of the theoretical reflectivity-film thickness curve might prove to be of value for kinetic studies of systems of this type.

Although the optical reflectivity method has been developed for studying anodic oxidation, there is no reason why it should not be used for thermal oxidation involving thin films.

To summarize, it is considered that the optical reflectivity method has the advantage that it is not subjective and provides a continuous method for studying anodic oxidation which is particularly useful when the rates of oxidation are high. Since monochromatic light is used there is no loss of resolution due to overlapping orders of interference beyond the second order as occurs with visual methods using white light. In addition, some information of the internal structure of the film may be obtained from the absorption which occurs in the oxide.

The method has, however, several disadvantages and, for example, the thickness of a given film cannot be measured unless the absolute reflectivity is determined. If the optical constants change during the course of oxidation, the method becomes invalid, but this objection applies equally to any other method of measurement.

Acknowledgments

Acknowledgments are made to the U. K. Atomic Energy Authority (Harwell) for kindly sponsoring this research and to Mr. O. Flint for helpful discussions.

Manuscript received March 11, 1960; revised manuscript received Aug. 20, 1960.

Any discussion of this paper will appear in a Discussion Section to be published in the December 1961 JOURNAL.

REFERENCES

1. O. Flint, J. J. Polling, and A. Charlesby, *Acta Met.*, **2**, 696 (1954).
2. A. E. Stebbens and L. L. Shreir, *Nature*, **183**, 1113 (1959).

3. E. C. Sykes, V. J. Hadrell, H. R. Haines, and B. W. Mott, *J. Inst. Met.*, **83**(5), 166 (1954).
4. A. Guntherschulze and H. Betz, *Z. Phys.*, **92**, 367 (1934).
5. A. Charlesby, *Proc. Phys. Soc.*, **66** (B), 533 (1953).
6. A. Charlesby, *Acta Met.*, **1**, 343 (1953).
7. A. E. Stebbens, Ph.D. Thesis, London University (1958).
8. D. A. Vermilyea, *Acta Met.*, **1**, 282 (1953).
9. L. Young, *Trans. Faraday Soc.*, **50**, 153 (1954).
10. W. H. J. Vernon, F. Wormwell, and T. J. Nurse, *J. Chem. Soc.*, 621, Pt. 1 (1939).
11. H. A. Miley, *J. Am. Chem. Soc.*, **59**, 2626 (1937).
12. O. S. Heavens, "Optical Properties of Thin Solid Films," p. 56, Butterworths, London (1955).
13. F. H. Constable, *Proc. Roy. Soc.*, **A115**, 570 (1929).
14. U. R. Evans, "Metallic Corrosion, Passivity and Protection," E. Arnold, p. 802 (1948). (appendix by A. B. Winterbottom)
15. A. J. Dekker and W. Ch. Van Geel, *Philips Research Repts.*, **2**, 313 (1947).
16. B. V. Deryagin and R. M. Friedland, *J. Tech. Phys. U.S.S.R.*, **18**, 1443 (1948).
17. D. A. Vermilyea, *This Journal*, **102**, 655 (1955).

Electrochemical Behavior of the Magnesium Anode

J. L. Robinson and P. F. King

Metallurgical Laboratory, The Dow Metal Products Company, Division of The Dow Chemical Company, Midland, Michigan

ABSTRACT

The anodic transient behavior of magnesium in aqueous environments is studied under controlled conditions. The steady-state behavior as reported by other investigators is reviewed, and pertinent additional observations are reported. A unified explanation of the aqueous electrochemical behavior of magnesium based on the concept that the inherent high reactivity of magnesium is masked by a highly protective $Mg(OH)_2$ film is presented. The unusual characteristics exhibited by the magnesium anode in many environments (invariance of steady-state working potential, "negative difference effect," and transient behavior) are related to processes leading to damage or repair of this film.

In the following aspects, the magnesium anode departs from what is considered normal electrochemical behavior. (*A*) Its steady-state working potential is usually more than a volt noble to its standard potential of −2.43 v (1), even at the low anodic currents associated with open circuit local action. (*B*) In some environments the steady-state potential is relatively insensitive to increasing anodic current. Robinson (2) shows that this is true up to at least 1 ma/cm^2 in chloride and sulfate electrolytes. (*C*) While in many environments the rate of magnesium anode consumption increases almost linearly with impressed current (2), the rate is substantially greater than that predicted by Faraday's law for divalent ion formation. This excess consumption manifests itself as an increase in hydrogen evolution at the anode with increasing anodic current (negative difference effect). (*D*) The magnesium anode also exhibits a transient behavior as it passes from one steady state to another. This was first mentioned by Kirk and Fry (3).

Gatty and Spooner (1) have attempted to explain the marked deviation of the open-circuit potential from the theoretical value. They point out that it is impossible to account for the magnitude of this polarization by a high magnesium ion activity at the magnesium surface, since the concentrations needed would be of astronomical magnitudes. To explain the nobility of the observed potential they postulate the formation of a hydride film. Whitby (4), on the other hand, proposes a filmed electrode of the type $Mg/MgO/OH^-$.

Several investigators have proposed explanations for the negative difference effect observed with magnesium. Whitby (4) proposes that the protective film on magnesium exercises control of the corrosion rate. Evans (5) implies that destruction of this film accounts for the increased hydrogen evolution observed with anodic current flow. Robinson (2) points out that the increased corrosion rate of Mg at low pH values could be due both to depolarization of the local anode by breakdown of the $Mg(OH)_2$ protective film and to depolarization of the cathode by the increased availability of protons for discharge. He shows that the pH decreases appreciably with increases of magnesium ion concentration and suggests that the local corrosion rate of the magnesium anode might well be expected to rise with increasing applied current density since the magnesium ion concentration at the anode-solution interface is increased. McNulty and Hanawalt (6) propose that the dissolution of the metal resulting from current flow uncovers additional local cathodes, which increases the amount of local action current which can flow until a balance between the uncovering of new cathodes and the loss of old ones is reached. Straumanis and Wang (7) prefer this explanation, but Straumanis (8) also points out that "the very active metals (Mg, Al, and Ti) react with the electrolyte (self-dissolution) in places where the protective scale is broken off from their surface." Glicksman (9) uses Casey and Bergeron's (10) model of proton transfer through the protective film along with film breakdown as an explanation of the phenomenon. The explanation offered by Tomashov, Komissarova, and Timonova (11) is similar, but they propose that the inclusion of chloride ion (in sodium chloride solution) in the film or adsorption of chloride ion on the film may be important to the film breakdown process. They suggest that the excess corrosion represented by the negative difference effect may be due either to chemical reaction

at the bare active surface where the film has broken down, or to the electrochemical reaction at microcathodes bared by the film destruction. They prefer the second possibility. Other investigators (12, 13) base their explanation on the anodic formation of unipositive magnesium ion, and its subsequent reaction with water to liberate hydrogen. Hoey and Cohen (14) consider the several possibilities and lean toward the enhancement of corrosion rate by anodic current as the explanation.

Glicksman and Morehouse (15) suggest that the voltage transient observed between two steady-state currents is due to the resistance of the protective film on magnesium which suffers partial breakdown with increasing currents.

It is our purpose in the present paper to attempt to build a self-consistent picture of the behavior of the magnesium anode in aqueous environments from the above-described phenomena and hypotheses and from some pertinent new data.

Experimental

The study of the anodic potential transient was carried out in a conventional one-compartment electrolysis cell utilizing a Luggin capillary reference probe with a saturated calomel electrode. The dimensions of the anode were 2.5 x 0.75 x 0.3 cm, and two 2.5 x 2.5 x 0.03 cm Pt cathodes were suspended parallel to and 2.5 cm from the anode faces. In all cases the anodes were prepared from commercial hard rolled 0.3 cm sheet containing a nominal 3% Al and 1% Zn, ASTM designation AZ31B-H24. A constant current was obtained by the use of a stable 600-v power source in conjunction with large swamping resistors. The artificially applied corrosion currents, referred to in the discussion, were imposed with a parallel power source. Potentials were recorded with a Sanborn oscillograph, except for detailed studies for which an oscilloscope was employed. The potential measurements were made 20 min after immersion of the anode in the electrolyte. Artificial corrosion rates were applied immediately upon the immersion of the anode. The experiments were carried out in duplicate in a constant temperature room at 21° ± 1°C. Reproducibility was better than ± 5%

Corrosion rates were determined in solutions of magnesium bromide (Dow MTG grade), sodium bromide (CP), and mixtures of the two in concentrations up to 5*N* by complete immersion of a 2.5 x 5.1 x 0.3 cm coupon in 200 cc of solution for one week. The specimens were cleaned in a 6% NaOH, 1% Na_3PO_4 cleaning bath at 90°C, pickled 1 min at room temperature in an acetic-nitrate pickle (266 cc acetic acid, 67 g sodium nitrate made up to 1 liter with distilled water), and then rinsed, dried, and weighed before immersion in the corroding medium. After exposure, they were removed from the solution, rinsed, cleaned in hot (90°C) 20% CrO_3 + 1% $AgNO_3$ cleaning solution, rinsed, dried, and weighed.

Results and Discussion

We consider the electrochemical behavior of magnesium as film controlled and dominated by processes of film damage and film repair. As pointed out above, even at the light anodic currents associated with open-circuit local action, magnesium's steady-state working potential is usually more than a volt noble to its standard potential of −2.43 v (1). At the outset this is an argument for a film of poor conductivity and reasonably good continuity. With such a pre-existing high degree of anodic polarization and intrinsically active electrochemical potential, processes leading to film damage or destruction should be productive of drastic changes with respect to such electrochemical properties as corrosion, anode potential, anode efficiency, and transient behavior.

The protective film on magnesium in most aqueous environments has been found by extensive x-ray and electron diffraction experiments to be magnesium hydroxide, never magnesium oxide. (Magnesium oxide has been observed to be formed at room temperature only by polishing in air or by dissolving magnesium in mercury.) Thus, the film repair process is merely the formation of magnesium hydroxide at the anode-solution interface. The film damaging process can then be considered as simply due to the build-up of soluble magnesium salts at the anode-solution interface. As Robinson (2) points out, this results in increased acidity and thus increased solubility of the magnesium hydroxide film. Evidence that the pH at the anode-solution interface can become very much lower than that of the bulk electrolyte is our observation that in NaCl electrolytes magnesium hydroxy chloride occurs as a corrosion product, even at relatively low anodic currents. The general mechanism which produces increased acidity at anodic sites is discussed by Evans (5). High concentrations of certain magnesium salts, such as halides, can also damage the film by modifying it through the incorporation of these salts between the magnesium hydroxide layers and consequently increasing the layer spacing. Such $Mg(OH)_2$ structural modifications have been reported by Feitknecht and co-workers (16, 17). Irrespective of the mode of protective film damage it is known that increasing concentrations of soluble magnesium salts markedly activate the potential and corrosion rate of magnesium. One example of this is reported by Glicksman (9) for magnesium bromide solutions with a small constant current imposed. Unpublished data in our laboratory show this activation on open circuit with a number of soluble magnesium salts. The simultaneous activation of corrosion rate and potential can best be explained by film damage.

Figure 1 shows the weight loss of magnesium as a function of applied anodic current density. For a large number of magnesium alloys and environments, the observed behavior is similar to that of curve 3 in this figure, but occasionally a magnesium alloy is found that behaves as shown by curve 1. The data for this curve were obtained on an atypical batch of cell magnesium tested in a saturated calcium sulfate-magnesium hydroxide solution. [The electrolyte and the test procedure employed in these measurements are standard for the evaluation of

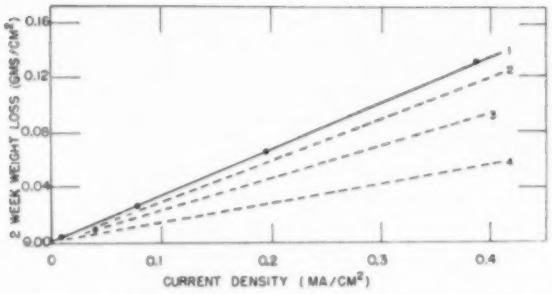

Fig. 1. Weight loss of magnesium alloys vs. applied anodic current adjusted to have a zero intercept by subtraction of the weight loss due to local action: 1, atypical behavior; 2, theoretical for unipositive ion formation; 3, typical behavior; and 4, theoretical for divalent ion formation.

magnesium anodes for cathodic protection applications (2).]

Curves 2 and 4 are the theoretical curves based on Faraday's law if all of the magnesium ionized to form univalent ions or divalent ions, respectively.

The typical behavior (Fig. 1, curve 3) corresponds to a mean valence of 1.3. This could be interpreted as the formation of the two ionic species, Mg^{+} and Mg^{++}. However, for data shown by curve 1 the mean valence would be less than 1, actually 0.8. In this instance a corrosion process which is current dependent must be postulated. We prefer to interpret *all* magnesium anodic behavior in terms of such a current-dependent reaction rather than to introduce the complication of two reactions and the hypothetical Mg^{+} ion. All that is necessary to have such a current-dependent corrosion reaction is to have current dependent formation of film-damaging soluble magnesium salts at the anode-solution interface. This can occur when magnesium ions enter the solution more rapidly than hydroxyl ions can diffuse to the surface. As a result, the magnesium ions pair with the anions of the supporting electrolyte forming film-damaging salts. Since anions arrive mainly by electrochemical transport, the formation of soluble salts at the anodic sites should be directly dependent on the magnitude of the current.

The total weight loss increases linearly with the magnitude of the applied anodic current, curve 3, of Fig. 1. The weight loss directly due to the applied current must increase linearly with its magnitude in accordance with Faraday's law. By difference, the corrosion rate must be increasing linearly with applied current. Such linearity has been observed to persist even to apparent applied current densities of 4 amp/cm² with AZ31B alloy in synthetic sea water. The unprotected area also increases with increasing current due to the formation of soluble salts as described above. If the increased corrosion is then considered to be caused by the direct reaction of magnesium with water in the same fashion as sodium reacts with water, the corrosion rate will be directly proportional to the unprotected area. Since the observed corrosion rate and the formation of soluble magnesium salts are both substantially directly proportional to the current, the film damage

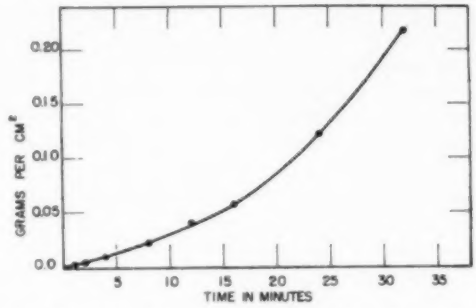

Fig. 2. Reaction of Mg-5% Hg (by weight) alloy with distilled water.

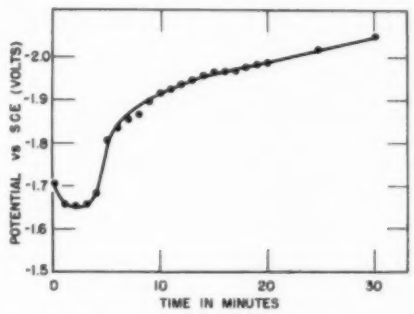

Fig. 3. Potential behavior of Mg-5% Hg (by weight) alloy during reaction with distilled water.

must also be directly proportional to the concentration of the soluble salts as anodic sites.

Pure magnesium alloyed with a fraction of an atomic percent of mercury demonstrates that extreme damage to the usually protective film on magnesium can cause the direct attack by water, as is assumed above. Figure 2 is the plot of the weight loss of such an alloy as a function of time in distilled water. The corrosion rates associated with these weight losses are in excess of one million mdd, a rate about one million times that of pure magnesium in the same environment. If the magnesium-mercury alloy specimen is removed from the distilled water, the heat evolved by the continuing corrosion reaction is so great that in a matter of seconds the specimen dries with the evolution of steam. The corrosion potential of this alloy becomes more active as the corrosion rate increases, as is shown in Fig. 3.

The above mechanism can be summarized as follows:

Since the production of Mg^{++} ions at the anode interface is directly proportional to the applied current and the anions arrive at the surface mainly by electrochemical transport, the average build-up of soluble magnesium salts (C_s) at the anode surface can be expressed as

$$C_s = k_1 i_a \qquad [1]$$

where i_a is the applied current and k is a constant.

Since film damage is due to the formation of soluble magnesium salts, the increase in effective area, A, is

$$A = f(C_s) \qquad [2]$$

Since we assume that the increase in corrosion (i_f) is due to direct reaction with water at damaged areas,

$$i_f = k_2 A \quad [3]$$

The observed increase in corrosion rate is linear with applied current (curve 3, Fig. 1); therefore

$$i_f = k_3 i_a \quad [4]$$

Thus, from Eq. [3] and [4]

$$A = (k_3/k_2) i_a \quad [5]$$

From Eq. [1] and [5], the function $f(C_r)$, Eq. [2], is the simple linear function

$$A = (k_3/k_2 k_1) C_r \quad [6]$$

Also, from Eq. [5]

$$i_a/A = k_2/k_3 \quad [7]$$

The above equations assume a constant corrosion rate (local action current). Since these equations hold for any constant local action current, they also hold for the artificially applied corrosion currents described in the experimental section.

The above anodic behavior should be limited to systems containing anions capable of forming soluble magnesium salts. Within our experience this is the case. Further, the potential, E, of the above system as a function of applied current should follow the general relation

$$E = f'(i_a/A) + E_{(i_a=\infty)} \quad [8]$$

but since (i_a/A) is a constant (Eq. [7]) it follows that E will be invariant with current. Our experience confirms Robinson's (2) observations on this point and, further, we have been unable to obtain appreciable polarization even at apparent current densities of 4 amp/cm^2 with AZ31B alloy in synthetic sea water.

The observed anodic potential transient behavior of magnesium can be considered a natural consequence of the above mechanism for the steady-state behavior. Essentially normal anodic polarization occurs when anions of soluble magnesium salts are absent from the environment, but transient polarization is observed when such anions are present. Figure 4 shows a generalized picture of the transient. It is a potential-time plot in which from A to B the anode is at a steady-state potential. When the anodic current is increased at B, the polarization increases. The Mg^{++} ions entering the system rapidly deplete the hydroxyl ions at the surface and pair with the other available anions. In turn the soluble magnesium salts formed to attack the protective magnesium hydroxide film at the anode-solution interface, and the effective anode area begins to increase. This increase in area reduces the effective current density and consequently the polarization; therefore, at point C reactivation of the potential begins. As the effective current density decreases, the relative rate of film damage decreases and causes a decrease in slope of the recovery portion of the curve. This decrease in slope continues until the rates of breakdown and repair are again equal and the steady state is re-established (point D). As pointed out above, the potential is invariant at steady-state irrespective of the magnitude of the applied current.

When the applied anodic current is removed at point D, the effective current density is reduced and the resulting depolarization of the anode manifests itself in an activation of the observed potential. Due to the decrease in rate of soluble salt formation resulting from the removal of the applied current, the protective film has a chance to repair itself until the steady state is reached and the observed potential decays to the initial value at point E.

Support for the contention that additional active area is being produced during the transient period is the observation, Fig. 5, that the magnitude of the activation of potential on removing the applied current is dependent on the fraction of the transient completed. This is direct evidence that the effective current density remaining on shutting off the current is decreasing throughout the transient and thus, since the current is fixed, the area is increasing.

The initial change in potential with an increase or decrease of anodic drain has been examined in detail with and without a resistor in series with the anode, Fig. 6. As can be seen, the potential drop produced by the resistance of the protective film is a trivial part of the total potential change. Since the initial portion of the transient appears to be more or less "normal" polarization of the anode, it is not surprising that its magnitude should depend on the magnitude of the applied current. In a given environment, *i.e.*, with a given corrosion rate, either natural or artificially applied, the magnitude of the potential change increases with applied current until an ill-defined plateau in the region of 1.30 v is reached. In Fig. 7 the maximum potential change is plotted vs. applied current for differing corrosion rates. Below the plateau, the higher the corrosion rate the smaller the maximum potential change for

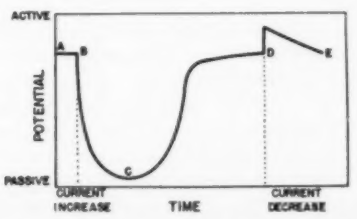

Fig. 4. Generalized anodic voltage transient observed with magnesium.

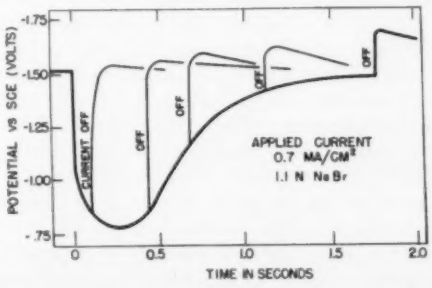

Fig. 5. Activation of potential on removing the applied anodic current as a function of the fraction of transient completed.

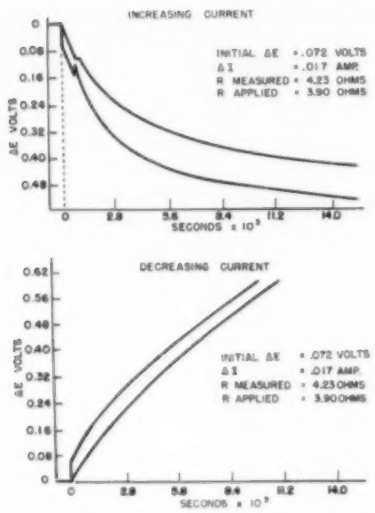

Fig. 6. Initial portion of the anodic voltage transient: (a) on closing the circuit; (b) on opening the circuit.

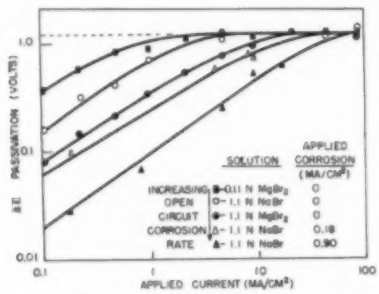

Fig. 7. Maximum potential change, passive direction, observed as a function of the applied current density at several corrosion rates.

a given applied current. This is to be expected since in the absence of applied current the effective anode area is directly proportional to the corrosion current, Eq. [8]. Thus, the greater the corrosion current, the greater the effective area and the lower the transient polarization resulting from a given applied current. Within the limits of our experimental methods the relationship

$$\Delta E = k_t \log (i_a + i_b)/i_b \qquad [9]$$

(i_a is applied current, i_b is observed corrosion current) reasonably represents the data obtained. Considerable scatter would be expected in a plot of these data (Fig. 8) since the i_b used is either the average observed corrosion current obtained from a 7-day corrosion test or the sum of this rate and an applied corrosion current. It is not to be expected that the instantaneous corrosion rate after 20 min immersion would be the same as that averaged over a week, and our experience has shown a marked time dependence of the corrosion rate in $MgBr_2$ solutions.

The magnitude of the transient potential change at any given applied current should be dependent on the relative rates of polarization and film breakdown. While both of these rates in a given environment tend to increase with increasing applied cur-

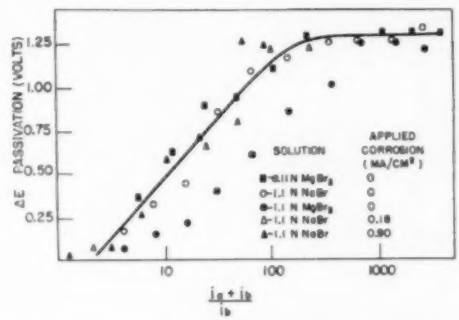

Fig. 8. Maximum potential change, passive direction, as a function of log $i_a + i_b/i_b$.

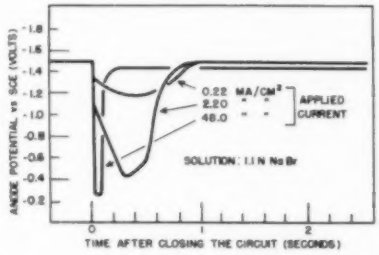

Fig. 9. Observed transients at various applied currents in 1.1N sodium bromide solution.

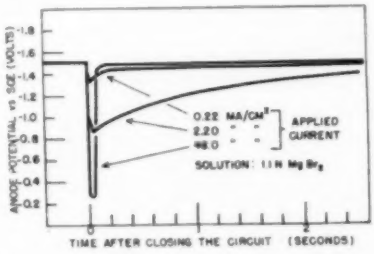

Fig. 10. Observed transients at various applied currents in 1.1N magnesium bromide solution.

rents, they need not increase at the same rate. The explanation for the plateau region observed, Fig. 8, probably lies in differences in these rate changes. The interaction between these rate changes undoubtedly also explains the varying shapes of the observed transients. In Fig. 9 and 10, transients are shown for varying applied currents under constant corrosion conditions and in Fig. 11 for varying corrosion rate at constant applied current. These curves appear to be members of a rather well behaved family. Within the limits of the data, the following observations arise from these curves. At approximately the same $(i_a + i_b)/i_b$ where the maximum polarization reaches a plateau, Fig. 8: (*a*) the number of millicoulombs passed during the passivation portion of the transient reaches a constant value of roughly 0.8; (*b*) the total transient time passes through a maximum; and (*c*) the magnitude of the activation of potential upon switching out of the applied current also reaches a plateau, Fig. 12. We do not believe that it is coincidence that all these transitions occur at the applied current which would tend to swamp out the corrosion current and in the case

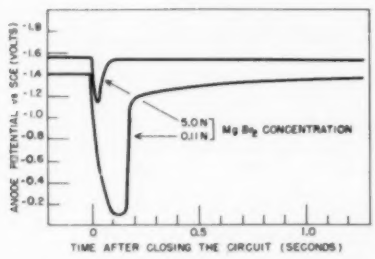

Fig. 11. Observed transients at an applied anodic current of 4.8 ma/cm² with two magnesium bromide concentrations.

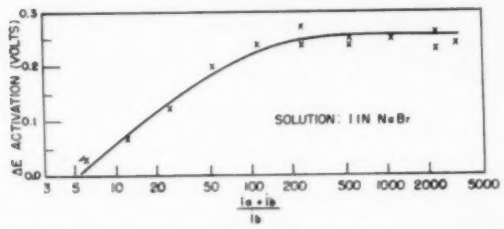

Fig. 12. Maximum potential change, active direction, on removing i_a, as a function of $(i_a + i_b)/i_b$.

of the activation plateau, a possible explanation is available.

The total weight loss at a magnesium anode (i_t) can be represented as the sum of the applied and local action currents and the excess weight loss caused by the applied current $i_t = k_2 i_a$ as defined by Eq. [4].

$$i_t = i_a + k_2 i_a + i_b \qquad [10]$$

The instant after the applied current is removed

$$i_t = k_2 i_a + i_b \qquad [11]$$

Since film repair has not yet occurred, Eq. [7] can be combined with Eq. [11] to give

$$i_t/A = k_2 + k_2/k_3\, i_b/i_a \qquad [12]$$

When i_a is very much larger than i_b, Eq. [9] simplifies to

$$i_t/A = k_2 \qquad [13]$$

Thus a limit should be reached in the magnitude of the potential activation as the increasing anodic current is removed.

Conclusions

1. Magnesium behaves electrochemically in a predictable manner.

2. The electrochemical behavior of magnesium can be satisfactorily explained solely on the basis of divalent ion formation.

3. The magnesium hydroxide film on magnesium in aqueous environments is extremely protective but quite responsive to electrochemical and environmental changes. This fact, coupled with the very negative reversible potential of magnesium, leads to film control of its electrochemistry in aqueous environments.

4. Where the protective $Mg(OH)_2$ film is damaged, magnesium reacts directly with water in a fashion comparable to the reaction between sodium and water. Such damage occurs from applied current as a result of the build-up of magnesium ion concentration at the anode interface.

5. The invariance of the steady-state potential, with applied anodic current, occurs only in environments containing anions capable of forming soluble magnesium salts. This phenomenon occurs because the effective area is proportional to the applied current and thus the effective current density is invariant.

6. The potential transients produced by changes in the applied anodic current are due to variations in the magnitude of the polarization resulting from transitory changes in the effective current density.

Acknowledgment

The authors are indebted to H. A. Robinson, L. Sturkey, and Dr. M. R. Bothwell for many helpful discussions and criticisms during the course of this work.

Manuscript received June 3, 1960. This paper was prepared for delivery before the Ottawa Meeting, Sept. 28-Oct. 2, 1958.

Any discussion of this paper will appear in a Discussion Section to be published in the December 1961 JOURNAL.

REFERENCES

1. O. Gatty and E. C. R. Spooner, "The Electrode Potential Behavior of Corroding Metals in Aqueous Solutions," p. 424, Oxford, at the Clarendon Press (1938).
2. H. A. Robinson, *Trans. Electrochem. Soc.*, **96**, 499, (1946).
3. R. C. Kirk and A. B. Fry, *J. (and Trans.) Electrochem. Soc.*, **94**, 277 (1948).
4. L. Whitby, *Trans. Faraday Soc.*, **29**, 1318 (1933).
5. U. R. Evans, "Metallic Corrosion, Passivity, and Protection," 2nd ed., Edward Arnold & Co., London (1946).
6. R. E. McNulty and J. D. Hanawalt, *Trans. Electrochem. Soc.*, **81**, 423 (1942).
7. M. E. Straumanis and Y. N. Wang, *This Journal*, **102**, 304 (1955).
8. M. E. Straumanis, *ibid.*, **105**, 284 (1958).
9. R. Glicksman, *ibid.*, **106**, 85 (1959).
10. E. J. Casey and R. E. Bergeron, *Can. J. Chem.*, **31**, 849 (1953).
11. N. D. Tomashov, V. S. Komissarova, and M. A. Timonova, *Trudy Inst. Fiz. Khim, Akad Nauk SSSR*, No. 5, Issledoran, Korrozii Metal No. 4, 172 (1955).
12. R. L. Petty, A. W. Davidson, and J. Kleinberg, *J. Am. Chem. Soc.*, **76**, 363 (1954).
13. D. V. Kokoulina and B. N. Kabanov, *Doklady Akad Nauk SSSR*, **112**, 692 (1957).
14. G. R. Hoey and M. Cohen, *This Journal*, **105**, 245 (1958).
15. R. Glicksman and C. L. Morehouse, *ibid.*, **102**, 273 (1955).
16. W. Feitknecht and M. Gerber, *Helv. Chim. Acta*, **25**, 131, 555 (1942).
17. W. Feitknecht and F. Held, *ibid.*, **27**, 1480 (1944).

Cyclic Photogalvanic Silver Halide Cells

S. Zaromb, M. E. Lasser, and F. Kalhammer

Research Division, Philco Corporation, Philadelphia, Pennsylvania

ABSTRACT

In order to distinguish between photoconductive or photocatalytic and "truly photogalvanic" effects, continuous photocurrent measurements were performed on cyclic Pt, Ag-AgCl, aqueous $FeCl_2$-$FeCl_3$, Pt and Pt, Ag-AgBr, aqueous $FeBr_2$-$FeBr_3$, Pt batteries in a state of nearly complete discharge. These batteries could be partly recharged by light of wave lengths shorter than 4300Å and 4800Å, respectively, with maximum photogalvanic quantum yields of 2-5%. These yields varied mainly with method of electrode preparation, electrolyte composition, and light wave-length, but not with light intensity for intensities equivalent to usual solar radiation levels. Direct recombination of photochemical reaction products, corrosion of Ag by an oxidant in the electrolyte, and electrode impedance and polarization effects were the main current limiting factors.

Photogalvanic Quantum Yield Studies

Since Becquerel (1) first discovered the photogalvanic effect, hundreds of papers on the subject appeared in the scientific literature (2, 3). However, most of these have dealt with open-circuit photopotentials rather than photocurrents. Although the former can offer interesting clues as to the type of photochemical products formed, if any, it is still essential for any practical photogalvanic cells and also for any thorough understanding of the kinetics of the photogalvanic process to obtain values of (*a*) the quantum yields of the individual photochemical reaction steps and (*b*) the net yields of the current that can be delivered for a given light input. Whereas the latter yields have been determined easily for dry photovoltaic cells such as the Si solar cells, there exist difficulties in measuring them in most photogalvanic systems.

To appreciate these difficulties it is necessary to distinguish at this point between those systems which in the dark: (*a*) are in or near a thermodynamic equilibrium and in which the light either gives rise directly to products dischargeable through a battery circuit or else generates an emf capable of producing chemical changes by electrolysis; and those which (*b*) are not in true thermodynamic equilibrium and in which the light catalyzes an otherwise extremely sluggish reaction or else accelerates the discharge of a battery by a photoconductive and/or depolarizing effect. Unfortunately, the systems for which photocurrent measurements have been reported seem to fall into group (*b*) (4-6). Furthermore, the term photocurrent (defined as the increase in current delivered by a cell when the potential of the illuminated electrode is returned to the value in the dark by applying or adjusting an external voltage (4, 5) does not distinguish between current generated by a photovoltage and that due to photoconductivity.

Let us consider for example a battery having an open circuit emf E_d in the dark and which comprises one electrode covered by a photosensitive material which also forms a current-limiting layer having a very high resistance R_d. When this electrode is illuminated, the current may increase from the value in the dark

$$I_d \cong E_d/R_d \qquad [1]$$

to a much higher value

$$I_l \cong E_d/R_l \qquad [2]$$

in light, due solely to a photoconductive effect. Now, it is known that photoconductors can have gains higher than one (7), *i.e.*, one photon of light may allow passage of hundreds of electrons when an electric field is applied across the photoconductor. Thus one may obtain deceptively high values for the photogalvanic quantum yields with batteries which would normally deliver a current in the dark, no matter how small (either spontaneously or with the aid of an external polarizing voltage), having the same polarity as the observed photocurrent.

Equations [1] and [2] describe essentially a conversion of chemical into electrical energy accelerated by light. If the term catalysis is generalized to include every type of acceleration of electrode discharge reactions, then Eq. [1] and [2] can be considered as describing a special form of the photocatalytic effect, and the current I_l can be considered as a "photocatalytic" rather than "photogalvanic" current. This objection seems to apply to the few reported photocurrent measurements in electrolytic systems (4-6).

On the other hand, in systems of group (*a*) the dark current I_d may again be described by Eq. [1]; however, its low value must be associated with a low value of E_d rather than with a high R_d. The current could then increase to a higher value

$$I_l \cong E_l/R_d \qquad [3]$$

due to a photogenerated emf. Since the latter implies actual conversion of light into electrical energy, Eq. [3] describes a truly photogalvanic current.

In frequent cases, however, both the emf and the resistance may change with illumination so that

$$I_i \cong E_i/R_i \qquad [4]$$

The distinction between the photoconductive and the truly photogalvanic effects may then pose a problem. Of course, when E_i and E_d have opposite polarity, then I_i must represent a truly photogalvanic current regardless of the value of R_i. However, even in batteries having an emf in the dark of the same sign as in light, it should be possible, in principle, to measure truly photogalvanic currents by a method of exhaustion, *i.e.*, by starting with a very limited quantity of reducible and/or oxidizable components and drawing much more current over a long period of time than could have been delivered by complete discharge with 100% current efficiency. Obviously, the method of exhaustion will be most sensitive when a battery can be completely discharged at the start of the illumination or, what is tantamount but simpler, when the battery is assembled with the discharge products replacing at least one essential but missing reactant.

If a completely discharged battery can deliver appreciable current upon illumination, then the light apparently effects at least a partial regeneration of the battery reactants. These regenerated reactants thus undergo *cyclic* chemical changes.

In the present work, the photogalvanic quantum yield Y_p is defined as the ratio of the number of electrons N_e caused to go around an external circuit per number of absorbed photons N_{ph} in a *cyclic* photogalvanic cell.

$$Y_p = (N_e/N_{ph})_{cyclic} \qquad [5]$$

For the most unambiguous measurements, the cell should have an initial open-circuit voltage in the dark close to zero or possibly even of a sign opposite to that observed upon illumination. It is not necessary that the cell voltage reverse or disappear when illumination is discontinued. In fact, it is preferable for the cell to have a certain ability to store the charge and emf generated by the light. However, one of the criteria for a truly light-induced current is a marked increase of emf from a negligibly low value or complete reversal of polarity upon illumination of the initially assembled cell.

A review of previously reported truly photogalvanic systems suggests that the photogalvanic currents are usually both transient and extremely low (*i.e.*, less than 1 μa) because of the absence of provisions for effective cyclic utilization and regeneration of reaction products. For instance, Becquerel's photogalvanic cells (1) consisted essentially of one bare Pt electrode and one Pt electrode covered with AgX (X = I, Br, or Cl) both immersed in the same electrolyte solution. However, the halogen formed in the photochemical reaction

$$AgX + h\nu \rightarrow Ag + 1/2\,X_2 \qquad [6]$$

cannot diffuse to the bare Pt electrode at a sufficiently high rate to give rise to appreciable electrode discharge reactions, because appreciable diffusion of the X_2 would require a rather high concentration of X_2 near the AgX. This would be difficult (if not impossible) to achieve by illumination on account of the tendency for the X_2 to recombine with the photolytically formed Ag.

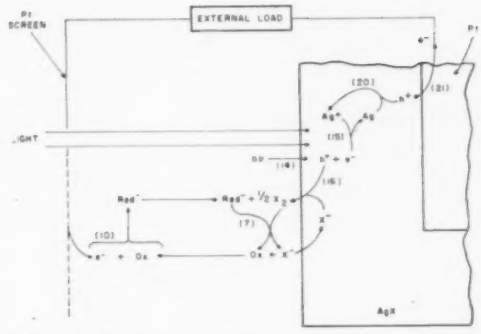

Fig. 1. Discharging and photochemical charging reactions at the electrodes of the cell.

The present studies are aimed at the development of cyclic photogalvanic cells and of methods of maximizing the quantum yield Y_p. A preliminary survey (8) led to the choice of photogalvanic cells based on reaction [6].

Cyclic Silver Halide Photogalvanic Cells

Photochemical charging and discharging reactions (Fig. 1).—In the present work, the cells differ from the Becquerel cell in that they contain in addition the components Red^- and Ox of a suitable reduction-oxidation couple which can remove the X_2 at the AgX-electrolyte interface via the reaction

$$1/2\,X_2 + Red^- \rightarrow Ox + X^-$$

$$E_7 = E_7^\circ - (RT/\mathbf{F})\ln\frac{(X^-)\quad(Ox)}{(Red^-)\,(X_2)^{1/2}} \qquad [7]$$

where the symbols in parentheses represent the activities of the respective components.

The net result of reactions [6] and [7] is then

$$h\nu + AgX + Red^- \rightarrow Ag + X^- + Ox \qquad [8]$$

which can be considered as a photochemical recharging of an Ag-Ox battery completely discharged via the reactions

$$AgX + e^- \rightleftharpoons Ag + X^-$$

$$E_9 = E_9^\circ - (RT/\mathbf{F})\ln(X^-) \qquad [9]$$

and

$$Ox + e^- \rightleftharpoons Red^- \quad E_{10} = E_{10}^\circ + (RT/\mathbf{F})\ln\frac{(Ox)}{(Red^-)} \qquad [10]$$

yielding an over-all discharge reaction

$$Ox + Ag + X^- \rightarrow Red^- + AgX \quad E_{11} = E_{10} - E_9 \qquad [11]$$

which is the reverse of reaction [8].

In order for the cell to be cyclic, the discharge reaction should occur spontaneously, *i.e.*, E_{11} should be positive. Furthermore, in order for reaction [7] to occur, it is necessary that the potential E_{12} for the reaction

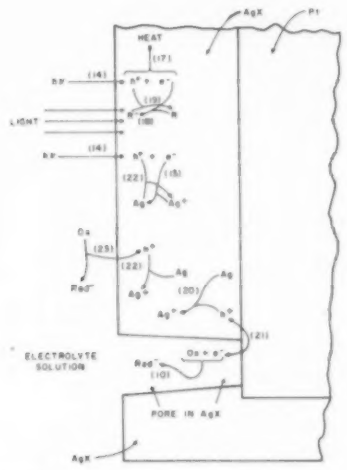

Fig. 2. Wasteful recombination mechanisms at the Pt-AgX electrode.

$$1/2\ X_2 + e^- \rightarrow X^-$$
$$E_{12} = E_{12}^\circ - (RT/F)\ln\ (X^-)/(X_2)^{1/2} \qquad [12]$$

be higher than E_{10}. Hence

$$E_0 < E_{10} < E_{12} \qquad [13]$$

which is a basic limitation on the choice of the $Red^- - Ox$ couple.

Competing wasteful reactions (Fig. 2).—Reaction [6] can be considered to be composed of the basic electronic process

$$h\nu \rightarrow e^- + h^+ \qquad [14]$$

where e^- and h^+ are electrons and holes, respectively, followed by

$$e^- + Ag^+ \rightarrow Ag \qquad [15]$$

and

$$h^+ + X^- \rightarrow 1/2\ X_2 \qquad [16]$$

as shown in Fig. 1

This suggests the possibility of several wasteful recombination reactions shown in Fig. 2

$$e^- + h^+ \rightarrow \text{heat} \qquad [17]$$

or, what is more likely,

$$e^- + R \rightarrow R^- \qquad [18]$$

followed by

$$R^- + h^+ \rightarrow R \qquad [19]$$

where R, R^- may be an impurity or lattice defect acting as a center for the recombination of holes with electrons.

On the other hand, the useful discharge reaction step [9] can also be regarded as the sum of

$$AgX \leftarrow Ag + h^+ + X^- \qquad [20]$$

and

$$e^- = -h^+ \text{ (at Pt-AgX interface)} \qquad [21]$$

where the h^+ originates at the Pt electrode as shown in Fig. 1. The last two steps must be differentiated on the one hand from the following wasteful reactions shown in Fig. 2

$$h^+ + Ag \rightarrow Ag^+ \qquad [22]$$

or

$$\text{Ox (at AgX-electrolyte interface)} \rightarrow Red^- + h^+ \qquad [23]$$

followed by reaction [22], where the h^+ originates from reaction [14] or [23], and on the other hand from the sequence of reactions [10], [20], and [21] all occurring at the Pt-AgX electrode in case of porosity of the AgX film, as shown at the bottom of Fig. 2. All these wasteful reactions represent short-circuiting paths for the recombination of e^- with h^+ without passage of the e^- through an external circuit.

Other current-limiting factors.—Even in the absence of the above parasitic reaction mechanism, the current density is limited by the resistance across the AgX film and by concentration and electrode polarization effects.

Attempts to reduce these limitations introduces other difficulties, *e.g.*, thinner films of AgX will have lower resistance, but they also form the short-circuiting pores considered in the preceding section. Furthermore, an appreciable fraction of the useful radiation of wave lengths approximating the absorption edge of the AgX may be lost by the thinner films but absorbed and converted into useful currents by the thicker ones. Similarly, concentration polarization effects are reduced with high (Ox) concentrations, but these accelerate the parasitic reaction (23).

Experimental Procedure

Optical system.—The optical arrangement is shown schematically in Fig. 3. Light from a 30-w microscope lamp having a color temperature of 2400°-2700°K was focused onto an area of 1-2 cm^2 of the Pt-AgX electrode g by means of the hemispherical mirror m and the condensing lens C. Most of the infrared radiation was absorbed by the water filter W. Filters B and D could be of the narrow-band interference type for experiments with monochromatic radiation, neutral density filters for studies with varying light intensities, or Wratten filters for cutting out some of the longer or shorter wave length components in special orienting experiments.

Relative light intensity measurements were performed with the photocell P located behind the transparent cell E. Absolute light intensity meas-

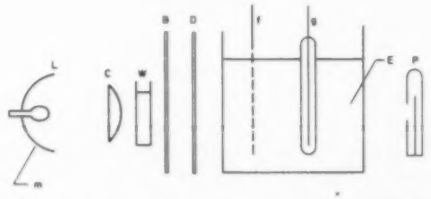

Fig. 3. Optical system for photogalvanic quantum yield measurements. Light from the 30-w microscope lamp L is focused by means of the adjustable reflecting mirror m and condensing lens C onto the Pt-AgX electrode g. Intensity and composition of the light are adjusted by means of the water filter W and interchangeable filters B and D. Phototube P located behind the test cell E measures relative light intensities when electrode g is temporarily removed.

urements were obtained by focusing the light source on a previously calibrated photovoltaic Si cell about 1 x 2 cm^2 in area (not shown in Fig. 1).

Test cell assembly.—The test cell E was a square transparent Lucite box with an outer jacket containing circulating water from a thermostat bath at 25°C. Electrode f was a 52 mesh Pt gauze made of 0.004-in. diameter wire, transmitting about 60-70% of the impinging radiation. Electrode g was prepared by abrading the surface of a 0.002-in. thick Pt foil with grade 320 emery paper, etching in aqua regia, rinsing, immersing in molten AgX contained in a porcelain crucible at about 500°C and slowly withdrawing the Pt while allowing the edge of the Pt to touch the crucible.

The resulting films of AgX over the Pt surface were well-adhering, about 5-20μ thick, and impervious to the electrolyte. The latter consisted of solutions of 0.001-0.1 (usually 0.01) M $FeCl_2$ plus 0.01-1 (usually 0.2) M HCl in experiments with Pt-AgCl electrodes, and of 0.01M NaBr plus 0.005M $FeSO_4$ with Pt-AgBr. The ratio of Fe^{+2} to Fe^{+3} ions was maintained nearly constant in some experiments by addition of $FeCl_3$ complexed with an excess of HF.

All reagents were of analytical grade. The AgCl was Baker Analyzed reagent, whereas the AgBr was prepared by precipitation of 0.2M $AgNO_3$ solutions with either 0.2M NaBr or 0.2M HBr.

Electrical measurements.—A model 153 X 12V-X-6 25-mv Brown potentiometer recorded the voltage drop across one of two resistance boxes connected in series with the test cell electrodes f and g of Fig. 1. Current-sensitivity and total external resistance could be adjusted at will by means of the two resistance boxes.

Internal cell resistances were not measured by means of the usual alternating current bridge method, in order to remove the possibility of any net charging effects resulting from the application of an external alternating voltage. Instead, the internal cell resistances were deduced from a series of current measurements with varying external resistances in the high external resistance range (10-100 kilo-ohms), where the current output was low enough to eliminate polarization effects. The same measurements also yielded the values of open-circuit cell voltage, which agreed with readings of a 10-megohm vacuum-tube voltmeter. On the other hand, the quantum yield measurements usually involved relatively low external resistances (10-100 ohms).

Photochemical quantum yield measurements.—The yields of reaction [8] were also measured by purely chemical methods. A beaker containing a stirred mixture of 4 g powdered AgX and 100 cc of 0.001M FeX_2 plus 0.02M HX was illuminated with the above mentioned 30-w microscope lamp for 1-10 min intervals. The powder was then allowed to settle and 10-cc samples of the solution were withdrawn and analyzed for Fe^{+2} ions by a permanganimetric method (9). Control titrations were also performed on samples from mixtures stirred in the dark and from illuminated mixtures of 4 g Cr_2O_3 with the same solution, to correct for any air oxidation of Fe^{+2} ions. The rates of conversion of Fe^{+2} to Fe^{+3} ions in the control experiments were negligibly low in comparison with those observed upon illumination of the AgX.

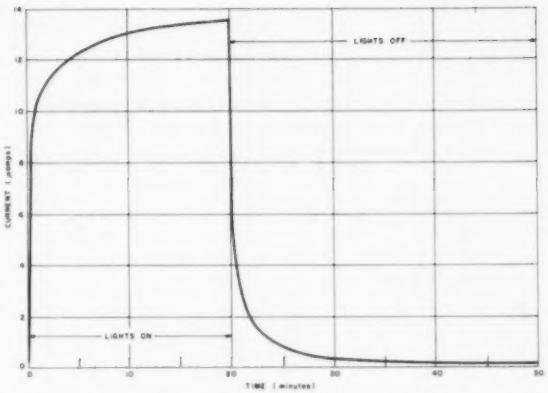

Fig. 4. Typical changes of current delivered by a Pt-AgCl, $FeCl_2$, Pt cell with and without illumination.

Experimental Results

The discharge characteristics of a typical Pt-AgCl, $FeCl_2$, Pt cell are shown in Fig. 4 Upon illumination of the Pt-AgCl electrodes in initially assembled test cells, the open-circuit emf rose from values of less than 50 mv to a value of about 0.4 v corresponding to the emf of an Ag-AgCl-$FeCl_2$-Pt battery. This satisfies, then, one basic criterion proposed near the end of the section on Photogalvanic quantum yield studies. Furthermore, the slow continuous rise in current and voltage over a period of more than 10 min indicates a gradual build-up of photochemical reaction products. Finally, a most convincing proof of true photochemical charging was obtained by illuminating the cells for varying time intervals while on open circuit and integrating the total current that could be withdrawn in the dark immediately following the illumination. The plot of charge withdrawn vs. time of illumination is linear (Fig. 5), in agreement with the charging reactions of the section on Photochemical charging and discharging reactions.

The electrodes used for the results of Fig. 5 were among the earliest and least efficient ones, yielding an average current of less than 10μa during continuous illumination. In order to optimize the current yields, the thickness of the AgCl-layers and

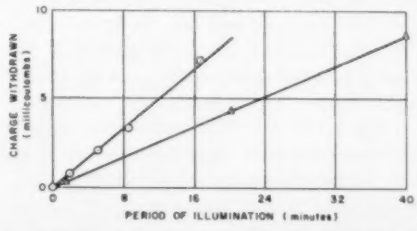

Fig. 5. Charge withdrawn from two different Pt-AgCl electrodes after various periods of illumination.

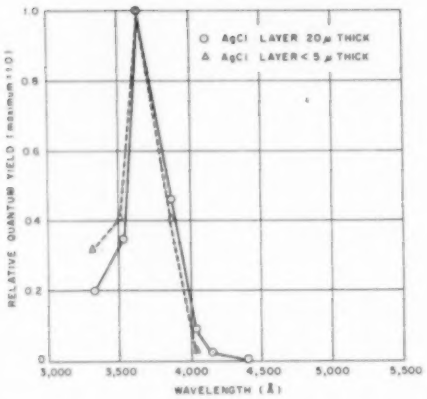

Fig. 6. Relative dependence of the photogalvanic quantum yield from Pt-AgCl electrodes on wavelength.

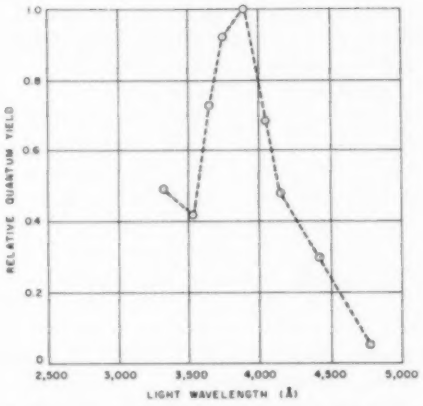

Fig. 7. Relative photogalvanic quantum yields from Pt-AgBr electrodes with light of various wave lengths.

composition of the solution were varied. Using a 1/100M solution of $FeCl_2$ which was approximately 1/1000M in $FeCl_3$, charging currents of up to 80μa for a short period of time and up to 40 μa for several hours were obtained when the AgCl layers were 5-20 μ thick.

With thinner layers, higher porosity and lower light absorption led to a lower efficiency whereas with thick layers ($> 20\mu$) the high impedance of the Pt-AgCl electrode limits the current. With carefully prepared electrodes (cf. section on test cell assembly), porosity was avoided, internal cell resistances ranged from 5 to 20 kilo-ohms, and results were reproducible within a factor of 2.

The best results obtained correspond to quantum yields of 2-5% for light of wave lengths shorter than 4000Å. The relative sensitivity of two Pt-AgCl electrodes to various wave lengths is shown in Fig. 6.

By varying the intensity of illumination with neutral density filters, it was found that the current yield increased linearly with intensity, showing no sign of any intensity saturation effect with the light source used.

With Pt-AgBr electrodes, the voltage and current changes upon illumination were small and usually in a direction opposite to that expected by the reaction scheme of the section on Photochemical charging and discharging reactions, when the AgBr was prepared from NaBr and $AgNO_3$ solutions. However, with AgBr prepared from HBr and $AgNO_3$ solutions, both the polarity of the photo-induced voltage and the photogalvanic quantum yields were comparable to those obtained with AgCl. Furthermore, since the fraction of light from tungsten at 2600°K absorbed by AgBr is about four times larger than the fraction absorbed by AgCl, the actual photogalvanic currents with the same illumination were correspondingly increased by a factor of three to four. With monochromatic light of various wave lengths, the relative photogalvanic quantum yields varied as shown in Fig. 7.

When exposed to the white light of a microscope lamp the AgBr electrodes showed a change of color and a simultaneous decrease in photogalvanic efficiency within a few hours. It is known (10) that light of wave lengths longer than the absorption edge may disperse the photolytically formed Ag, forming an Ag colloid with an absorption band extending into the intrinsic absorption region of the AgX. This colloid may decrease the amount of light available for photolytically active absorption. Furthermore, the colloidal Ag may accelerate hole-electron recombination via the reaction steps [15] and [22] (cf. Fig. 2).

This possibility was partly confirmed when filtered light in the range of 3300-4400Å was used for illumination of the AgBr. Almost no color change could be observed under steady-state conditions, and the photolytic sensitivity of the electrodes decreased only after a few days, this decrease being probably due to the formation of pores.

It is noteworthy that the spectral sensitivity curves for both AgCl and AgBr (Fig. 6 and 7) show maximum quantum yields for wave lengths just below the absorption edges of the respective halides. To explain the decrease in quantum yield with decreasing wave lengths one may assume that the latter, being highly absorbed at the surface of the AgX, result in the formation of Ag near the AgX-electrolyte interface where re-oxidation by Fe^{+3} ions is relatively fast. Evidence for this kind of recombination is given in Fig. 8 and 9. In Fig. 8, 80% of the charge formed by illumination of a Pt-AgCl, $FeCl_2$, Pt cell for 8.5 min is shown to disappear within 20

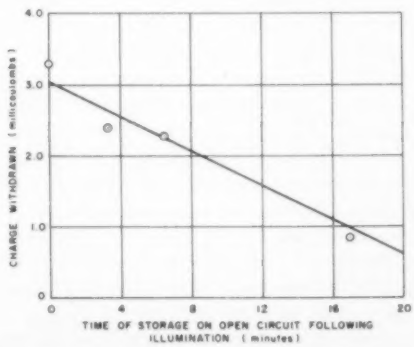

Fig. 8. Loss of charge during open circuit storage

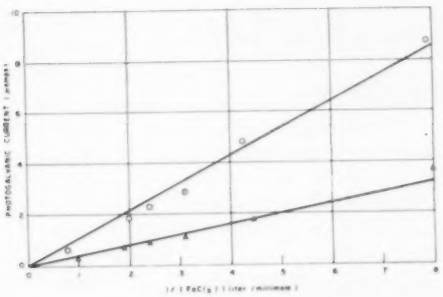

Fig. 9. Inverse proportionality of photogalvanic current to the $FeCl_3$ concentration observed with two Pt-AgCl electrodes.

min. In Fig. 9, the photogalvanic current is found to be inversely proportional to the Fe^{+3} ion concentration, for concentrations above 10^{-4}M $FeCl_3$.

Whereas the photogalvanic quantum yields were usually less than 5% with both Pt-AgCl and Pt-AgBr electrodes, the photochemical quantum yields for the conversion of Fe^{+2} to Fe^{+3} ions by illumination of both AgCl and AgBr powders (cf. section on Photochemical quantum yield measurements) were 50-100%. These high yields may be attributed partly to the absence of the stringent electrochemical requirements for the delivery of useful photogalvanic currents and partly to the large effective surface area of the powdered AgX with a corresponding low surface density of photochemically formed Ag taking part in wasteful recombination reactions.

Conclusions

Partial photochemical charging of Pt-Ag-AgX, aqueous FeX_3, Pt cells was achieved with maximum photogalvanic quantum yields of 2-5% in cells remaining in a state of nearly complete discharge.

In partly charged batteries, i.e., containing more than 10^{-4}M FeX_3 or an appreciable surface concentration of Ag, direct attack of the Ag by Fe^{+3} ions appreciably reduces the photogalvanic quantum yields in direct proportion to the Fe^{+3} ion concentration. When the latter reaches or exceeds 0.001M, the quantum yield may be reduced by a factor of ten or more. On the other hand, for Fe^{+3} ion concentrations below 10^{-4}M the photogalvanic current is severely limited by concentration polarization at the Pt-FeX_3 electrode. The optimum Fe^{+3} ion concentration is therefore limited to the fairly narrow range of 10^{-3} to 10^{-4}M.

However, the most serious drawback of these cells is the deterioration observed after 1 to 5 days of illumination, attributable mainly to the development of pores in the AgX film (cf. Fig. 2).

Whereas the last difficulty applies only to AgX-covered Pt electrodes, the problem of diffusion-limited current with low photochemical product concentrations and of recombination with higher concentrations is likely to be encountered in most photogalvanic systems. Some approaches toward a solution of this problem are to be presented in a later publication.

Acknowledgments

Thanks are due to Drs. N. Winogradoff, J. O'M. Bockris, and Gerald Oster for fruitful discussions and to Mr. W. Jann for help in the performance of the experimental work.

Manuscript received April 12, 1960.

Any discussion of this paper will appear in a Discussion Section to be published in the December 1961 JOURNAL.

REFERENCES

1. E. Becquerel, *Compt. rend.*, **9**, 561 (1839).
2. A. W. Copeland, O. D. Black, and A. B. Garrett, *Chem. Rev.*, **31**, 177 (1942).
3. K. M. Sancier, Trans. Conf. Use of Solar Energy, **V**, p. 43-56, University of Arizona Press (1958).
4. H. Luggin, *Z. physik. Chem.*, **23**, 577 (1897).
5. V. I. Veselovsky, *J. Phys. Chem. (U.S.S.R.)*, **22**, 1302 (1948).
6. A. Goldman and J. Brodsky, *Ann. Physik*, **44**, 849 (1914); C. G. Fink and D. K. Adler, *Trans. Am. Electrochem. Soc.*, **58**, 175 (1930).
7. A. Rose, *Proc. I.R.E.*, **43**, 1850 (1955).
8. M. E. Lasser, S. Zaromb, and F. Kalhammer, Proc. 13th Ann. Power Sources Conf., p. 66-68, (Power Sources Div., U.S. Army Signal R and D Lab., Ft. Monmouth, N. J. (1959).
9. I. M. Kolthoff and E. B. Sandell, "Textbook of Quantitative Inorganic Analysis," p. 592, Macmillan Co., New York (1946).
10. C. E. K. Mees, "The Theory of the Photographic Process," p. 285, Macmillan Co., New York (1946).

The A-C Properties of Tantalum Solid Electrolytic Capacitors

D. A. McLean

Bell Telephone Laboratories, Incorporated, Murray Hill, New Jersey

ABSTRACT

The two basic elements in the dissipation factor of tantalum solid electrolytic capacitors are tan δ', the substantially frequency independent dissipation factor of the tantalum oxide, and R_s, the lumped effective resistance of MnO_2 or other series constituents. These elements can be separated and evaluated from measurements at two frequencies. Use of such evaluation in applied research is illustrated. The value of R_s is related analytically to the resistivity of the MnO_2 network and the dimensions of an idealized right cylindrical porous capacitor structure. Variation of capacitance with frequency for a large number of commercial capacitors was found to be related to tan δ' in a way proposed in the literature for anodic oxides.

The tantalum solid electrolytic capacitor (1) is a relatively new component which is enjoying increasing use but which is still under active development. It is important to understand the measured electrical characteristics of these capacitors for purposes both of analyzing the results of research and development investigations and of applying logical requirements to manufactured products.

Attempts to evolve equivalent circuits to represent the a-c behavior of conventional wet electrolytic capacitors have met with only moderate success owing to limitations of the theories and to vagaries of the capacitors themselves. The tantalum solid capacitor is simpler and more reproducible, and has superior a-c properties, offering hope for better understanding. This is a significant advantage of this capacitor, since analytical methods can be evolved to aid in interpreting experimental values. The purposes of this paper are to propose explanations of some of the principal a-c properties of tantalum solid capacitors, to confirm these explanations with experimental data, and to apply the proposed analysis to several development studies. Within limits, the methods advanced can be applied to aqueous electrolyte types to aid in understanding these capacitors also.

This paper deals primarily with power dissipation under a-c stress and secondarily with capacitance. Several terms are commonly used to express the dissipation in capacitors, the principal ones being defined in Fig. 1. All of these express in one way or another the phase relation between current and voltage. The value of dissipation factor, or "tan δ," is the most convenient for treating the material given here. Reference is made also to "effective series resistance" which is the hypothetical lumped resistance required to produce the observed dissipation. Many bridges for measuring capacitors give directly the capacitance and either the dissipation factor or the effective series resistance.

All measurements reported in this paper were made without d-c bias and with an applied a-c voltage of a fraction of a volt rms at balance. Studies have shown that the application of a bias to solid electrolytic capacitors has only a very small effect on the a-c properties and would not alter the conclusions reached herein. Figure 2 shows values of capacitance, effective series resistance and tan δ as

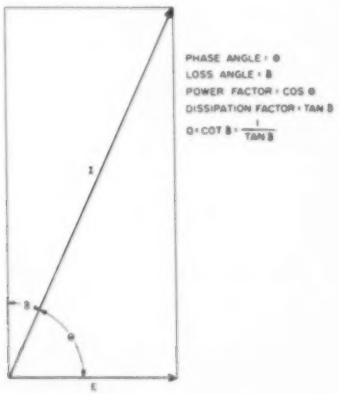

Fig. 1. Relationship of terms commonly used to define dissipation in capacitors.

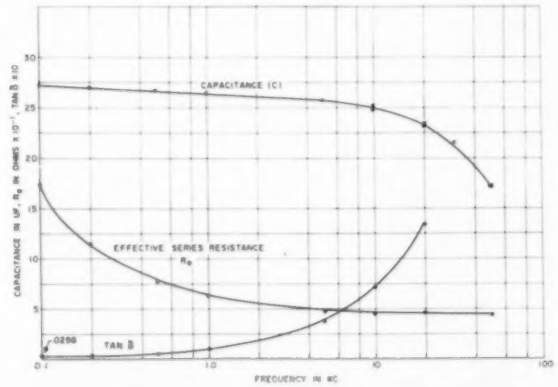

Fig. 2. Typical frequency dependence of a-c properties of porous tantalum solid electrolytic capacitors.

a function of frequency for a 25 UF, 35 v capacitor. The general behavior is typical of all capacitors of this type, but the frequency at which the capacitance falls off rapidly shifts with capacitor size, porosity, and other composition and processing factors.

The scope of this paper is limited to frequencies below those at which capacitance falls off steeply, which is the normal region of practical capacitor measurements. In this region, the a-c properties can be discussed in simple terms of lumped constants, whereas at higher frequencies more complex analysis based on distributed parameters is required. The applicable range of the present discussion for the capacitor of Fig. 2 is up to 10-20 kc.

Equivalent circuit.—The equivalent circuit suggested to explain the most important a-c characteristics is shown in Fig. 3. Each of the elements in this circuit has a definite physical significance.

The losses consist of two types: the dielectric loss of the dielectric itself, and dissipation in the series resistance residing mainly in the MnO_2 semiconductor, but including also any carbon coat, metal layers, and leads. These two types of loss are represented by two series resistances, R_1 and R_2, respectively. Considering first the dielectric loss produced in a hypothetical R_1, it is apparent from Fig. 2 and from other voluminous data that at the lowest frequencies tan δ is relatively independent of frequency. This is the region where dissipation in the dielectric predominates. Variation in tan δ in this region is extremely small compared to that which would be produced by a true series resistance such as R_2 or by a parallel leakage path. Furthermore, the values of tan δ at the lowest frequencies are relatively independent of geometry and capacitance and therefore must be a property of the oxide film. The low-frequency values of tan δ are, however, somewhat dependent on tantalum purity and structure and on processing steps, as might be expected since these are likely to influence the quality of the dielectric. Figure 4 shows the values of capacitance and tan δ for 0.1 UF wire-anode capacitors where the geometry is especially favorable to low series losses in R_2 and hence where only dielectric loss is involved. Over a thousandfold range in frequency, tan δ varies only about twofold, ignoring one 100 kc value. Purifying the surface by etching decreases the dissipation factor by a much greater factor than this. Hence it is a useful approximation to say that the loss in the dielectric, which shall be called tan δ′, is independent of frequency.

Tantalum oxide is not unique in exhibiting substantial independence of tan δ′ with frequency. This

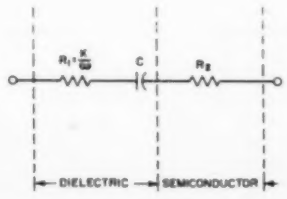

Fig. 3. Proposed equivalent circuit of tantalum solid electrolytic capacitors.

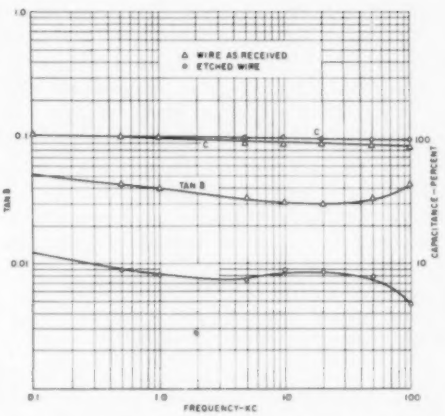

Fig. 4. Dependence of capacitance and tan δ on frequency. Tantalum wire solid electrolytic capacitors. 0.10 UF.

property has been observed and discussed for many years on a wide variety of ceramics, glasses, and organic polymers (2-5). No entirely satisfactory explanation has been advanced, but for the most part theories which have been proposed assume a wide distribution of relaxation times in the polarizable constituents. To have tan δ′ ($=\omega CR_1$) independent of frequency, the hypothetical resistance, R_1, must vary inversely with frequency and is given in Fig. 3 as K/ω where K is a constant. One could as well employ a parallel resistance varying directly with frequency, but this has a slight mathematical disadvantage. R_2, residing principally in the MnO_2 semiconductor layer, can reasonably be assumed to be a true ohmic resistance. The dissipation factor which would be observed if there were no dielectric loss is, then, ωCR_2.

Tan δ equation.—The dissipation factor, or tan δ, in a capacitance-resistance series network is given by ωCR. For the equivalent circuit of Fig. 3,

$$\tan \delta = \omega C(R_1 + R_2) \qquad [1]$$

When "effective series resistance" is measured on a bridge, the value observed is $R_1 + R_2$.

Since $\omega CR_1 = \tan \delta'$

which is independent of frequency

$$\tan \delta = \tan \delta' + \omega CR_2 \qquad [2]$$

Evaluation of constants.—If the dissipation factor obeys Eq. [2], then when log tan δ is plotted against log f over a suitable frequency range, tan δ′ will predominate at low frequencies and tan δ will vary little with frequency. At higher frequencies, ωCR_2 will predominate, and the curve will approach a 45° slope. Figure 5, in which data are plotted for two 25 UF capacitors, shows conformance with this expectation, providing a confirmation of Eq. [2]. Strictly speaking, a limiting slope slightly less than 45°C is expected, since the capacitance decreases moderately with increasing frequency. The tan δ at 10 kc for one capacitor is about twice that of the other, indicating a variation of about that factor in R_2. However, the tan δ′ values at 50 cycles are

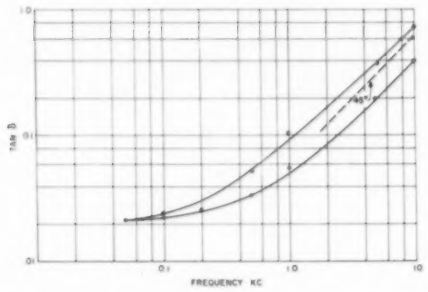

Fig. 5. Relationship of tan δ and frequency for two 25 UF porous tantalum solid electrolytic capacitors.

equivalent, indicating a similarity in the quality of the tantalum oxide film.

If C and tan δ are measured at two frequencies, one can determine the two constants, tan δ′ and R_s, by use of Eq. [2]. Further test of Eq. [2] consists of the reasonableness and consistency of values obtained in this way. Evaluation of tan δ′ and R_s for a capacitor using different pairs of frequencies usually gives satisfactorily consistent results, as is demonstrated below. Nevertheless, since the theory is regarded as approximate and for other evident reasons, certain criteria are recommended for selecting the frequencies employed. Greatest precision will result from using widely separated frequencies, with the lower one at a point where tan δ′ predominates and the higher one in a region where R_s predominates. It is suggested on the basis of experience that, when possible, the low frequency be one at which tan δ does not exceed about 0.05 since the upper limit for tan δ′ in a good quality tantalum oxide film is about 0.03. The high frequency should be chosen so that tan δ is about 0.1 or greater. An upper limit must be placed on the higher frequency, to avoid the region of precipitous capacitance decline illustrated in Fig. 2. Beyond this frequency, other complicating factors enter the picture. The upper limit can be estimated directly from capacitance plots such as the one in Fig. 2. In this case, this limit would be about 10 kc. One may also estimate the upper limit of frequency on the expectation that extraneous factors will enter before the point where the effective time constant CR_s exceeds, say, the time of 1/4 cycle. The selection of 1/4 as the factor is liberal and somewhat arbitrary, based only on the qualitative knowledge that an appreciable phase shift will occur unless the time constant is substantially less than the deviation of 1/2 cycle. If this frequency is f_{max},

$$CR_s = \frac{1}{4f_{max}} \sec$$

$$2\pi f_{max} CR_s = \frac{\pi}{2}$$

or

$$\omega_{max} CR_s = \frac{\pi}{2}$$

At such a frequency, ωCR_s will predominate in the loss, and the left-hand term approximates tan δ. Therefore, the absolute maximum frequency is that at which tan $\delta = \pi/2$. Owing to the distributed nature of the resistance one should stay well below this. Good results have been obtained using tan δ values as high as 0.75, but it is recommended that values in excess of 0.50 not be used. It will be noted in Fig. 2 that at 10 kc, tan $\delta = 0.72$; hence the two rules suggested for the maximum allowable higher frequency are approximately equivalent. To summarize, the suggested criteria for sets of values to use in calculating tan δ′ and R_s are: (*a*) tan δ at the lower frequency should not exceed about 0.05, and (*b*) tan δ at the higher frequency should lie between 0.10 and 0.50.

In order to apply this analysis successfully, one must be able to make accurate capacitance and tan δ determinations over a substantial frequency range. For the bulk of commercial porous tantalum solids, a range of 100 cycles to 10 kc is adequate. For very small capacitors, wire types, and others with unusually favorable geometries, it is desirable to be able to make measurements at frequencies as high as 50-100 kc. In some instances, data up to 200 kc or more are required if one wishes to evaluate R_s. In general, if tan δ is plotted against frequency over a suitable frequency range, tan δ at low frequencies approximates tan δ′ and at high frequencies it approximates ωCR_s. In some instances this may serve to estimate these factors, but tan δ′ and R_s are never completely separated in this manner.

Test of Eq. [2].—The results of evaluating tan δ′ and R_s for a particular 50 UF capacitor are given in Table I. For this illustration, six different frequencies were used. The three low-frequency values of tan δ are all in or close to the range recommended above for the lower frequency. The three high-frequency values correspond with a minor exception (tan δ at 20 kc = 0.664) to the criterion for the higher frequency. At the right hand side of Table I are shown the values of tan δ′ and R_s calculated for seven different frequency pairs. The remarkable consistency of the calculated values confirms the basic correctness of Eq. [2]. Test No. 3 does not fulfill the suggested criterion for the higher frequency; yet when it is combined with Test No. 1 or Test No. 2, calculated values correspond with those for other data pairs. Consistency such as shown in Table I may be somewhat better than average, but other calculations have always given reasonable agreement with theory. Evaluations of constants have been made on large numbers of units, and the

Table I. Frequency characteristics of a 50 UF tantalum solid capacitor

Measured properties				Calculated constants		
Test No.	*f*, kc	C, UF	tan δ	Data combination	tan δ′	R_s, ohm
1	0.05	51.47	0.0215	(3)-(1)	0.0196	0.116
2	0.1	51.06	0.0224	(3)-(2)	0.0186	0.120
3	1.0	49.99	0.0562	(4)-(1)	0.0197	0.114
4	5.0	49.10	0.196	(4)-(2)	0.0187	0.115
5	10.	48.3	0.394	(5)-(2)	0.0186	0.126
6	20.	46.0	0.664	(6)-(2)	0.0188	0.111
				(5)-(3)	0.0166	0.126

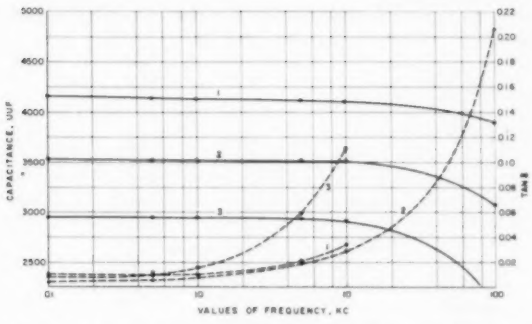

Fig. 6. Variation of capacitance and tan δ with frequency for three tantalum printed capacitors; 90-mil diameter anodes.

results are such as to establish a high degree of confidence in Eq. [2] as a close approximation, and to indicate that this equation can be used safely as an analytical tool.

Data for an entirely different type of tantalum oxide capacitor have also been treated by this method. This is the "printed" capacitor described by Berry and Sloan (7). To produce the capacitor, a film of tantalum is sputtered onto a substrate of glass or ceramic. This tantalum is anodized, and a counter-electrode of gold is applied by evaporation. These capacitors have no semiconductor, and the true series resistance is governed by the resistivity and thickness of the sputtered tantalum since the resistance of the gold layer is much lower. The capacitance values are orders of magnitude lower, and the effective series resistance ($R_1 + R_2$) orders higher than for the cases cited above. Figure 6 shows the capacitance-frequency and tan δ-frequency curves for three such capacitors. The relative constancy of tan δ at the lower frequencies is again evident. Calculated values of tan δ′ and R_2 are shown in Table II for these three samples. The upper half of the table presents the experimental results, and the lower half calculations made from widely separated frequency pairs. The agreement between values for any given capacitor is considered good.

Table II. Properties of tantalum printed capacitors, 90-mil diameter

A. Bridge measurements

Sample	0.1 kc C_1, MMF	0.1 kc tan δ	1.0 kc C_1, MMF	1.0 kc tan δ	10 kc C_1, MMF	10 kc tan δ	100 kc C_1, MMF	100 kc tan δ
1	4323	0.0103	4262	0.0106	4205	0.0345	3800	0.252
2	3574	0.0053	3554	0.0095	3525	0.0288	3160	0.206
3	2897	0.0082	2882	0.0172	2818	0.111	1350	0.976

B. Calculated values of tan δ′ and R_2, using various frequency pairs

Sample	10-0.1 kc tan δ′	10-0.1 kc R_2, ohm	1.0-0.1 kc tan δ′	1.0-0.1 kc R_2, ohm	100-1.0 kc tan δ′	100-1.0 kc R_2, ohm
1	0.0100	92.6			0.0080	102.5
2	0.0051	112.3			0.0073	100.5
3	0.0071	589	0.0072	553	*	

* tan δ at 100 kc beyond usable range for calculations.

As discussed by Berry and Sloan, the tantalum produced by sputtering produces a superior oxide film. One evidence is the low values of tan δ′, ranging from 0.010 downward. Data on these capacitors provide a goal toward which to work in all tantalum capacitor investigations, since the values of tan δ′ should approximate the intrinsic dissipation factor of amorphous tantalum oxide. In an attempt to evaluate this goal, twenty printed capacitors selected at random were studied in detail. The anodes were 0.250 in. in diameter, and formation was at 100 v. The average tan δ′ was 0.0050 with a standard deviation for the lot of 0.0021. The lowest value was 0.0028, and eight values were between 0.0030 and 0.0040.

Further evidence of the value and applicability of Eq. [2] evolves from the following section on applications.

Applications

The methods described have been used to analyze the results of several experimental programs. Several of the more important applications are presented here, primarily as examples of the wide applicability of the method, but partly because of the significant results of the experiments themselves.

Experiment 1. Influence of porosity of the anode.— Anodes of 1-g weight were pressed and sintered from a particular lot of tantalum powder. Two batches were produced, pressed to different densities, but sintered in the same sinter run at 2000°C. The only variation should be one of porosity. Each lot was divided into three groups of six each and anodized at 110, 130, and 150 v, after which they were processed into solid electrolytic capacitors by a standard procedure. Calculated values of tan δ′ and R_2 on two capacitors from each group are given in Table III. Evaluations of tan δ′ and R_2 are given for four pairs of frequencies and for the most part satisfactory consistency is observed.

One concludes that there is little effect of density on tan δ′ which is to be expected if this is a characteristic of the oxide film. If the slight evidence of lower tan δ′ in the low density anode is real, this can be explained by a greater degree of purification during sintering owing to the open structure. Average values of tan δ′, based on the 1-0.05 kc range, are: low density, 0.0248; high density 0.0273.

Values of R_2 for the higher density samples are much greater than for the low density samples. This is to be expected on the basis of the smaller pore structure which results in less MnO_2 and narrower conducting paths. Based on the 1-0.05 kc values, the average values of R_2 are: low density, 0.465 ohm; high density, 1.34 ohm.

Experiment 2. Comparison of tantalum powders.— The experiment cited above shows the effect of density on tan δ′ and R_2 for a given tantalum powder. However, particle size distribution and particle shape may have a very large influence on R_2. In another lot of anodes made from a powder produced by a different supplier, 1-g anodes were made with a density of 8.20, almost identical with that of the low density anodes of Table II. The capacitance per unit volume at a given formation voltage was like-

Table III. Calculated tan δ and R_2 of capacitors using 1-g anodes, all from the same tantalum powder. Two densities, three formation voltages. Capacitance (100~) 13-27 UF depending on density and anodizing voltage. tan δ at 0.1 kc 0.03-0.05

		Calculated constants							
		tan δ′				R_2			
Density	Formation voltage	1 kc 0.05 kc	1 kc 0.1 kc	5 kc 0.05 kc	5 kc 0.1 kc	1 kc 0.05 kc	1 kc 0.1 kc	5 kc 0.05 kc	5 kc 0.1 kc
8.13	110	0.0191	0.0210	0.0199	0.0228	0.525	0.512	0.413	0.416
		0.0258	0.0249	0.0263	0.0273	0.423	0.494	0.362	0.360
	130	0.0246	0.0251	0.0246	0.0234	0.387	0.383	0.387	0.386
		0.0234	0.0236	0.0234	0.0238	0.675	0.671	0.669	0.656
	150	0.0285	0.0250	0.0284	0.0252	0.493	0.522	0.500	0.507
		0.0272	0.0275	0.0266	0.0268	0.288	0.281	0.378	0.378
10.13	110	0.0270	0.0337	*	*	0.675	0.622	*	*
		0.0237				1.16	1.06		
	130	0.0278	0.0296			1.39	1.42		
		0.0296	0.0313			1.88	1.86		
	150	0.0273	0.0316			1.40	1.35		
		0.0339	0.0403			1.48	1.39		

* Values of tan δ at 5 kc were outside the recommended range for use in calculations.
· These rows give frequency pairs used in making calculations.

wise the same within 10%, indicating equivalent specific surface. The average tan δ′ calculated from the 1 and 0.05 kc data was 0.0229, as compared with 0.0248 from Table II. This signifies equivalent quality in the oxide film. Yet despite these similarities, the physical nature of the pore space was obviously quite different and substantially more favorable, since the average R_2 was only 0.176 ohm, as compared with 0.465 ohm.

Experiment 3. Evaluation of the process of Applying MnO_2.—All samples referred to above had MnO_2 applied by identical procedures. The electrical conductivity of MnO_2 depends critically on temperature and time used in its formation by pyrolysis of manganous nitrate. It is obvious that the analysis described can give relative values of conductivity of MnO_2 produced within the porous capacitor structure by various procedures. No data will be given here, but this method has been used extensively for this purpose in our laboratory.

Experiment 4. Effect of number of coats of MnO_2.—In the formation of MnO_2 in the capacitor structure, the element is saturated with aqueous manganous nitrate and heated to 300°-500°C. To obtain complete coverage and adequate conductance, a series of consecutive MnO_2 treatments is given.

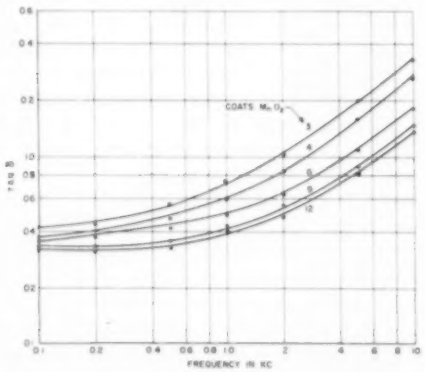

Fig. 7. Relationship of tan δ and frequency for porous tantalum electrolytic capacitors having various numbers of MnO_2 coats.

A study was made of the effect of number of MnO_2 applications on the electrical characteristics. The anodes consisted of 2-g porous tantalum pellets with integral leads, anodized at 100 v. Separate groups were given various numbers of MnO_2 coats by a standard procedure, made into finished capacitors, and electrical properties determined over a frequency range. The average values of tan δ as a function of frequency are plotted in Fig. 7, and average capacitance values in Fig. 8. With respect to capacitance, the principal variation is in the frequency at which rapid capacitance decrease sets in. The 0.1 kc and 10 kc values of tan δ conform to the criteria given for pairs of values to be used in calculating tan δ′ and R_2. Results of these calculations are presented in Table IV.

The value of tan δ′ appears to decrease with increasing amount of MnO_2. This may not be particularly significant since, excluding the samples with three coats, all values fall within a 10% range. If the trend is real, it could be produced by the additional thermal history or by reformings which are given after each three coats. This reforming consists of immersing the anodes in electrolyte and applying a positive potential for a short period of time.

The value of R_2 decreases regularly with the addition of MnO_2. A simple picture is that each MnO_2 treatment adds a fixed amount of material to the pore walls until the channels begin to be restricted. Additional treatments add only a small amount of

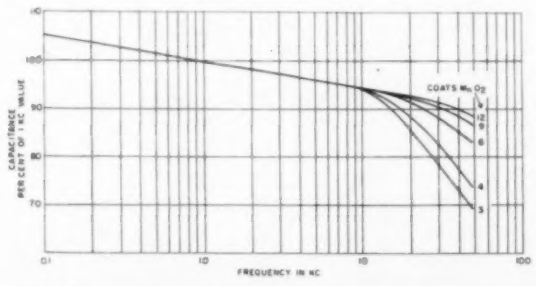

Fig. 8. Capacitance-frequency relationships for porous tantalum electrolytic capacitors of Fig. 7.

Table IV. Effect of number of MnO_2 coats on tan δ' and R_2

No. coats	100 Cycles		10 kc			
	C	tan δ	C	tan δ	tan δ'	R_2
3	20.99	0.041	18.83	0.330	0.0377	0.248
4	20.54	0.036	18.35	0.266	0.0334	0.202
6	20.69	0.034	18.63	0.180	0.0324	0.126
9	20.77	0.033	19.05	0.144	0.0318	0.094
12	20.70	0.031	19.07	0.135	0.0300	0.088

MnO_2. This simple theory predicts that the series conductance $1/R_2$ would initially increase in proportion to the number of coats and later would increase at a much lower rate. The data plotted in Fig. 9 fit this simple theory surprisingly well. The results indicate that for these particular anodes about 10 coats are required to approach pore filling. This number may well vary with anode size, pore size, pore volume, concentration of manganous nitrate, and other factors.

Significance in specifications.—The presence of two important factors in the dissipation factor complicates the problem of specifications and quality control. Nevertheless, their recognition should lead to more adequate and significant requirements. If a capacitor has, for example, a tan δ of 0.06 at 100 cycles, this is far too high if the loss is primarily due to tan δ', since it indicates a poor grade of tantalum, poor processing, or both. If half or more of this loss is due to R_2 on the other hand, the capacitor may be satisfactory for low-frequency applications. Similar ambiguity applies to measurements made at any other single frequency. It is desirable that measurements be made at a minimum of two frequencies, and tan δ' and R_2 evaluated. An alternative to evaluation of these constants would be to set tan δ limits at two frequencies, but this would be complex since each capacitor size, shape, and voltage rating would require different limits. Furthermore, tan δ' and R_2 furnish much more information than the raw data.

Basically, tan δ' is a measure of tantalum oxide quality. R_2 is a measure of anode structure and adequacy of the MnO_2 semiconductor.

There has been a tendency to refer to the measured value of $C(R_1+R_2)$ as the "time constant" of the capacitor. This is obviously inaccurate as a different value will be obtained for each value of frequency. A closer approximation to the actual time constant is CR_2.

Physical meaning of R_2; effect of form factor and size.—Neglecting a normally minor portion of R_2 residing in a layer of MnO_2 external to the anode of the finished capacitor and any carbon coat or other series element introduced in fabrication, one may easily estimate the effect of form and size of capacitor on R_2 and at the same time establish the significance of R_2. A useful example treated here is that of a right cylinder of porous sintered tantalum formed into a solid capacitor. This form is chosen both because of simplicity and because it is the most common form of porous anode. It is assumed that the cylinder is long with respect to diameter and can therefore be treated as semi-infinite, with all current flow radial. The analysis will apply as well to a cylinder of any proportions if the MnO_2 or other conducting material does not cover the ends of the cylinder.

For this analysis, reference is made to Fig. 10. The general method of procedure is to consider separately the power dissipation on a distributed and a lumped basis and then to equate the two.

One can consider that the channels containing MnO_2 constitute a conducting network with an effective resistivity, ρ ohm cm. The value of ρ will be governed by the porosity, size and shape of pores, degree of pore filling, and conductivity of the MnO_2. The cylindrical element in Fig. 10 having radius r and thickness dr, has, in the radial direction, a resistance of $\rho\, dr/2\pi rl$.

One may denote the amount of capacitance possessed by the anode per unit volume by $k(=C/V)$ farads/cm^3. k is determined by the specific surface area of the sintered anode and the thickness of the dielectric oxide film. The current flowing in the cylindrical element is that required by the capacitance contained in the right cylinder which it envelops.

$$I = \frac{\omega C_r E}{\sqrt{1 + \omega^2 R_s^2 C_r^2}}$$

where R_s is the effective series resistance for the cylindrical portion within r, and C_r is the capacitance of this portion, equal to $k\pi r^2 l$. However, if one limits conditions to those where $\omega^2 R^2 C_r^2$ is small

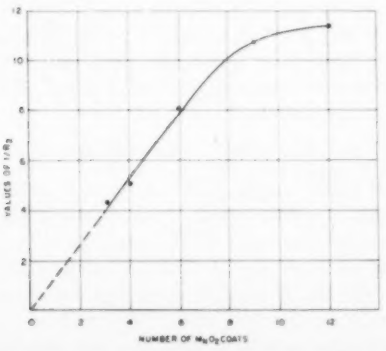

Fig. 9. Effect of number of MnO_2 coats on value of R_2; 20 UF, 35-v capacitors.

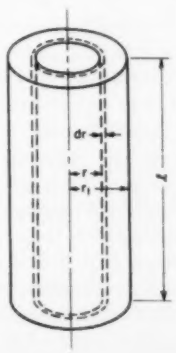

Fig. 10. Schematic diagram of cylindrical anode used to derive Eq. [6].

compared to unity, the equation for current becomes simply:

$$I = \omega C_r E$$

This implies moderate frequencies and is not an important limitation, since ω cancels out before one reaches the important relations of Eqs. [5] and [6]. The reasonableness of the simplification is seen from the fact that if tan δ for the section under consideration is as high as 0.10, the error involved is only 1%.

Denoting the power-dissipation as P, then dP, the dissipation in the cylindrical element (I^2R), is

$$dP = \frac{\pi\omega^2 lk^2 E^2 \rho}{2} r^3 dr$$

Total dissipation in the capacitor is

$$P = \int_{r=0}^{r=r_1} dP = \frac{\pi\omega^2 lk^2 E^2 \rho}{8} r_1^4 \qquad [3]$$

Now considering lumped constants and employing the same simplification as above, the current drawn by the whole capacitor is $\omega\pi r_1^2 lkE$ and the series resistance is the R_s of Eq. [1]-[2].

$$P = I^2R = \pi^2\omega^2 l^2 k^2 E^2 r_1^4 R_s \qquad [4]$$

Combining Eq. [3] and [4],

$$R_s = \frac{\rho}{8\pi l} \qquad [5]$$

A striking conclusion from this equation is that for a fixed value of l, R_s is independent of the value of the anode radius r_1. However, it should be noted that since the capacitance increases with r_1 the total dissipation will increase.

If one desires a given capacitance C, then, since

$$C = \pi r_1^2 lk, \; R_s = \frac{\rho r_1^2 k}{8C} \qquad [6]$$

This shows that for a fixed capacitance (hence fixed volume equal to C/k) it is advantageous to keep the anodes as slender as practical. This is not a surprising conclusion, but Eq. [6] is useful in giving a quantitative measure of the advantage.

Using a suitable form of sample and measuring R_s, Eq. [5] permits one to evaluate ρ and also to judge the effect of porosity, tantalum particle form, and procedures for applying MnO_2.

Other conclusions from Eq. [5] are expected ones: that R_s is proportional to ρ, inversely proportional to l, and independent of the other factors.

Capacitance-frequency characteristics.—From the lowest frequencies at which measurements were made up to some higher frequency related to C and R_s, plots of C *vs.* log f are linear. This linearity is observed up to 5 kc in Fig. 2, and up to about 10 kc in Fig. 6. In Fig. 11 are plotted data for three capacitors of the same structure but various characteristics showing linearity up to 1.0-5 kc. Some wire anode capacitors such as those used for obtaining the data of Fig. 4 exhibit linearity up to 100 kc or more.

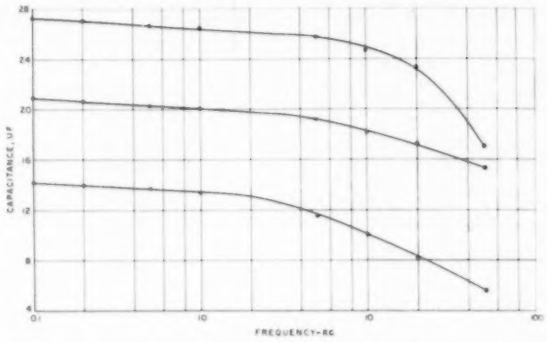

Fig. 11. Capacitance-frequency characteristics for three porous tantalum solid electrolytic capacitors.

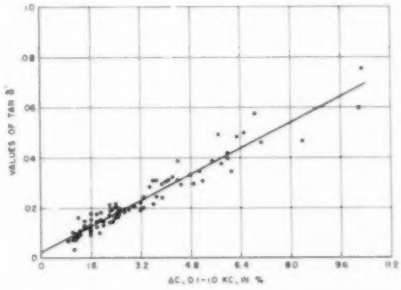

Fig. 12. Plot of tan δ' vs. change in capacitance between 0.1 and 1.0 kc for a wide variety of porous tantalum solid electrolytic capacitors. 21 Points are from laboratory produced samples; remaining 59 points are from product of eight commercial suppliers, in quantities of 3-15 from each.

The large frequency range over which this linear behavior was observed, particularly for wire anodes and other anodes of particularly favorable geometry, prompted the assumption that this must be simply the frequency characteristic of Ta_2O_5. Further study proved that this assumption requires critical examination and elaboration.

In the first place, the relative change in capacitance with frequency is not constant but varies by more than an order of magnitude when a large number of samples are tested. Second, the capacitance variation depends in an interesting and simple way on tan δ'. This dependence was obvious from inspection of a large body of data, and is illustrated by the plot of Fig. 12 for 90 capacitors from a wide variety of sources. In this figure, calculated values of tan δ' are plotted against change in capacitance between 100~ and 1 kc. The best line determined by least squares fit is drawn on Fig. 12, and corresponds to the equation

$$\tan \delta' = 0.0028 + 0.00642 \, \Delta C \; (\%) \qquad [7]$$

The root mean square residual for the points plotted is 0.00385. A consequence of this relationship is that, if one knows the slope of the capacitance curve, one can estimate tan δ' with fair precision. The intercept on the tan δ' axis is small but statistically significant. If one ignores this intercept and forces the line through the origin, then the relationship is

$$\tan \delta' = 0.00703 \, \Delta C \; (\%) \qquad [8]$$

In this case, the root mean square residual is slightly higher, 0.00412.

No correlation has been found between ΔC and any other properties such as R_s, capacitance value, or capacitor volume, shape, or structure.

By plotting the individual residuals against the capacitor supplier, one can detect a slight correlation, with some suppliers' product tending to fall above and some others below the line of Fig. 12. However, that this correlation is small is attested by the fact that the product from several suppliers cover a wide range of tan δ' and ΔC, yet produce no serious outlying values.

Since ΔC is related only to tan δ', which has been established as a characteristic of the tantalum oxide film, it follows that the variation in capacitance in the low-frequency range must also be characteristic of the oxide, in confirmation of the original assumption. The same factors which produce high values of loss in the film also produce relatively large variations in capacitance with frequency.

Both Winkel and de Groot (8) and Young (9) have treated the relationship between capacitance-frequency dependence and dissipation factor. Although starting with different theoretical assumptions, they arrive at identical expressions. Winkel and de Groot, based on a distribution of relaxation times, arrive at the expression

$$\frac{1}{C}\frac{\partial C}{\partial \ln \omega} = -\frac{2}{\pi}\tan \delta \qquad [9]$$

Since the authors are concerned with properties of the dielectric, it is obviously more accurate to refer to tan δ'. Inasmuch as $C/\ln\omega$ is a constant in the low-frequency range, increments can be employed instead, and

$$\Delta C\ (\%) \text{ is equivalent to } \partial C/C \times 100$$

Equation [9] can now be rewritten

$$\frac{\Delta C}{100} = \frac{2}{\pi}\Delta \ln \omega \tan \delta'$$

since the change of C is small and ΔC is negative.

In going from 100~ to 1 kc, $\Delta \ln \omega = 2.303$ so that,

$$\tan \delta' = 0.00682\ \Delta C \qquad [10]$$

Young, using a modification of Van Geel's theory involving an exponential variation of resistivity across the dielectric oxide, arrives at the following expressions, which were found to check experimental data for columbium oxide:

$$1/C = k_1 \log f + K \qquad [11]$$

$$Rf = k_2 \qquad [11a]$$

and

$$k_1/k_2 = 9.2 \qquad [11b]$$

Differentiating Eq. [11],

$$dC/C^2 = -k_1\, d \log f$$

Since C varies by a very small amount over a small frequency range such as a decade,

$$dC/C = -k_1\, C\, d \log f$$

Since

$$k_1 = 9.2\ k_2 = 9.2\ Rf$$

$$dC/C = -9.2\ RfC\ d \log f$$

$$= -9.2/2\pi \tan \delta\ d \log f$$

Inasmuch as tan δ (in this case equivalent to tan δ') is independent of frequency, one can take increments, and for 1 decade change in frequency, $d \log f$ can be replaced by unity and dC/C by $\Delta C/100$, where ΔC is the percentage decrease in capacitance.

$$\Delta C\ (\%) = \frac{9.2 \times 100}{2\pi}\tan \delta'$$

$$\tan \delta' = 0.00682\ \Delta C \qquad [12]$$

Equation [12] is seen to be identical with Eq. [10] derived from the Winkel and de Groot development.

These equations are in remarkable agreement with the empirically determined constants of Eq. [7] and [8] and confirm quantitatively the relations of Young and Winkel and de Groot, although in no way distinguishing between their theoretical approaches. This agreement gives further evidence that the analysis presented in this paper allows one to arrive at the true values of tan δ'.

Conclusions

Using a-c properties measured at two or more frequencies, it is possible to explain the a-c losses in tantalum solid electrolytic capacitors in terms of two factors, one a frequency independent dissipation factor in the tantalum oxide, and the other the series losses residing principally in the manganese dioxide semiconductor. This simple analysis allows one to rationalize the a-c properties of capacitors and to attach significance to many types of experiments. The two types of loss should be taken into account in setting up specifications for capacitors.

By treating the case of a right cylinder of porous tantalum, a quantitative meaning of the series losses is arrived at in terms of the specific resistivity of a manganese dioxide network. This treatment also provides a measure of the influence of form factor on the a-c losses.

The relation between the a-c losses in the oxide and the variation of capacitance with frequency is in good agreement with previously published data and theories.

Acknowledgments

The data used in these studies are exclusively data obtained by the author's associates in their regular development studies. The author has also had assistance with certain of the calculations. He is especially indebted to Mr. C. C. Houtz, Mrs. F. S. Power, Mr. R. W. Berry, Miss Dolores Farrell, Miss Doris Sloan, Mr. M. J. Urban, Mr. S. Karlik, and Mr. Fred Watkins. Special appreciation is due Mr. G. J. Levenbach for the statistical work.

Manuscript received May 13, 1960. This paper was prepared for delivery before the Chicago Meeting, May 1-5, 1960.

Any discussion of this paper will appear in a Discussion Section to be published in the December 1961 JOURNAL.

REFERENCES

1. D. A. McLean and F. S. Power, *IRE Proc.*, **44**, 872 (1956).
2. J. D. Hoffman, *IRE Trans. on Component Parts*, **CP-4**, 42 (June 1957).
3. Blowden Piercy, Annual Report, Conf. on Electrical Insulation, p. 1 (1956).
4. M. Gevers and F. K. du Prè, *Trans. Faraday Soc.*, **42**, 47 (1946).
5. M. Gevers, *Philips Research Repts.*, **1**, 279 (1946).
6. C. G. Garton, *Trans. Faraday Soc.*, **42**, 56 (1946).
7. R. W. Berry and Doris Sloan, *IRE Proc.*, **47**, 1070 (1959).
8. P. Winkel and P. de Groot, *Philips Research Repts.*, **13**, 489 (1958).
9. L. Young, *Trans. Faraday Soc.*, **51**, 1250 (1955).

The Chemistry of Cable-Oil Deterioration

George Feick and Walter F. Olds

Arthur D. Little, Inc., Cambridge, Massachusetts

and Edward D. Eich

Anaconda Wire and Cable Company, Hastings-on-Hudson, New York

ABSTRACT

The known chemistry of cable-oil deterioration is reviewed and some of the current theories are examined. It is shown that none of these is adequate to explain all the observed facts. A new theory of oil deterioration, based on the known electron transfer reactions of organic peroxides, is advanced and compared with the available data. The results of some experiments suggested by the theory are discussed.

The control of power factor in electrical oils has always been one of the major problems of the cable engineer and others concerned with liquid dielectrics. Although the problem of oil deterioration has been studied for many years, a fully satisfactory explanation of the chemistry involved has not yet been forthcoming.

A recent review by Piper (1) indicates that much of the research in the field has been concerned with the addition of various electrolytes such as organic acids, amines and their salts to hydrocarbon liquids in the hope of reproducing the high values of power factor found in aged oils. At low concentrations (when they are present in true solutions), these additives give only a negligible increase in conductivity, indicating that no significant electrolytic dissociation takes place. There is evidence, however, that high losses are often associated with the presence of colloidal materials in the oil. Piper concludes that the increased conductivity of deteriorated oils is caused primarily by the formation of colloidal ions. He has been unable, however, to correlate conductivity with the movement of colloidal particles observable under the ultramicroscope.

Recent work by Gemant (2, 3) has shown that oils containing small concentrations of aliphatic acids become highly conducting when treated with ozone. Gemant attributes this conductivity to ions formed by reaction of the acid with the ozonides of aromatic hydrocarbons present in the oil. Since it is known that electrical oils will deteriorate in the absence of ozone, these observations must be regarded as a special case.

In the present paper we consider an aspect of oil chemistry which we believe has received too little attention in the past. This is concerned with the reactions of organic peroxides or hydroperoxides commonly found in oxidized oils—even those which have merely been stored at room temperature. We will try to show that the reactions of these peroxides explain, at least qualitatively, many of the known facts of oil deterioration and give some indication of the nature of the ions present in deteriorated oil.

Experimental

Materials.—The oil used in these experiments was a commonly used electrical oil sold under the name of Univolt 35 by the Esso Standard Oil Company. The N, N′-disalicylidene 1, 2-propanediamine was a product of the DuPont Company and was furnished as an 80% solution under the name of DMD. The dibutyl paraphenylene diamine was furnished by the DuPont Company under the name of Gasoline Antioxidant No. 22. The activated clay used for removing peroxide from the oil was produced by the Minerals and Chemicals Corporation of America and is sold by the Harshaw Chemical Company under the name of Attapulgite No. 12104/81.

Apparatus and Procedure.—The aging tests described herein were carried out at 85°C in glass cells of about 100 ml capacity equipped with concentric cylindrical nickel electrodes with an air capacitance of around 50 $\mu\mu f$. About 60 ml of oil was used in each test and was degassed in the cell by heating at 85° under vacuum (40μ) for at least 1 hr. Provision was made for admitting measured amounts of oxygen to the cell, although unless otherwise noted all the runs reported herein were carried out under vacuum.

The dissipation factor of the oils during aging was measured with a General Radio Type 1610A a-c

bridge assembly at 60 cycles. Alternatively, the d-c conductivity of the oil was measured with a source of 1.5 v (applied intermittently to avoid polarization) and a Kiethley Model 410 micromicroammeter. The results were then converted to equivalent dissipation factor at 60 cycles, assuming all the loss to be due to electrolytic conductance. Agreement between the two methods was good.

When a peroxide-free oil was desired, the sample was purified by heating with stirring to 100°C for 1½ hr under oxygen-free nitrogen with 1% W/V of clay, followed by cooling and filtering.

Peroxide analyses were made by iodometric titration of 10-ml samples following the procedure of Cass (4).

Nature of Dielectric Losses

It is generally assumed that the losses in oxidized oils are due entirely to ionic conductance. This assumption may be tested by measuring the dissipation factor, tan δ, as a function of frequency.

If we assume an equivalent parallel circuit to represent the oil sample, then the usual expression for dissipation factor:

$$\tan \delta = 1/\omega CR \qquad [1]$$

becomes to a close approximation[1]

$$\tan \delta = 9 \times 10^{12} \Psi / 5\epsilon' f \qquad [2]$$

where f is the measuring frequency, ϵ' is the dielectric constant of the oil, and Ψ is the specific conductance measured by an a-c bridge circuit. In general, Ψ is the sum of two components:

$$\Psi = \Psi_o + \Psi_a \qquad [3]$$

where Ψ_o is the electrolytic contribution to conductance and Ψ_a is the in-phase component of conductance arising from purely a-c relaxation mechanisms such as dipole orientation or the Maxwell-Wagner mechanism. If we assume the sample to have no such a-c losses, Ψ_a is zero and ϵ' is independent of frequency. Under these conditions, Eq. [2] can be written in the form:

$$\log \tan \delta = -\log f + \text{const} \qquad [4]$$

which shows that a plot of log tan δ vs. log f will give a straight line inclined at an angle of −45° to the log f axis.

Figure 1 is such a plot for a typical sample of Univolt 35 oil aged with oxygen in the presence of copper. The slope and linearity show that the assumption underlying Eq. [4] is entirely justified, namely, that all the observed loss is due to ionic conductivity.

In view of this fact, we have felt justified in using d-c conductance measurements interchangeably with a-c bridge readings. In all cases we have found good agreement between the two methods, a further indication that we are concerned only with ionic loss.

Role of Copper and Peroxides

We will now discuss the experimental evidence which indicates that the reaction of metallic copper with organic peroxides present in the oil is one mechanism leading to a high ionic conductivity. Such peroxides are formed in the oil merely on standing in the presence of air at normal temperatures. Their formation is accelerated by light or heat and is inhibited by certain antioxidants. Most commercial electrical oils contain measurable quantities of peroxides, which are detectable by iodometric titration.

[1] Taking the velocity of light to be 3.0 × 10^{10} cm/sec.

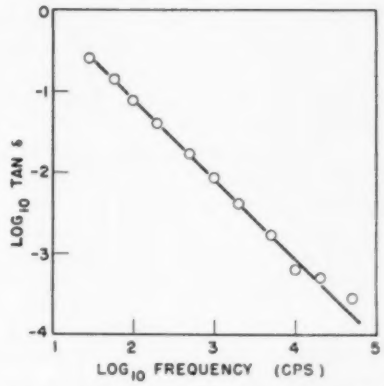

Fig. 1. Dissipation factor vs. frequency for Univolt-35 oil, aged 3050 hr with 36 meq. of oxygen and 1600 cm² of copper surface per liter of oil. Aged and measured at 85°.

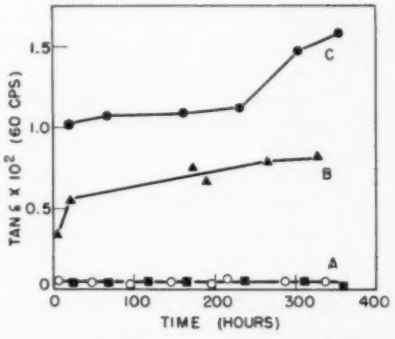

Fig. 2. Dissipation factor vs. time for Univolt-35 oil at 85°C. Curve A: ○ 3.6 meq./l peroxide, no copper; ■ no peroxide, 1600 cm² copper surface per liter; curve B: 1.85 meq./l peroxide, 1600 cm² Cu/l; curve C: 3.6 meq./l peroxide, 1600 cm² Cu/l.

Evidence for reaction of peroxides with metallic copper is shown in Fig. 2. Curve A shows that if either peroxide or copper foil is present in the cell, no ions are formed in the oil since the dissipation factor remains constant at its low initial value. If both copper and peroxide are present, however, the dissipation factor rises in a few hundred hours to a value roughly proportional to the amount of peroxide present, as shown by curves B and C.

The peroxide-free oil used for the data of Fig. 2 was prepared by treatment of the oil as received with activated clay. In order to show that peroxides are responsible for the reaction with copper and not some other material removed from the oil by the clay treatment, two runs were made with clay-treated and re-oxidized oil as shown in Fig. 3. Curve A of this figure shows that the dissipation factor of a clay-treated, peroxide-free oil rose only slightly on aging under vacuum with copper for 161 hr. At

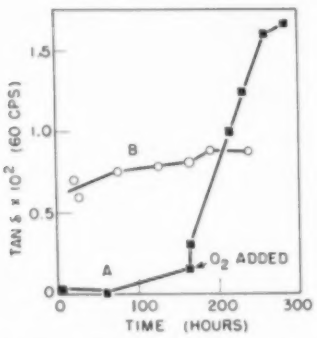

Fig. 3. Dissipation factor vs. time for purified and re-oxidized Univolt-35 oil at 85°C. Curve A: purified oil (no peroxide), 18 meq. O_2/liter of oil added at 161 hr; curve B: oil purified and re-oxidized before test to 1.85 meq. peroxide/l. Note: The rise in curve A before 161 hr may be due to slight air leakage.

this point, oxygen gas corresponding to 18 meq. (milliequivalents) of oxygen per liter of oil was admitted to the cell. The dissipation factor started to rise immediately and reached a value of 0.015 after about 100 hr.

The second experiment, shown in curve B of Fig. 3, was made with clay-treated, peroxide-free oil which was re-oxidized by saturating with oxygen and allowing to stand for a few days in sunlight. The peroxide analysis after re-oxidation was 1.85 meq./l. The behavior of this oil on aging with copper is almost identical with that of fresh oil containing the same amount of peroxide as shown in curve B of Fig. 2.

The above facts indicate that an essential feature of cable-oil deterioration is the reaction of organic peroxides, either with copper or by a copper-catalyzed mechanism, to form ionized products. The free radical reactions usually postulated in oil oxidation mechanisms may play a role, but by themselves are not sufficient to account for the observed increase in conductivity. Since the reaction of free oxygen with oils is known to proceed through the intermediate stage of hydroperoxide formation, it may be further postulated that those reactions of the hydroperoxides which lead to ionic products are sufficient to account for the deterioration of oils under the oxidizing conditions generally encountered in service.

Chemistry of Ion Formation from Metals

In seeking a more detailed explanation of these peroxide reactions, we find that the so-called Haber-Weiss mechanism (5) agrees well with the observed facts. The general equation for this reaction may be written

$$ROOR' + D \rightarrow D^{\cdot} + RO\cdot + R'O^{-} \qquad [5]$$

where D is an electron donor substance which transfers an electron to the peroxide molecule during the decomposition process. This type of reaction produces the ions necessary to account for the observed rise in conductivity, as well as a free radical (RO ·) capable of carrying on the oxidation chain if free oxygen is present.

If metallic copper is present, we may postulate that it will serve as the required electron donor. In donating electrons to the peroxide, the copper will become oxidized first to cuprous, and then to cupric ions, as shown by the following over-all reaction

$$2ROOR' + Cu \rightarrow Cu^{\cdot\cdot} + 2RO\cdot + 2R'O^{-} \qquad [6]$$

The same reaction has been postulated to explain the formation of copper mercaptides in petroleum distillates (6).

The free radicals may remove electrons from metallic copper to form further ions:

$$2RO\cdot + Cu \rightarrow Cu^{\cdot\cdot} + 2RO^{-} \qquad [7]$$

or they may decompose to stable species by non-ionic mechanisms.

In any event we must suppose that, concurrent with the above reactions, the peroxide decomposes by free radical mechanisms into non-ionized products, thus

$$ROOR' \rightarrow RO\cdot \rightarrow \text{non-ionized products} \qquad [8]$$

This is shown by the fact that when a peroxide-containing oil is heated for a number of hours in the absence of an electron donor, some or all of the peroxide is found to have disappeared, although no increase in power factor has taken place.

There is evidence, however, that the reaction of peroxides with copper is more rapid than this homolytic reaction to free radicals. In taking data shown in Fig. 2, for example, the two oils which were started with 3.6 meq. of peroxide per liter were again analyzed for peroxide after about 355 hr of aging. The oil aged with copper (curve C) contained no detectable peroxide, while that aged without copper (curve A) still contained 0.9 meq./l of peroxide or a quarter of the original amount.

The formation of copper ions in these reactions is confirmed by experiments in which N, N′-disalicylidene-1, 2-propanediamine (DMD) is added to the reaction mixture. This oil-soluble compound is a powerful complexing agent for cupric ion, with which it forms a tetradentate chelate compound of the following structure

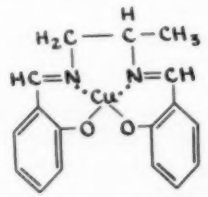

The addition of DMD to oils oxidized in the presence of copper is found to produce a marked decrease in conductivity. For example, the badly oxidized oil shown in Fig. 1 had a dissipation factor of 0.114 (at 60 cps) after 3500 hr of aging with copper and oxygen. The addition of 0.12% of DMD to this oil reduced the dissipation factor to 0.016; a sevenfold decrease. A sample of a different oxidized oil gave a decrease in dissipation factor from 0.0175 to 0.0025 on addition of 0.12% DMD, again a sevenfold reduction. We postulate that, in combining with cupric ion, the complexing agent releases hydrogen

ions which combine with the negative ions present to form weakly ionized products responsible for the small residual conductivity.

The use of a copper complexing agent is even more beneficial if it is added to the oil-copper system at the beginning of the oxidation process. In this case, 0.06% of DMD will hold the dissipation factor of Univolt 35 oil to a value of 0.001 or less after aging for 600 hr with copper and 18 meq. of oxygen per liter of oil. A control sample without DMD reached a dissipation factor of 0.0175 in less than 200 hr.

A possible explanation of the increased benefit of adding DMD at the beginning of the oxidation lies in the fact that the copper ions are complexed as soon as they are formed and are thus prevented from exerting any catalytic action on the oxidation process.

The nature of the negative ions formed in the above reaction depends on the particular peroxides present. In oxidized petroleum oils, the active oxygen is probably present as a mixture of a large number of organic hydroperoxides for which the general formula may be written ROOH. When such compounds are decomposed by an electron donor, we expect either oxyhydrocarbon ions (RO^-) or hydroxyl ions (OH^-) or both. Neither of these species would be expected to be very stable in oil solution nor to form highly dissociated compounds with copper. Possibly these ions react further to form charged colloidal particles, although nothing in our results appears to require such an hypothesis. Pending further work, therefore, the exact identity of the negative ions must be considered an open question.

We expect that considerable light may eventually be thrown on the process of ion formation, as well as on the nature of the negative ions, by studying the reactions of various classes of pure organic peroxides rather than the indeterminate mixtures found in petroleum oils. A few preliminary experiments along this line indicate that both benzoyl peroxide and di-cumyl peroxide produce much smaller increases in power factor than the native peroxides formed by oxidation of Univolt-35 oil. This result indicates that we may expect a considerable variation in reactivity among various peroxides and that improved cable oils might be made by identifying and eliminating substances which form highly reactive peroxides.

The electron-transfer mechanism can be generalized to account for the effect of other metals such as iron and lead, which are known to have an adverse effect on the electrical properties of oil. The fact that metals such as nickel, stainless steel, and aluminum fail to react may be attributable to the insolubility of their salts, or to the presence of an insulating oxide film on the metal which prevents transfer of electrons. In this connection it may be noted that Balsbaugh and Assaf (7) found that oxidized copper has less deleterious effect on oil than clean copper.

Amines as Electron Donors

In studying the action of antioxidants on the oxidation of Univolt-35 oil with copper, we found that in the presence of dibutyl paraphenylene diamine (AO-22) a considerable increase in conductivity was observed which was not prevented by the presence of DMD. This led us to suspect the presence of other cations beside those of copper and to consider possible reactions of amines with peroxides.

The reaction of benzoyl peroxide with amines such as aniline is well known. Horner and Schlenk (8) have proposed mechanisms for these reactions, the first step of which is an electron transfer from the amine to the peroxide with ion formation in the following manner:

$$ROOR + 2R_2'N \longrightarrow 2RO^- + 2R_2'N^{\cdot +} \qquad [9]$$

Both the negative ion (RO^-) and the positive radical-ion ($R_2'N^{\cdot +}$) will probably be unstable and may react further to final products.

Preliminary experiments with AO-22 and various peroxides have been somewhat inconclusive because the antioxidant gives fairly high values of dissipation factor (around 0.0075 to 0.010) in control experiments with peroxide-free oil. This may be attributable to oxidation products or other impurities in the commercial sample of AO-22 used.

The increases in conductivity obtained by reacting AO-22 with cumene hydroperoxide, dicumyl peroxide, or peroxide-containing oil have been rather small and difficult to distinguish from the control experiments. Work with purer materials is needed. With benzoyl peroxide and AO-22 (3 meq./l of each), however, we obtained a dissipation factor in the vicinity of 0.05 to 0.06 after 24 hr of aging. The dissipation factor remained in this range until the experiment was terminated after 450 hr.

Conclusions

We conclude that our results are consistent with the hypothesis that the ions responsible for the conductivity of oils deteriorated in service are formed by the reaction of organic peroxides or hydroperoxides with electron donor substances. Such electron donors may be metals such as copper, iron, or lead, or they may be organic compounds such as amines. Considerable variation in the reactivity of individual electron donors and individual peroxides has been observed.

In the case of oils aged in the presence of copper, the major conductive cation is cupric ion. The nature of the negative ions is less well understood, but further light may be thrown on this question by studying the reactions of pure organic peroxides of various types.

Acknowledgment

The authors take pleasure in acknowledging the help of many of their colleagues both of Anaconda Wire and Cable Company and of Arthur D. Little, Inc. In particular we wish to thank Dr. Raymond M. Fuoss, Mr. Glenn E. Andrews, Dr. Jay Vreeland, and Mr. Jay C. Balsbaugh for valuable discussion and assistance, and Mr. Henry Murphy for making most of the electrical measurements.

Manuscript received Feb. 24, 1960. This paper was prepared for delivery before the Philadelphia Meeting, May 1-5, 1959.

Any discussion of this paper will appear in a Discussion Section to be published in the December 1961 JOURNAL.

REFERENCES

1. A. R. von Hippel, Editor, "Dielectric Materials and Applications," p. 156, John Wiley & Sons, Inc., New York (1954).
2. A. Gemant, *This Journal*, **102**, 454 (1955).
3. A. Gemant, *Appl. Sci. Res.*, **A6**, 1 (1956).
4. W. E. Cass, *J. Am. Chem. Soc.*, **68**, 1981 (1945).
5. A. V. Tobolsky and R. B. Mesrobian, "Organic Peroxides," p 95, Interscience Publishers, Inc., New York (1954).
6. Petroleum Chemicals Div., E. I. Du Pont de Nemours and Co., Technical Memorandum No. 231, "Formation of Copper Mercaptides in Light Hydrocarbons," Wilmington, Del. (1954).
7. J. C. Balsbaugh and A. G. Assaf, *Trans. AIEE*, **62**, 311 (1943).
8. See Ref. 5, p. 104.

Electrodeposition of Cobalt-Molybdenum Alloys

Albertine Krohn and Theodore M. Brown[1]

Chemistry Department, University of Toledo, Toledo, Ohio

ABSTRACT

Previous studies showed that iron-molybdenum alloys could be deposited from pyrophosphate solutions. This investigation shows that a similar bath can be used to deposit cobalt-molybdenum alloys. The addition of hydrazine sulfate to the plating bath prevents anodic oxidation of Co(II) to Co(III). It also causes an increase in the cathode current efficiency and in the molybdenum content of the deposits. Efficiency is further increased by wiping the cathode during plating. The average content of the deposits was about 56% molybdenum, 37% cobalt, and 7% nonmetallic material. The cathode current efficiency was about 46%. The deposits were bright and adherent but tarnished readily unless a protective coating was applied.

The codeposition of molybdenum with iron, cobalt, nickel, copper, and zinc from pyrophosphate baths was studied extensively by Myers (1). Recent studies by Case and Krohn (2) have shown that it is possible to electrodeposit iron-molybdenum alloys with greater efficiencies than previously reported by using a specially designed plating cell incorporating cathode rotation, stirring, and wiping.

The present study was undertaken as part of a continuing research program concerned with the deposition of molybdenum with various metals from pyrophosphate baths using this specially designed plating apparatus. More specifically, this paper describes the results of the effect of certain variables on the cobalt-molybdenum system, beginning essentially with the plating bath developed by Myers and the special plating apparatus designed by Case and Krohn.

Experimental

Apparatus.—The plating cell and auxiliary equipment used in this study have been described previously (2).

Plating bath.—The bath used at the beginning of this investigation was essentially that of Myers (1) modified by the addition of hydrazine sulfate. Preliminary experiments showed that the cobalt(II) present in the bath was oxidized at the anode to cobalt(III) products resulting in a decrease in the efficiency of the plating process, especially if a number of runs were made using the same plating solution. The oxidation of cobalt(II) was prevented by the use of hydrazine sulfate which acted as a potential buffer, being oxidized at the anode in preference to the cobalt(II) ions. It was further found that the use of hydrazine resulted not only in improving the efficiency of the plating process but also increased the molybdenum content of the deposits.

Analysis of the deposits.—The alloy deposits were dissolved in 5*N* nitric acid. The molybdenum and cobalt were analyzed colorimetrically, based on the fact that they react with mercaptoacetic acid to form colored solutions (3, 4). In the determination of molybdenum, the interfering color due to the presence of cobalt was eliminated by the addition of EDTA (ethylenediaminetetraacetic acid).

Experimental Results

Unless otherwise stated, the plating runs were made using a current density of 17.8 amp/dm^2 (160 amp/ft^2) and a bath temperature of 60°C. Most of the plating runs were of 10-min duration. The speed of rotation of the cathode during this investigation was maintained at 1750 rpm, a speed previously established as the optimum (2). The deposits were found to contain a small amount of nonmetallic material (NMM) which may have been oxygen (1, 2), hydrogen (5, 6), or both. The percentage of NMM was obtained by subtracting the total percentage of molybdenum and cobalt from 100. The calculation of the cathode current efficiency (CCE) was based on the oxidation states of molybdenum(VI) and cobalt(II). The effects of changes in plating conditions and solution composition on the deposits and on cathode current efficiency are summarized by the following graphs and discussion. When conditions encountered were better than those previously used, these were retained for the remainder of the investigation.

Effect of current density.—The plating solution in this series of tests had the following composition:

[1] Present address: Chemistry Department, Iowa State University, Ames, Iowa.

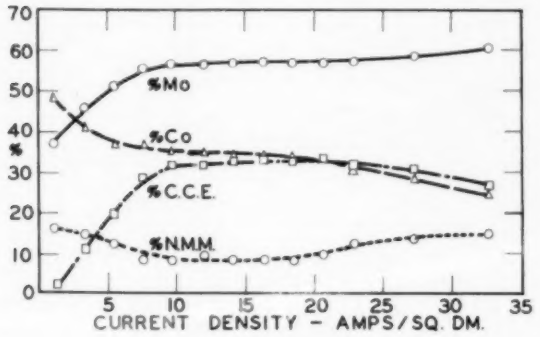

Fig. 1. Effect of current density

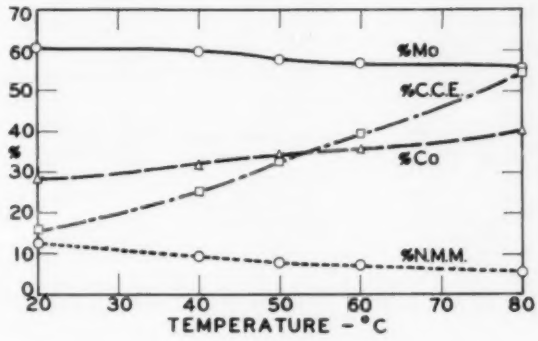

Fig. 3. Effect of temperature

33.6 g/l (0.83*N*) $Na_2MoO_4 \cdot 2H_2O$, 8.1 g/l (0.068*N*) $CoCl_2 \cdot 6H_2O$, 60.0 g/l (0.54*N*) $Na_4P_2O_7 \cdot 10H_2O$, 80.0 g/l (0.95*N*) $NaHCO_3$, and 1.5 g/l $N_2H_4 \cdot H_2SO_4$. The temperature of the plating bath was maintained at 50°C.

Runs were made at current densities varied from 1.1 to 33.3 amp/dm² (10 to 300 amp/ft²). The length of each plating run was adjusted so that a total of 2000 coulombs passed through the solution during each run. The deposits obtained from runs at low current densities were almost black in appearance, thin, and not very adherent. As shown in Fig. 1, the molybdenum content was low, cobalt content high, and nonmetallic material content high as compared to the deposits obtained at higher current densities. As the current density was increased, the deposits became more adherent and were of a metallic steel-gray color. The molybdenum content as well as the current efficiency was greater at these higher current densities. At extremely high current densities, the color of the deposits changed to a light gray and the efficiency decreased. Good deposits were obtained with high efficiency and molybdenum content at current densities ranging from 12.3 to 23.4 amp/dm² (110 to 210 amp/ft²).

Effect of the length of plating time.—Using the same bath composition and temperature as for the study of the effect of current density, runs of 2- to 60-min duration were made.

The deposits obtained from runs of 2- to 20-min duration were adherent and of pleasant appearance. The 20-min plate was about 10 μ thick. The composition of these deposits varied only slightly as shown in Fig. 2. As the length of the plating time was increased, the deposits became grayish and less adherent. The efficiency decreased continuously as the length of plating time was increased.

Effect of temperature.—Again the composition of the plating solution was the same as that used for the study of the effect of current density. Runs were made at varying temperatures from 20° to 80°C using a current density of 17.8 amp/dm² (160 amp/ft²). At low temperatures the deposits were dull gray in color. As the temperature of the bath was increased the deposits became very bright. At 80°C the plating bath contained some colloidal material. As shown in Fig. 3, the molybdenum content was found to decrease with a corresponding increase in the cobalt content as higher temperatures were used. The current efficiency increased continuously as the temperature was increased.

Effect of molybdenum(VI) concentration.—The concentration of Mo(VI) was varied from 0.0 to 2.0*N* (0 to 80.0 g/l $Na_2MoO_4 \cdot 2H_2O$). The concentration of the other bath components was the same as listed previously.

With no molybdenum present, a very silvery nonadherent deposit containing 86.3% Co and 13.7% nonmetallic material was obtained. As the Mo(VI) concentration in the bath was increased, the molybdenum content of the deposits increased (Fig. 4) and the cobalt content decreased. The current efficiency rose very rapidly as the Mo(VI) concentration was increased to 0.05*N*. Beyond this concentration the molybdenum content of the deposits did not increase to any great extent whereas the current

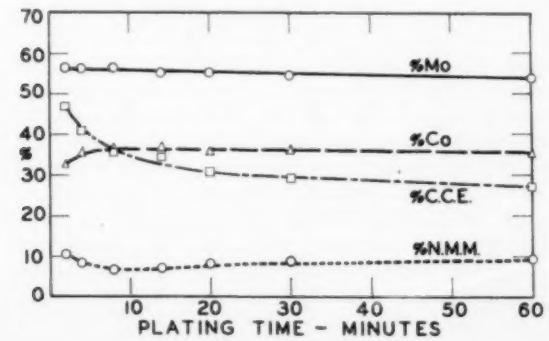

Fig. 2. Effect of length of plating time

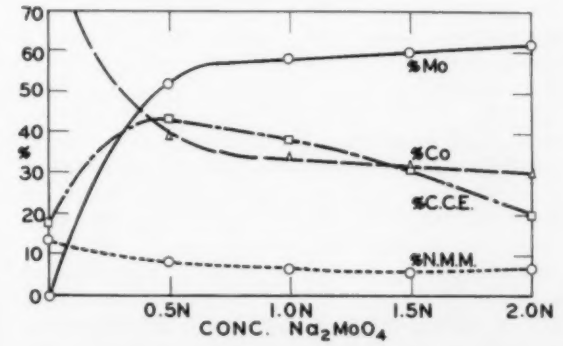

Fig. 4. Effect of Mo(VI) concentration

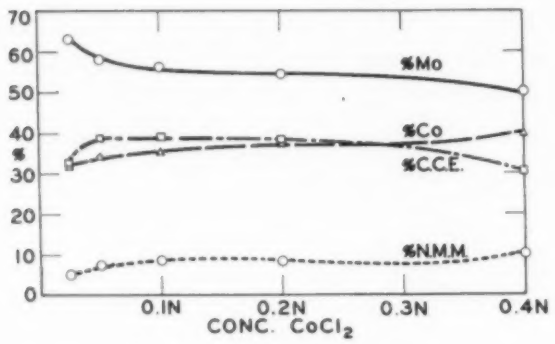

Fig. 5. Effect of Co(II) concentration

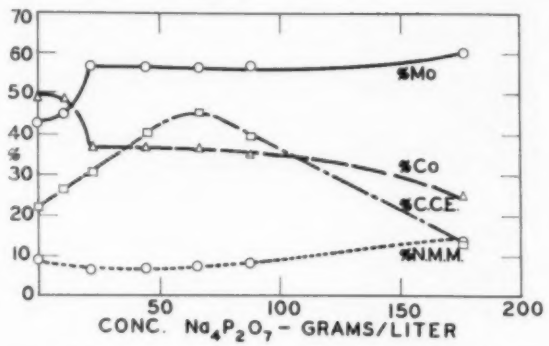

Fig. 6. Effect of sodium pyrophosphate concentration

efficiency decreased rapidly. All of the deposits containing molybdenum were smooth and adherent.

Effect of cobalt(II) concentration.—Runs were made at varying Co(II) concentrations between 0.0 and 0.4*N* (0 to 47.5 g/l $CoCl_2 \cdot 6H_2O$). The amount of $Na_4P_2O_7 \cdot 10H_2O$ was varied correspondingly to keep all of the Co(II) complexed with pyrophosphate in each solution. Except in the solution containing no Co(II) where the usual 60.0 g/l $Na_4P_2O_7 \cdot 10H_2O$ was added, the normality of the pyrophosphate was exactly eight times that of the Co(II) used. Concentrations of the other bath components were as follows: 32.2 g/l (0.8*N*) $Na_2MoO_4 \cdot 2H_2O$. 80.0 g/l (0.95*N*) $NaHCO_3$, and 1.5 g/l $N_2H_4 \cdot H_2SO_4$.

Only a flash deposit which was blue-black in appearance was obtained from the solution which contained no Co(II). As would be expected, the molybdenum content of the deposits decreased and the cobalt content increased as the concentration of Co(II) in the bath was increased (Fig. 5). The current efficiency was constant over a range of 0.05 to 0.2*N* (5.9 g/l to 23.8 g/l $CoCl_2 \cdot 6H_2O$) and then decreased slowly with increasing cobalt concentration.

Effect of sodium pyrophosphate concentration.—Runs were made at varying concentrations of $Na_4P_2O_7 \cdot 10H_2O$ from 0 to 176.4 g/l, the other bath components being present in the following concentrations: 32.2 g/l (0.8*N*) $Na_2MoO_4 \cdot 2H_2O$, 11.9 g/l (0.1*N*) $CoCl_2 \cdot 6H_2O$, 80.0 g/l (0.95*N*) $NaHCO_3$, and 1.5 g/l $N_2H_4 \cdot H_2SO_4$.

The plating solutions containing a mole ratio of pyrophosphate to Co(II) of 0:1 and 0.5:1 (11.2 g/l $Na_4P_2O_7 \cdot 10H_2O$) were pink in color and contained precipitates of cobalt(II) hydroxide and cobalt- pyrophosphate complexes. In solutions containing small amounts of pyrophosphate, precipitates having the composition $Co_5(P_2O_7)_3^{-2}$, $Co_2(P_2O_7)_4^{-6}$, and $Co_3(P_2O_7)_3^{-2}$ have been observed (7). The deposits were black and had a lower molybdenum content and higher cobalt content than the deposits obtained from solutions containing higher concentrations of pyrophosphate (Fig. 6). By increasing the mole ratio of pyrophosphate to Co(II) to 1:1 (22.3 g/l $Na_4P_2O_7 \cdot 10H_2O$) where a soluble complex of $Co(P_2O_7)^{-2}$ forms (7), a great increase in the molybdenum content of the deposits and a corresponding decrease in the cobalt content was obtained. The solution was light purple and contained a colloidal precipitate since the amount of pyrophosphate was not sufficient to keep all of the Co(II) complexed. No precipitate was obtained when the mole ratio of pyrophosphate to Co(II) was increased to 3:1 (66.9 g/l $Na_4P_2O_7 \cdot 10H_2O$). The color of the solution at this concentration was a deep purple. At high concentrations of pyrophosphate, the amount of cobalt in the deposits decreased due to the Co(II) being more tightly bound in the pyrophosphate complex. The efficiency of the process increased rapidly to a maximum at a mole ratio of pyrophosphate to Co(II) of 3:1 and then decreased with increasing concentrations of pyrophosphate. The static potentials of both molybdenum and cobalt became more negative as the concentration of pyrophosphate was increased, indicating that, in addition to the cobalt forming a complex with the pyrophosphate, the molybdenum may also form some sort of complex with pyrophosphate.

Effect of pH.—Using a bath having the composition 32.2 g/l (0.8*N*) $Na_2MoO_4 \cdot 2H_2O$, 11.9 g/l (0.1*N*) $CoCl_2 \cdot 6H_2O$, 66.9 g/l (0.6*N*) $Na_4P_2O_7 \cdot 10H_2O$, and 1.5 g/l $N_2H_4 \cdot H_2SO_4$, runs were made at *p*H values from 7.0 to 9.8. A pH of 7.0 was obtained by replacing the $NaHCO_3$ by an equivalent amount of NaCl (56.5 g/l) and adding dilute HCl to give the desired *p*H. The *p*H of 7.6 was obtained in a similar manner except that no HCl was added. The plating solution containing the usual amount of $NaHCO_3$ had a *p*H of 8.3. By using 56.3 g/l $NaHCO_3$ and 23.8 g/l Na_2CO_3, a *p*H of 9.0 was obtained. When the $NaHCO_3$ was replaced by 80.0 g/l Na_2CO_3, the solution had a *p*H of 9.8.

At a *p*H of 7, the solution was light pink in color and only a flash deposit was obtained. As the *p*H was increased to 7.6, the color of the solution darkened and a reddish-pink colloidal material was formed. The deposit obtained at this *p*H was neither bright nor adherent. As the *p*H was increased, the solution assumed the usual deep purple color and the deposits became brighter and more adherent. As shown in Fig. 7, a maximum molybdenum and minimum cobalt content was achieved at a *p*H of 8.3. The efficiency reached a maximum at a *p*H of 9.0 where the pyrophosphate complex appeared to be the most soluble. At a *p*H of 9.8, a deep blue precipitate was obtained, and the deposit was poor and grayish in appearance. It is seen that small changes in *p*H result in great changes in the molybdenum

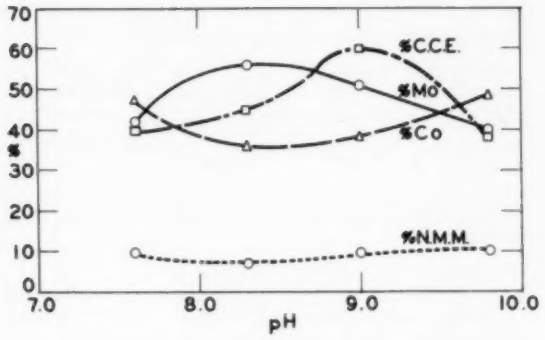

Fig. 7. Effect of pH

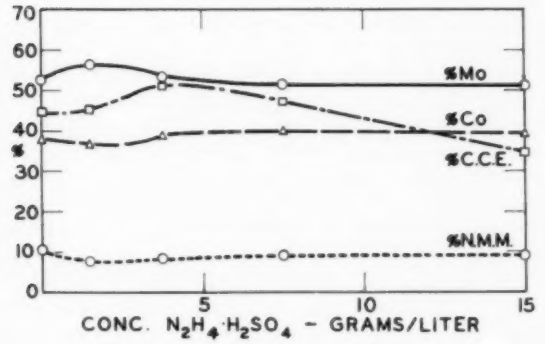

Fig. 8. Effect of hydrazine concentration

content and current efficiency. The highest molybdenum content was obtained at a pH of 8.3, easily reproducible by adding an excess of $NaHCO_3$.

Effect of hydrazine concentration.—The plating solution used had the following composition: 32.2 g/l (0.8*N*) $Na_2MoO_4 \cdot 2H_2O$, 11.9 g/l (0.1*N*) $CoCl_2 \cdot 6H_2O$, 66.9 g/l (0.6*N*) $Na_4P_2O_7 \cdot 10H_2O$, 80.0 g/l (0.95*N*) $NaHCO_3$, and varying amounts of hydrazine sulfate from 0 to 15.0 g/l.

During the plating run, the solution containing no $N_2H_4 \cdot H_2SO_4$ became very dark green in color and contained finely dispersed oxides of cobalt due to the oxidation of Co(II) to Co(III) products at the anode. As the concentration of $N_2H_4 \cdot H_2SO_4$ was increased the color of the solution changed from purple to wine red. Figure 8 shows that the molybdenum content of the deposits increased and then decreased, finally leveling off. The efficiency reached a peak at a concentration of approximately 3.5 g/l $N_2H_4 \cdot H_2SO_4$.

The addition of hydrazine sulfate to the plating solution prevents the oxidation of Co(II) to undesirable Co(III) products. Thus the current efficiency does not decrease as rapidly when consecutive runs are made on the same solution containing sufficient hydrazine sulfate as compared to a solution which does not contain hydrazine sulfate.

Reproducibility.—Four identical runs were made, keeping all factors as nearly constant as possible. The composition of the deposits was found to be reproducible to within ±0.9% which was within the experimental error of the analytical methods used. The four deposits were nearly identical in appearance.

Summary and Conclusions

Eight variables as given in Table I were examined. Since the primary purpose of this investigation was to obtain a deposit containing a high molybdenum content with the greatest current efficiency possible, values of each variable are given for the conditions under which the highest molybdenum content and the greatest current efficiency were obtained. Finally, there appears the value chosen as the one felt best suited for practical operation. In all cases it was not possible to choose a value for practical operation which gave the maximum molybdenum content as well as the maximum current efficiency.

Using the solution composition and conditions indicated in the last column of Table I, deposits weighing about 0.23 g were obtained using a platinum electrode having an effective plating area of 21.7 cm^2. Such deposits were about 10 μ thick. A typical deposit is shown in Fig. 9. The average composition of the deposits was 56% Mo, 37% Co, and 7% nonmetallic material which may have been oxygen, hydrogen, or both. If this material is oxygen, and if the oxygen is tied up with the molybdenum, then all of the molybdenum is not in the metallic state.

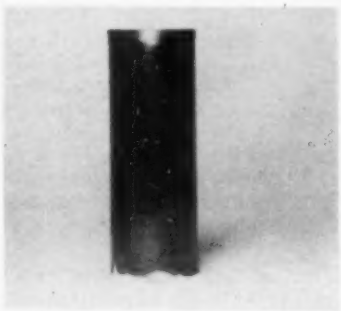

Fig. 9. Typical cobalt-molybdenum deposit

Table I. Optimum solution composition and plating conditions using cathode stirring and wiping

Variable	Value for highest % Mo	Value for greatest % CCE	Value for practical operation
Current density	300 amp/ft^2	150 amp/ft^2	160 amp/ft^2
Length of plating time	2 min	2 min	10 min
Temperature	20°C	80°C	60°C
Mo(VI) conc.	2.0*N* (80 g/l)	0.5*N* (20 g/l)	0.8*N* (32.2 g/l)
Co(II) conc.	0.025*N* (3.0 g/l)	0.1*N* (11.9 g/l)	0.1*N* (11.9 g/l)
Sodium pyrophosphate conc.	1.6*N* (176.4 g/l)	0.6*N* (66.9 g/l)	0.6*N* (66.9 g/l)
pH	8.3	9.0	8.3
$N_2H_4 \cdot H_2SO_4$ conc.	1.5 g/l	3.75 g/l	1.5 g/l

Calculations show that each per cent of oxygen ties up approximately 4% of molybdenum. Assuming that all the oxygen is combined with molybdenum, the composition would be 28% Mo, 37% Co, and 35% Mo_2O_3. The current efficiency under these conditions was about 46%. Deposits were bright and adherent but tarnished readily unless a protective coating was applied.

These results compare favorably with those of other investigators. Ernst, Amlie, and Holt (8) report molybdenum-cobalt alloys containing up to 40% Mo plated from an ammoniacal citrate bath with cathode current efficiencies between 50 and 60%. A Russian paper (9) reports alloys of 10 to 40% Mo from a similar bath, but claims efficiencies up to 90% with the use of alloy anodes. Seim and Holt (10) also obtained alloys from citric acid baths with about the same composition and 50% C.C.E. Previous work with pyrophosphate solutions (1) had produced alloys with less than 50% Mo and efficiencies generally below 40%.

As pointed out previously (2), there is as yet no theoretical explanation which is entirely satisfactory to describe the mechanism of the electrodeposition of molybdenum alloys. At present, the hydroxide film theory provides reasonable explanations for most of the experimental data. It is hoped that by complete studies of the plating of molybdenum with each of the codepositing metals, the mechanism may become more apparent.

Manuscript received June 23, 1960. This paper was prepared for delivery at the Houston Meeting, Oct. 9-13, 1960. It is abstracted from a thesis presented by T. M. Brown to the University of Toledo in partial fulfillment of the requirement for the degree of Master of Science.

Any discussion of this paper will appear in a Discussion Section to be published in the December 1961 JOURNAL.

REFERENCES

1. H. S. Myers, "The Electrodeposition of Molybdenum," unpublished Ph.D. thesis, Columbia University (1941).
2. L. O. Case and A. Krohn, *This Journal*, **105**, 512 (1958).
3. F. Will, III, and J. H. Yoe, *Anal. Chem.*, **25**, 1363 (1953).
4. D. A. Otterson and J. W. Graab, *ibid.*, **30**, 1282 (1958).
5. D. W. Ernst and M. L. Holt, *This Journal*, **105**, 686 (1958).
6. F. B. Saubestre, *ibid.*, **106**, 1305 (1959).
7. L. B. Rogers and C. A. Reynolds, *J. Am. Chem. Soc.*, **71**, 2081 (1949).
8. D. W. Ernst, R. F. Amlie, and M. L. Holt, *This Journal*, **102**, 461 (1955).
9. T. F. Frantsevich-Zabludovskaya, *Ukrain. Khim. Zhur.*, **25**, 463 (1959).
10. H. J. Seim and M. L. Holt, *J. (and Trans.) Electrochem. Soc.*, **96**, 205 (1949).

Electrodeposition of Nickel-Cobalt Alloys from the Pyrophosphate Bath

Vasanta Sree and T. L. Rama Char

Electrochemistry Laboratory, Department of Inorganic and Physical Chemistry, Indian Institute of Science, Bangalore, India

ABSTRACT

Nickel has been codeposited with cobalt from the pyrophosphate bath. Detailed studies on alloy composition, cathode efficiency, and potential have led to the optimum conditions for obtaining satisfactory alloy plates with 10-91% nickel. The efficiency of cast alloy anodes is quite high. X-ray patterns of the deposits show the existence of f.c.c. and hexagonal structures. The deposit composition could be altered appreciably only by varying the metal content of the bath.

Alloys of nickel and cobalt have been deposited from sulfate (1), chloride (2), sulfate-chloride (3-5), sulfamate (6) and triethanolamine (7) solutions. It has been shown in this laboratory that the pyrophosphate bath is suitable for the plating of nickel (8) and cobalt (9). The preliminary work on the codeposition of nickel with cobalt from the bath has been reported briefly (10).

Experimental

Plating solutions were prepared from potassium pyrophosphate, nickel chloride, and cobalt chloride. Ammonium citrate was added as a bath constituent since it was beneficial from the view point of buffering of solution, limiting cathode current density, cathode efficiency, and deposit composition range Its concentration was based on previous studies on nickel (8) and cobalt (9) plating from the pyrophosphate bath. The effect of the chloride ion on anode corrosion has been shown with solutions containing the pyrophosphates of potassium, nickel, and cobalt. The pyrophosphate content of the solution was always in excess of that required for complex formation, and the molar ratio of pyrophosphate (P_2O_7) to metal has been given. Physicochemical measurements have shown that the metal ion concentration (g ion/l) and instability constant for the pyrophosphate complexes are of the order of 10^{-9} for nickel (8) and 10^{-4} for cobalt (11). The nickel content was estimated by the dimethyl-

glyoxime method in presence of sodium acetate, cobalt gravimetrically by precipitation as cobalt anthranilate, and pyrophosphate by the ammonium phosphomolybdate method. For control experiments the solutions were analyzed by the same procedure as for the alloy. The deposit was stripped from the cathode with a solution containing 50 ml conc. HNO_3 (sp gr 1.38), 5 ml conc. HCl (sp gr 1.17), and 45 ml water. Nickel and cobalt were estimated as mentioned above.

Fresh solutions, 200 ml, of one concentration, were taken for each experiment—determination of current efficiency, plate composition and electrode potential at a given current density, with insoluble anodes. The same solution was, however, used for determinations at a number of current densities, for experiments with soluble anodes. A cylindrical hollow cathode of Pt or Cu (1½ in. length x ⅜ in. diameter) slipped over a stainless steel rod was placed inside a ring shaped Pt anode used for electroanalysis, or an alloy anode (7/10 in. height x 1½ in. diameter x ¼ in. thickness). The inter-electrode distance was ½ in. Cast alloy anodes containing 32 and 74% Ni were used, the anode area being four times the cathode area. The bath was worked under still conditions as agitation did not offer any advantage. The plating time varied from 10 to 45 min.

Electrode efficiencies were determined by the usual method for alloys (12), and the Philips Conductivity Bridge was used for specific resistivity. The pH was measured with a glass electrode, the adjustments being made with hydrochloric acid or potassium hydroxide. Conditions were controlled carefully to obtain electrode potential values (hydrogen scale) to the accuracy of ± 0.005 v. The data, however, have been presented to the second decimal place, the sign of the potential being negative for the cathode and positive for the anode unless otherwise stated. A decrease in the cathode potential means that the potential is less negative. The rest of the experimental details were the same as described before (13). The conventional throwing number was calculated from the equation of Gardam (14) for a linear relationship between cathode potential and log current density. Photomicrographs of the surface of a thick coating (0.001 in.) of the deposit were taken with a Leitz-Metallux metallographic microscope. X-ray powder patterns of the deposit were obtained from a Hilger x-ray diffraction unit and a Ninus G.P.57.3 mm diameter camera. Iron Kα radiations with manganese filter at 25 kv and 10 ma were utilized.

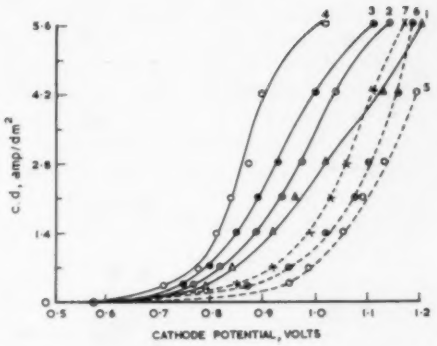

Fig. 1. Cathode potential curves for nickel and cobalt. Ratio 2.5, temp. 60°C, pH 9.1-9.5, 20 g/l am. citrate throughout unless otherwise stated. 1-4 Co: curve 1, 0.025; 2, 0.05; 3, 0.1; 4, 0.2M; 5-7 Ni: 5, 0.1; 6, 0.2; 7, 0.3M.

Experimental Results

Figure 1 shows that the cathode potential curves for nickel and cobalt in pyrophosphate solutions are close together, indicating the possibility of codeposition. Some of the curves intersect at higher current densities. In general, nickel is the baser metal of the system.

Alloy deposition was carried out under different conditions with respect to electrolyte concentration, addition agents, pH, and temperature. A detailed study was made of the effect of the variables on plate composition, cathode efficiency, and cathode potential. Alloy anodes have also been used to study the effect of electrolyte concentration, citrate and chloride ions, and temperature. Results are presented in Fig. 2 to 14, and Tables I to IV. All the data have not been covered to avoid overlapping. Except for cathode efficiency there is no significant difference in the plating characteristics with insoluble and soluble anodes. Some of the results, therefore, have been presented with insoluble, and

Table I. Effect of variables on alloy deposition

Variable	% Ni in deposit	Cathode efficiency	Limiting c.d.	Cathode potential
Fig. No.	2-4	5-7	2-4	8
Increase in c.d.	Little change	Slight decrease at high c.d.	—	Increase
Increase in Ni content of soln.	Increase	Slight increase	Increase	Little change
Increase in Co content of soln.	Decrease	Little change	Increase, then decrease	Little change
Increase in P_2O_7 content of soln., ratio 2.1, 2.5, and 3.	No change	Little change	No change	Little change
Increase in total metal content of soln.—0.1, 0.2, 0.4, 0.6M.	No change	Slight increase	Increase	Slight decrease
Increase in pH of soln.	Slight increase	Increase	Slight decrease	Little change
Anodes, insoluble and soluble—74 and 32% Ni	No change	Slight increase	No change	Little change
Increase in temperature—40, 50, 60, 70, 80°C	No change	Slight increase	Increase	Decrease
Agitation	Increase	Decrease at low c.d.	No change	Slight decrease
Addition agents				
Gelatin, fuchsin	No change	Slight decrease	Decrease	Little change
Salicylic acid, resorcinol	Slight increase	No change	No change	No change

the rest with soluble anodes. The data recorded correspond to good quality deposits. Table I summarizes the effect of the variables on alloy deposition.

The bath gives bright, adherent, and smooth alloy deposits with 10-91% Ni, the color ranging from bluish white to white with an increase in the nickel content. It was stable and did not present any difficulty. The performance of the alloy anodes was fairly satisfactory, as substantiated by the control

Table II. Control experiments

Electrolyte: Ni 0.3M (17.64 g/l), Co 0.1M (5.90 g/l); ammonium citrate 20 g/l; pH 9.3; sp. resistivity 4.43 ohm/cm³; vol. of electrolyte 200 ml; plating time, 1 hr; c.d.—cathode 2.8 and anode 0.7 amp/dm². Change in pH, sp. resistivity and pyrophosphate—not appreciable.

Anode % Ni	Potential, v		% Ni in deposit	Efficiency %		Change in metal conc., g/l	
	Cathode	Anode		Cathode	Anode	Ni	Co
74	0.99	0.62	74	92	87	−0.27	−0.11
32	1.01	0.20	73	91	63	−1.31	+0.04

experiments summarized in Table II, and the anode potential curves of Fig. 10. The solutions could be used for several runs, and aging up to six months had little effect on their performance. Thick coatings from 0.0005 in. onwards, calculated from area, weight, and analysis could be obtained. High cobalt alloy (80% and above) deposits above thickness 0.002 in. showed a tendency toward cracking. They were resistant to the laboratory atmosphere (1-2 years) and did not change in appearance or color.

Operating conditions.—Table III gives the operating conditions for obtaining satisfactory deposits over a wide composition range, together with the plating characteristics under optimum conditions for the pyrophosphate and sulfate-chloride baths for nickel-cobalt deposition. The data recorded for the acid bath have been obtained experimentally for a typical composition (5). The pyrophosphate bath has some advantages over the acid bath, the favorable points being: (*a*) total metal content of the solution, (*b*) specific resistivity and throwing power, (*c*) bath control in view of the low nickel to cobalt ratio in the solution, (*d*) speed of plating, and (*e*) cathode efficiency.

Discussion

The experimental results show that the pyrophosphate bath is suitable for plating alloys of nickel with cobalt. Detailed studies of an academic character on the effect of variables on alloy deposition have not been made by previous workers. Alloy anodes have not been used, and the current density did not go beyond 5 amp/dm² except in the sulfate-chloride bath employed by Weisberg (5). The pyrophosphate bath can be worked up to 8.4 amp/dm² cathode current density under still conditions and gives deposits over a wide composition range.

Alloy composition.—The nickel content of the deposit could be increased chiefly by an increase in the nickel or decrease in the cobalt content of the solution, and to some extent by an increase in the pH or agitation of the solution (Fig. 2-4). The other variables had no significant effect on the alloy com-

Table III. Operating conditions

	Pyrophosphate		Sulfate-chloride	
	Range	Optimum		
Bath composition, g/l				
Nickel chloride ($NiCl_2$, $6H_2O$)	11.9-95.0	71.4	Nickel sulfate ($NiSO_4$, $7H_2O$)	240
Cobalt chloride ($CoCl_2$, $6H_2O$)	6.0-71.4	23.8	Nickel chloride ($NiCl_2$, $6H_2O$)	45
Pyrophosphate (P_2O_7)	43.5-261.0 (0.25-1.5M)	174.0 (1.0M)	Cobalt sulfate ($CoSO_4$, $6H_2O$)	15
Ammonium citrate	2-40	20	Sodium formate	35
Nickel	3.0-23.5 (0.05-0.4M)	17.6 (0.3M)	Boric acid	30
Cobalt	1.5-17.7 (0.025-0.3M)	5.9 (0.1M)	Ammonium sulfate	2.5
			Formaldehyde	1
			Nickel	61.55 (1.05M)
			Cobalt	3.37 (0.06M)
pH	8.3-10.1	9.3	3.7	
Temperature, °C	40-80	60	60	
Sp. resistivity, ohm/cm³	4.46-7.60	4.65	10.08	
Bath voltage, v	1.1-3.0	1.1-2.3	0.7-2.1	
Agitation, rpm	nil	nil	800	
Cathode	Pt, Cu	Pt, Cu	Pt, Cu	
Anode, % Ni	32, 74; Pt	74	74	
Cathode c.d., amp/dm²	0.35-8.40	0.35-8.40	0.35-8.40	
Anode, c.d., amp/dm²	0.1-2.1	0.1-2.1	0.1-2.1	
Cathode efficiency, %	34-99	63-99	57-73	
Anode efficiency, %	63, 87	87	98	
Cathode potential, v	0.67-1.35	0.79-1.24	0.56-1.01	
Anode potential, v	0.13-1.26	0.37-0.76	0.08-0.60	
Throwing number, N	—	0.0316	0.0139	
Deposit				
Composition, % Ni	10-91	69-74	69-75	
Time to deposit 0.0005 in., min (2.8 amp/dm²)	—	10	16	

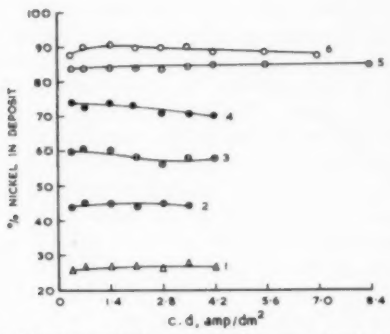

Fig. 2. Effect of cobalt concentration and citrate in solution on deposit composition. Anode Pt unless otherwise stated. Ni 0.3M, Co: curve 1, 0.2; 2, 0.1; 3, 0.05; 4, 0.025; 5, 0.05 with citrate; 6, 0.025 with citrate.

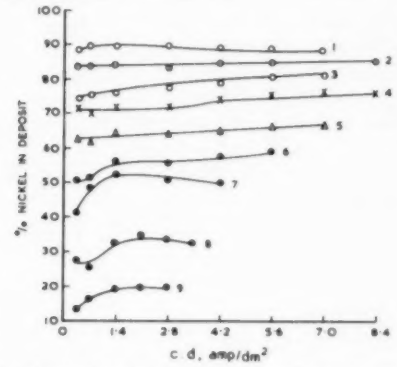

Fig. 3. Effect of nickel and cobalt concentration in solution on deposit composition. Electrolyte: curve 1, Ni 0.3, Co 0.025; 2, Ni 0.3, Co 0.05; 3, Ni 0.4, Co 0.1; 4, Ni 0.3, Co 0.1; 5, Ni 0.2, Co 0.1; 6, Ni 0.3, Co 0.2; 7, Ni 0.1, Co 0.1; 8, Ni 0.05, Co 0.1; 9, Ni 0.05, Co 0.2M.

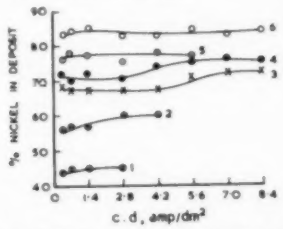

Fig. 4. Effect of citrate concentration in solution, pH and agitation on deposit composition. Ni 0.3M, Co 0.1M, pH 9.3. Curve 1, citrate nil; 2, citrate 5 g/; 3, citrate 20 g/l, pH 8.3; 4, citrate 20 g/l; 5, citrate 20 g/l, pH 10.1; 6, citrate 20 g/l, agitation 1200 rpm.

position, the maximum variation being 5% Ni. The constancy in alloy composition over a wide range of current density is a conspicuous feature during the deposition of this alloy. This has been noticed also during the deposition of nickel-cobalt alloys by most of the previous workers (1, 2, 4-7). However, variations in composition with current density, pH, and temperature have been reported by Fink and Lah (3), and Pletenew and Kusnezowa (15). Work done in this laboratory has shown a similar constancy of composition during the deposition of alloys of nickel with tin (16), iron (10), and zinc (17), and of iron with zinc (18) from pyrophosphate solutions.

In the deposition of nickel and cobalt, the free pyrophosphate content of the solution had little effect on the plating characteristics. The observed behavior in alloy deposition is to be attributed to the presence of the same complexing anion for both metals and the excess of free pyrophosphate in the bath. Ammonium citrate increased the nickel content of the alloy deposit (Fig. 2 and 4), and the addition agents mentioned in Table I had no appreciable effect.

In acid solutions the total metal content is higher than that in the pyrophosphate bath in order to obtain alloys in a similar composition range. Weisberg (5) as well as Young and Struyk (2) have used a high nickel to cobalt ratio of 17 and 26 in the solution, respectively, in order to obtain deposits containing 73 and 89% nickel, respectively. In the present investigations, however, it was possible to deposit alloys containing 73 and 90% nickel from solutions containing a nickel to cobalt ratio of 3 and 12, respectively. The other workers (3, 4, 15) have used solutions containing a maximum ratio of 10. The results show that the deposit composition can be controlled easily during deposition from the pyrophosphate bath, whereas the acid solutions require careful control of pH and other variables.

Cathode efficiency.—The cathode efficiency in the deposition of nickel and cobalt from pyrophosphate solutions is 80-94 and 4-38%, respectively, under the conditions employed for alloy deposition. Ammonium citrate increases the efficiency of nickel deposition, whereas it decreases the efficiency of cobalt deposition from this bath. Since it increases the percentage of nickel in the alloy, there is an over-all increase in the efficiency during codeposition. The alloy efficiency was in general close to that of nickel irrespective of the deposit composition, indicating that the cobalt efficiency is increased by codeposition (Fig. 5-7). Efficiency values of the

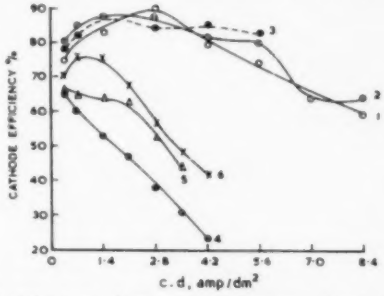

Fig. 5. Effect of cobalt concentration and citrate in solution on cathode efficiency. 1-3, with citrate; 4-6, citrate nil. Ni 0.3M, Co: 1 and 4—0.05M, 2 and 5—0.1M, 3 and 6—0.2M.

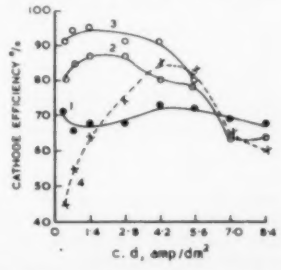

Fig. 6. Effect of pH and agitation on cathode efficiency. Ni 0.3M, Co 0.1M. Curve 1, pH 8.3; 2, pH 9.3; 3, pH 10.1; 4, pH 9.3; agitation 1200 rpm.

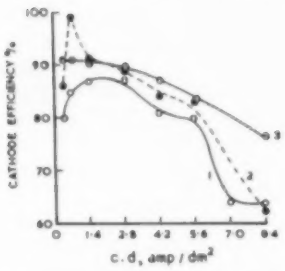

Fig. 7. Effect of anode composition on cathode efficiency. Ni 0.3M, Co 0.1M, pH 9.3. Anode: curve 1, Pt; 2, alloy 74% Ni; 3, alloy 32% Ni.

order of 70% and below have been reported for acid solutions (1, 2, 5, 15). Bonn and Wendell (19) as well as Young and Struyk (2) have observed efficiency values greater than 100%, the former with hypophosphite solutions and the latter with superimposed alternating current. Figure 6 shows that increase in the pH of the solution increases the cathode efficiency; agitation decreases the efficiency at low current density. The other variables had no marked effect, the maximum change being about 15%. Increase in the metal content of the solution and temperature increased the limiting current density. Under optimum conditions, the limiting current density values for nickel, cobalt, and the alloy are 6.0, 9.8, and 8.4 amp/dm². The deposits were satisfactory although the efficiency was much below 100%.

Cathode potential.—The cathode potential during alloy deposition decreased with decrease in current density or increase in temperature (Fig. 8). The effect of the other variables was not significant, the variations being not more than 0.14 v. The plating solutions possessed good throwing power as observed visually. The deposition potentials for nickel, cobalt, and nickel-cobalt alloy in pyrophosphate solutions under optimum conditions are 0.66, 0.60, and 0.70 v, respectively. An alloy deposit with more or less a constant composition is to be expected, as is borne out by the experimental results. In sulfate solutions Glasstone (1) has obtained deposition potentials of 0.57 v for cobalt and alloy, and 0.56 v for nickel. The values in pyrophosphate solutions are about the same order. He also has attributed the constancy of composition to the deposition potentials of the two metals and the alloy being almost the same for different concentrations, so that there is no tendency for one metal to deposit more readily than the other with a variation in the current density. He has stated that at low current densities the effect of temperature on deposit composition is due to the depolarization of nickel and the impoverishment of cobalt in the electrolyte. At higher current densities and temperatures the composition change is very little, and this has been explained as being due to the retarding effect of cobalt on nickel deposition.

Temperature has no effect on the deposit composition between 40° and 80°C. Figure 12 shows the effect of temperature on the cathode potentials of

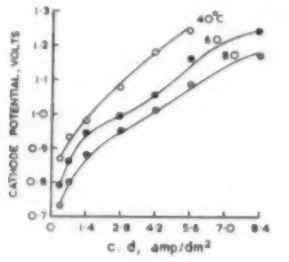

Fig. 8. Effect of temperature on cathode potential. Conditions same as in Fig. 7, anode 74% Ni.

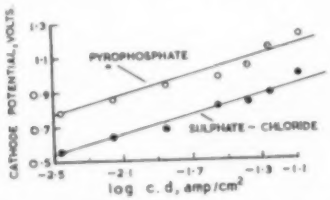

Fig. 9. Cathode potential—Log c.d. lines. Pyrophosphate bath—nickel chloride 71.31, cobalt chloride 23.80, pyrophosphate 174, citrate 20 g/l; pH 9.3, 60°C, anode 74% Ni. Sulfate-chloride bath—nickel sulfate 240, nickel chloride 45, cobalt sulfate 15, sodium formate 35, boric acid 30, ammonium sulfate 2.5, formaldehyde 1 g/l; pH 3.7, 60°C, anode 74% Ni.

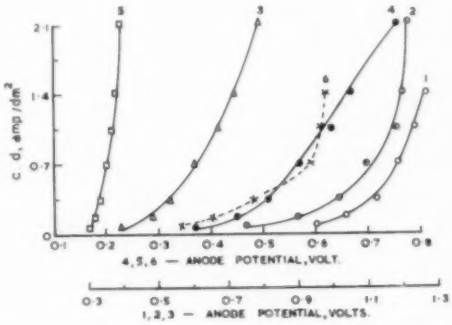

Fig. 10. Anode potential curves. Anode c.d. is given. Bath prepared from: 1-3, nickel pyrophosphate, cobalt pyrophosphate, potassium pyrophosphate, citrate 20 g/l; 4-6, nickel chloride, cobalt chloride, potassium pyrophosphate, citrate 20 g/l. Temp, 60°C; Ni 0.3M; Co 0.1M; pH 9.3. Anode: 1-4, 74% Ni; curve 5, 32% Ni; 6, Ni in Ni 0.3M; 1, KCl nil; 2, KCl 15 g/l; 3, KCl 50 g/l.

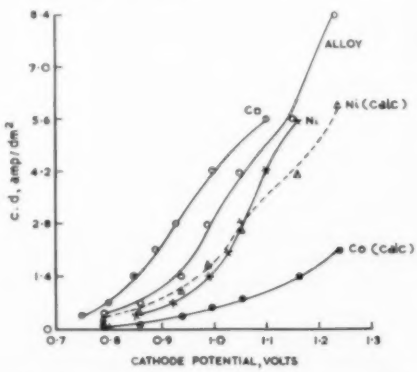

Fig. 11. Reconstruction of single metal potential curves from alloy composition and potential. Bath composition: Ni, 0.3M; Co, 0.1M; alloy, Ni 0.3M, Co 0.1M, other conditions same as in Fig. 9.

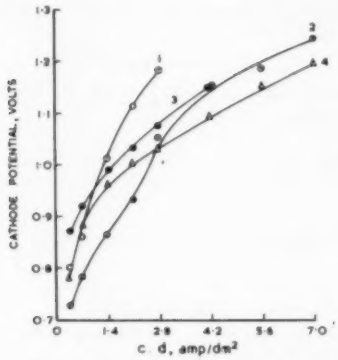

Fig. 12. Effect of temperature on cathode potentials of nickel and cobalt. 1-2, Co 0.1M; 3-4 Ni 0.3M; temp, 1 and 3, 40°C; 2 and 4, 80°C.

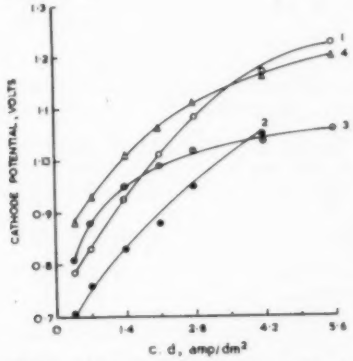

Fig. 13. Effect of pH on cathode potentials of nickel and cobalt. 1-2 Co 0.1M; 3-4 Ni 0.3M; curve 1, pH 8.8; 2, pH 10.8; 3, pH 8.5; 4, pH 10.5.

nickel and cobalt. The values for 60°C have not been plotted as the curve somewhat overlaps and comes in between the curves for 40° and 80°C. The results show that temperature has no significant effect on the cathode potentials of the single metals or the alloy (Fig. 8). Second, the relative effect of temperature is on cobalt rather than on nickel which has a greater tendency to deposit. The net result is that the effect of temperature on nickel deposition will be the dominating factor during co-deposition. One can therefore expect little variation in composition with temperature. Last, the deposition potentials of the two metals and the alloy in pyrophosphate solutions are practically the same at 40° and 80°C, as given above for 60°C. This is also in favor of constancy of composition. Figure 4 shows that there is a slight increase in nickel content of the deposit with increase in pH. This is in accordance with the appreciable effect of pH on the cathode potentials of nickel and cobalt, see Fig. 13.

The cathode potential curves (Fig. 1) for nickel and cobalt belong to two types (12): (A) curves are close and the same vertical line cuts both, and (B) curves intersect (in a few cases). From the alloy potential and composition, however, it is possible to determine the proportion of the current that is used in the deposition of each metal and to plot corresponding potential curves for each. Such studies are rare, and the metal ratios in the deposit have been found to vary widely from those predicted from the single metal potential curves (12, 20). Calculations of this nature, wherever possible, will at least give a fairly quantitative picture of the extent of influence of one metal over the other during alloy plating. Figure 11 presents the cathode potential curves of the nickel-cobalt system under optimum conditions: alloy potential, single potentials—observed and calculated. The alloy curve is in between the experimental curves for nickel and cobalt. When the curves are reconstructed the nickel curve is practically unchanged at lower current densities, and there is a small polarization beyond 2.8 amp/dm². On the other hand there is a large polarization of the deposition of cobalt, which is now the baser metal in the system. The alloy curve is closer to the calculated curve for nickel, indicating that a deposit with a high nickel content is to be expected. This is in fair agreement with the results.

Structure of deposits.—The photomicrographs in Fig. 14 show that the electrodeposited alloy has a

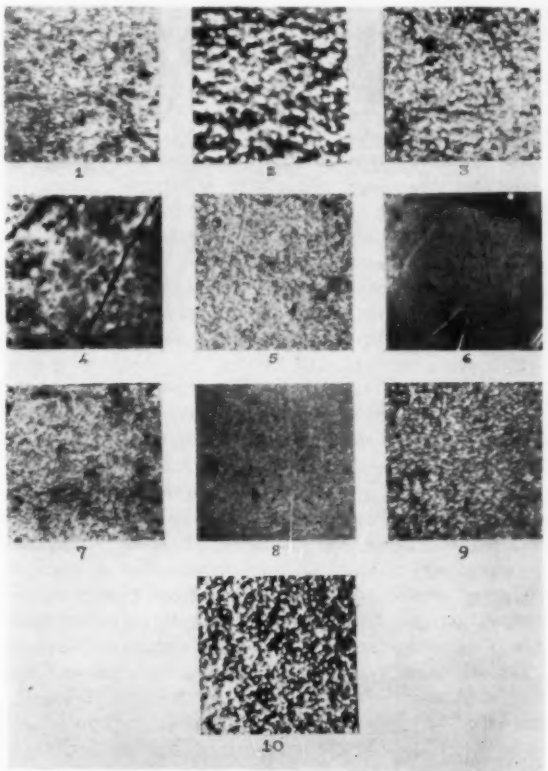

Fig. 14. Photomicrographs of deposits. Copper base, magnification 1 x 200. Soluble anodes, 74% Ni for plates 2 to 5; and 32% Ni for plates 6 to 9. Plate 1. Ni only—Ni 0.3, am. citrate 20 g/l, 2.8 amp/dm²; plate 2, 86% Ni-Ni 0.3M, Co 0.05M, am.citrate 20 g/l, 2.8 amp/dm²; plate 3, 73% Ni-Ni 0.3M, Co 0.1M, am.citrate 20 g/l, 2.8 amp/dm²; plate 4, 70% Ni, acid bath—nickel sulfate 240, nickel chloride 45, sodium formate 35, boric acid 30, cobalt sulfate 15, am. Sulfate 2.5, formaldehyde 1 g/l, 2.8 amp/dm², 800 rpm; plate 5, 57% Ni-Ni 0.3M, Co 0.2M, am.citrate 20 g/l, 2.8 amp/dm²; plate 6, 49% Ni-Ni 0.3M, Co 0.1M, 2.8 amp/dm²; plate 7, 42% Ni-Ni 0.1M, Co 0.1M, am. citrate 20 g/l, 2.1 amp/dm²; plate 8, 28% Ni-Ni 0.05M, Co 0.1M, am.citrate 20 g/l, 0.7 amp/dm²; plate 9, 14% Ni-Ni 0.05M, Co 0.2M, am.citrate 20 g/l, 1.4 amp/dm²; plate 10, Co only—Co 0.1M, am.citrate 2 g/l, 2.8 amp/dm².

Table IV. X-ray studies

Conditions as in Fig. 14.

Plate No.	% Ni	Phase	Lattice	Experimental, A		Reported, A	
				a	c	a	c
1	Ni only		f.c.c.	3.501		3.517	
2	86	α	f.c.c.	3.4824			
3	73	α	f.c.c.	3.4886		3.5221	
5	57	α	f.c.c.	3.5078			
7	42	α	f.c.c.	3.5334		3.5286	
8	28	α	f.c.c.	3.5292			
9	14	β	c.p.h.	2.492	4.037		
10	Co only		c.p.h.	2.4796	4.067	2.5014	4.0616

fine-grained structure. X-ray studies of the deposits showed the existence of the alpha solid solution with f.c.c. structure and beta solid solution with c.p.h. structures as in the phase diagram (Table IV). There was an increase in the lattice constant value as the nickel content of the deposit decreased (except in case of 28% Ni). The reported values in the table have been presented for the nearest composition of the thermal alloy (21). Aotani (22) observed that nickel-cobalt alloys deposited from sulfate solutions had a magnified range of solid solutions containing 11-79% nickel.

Anode corrosion.—The nickel anode corrodes satisfactorily in pyrophosphate solutions containing the chloride ion (8), the anode efficiency being close to 100%. On the other hand, the cobalt anode, cast or electrolytic, was totally passive in solutions with or without chloride. Anode corrosion was, however, satisfactory with nickel-cobalt alloys of both compositions; they are solid solutions. Young and Struyk (2) have used separate anodes and observed a preferential dissolution of cobalt. Nickel wire wound over cobalt strips was employed as the anode by Brockman and Nowlen (7). There is a mention of the use of alloy anodes by Brockington (23). The performance of the alloy anodes checked well with anode potential curves of Fig. 10 and analysis of the plating solutions, see Table II. There is a decrease in the metal content of the solution due to the difference in the electrode efficiencies. The bath requires careful control in industrial plating since there is a tendency for sludge formation. Without chloride ion in solution, nickel-cobalt anodes are totally passive as found from anode potentials (Fig. 10).

Acknowledgment

Our thanks are due to Professor M. R. A. Rao for his keen interest in the work.

Manuscript received June 20, 1960. Paper prepared for delivery before the Houston Meeting, Oct. 9-13, 1960.

Any discussion of this paper will appear in a Discussion Section to be published in the December 1961 JOURNAL.

REFERENCES

1. S. Glasstone and J. C. Speakman, *Trans. Faraday Soc.*, **26**, 565 (1930); **27**, 29 (1931).
2. C. B. F. Young and C. Struyk, *Trans. Electrochem. Soc.*, **89**, 383 (1946).
3. C. G. Fink and K. H. Lah, *Trans. Am. Electrochem. Soc.*, **58**, 373 (1930).
4. C. B. F. Young and N. A. Gould, *Trans. Electrochem. Soc.*, **69**, 585 (1936).
5. L. Weisberg, *ibid.*, **73**, 435 (1938).
6. R. Piontelli and L. Canonica, *Proc. Third International Electrodeposition Conference*, p. 121 (1948).
7. C. J. Brockman and J. P. Nowlen, *Trans. Electrochem. Soc.*, **69**, 553 (1936).
8. S. K. Panikkar and T. L. Rama Char, *This Journal*, **106**, 494 (1959).
9. Vasanta Sree and T. L. Rama Char, *Bull. India Section, Electrochem. Soc.*, **9**, 59 (1960).
10. Vasanta Sree and T. L. Rama Char, *ibid.*, **7**, 72 (1958).
11. J. Vaid and T. L. Rama Char, *ibid.*, **7**, 5 (1958).
12. A. G. Gray (Editor), "Modern Electroplating," John Wiley and Sons, New York (1953).
13. Vasanta Sree and T. L. Rama Char, *Electroplating and Metal Finishing*, **12**, 326, 385 (1959).
14. G. E. Gardam, *Trans. Faraday Soc.*, **34**, 698 (1938).
15. S. A. Pletenew and W. W. Kusnezowa, *Z. Elektrochem.*, **39**, 201 (1933).
16. J. Vaid and T. L. Rama Char, Unpublished work.
17. S. K. Panikkar and T. L. Rama Char, *J. Sci. and Ind. Research*, **17A**, 95 (1958).
18. Vasanta Sree and T. L. Rama Char, *ibid.*, **17B**, 439 (1958).
19. T. H. Bonn and D. C. Wendell, Jr., U. S. Pat. 2,644,787 (1953).
20. W. Blum and G. B. Hogaboom, "Principles of Electroplating and Electroforming," Third Ed., McGraw-Hill Book Co., New York (1949).
21. A. Taylor, *J. Inst. Metals*, **77**, 585 (1950).
22. K. Aotani, *Nippon Kinzoku Gakukai-Shi*, **B14**, No. 5, 52, (1950); *Chem. Abs.*, **47**, 7917 (1953).
23. A. F. Brockington, *Metal Ind. (London)*, **69**, 468 (1946).

Electrolysis in Anhydrous Ether

Ivan E. Gillet

Electrochemistry Laboratory, University of Liege, Liege, Belgium

ABSTRACT

Electrolyses have been carried out on anhydrous ethyl ether made conductive by dissolution of inorganic salts or Grignard reagents ($AlCl_3$ or $AlCl_3$ + LiCl or $MgBr_2$ or RMgBr). Polarization curves have been determined and products analyzed. Results and conclusions are presented, the main conclusion being that ether itself reacts easily at both electrodes and is sometimes the only reacting substance, the dissolved salt being used only to conduct the current in solution.

Jolibois (1), Evans (2), Brenner (3), and we (4) have used anhydrous diethyl ether as a solvent for electrolysis. The products obtained indicated decomposition of the solvent in several cases at the anode or at the cathode and suggested the problem of the behavior of the solvent itself during electrolysis. As a preliminary approach to the description of this behavior, two questions are considered in this paper for both anodes and cathodes: 1. Under what circumstances does the solvent react, and when does it act only as a solvent? 2. Where does the solvent react—on the electrode surface, a true electrode reaction, or in solution, a chemical reaction with faradaic products of the solute?

Experimental

Cells.—Four types of Pyrex cells were used, containing 3-250 ml of solution and differing mainly in size, shape, and position of the electrodes. The fourth cell had a capillary probe to provide an electrolytic junction to a reference electrode.

Electrodes.—All were of bright platinum. In the first cell, a small wire (0.04 cm^2) was the electrode under study in the middle of a cylindrical basket used as a larger counter electrode (40 cm^2) (4). In a second cell (microcell) two small wires were used (0.07 cm^2) 2 cm apart. In a third cell (preparative) two rectangular platinum foils (5 cm^2) were set parallel to each other at a distance of 2 cm. In the fourth cell the two 2 cm^2 circular parallel foils were set 15 cm apart.

Reference electrode.—The first part of this work was done without a reference electrode because such an electrode was not known for anhydrous ether. Subsequently, we made a suitable reference electrode of silver/silver chloride prepared in the usual aqueous way [Brown's procedure (5)]. It was washed thoroughly by prolonged and repeated soaking first in distilled water, then successively in alcohol, ordinary ether, and anhydrous ether, and finally was put in anhydrous ethereal 3M $AlCl_3$ saturated with 0.75M LiCl. The potential was stable and reproducible. An analogous Ag/AgBr electrode was used by Berglund and Sillen (6) as indicating electrode in potentiometric titrations in anhydrous ether; their solutions contained LiBr and a large amount of $LiClO_4$ as supporting electrolyte.

Materials.—Commercial diethyl ether was purified and dried in the usual way (7), then distilled over fresh sodium wire directly into the preparation flask.

To make the solutions conducting, various anhydrous substances were used: organo-magnesium halides (R-Mg-X), $MgBr_2$, $AlCl_3$, and $AlCl_3$ plus LiCl.

To keep the solutions anhydrous during preparation and electrolysis and to avoid the possible action of oxygen, all experiments were made under an atmosphere of pure dry nitrogen. Classical methods of gas analysis were used at first; and more recently, gas chromatography was used.

Results and Discussion

For answering the questions about when and where the solvent reacts, two sets of facts are available: the products obtained and the dynamic electrode potentials involved.

Products

At the anode.—With organo-magnesium compounds, the main products are hydrocarbons from the solute plus CO_2, oxygen, and alcohols, as shown by Evans (2e, f, g, h, i).

With 2.5M $MgBr_2$, the anodic reaction gives a gas consisting principally of CH_4 and CO_2; the presence of oxygen is uncertain.

At the cathode.—With 2.5M $MgBr_2$ there is no Mg deposition as with Grignard reagents, but hydrogen evolution occurs with high yield (> 80%).

With 3M $AlCl_3$ in the preparative cell containing 50 ml of solution and at a cathodic current density of 30 ma/cm^2, there also is evolved a gas composed of ethylene and hydrogen chloride. After 3 hr of electrolysis, however, HCl stopped coming off and H_2 appeared and was produced for the rest of the electrolysis time (10 hr). Three hours of electrolysis corresponded to 0.016 **F** of electricity passed in a cell containing 0.15 mole of $AlCl_3$.

With 3M $AlCl_3$ + 0.75M LiCl the products are identical with those obtained with $AlCl_3$ alone for the first 3 hr.

If the solvent reacted chemically in solution with faradaic products of the solute, the products from the solvent should change with the nature of the solute. Clearly this is not the case either at the anode or at the cathode. Thus the solvent reaction

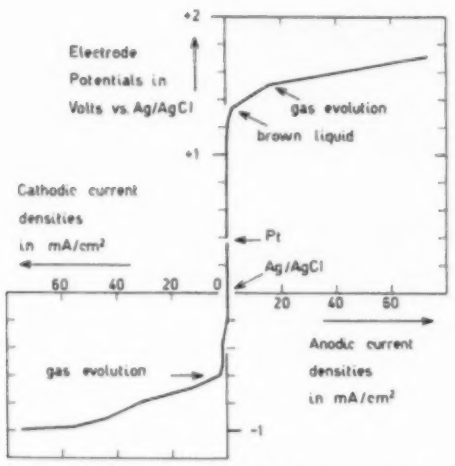

Fig. 1. Anodic and cathodic polarization curves for a solution of 3M $AlCl_3$ + 0.75M LiCl in anhydrous ether between bright platinum electrodes.

at either electrode seems to be a true electrode reaction.

Dynamic Potentials

Figure 1 shows polarization curves (anodic and cathodic) for an ether solution of 3M $AlCl_3$ saturated with 0.75M LiCl between bright platinum electrodes. This was done with the new reference electrode mentioned above. The potential of this silver chloride electrode has been taken as zero on the diagram.

The static potential of bright platinum on this scale is + 0.38 v. The dynamic potential of the anode, when the current starts to increase sharply from negligible values, is + 1.35 v. The dynamic potential of the cathode under the same conditions is − 0.60 v. The so-called "decomposition voltage" for this solution between bright platinum electrodes is thus 1.35 + 0.60 = 1.95 v.

This seems to be characteristic of the solvent for the following reasons: (*A*) No products were obtained coming exclusively from the solute, no aluminum or lithium deposition at the cathode, no chlorine evolution at the anode. (*B*) The products obtained require the decomposition of ether; at the cathode, ethylene (C_2H_4) as well as hydrogen atoms to form H_2 or HCl must come from the solvent; at the anode, the brown liquid formed at + 1.35 v is probably an organic polymer of low molecular weight. (*C*) This decomposition voltage seems to be the same with different solutes when the products show a decomposition of the solvent: Evans and coworkers have shown by analysis of the products obtained from the electrolysis of Grignard reagents that the highest rate of solvent decomposition was obtained with CH_3Mg-X (2e, f) and C_2H_5-Mg-Br (2i) as solutes. With t-butyl-magnesium bromide, on the contrary, the products, butane and butene, come exclusively from the solute, with no solvent decomposition at all (2h)

$$2(CH_3)_3C\text{-Mg-Br} \rightarrow C_4H_{10} + C_4H_8$$

For the first two, with solvent decomposition, methyl- and phenyl-magnesium bromides, the decomposition voltages are 1.94 and 2.17 v, respectively (2d). For t-butyl-magnesium bromide, without solvent decomposition, the decomposition voltage is 0.97 v (2d).

Comparison of these voltages with the value of 1.95 v for the $AlCl_3$ solution (Fig. 1) shows that the solvent reacts only when a minimum voltage is reached (between 1.9 and 2 v). Below this value only the solute reacts, as in the case of t-butyl-magnesium bromide at 0.97 v. At or above this value, either the solvent reacts alone, as with $AlCl_3$, or both solvent and solute react, as with methyl- and phenyl-magnesium bromides.

The fact that the solvent reaction depends on a definite electrode potential is a further indication that it is a true electrode reaction.

Actually, the decomposition voltage is the sum of anode and cathode potentials, and only the reaction potentials for each electrode separately have a conclusive worth. Nevertheless, the above conclusion holds true at least qualitatively and probably quantitatively for the following reasons: (*A*) The difference between 0.97 and 1.95 v is large enough for a qualitative conclusion in any case. (*B*) In Evans' measurements, organic products being formed at the anode and magnesium being deposited at the cathode, the decomposition voltages can be taken as anodic reaction potentials *vs.* a magnesium reference electrode if one assumes, as did Evans, that the deposition potential of magnesium is constant. (*C*) For an almost quantitative conclusion, it is only necessary to assume that, within a certain limit of error, the deposition potential of magnesium is close to the potential for the cathodic evolution of ethylene and hydrogen. This might well be the case in spite of the fact that the metal is deposited with 100% current efficiency from Grignard solutions while it is not deposited at all from ether solutions of $MgBr_2$ or $AlCl_3$. This last fact is not accounted for on the basis of potentials but on the basis of reacting species, as Dessy and Handler (8) have shown with radioactive magnesium that the metal deposited from Grignard solutions comes exclusively from RMg^+ or R_2Mg in solution and not at all from MgX^+ or MgX_2.

Conclusions

In electrolyses of various solutions in anhydrous diethyl ether the products obtained show that ether itself can react at both electrodes and is sometimes the only reacting substance, solutes being only conducting additives.

The dynamic potentials involved indicate that at both electrodes the electrolytic decomposition of ether is a true electrode reaction, responsible for the faradaic current and occurring at a definite electrode potential, independently of the nature of the solute.

Manuscript received June 20, 1960. This paper was prepared for delivery before the Columbus Meeting, Oct. 18-22, 1959.

Any discussion of this paper will appear in a Discussion Section to be published in the December 1961 JOURNAL.

REFERENCES

1. P. Jolibois, *Compt. rend.*, **155**, 353 (1912); *ibid.*, **156**, 712 (1913).

2. a, J. M. Nelson and W. V. Evans, *J. Am. Chem. Soc.*, **39**, 82 (1917); b, W. V. Evans and F. H. Lee, *ibid.*, **55**, 1474 (1933); c, W. V. Evans and F. H. Lee, *ibid.*, **56**, 654 (1934); d, W. V. Evans, F. H. Lee, and C. H. Lee, *ibid.*, **57**, 489 (1935); e, W. V. Evans and E. Field, *ibid.*, **58**, 720 (1936); f, W. V. Evans and E. Field, *ibid.*, **58**, 2284 (1936); g, W. V. Evans and D. Braithwaite, *ibid.*, **61**, 898 (1939); h, W. V. Evans, D. Braithwaite, and E. Field, *ibid.*, **62**, 534 (1940); i, W. V. Evans, R. Pearson, and D. Braithwaite, *ibid.*, **63**, 2574 (1941); j, W. V. Evans and R. Pearson, *ibid.*, **64**, 2865 (1942); k, R. Pearson and W. V. Evans, *Trans. Electrochem. Soc.*, **82**, 297 (1942).
3. A. Brenner, *This Journal*, **106**, 148 (1959).
4. I. Gillet and F. Bloyaert, *Ind. Chim. Belge*, **16**, 78 (1951).
5. A. S. Brown, *J. Am. Chem. Soc.*, **56**, 646 (1934).
6. U. Berglund and L. G. Sillen, *Acta Chem. Scand.*, **2**, 123 (1948).
7. A. I. Vogel, "Practical Organic Chemistry," p. 161, Longmans, Green and Co., London (1951).
8. R. E. Dessy and G. S. Handler, *J. Am. Chem. Soc.*, **80**, 5824 (1958).

The Elastic Modulus and Internal Friction of Electrodeposited Copper

Harold J. Read and Arthur H. Graham

Department of Metallurgy, Pennsylvania State University, University Park, Pennsylvania

ABSTRACT

Experimental techniques and calculations for the determination of elastic modulus and internal friction from sonic measurements on thin-walled tubes prepared by electrodeposition are described. A method of making the tubes with the necessary precision is presented. Data on the effects of some plating variables are given, but special attention is devoted to relationships between the structures of the deposits and the elastic properties under study.

There has developed in recent years an increasing awareness of the importance of the mechanical properties of electrodeposited metals, and many investigators have gathered data on tensile strength, ductility and hardness. But two mechanical properties which have received little or no attention are the elastic modulus and internal friction.

Although the elastic modulus is involved in the calculation of internal stress of electrodeposits, there are no published data on actual measurements of elastic modulus in electrodeposited copper—a metal which has received considerable attention so far as internal stress is concerned. Handbook values for wrought copper have been used. It is well known, however, that the elastic modulus of cold-worked copper may vary from 14.5 to 17.0 x 10^6 psi (1). Structural anisotropy may also greatly affect the elastic modulus. Weertman and Koehler (2) found that the elastic modulus of a single crystal of annealed copper in the [100] direction was 9.55 x 10^6 psi. Inasmuch as structural anisotropy is far from unknown in electrodeposits, this factor conceivably could have considerable effect on the elastic modulus of a given deposit.

Because the technique used to measure the modulus in this investigation can also be employed in the determination of internal friction, exploratory measurements were made on some of the deposits. This part of the investigation was undertaken for reasons other than scientific curiosity. Damping capacity is a manifestation of internal friction and is a significant property in the selection of materials for certain components of mechanical devices. It is probable also that internal friction measurements will be of value in the study of intergranular corrosion, diffusion, and impurity concentration in electrodeposits. It is known that the internal friction of copper varies considerably, depending on the degree of cold work (3), the oxygen content (4) and other factors (5, 6). No measurements have been reported for electrodeposited copper.

Experimental Procedures

Foerster (6) developed the sonic technique which was used in this investigation. Although solid bars are commonly used in the ordinary adaptations of Foerster's method, such specimens are not practical for electrodeposits of the thicknesses usually encountered in protective and decorative coatings. The method can be used, however, just as satisfactorily with thin-walled tubes as with solid bars. It was found that tubes with walls of 33-mil thickness were rigid enough to be handled in the preparative and measuring procedures. Although this is considerably thicker than deposits that are used for ordinary commercial processes, it is at least of the same order of magnitude. Experience with the measurement of other mechanical properties indicated that the difference in thickness is not important so long as massive deposits are avoided.

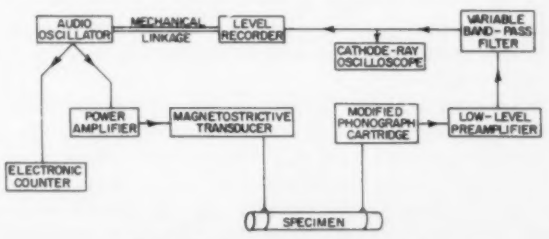

Fig. 1. Block diagram of apparatus

Table I. Components of the apparatus Shown in Fig. 1

Component	Manufacturer	Model No.
Audio oscillator	Hewlett Packard	DY 2200
Electronic counter	Hewlett Packard	521C
Power amplifier	Dyna Company	Mark III
Magnetostrictive transducer	Specially constructed	
Phonograph cartridge	Unidentifiable	
Low-level preamplifier	Tektronix	112
Variable band-pass filter	Krohn-Hite	310-AB
Cathode-ray oscilloscope	Tektronix	315-D
Level recorder	Bruel and Kjaer	2304

The array of apparatus employed for the sonic tests is indicated as a block diagram in Fig. 1, and the components are identified in Table I. After a specimen is suspended between the transducer and the pickup by two fine cotton strings, a run is made by starting the audio oscillator at a low frequency. Gradual increase of the frequency is achieved by action of a constant-speed motor which is located in the level recorder and is connected to the oscillator by a mechanical linkage. When the resonant frequency is reached, the resonance curve is plotted by the recorder and simultaneously displayed visually on the screen of the oscilloscope.

Calculation of the elastic modulus from the resonant frequency of a freely suspended body vibrating in a transverse mode is based on a well-known relationship:

$$E = \frac{4\, l^4 f_r^2 \rho}{\pi^2 \beta_n^2 K^2}$$

where E is the elastic modulus, l length of the tube, f_r resonant frequency, ρ mass density, π 3.1416, β_n constant that depends on the particular harmonic excited $\beta_1 = 1.5056$, $\beta_2 = 2.4997$, β_3 to $\beta_n = n + 0.5$, and K is radius of gyration.

For a thin-walled tube

$$K = \tfrac{1}{2}\,(r_1^2 + r_2^2)^{1/2}$$

where r_1 is the inner radius of the tube and r_2 the outer radius of the tube, and

$$E = \frac{16\, l^4 f_r^2 \rho}{\pi^2 \beta_n^2 (r_1^2 + r_2^2)} \qquad [1]$$

All values required for the solution of Eq. [1] can be determined with considerable accuracy; hence, the method as a whole is quite accurate. An analysis of the probable errors in the measured quantities indicates that the elastic moduli of the deposits studied in this investigation should be accurate to three significant figures.

Foerster (6) has shown that the maximum stress during a determination never exceeds 14 psi and is usually less than 2 psi. It is apparent, therefore, that the elastic modulus determined by the sonic technique represents the tangent to the stress-strain curve at zero stress; hence, the measured modulus is that defined by usual engineering practice.

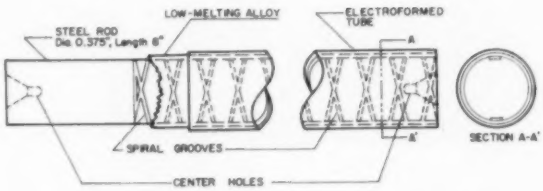

Fig. 2. Cathode assembly for electrodeposition of tubes

Proper calibration of the apparatus makes possible the direct determination of internal friction from a measurement of the distance between the half-power points on the resonance curve. It is convenient to use the concept of mechanical Q, which is analogous to the well-known electrical Q. Internal friction designated as Q^{-1} is defined by the equation:

$$Q^{-1} = \frac{f_2 - f_1}{f_r} \qquad [2]$$

where the term f_r is the resonant frequency, and f_1 and f_2 denote the frequencies at which the resonance curve falls to half of its maximum power. In most cases, internal friction measured in terms of the logarithmic decrement, δ, may be converted (3) to Q^{-1} by the equation:

$$Q^{-1} = \delta/\pi \qquad [3]$$

Specimen preparation.—All of the specimens were thin-walled tubes approximately 0.4 in. in diameter and 4 to 6 in. in length. The cathodes on which the tubes were deposited were steel rods coated with a thin layer of low-melting alloy. Figure 2 shows the details of the cathode rods. A steel rod was used as the main part of the cathode rather than a solid rod of low-melting alloy because the alloy has not sufficient strength or rigidity to permit accurate machining of its surface prior to deposition of copper. The internal diameter of the finished tube must be both uniform and accurately known; hence, the cathode must be a true circular cylinder.

The coating of low-melting alloy was applied by dipping a cold steel cathode rod into a crucible of molten alloy held just above its melting point. A layer of the alloy immediately froze on the cold rod, which was then withdrawn promptly. The surface of the alloy coating was machined accurately in a lathe; at the completion of this operation the alloy thickness was but a few thousandths of an inch. The spiral groves on the steel rod are necessary to provide a mechanical key to hold the low-melting alloy in place, particularly during the machining operations.

After copper had been deposited to the desired thickness, the entire cathode was immersed in hot water to melt the alloy, thus making it possible to slip the tube off the steel rod. Most of the residual alloy adhering to the internal surface of the tube was removed by forcing cylindrical sponges through the tube while it was immersed in hot water.

In those instances where a rough deposit was to be machined on its outer surface the operation was carried out prior to the removal to the electroformed tube from the cathode rod. This procedure assured

concentricity of the inner and outer surfaces of the copper tube.

Plating details.—Three copper plating baths were employed in the preparation of specimens; their compositions were as follows: Purified acid-sulfate bath, $CuSO_4 \cdot 5H_2O$-200 g/l, H_2SO_4-50 g/l; impure acid-sulfate bath, $CuSO_4 \cdot 5H_2O$-150 g/l, H_2SO_4-60 g/l, C_2H_5OH-50 g/l; duPont's P. R. Cyanide Bath,[1] CuCN-74-90 g/l, "Cyanobrik" NaCN-84-102 g/l, KOH (85%)-16-30 g/l, Elchem 1442-10 ml/l, Elchem 1396-10 ml/l.

The acid-sulfate baths were operated at room temperature without agitation, and the du Pont bath was used in conformance with the instructions furnished by its purveyors.

These baths were selected for the production of copper deposits with different kinds of microstructures. The pure acid-sulfate bath should yield a large-grained columnar structure. The impure acid-sulfate bath was a coulometer solution which had been in use for a long time; it was known to produce a very fine-grained structure in which there was no indication whatever of a preferred direction of growth. The du Pont proprietary bath is known to yield a structure in which the individual grains are exceedingly small, but the structure also possesses the so-called laminated appearance which is commonly encountered in deposits which have been prepared by P. R. plating. Another reason for choosing the P. R. proprietary bath was the assurance that one could deposit a thick coating without the development of the roughness so often encountered in cyanide deposits which are more than 1 mil thick.

Purification of the simple acid-sulfate bath involved treatment with 7 g/l of activated charcoal, agitation at 70°C for 3 hr, and filtration through a fine paper. Previous experience had indicated that the technical chemicals used for bath preparation would give deposits with a very large grain size after such purification.

The plating was carried out in 2-l beakers which were lined with sheets of copper that served as anodes. Cathodes were carefully positioned in the center of the beakers to insure uniform current distribution.

The low-melting alloy was always plated with a thin copper strike from a Rochelle-cyanide bath operated at room temperature and at 5 asf. A strike was not really necessary before plating with the du Pont solution, but it was used for the sake of uniformity in procedure.

Reference standard.—In order to check the sonic technique of measuring the elastic modulus and to provide a reference against which modulus determinations for electrodeposited copper could be compared, commercially drawn copper tubing was selected. Microscopic examination of the tubing revealed many annealing twins and only slight elongation of the grains in the longitudinal direction. It was evident, therefore, that the tube had been thoroughly annealed and then only slightly cold worked in the final drawing operation; hence, its modulus should have been very close to that which has been reported for annealed copper, 18 x 10^6 psi. Experimental determination with the sonic equipment gave 18.1 ± 0.1 x 10^6 psi. The internal friction measurement yielded 4 x 10^{-4}, which represents the lower limit of sensitivity of the sonic technique, but the value compares favorably with that reported for annealed copper by Lawson (7). On the other hand, it is considerably lower than values which have been cited by other investigators (4-6).

[1] du Pont's "Leveled Copper Plating Process" with du Pont addition agents Elchem 1442 and Elchem 1396. The complete solution, fully compounded and ready for use, was furnished by the Electrochemicals Division of E. I. du Pont de Nemours and Company.

Results and Discussion

Elastic modulus measurements.—Inasmuch as current density and thickness of deposit may each have some effect on the structure of electrodeposited copper and hence on the elastic modulus, these variables were studied first. The impure acid-sulfate solution was used at current densities of 5 and 10 asf to prepare deposits in the thickness range from 3 to 10 mils. Current densities greater than 10 asf did not yield specimens with sufficiently smooth surfaces for sonic determinations of the elastic modulus.

The results summarized in Table II indicate that there is no significant effect of either current density or thickness on the elastic modulus. They indicate also that the reproducibility is quite satisfactory. So far as precision of replicate measurements is concerned, the sonic technique is known to be very good, but it was gratifying to find that good reproducibility could be obtained for a group of plated specimens. The sensitivity of some mechanical properties to plating variables often complicates the preparation of truly replicate specimens.

As a result of these preliminary experiments a nominal thickness of 6 mils was employed for subsequent work. Tubes having this wall thickness can be handled easily and are still representative of electrodeposits rather than of massive metal.

Comparisons of deposits from the three types of baths as well as comparisons with the commercially drawn tubing used as a reference material are sum-

Table II. Effects of current density and thickness on the elastic modulus of electrodeposited copper

Impure Acid-Sulfate Bath

Current density, asf	Elastic modulus—psi × 10^{-6}		
	Plated thickness—mils		
	3	6	10
5	15.3	15.4	15.5
	15.3	15.7	15.7
	15.4	16.0	15.8
	15.5		
(average)	(15.4 ± 0.1)	(15.7 ± 0.3)	(15.7 ± 0.2)
10	15.2	15.7	15.4
	15.3	15.8	15.4
	15.3	16.2	15.6
	15.4		15.7
	15.4		15.3
(average)	(15.3 ± 0.1	(15.9 ± 0.3)	(15.5 ± 0.2)

Table III. Elastic moduli of copper deposits compared to modulus For drawn copper tubing —18.1 ± 0.1 × 10^6 psi

Plating bath	Current density, asf	As-plated surface: Elastic modulus psi × 10^{-6}	As-plated surface: Deviation from reference, %	Machined surface: Elastic modulus, psi × 10^{-6}	Machined surface: Deviation from reference, %
Purified acid copper sulfate	10	13.9		16.2	
		13.9		16.1	
		14.0		16.0	
		14.2		16.1	
	(average)	(14.0 ± 0.2)	22.7	(16.1 ± 0.1)	11.0
Impure acid copper sulfate	10	15.7		17.1	
		15.8		16.9	
		16.2		16.9	
	(average)	(15.9 ± 0.3)	12.2	(16.9 ± 0.1)	6.6
du Pont's P. R. copper cyanide	40	16.1		16.8	
		16.0		16.9	
		15.8		16.8	
	(average)	(15.9 ± 0.2)	12.2	(16.8 ± 0.1)	7.2

marized in Table III. The striking item in this table is the low modulus for the deposits from the purified acid-sulfate bath. There is no great difference between the results for the deposits from the impure acid-sulfate bath and the cyanide bath. Examination of the microstructures of the deposits showed that plating from the pure acid-sulfate solution produced large, columnar grains normal to the basis metal surface, whereas the deposits from the other two solutions were fine grained. Some trace of columnar structure was discernible in the deposits from the impure acid-sulfate bath, but twins and other subgrain discontinuities broke up the columnar pattern. The P. R. cyanide deposits showed, of course, the so-called laminations that are expected from P. R. plating.

If one assumes that the columnar structure represents a certain degree of preferred orientation, the result should be a decrease of the elastic modulus just as the preferred orientation resulting from the cold working of copper causes a decrease of modulus. If this be true, one could speculate that anything which might be done to destroy or decrease the perfection of preferred orientation in the deposit would increase the modulus. To test this speculation several specimens from each of the three baths were machined on a lathe before the tubes were removed from the cathode assembly. The tool used for this purpose "smeared" the surface of the tube considerably. This was evident particularly for the specimens from the pure acid-sulfate bath. Microscopic examination showed that the columnar structure was bent and distorted to a high degree near the surface, and the effects were noticeable for a ½ mil or so in depth. Reference to Table III shows that reduction of the preferred orientation in the columnar deposits increases the elastic modulus, thereby confirming the speculation that preferred orientation causes a decrease in the modulus. Distortion caused by machining has little effect on the deposits which had no oriented structure initially.

There is no indication that hardness can be correlated with the elastic modulus. This is just one more bit of evidence that hardness is a property which electrodepositers should ignore.

The question arises as to whether the data reported in Table III deviate sufficiently from each other and from handbook values of the modulus to be significant. It would appear that for the purposes of calculating internal stress it is not acceptable to use 18 x 10^6 psi, the value found in some handbooks. This can result in an error of 23% for columnar deposits and about 12% for fine-grained deposits. Whether this is significant will depend on the purposes to which stress calculations are put. Some investigators in the field of stress determination in copper have used 16 x 10^6 psi, and the sonic technique indicates that this is satisfactory, except possibly for extremely columnar deposits.

Internal friction measurements.—The first measurements of internal friction on several groups of specimens showed large variations among specimens of identical thickness as well as among sets of specimens representing different thickness. It seemed possible that the decrease in internal friction with increasing plated thickness (see Table IV) might

Table IV. Effect of removal of residual alloy on elastic modulus and internal friction

Deposits from impure acid-sulfate bath

Plated	Elastic modulus—psi × 10^{-6}: Before removal of residual alloy	Elastic modulus—psi × 10^{-6}: After removal of residual alloy	Internal friction Q^{-1} × 10^4: Before removal of residual alloy	Internal friction Q^{-1} × 10^4: After removal of residual alloy
6	15.7	15.8	27-40	11
	15.8	15.9	32	16
	16.2	16.3	102	16
(average)	(15.9 ± 0.3)	(16.0 ± 0.3)		(14)
10	15.3	15.5	29-62	19
	15.4	15.4	10	11
	15.6	15.7	19	12
	15.7	15.7	14	10
(average)	(15.5 ± 0.2)	(15.6 ± 0.2)		(10)
30	15.3	15.3	9	9

be due to diminishing effects from the residual alloy on the inner surfaces of the tubes. Lead and other metals used in the low-melting alloy have much higher values of internal friction than copper. Variations among specimens of identical nominal thickness could be ascribed to differences in the amount of residual alloy left on individual specimens.

Several attempts were made to remove the residual alloy by chemical methods. None was satisfactory. It was found, however, that the alloy could be moved by grinding the bores of the tubes with emery paper wrapped around a mandrel. The results of this treatment appear in Table IV and show that the reproducibility of the data was much improved. The fact that the elastic modulus was not appreciably changed indicates that the grinding operation did not introduce any severe mechanical effects. Furthermore, it has been well established that limited plastic deformation increases the internal friction of metals; hence, it can be assumed that no change in mechanical properties was brought about by the grinding of the surface, otherwise the internal friction should have increased rather than decreased. The large decrease caused by the removal of the residual alloy indicates the extreme importance of surface effects in internal friction measurements by the sonic method.

There is good agreement amongst the internal friction measurements reported in Table IV after removal of residual alloy, and one might readily assume that the average value, about 10×10^{-4}, is well representative of copper electrodeposits from an impure acid-sulfate bath. This is 2½ times the measured value of 4×10^{-4} for the internal friction in the copper tubing which was chosen as a reference material.

Continued work on measurements of internal friction disclosed two serious sources of variations in the measurement for individual specimens. The most serious was the dependence of the measured value on the amplitude of vibration imposed upon the specimens. Representative data are given in Table V. A significant increase in the electrical power applied to the transducer by changing the amplitude of the oscillator signal will increase the measured value of internal friction by a factor of 2 or more. The location of the supporting strings with respect to the location of the nodes on the vibrating specimen also affects the amplitude of vibration and the measurements of internal friction.

Energy losses to the surroundings comprise another source of variation in the sonic technique. The dissipation of energy which is measured in the sonic method represents the summation of damping among the fibers of the supporting string, damping within the loops of string that are in contact with the specimen, acoustical radiation from the specimen to the atmosphere, and the internal friction of the metal.

Table V. Amplitude dependence of measurements of internal friction

Purified copper sulfate bath

Specimen No.	Length, mm	Distance between nodes, mm	Distance between supports, mm	Oscillator amplitude setting, range 0 to 100	Internal friction, $Q^{-1} \times 10^{+4}$
1	138	76	100	0	9.6
			100	5	18.3
			100	10	19.5
2	107	59	70	0	19.1
			100	0	43.0

The observed amplitude dependence could be related to any of the factors which contribute to the total dissipation of energy. Adiabatic conditions must be attained, therefore, before the amplitude dependence can be attributed with certainty to the internal friction in the metal. Energy dissipation in the supports could have been minimized by the use of single silk fibers or iron wire approximately 1 mil in diameter in place of cotton strings. Zener has shown that if the internal friction is 1×10^{-4} or lower, the energy losses owing to acoustical radiation become significant and the specimen should be enclosed in an evacuated chamber (8). However, modification of the apparatus was impractical because the measurements of internal friction in the electrodeposits of copper were of an order of magnitude equal to the lower limit of sensitivity for the sonic method (9, 10). Any improvement of the experimental techniques along the lines indicated above would decrease the internal friction values. It is apparent, therefore, that the sonic method is not suitable for a detailed study of internal friction in electrodeposited copper.

Summary

The elastic modulus of electrodeposited copper, measured by the sonic technique, is not affected by current density or thickness of deposit, but ranges from 17×10^6 psi for fine-grained deposits to 14×10^6 psi for large-grained columnar structures.

The internal friction of copper deposits appears to be considerably greater than that of wrought copper, but the very low values encountered are near the limit of sensitivity for the sonic technique.

Acknowledgments

The authors are indebted to the Electrochemicals Department of E. I. du Pont de Nemours and Company for the proprietary cyanide plating solution and to the Physics Department of the Pennsylvania State University for use of sonic testing apparatus. Dr. J. D. Wolf contributed valuable suggestions and discussion.

Manuscript received July 11, 1960. This paper was prepared for delivery before the Columbus Meeting, Oct. 18-22, 1959.

Any discussion of this paper will appear in a Discussion Section to be published in the December 1961 JOURNAL.

REFERENCES

1. "Handbook of Chemistry and Physics," 39th Edition, p. 2007, Chemical Rubber Publishing Co., Cleveland (1957).
2. J. Weertman and J. S. Koehler, *J. Appl. Phys.*, **24**, 624 (1953).
3. A. S. Nowick, "Internal Friction in Metals," *Progress in Metal Physics*, **4**, Interscience Publishers, Inc., New York, 1-70 (1953).

4. R. Cabarat, L. Guillet, and R. LeRoux, *J. Inst. Metals*, **75**, 391 (1949).
5. V. S. Postinkov, *Doklady Akad. Nauk. S.S.S.R.*, **91**, 79 (1953).
6. F. Foerster and W. Koester, *J. Inst. Elect. Eng.*, **84**, 558 (1939).
7. A. W. Lawson, *Phys. Rev.*, **60**, 330 (1941).
8. C. Zener, "Elasticity and Anelasticity of Metals," p. 65, University of Chicago Press, Chicago (1948).
9. D. E. Kline, "Internal Friction Phenomena in Solids," Ph.D. Thesis, The Pennsylvania State University (1955).
10. D. E. Kline, "Temperature Dependence of Internal Friction," M. S. Thesis, The Pennsylvania State University (1953).

The Significance of the Temperature Dependence of Fluorescence Intensity

C. H. Haake

Research Department, Westinghouse Electric Corporation, Bloomfield, New Jersey

ABSTRACT

For some phosphors the fluorescence intensity increases with increasing temperature, reaches a maximum, and then decreases. This behavior arises from a competition of an increasing absorption for the exciting radiation and thermal quenching of the emitted radiation. However, the slope of the initial rise of fluorescence and the temperature of the maximum also depend rather strongly on the thickness of the sample considered. Thin samples, i.e., those in which the penetrating exciting radiation is not absorbed completely, in comparison with thick samples exhibit a steeper slope and a maximum at higher temperature. If the phosphor is in powder form, the average particle size also influences the slope and the position of the maximum although generally to a lesser degree than the sample thickness. Experimental data are presented for magnesium fluorogermanate and magnesium fluoroarsenate, both activated with manganese.

Experimental data on the temperature dependence of the fluorescence intensity of phosphors are of interest for several reasons. For one, in combination with other pertinent data, they yield qualitative and sometimes also quantitative insight into the mechanism of luminescence. An increase of intensity with rising temperature may indicate an increasing absorptivity of the phosphor material for the exciting radiation (1). Thermal quenching of the emitted fluorescence, on the other hand, causes an opposite trend (2). If both processes occur simultaneously, the fluorescence intensity shows a maximum. The many phosphors which produce no such maximum are not considered here. Another reason for studying the temperature dependence of fluorescence is the practical value of such data for designing new phosphors or improving existing ones. Phosphors with good temperature dependence find application, for instance, in high-pressure mercury-vapor lamps (3) and in highly loaded fluorescent lamps where they are operated at relatively high temperatures.

Since it is impractical to measure the performance of experimental phosphors in lamps, one usually resorts to measurements on small plane phosphor layers (4). It is the object of this paper to investigate the significance of the temperature dependence of fluorescence as it may appear from such measured data.

Theory

The fluorescence of several phosphor systems shows temperature dependencies of the general form depicted in Fig. 1 (3, 5). The shape of such plots, particularly below the temperature, T_B, of the break point, usually varies drastically with the wave length of excitation (3, 6). The initial rise of fluorescence will in most cases be due to an increasing absorption, as the occupancy of higher phonon levels in the ground state of the absorbing center increases with temperature (1).

The number of quanta $Q\ (\lambda, T)$ emitted from a phosphor layer per cm^2 and sec when excited by radiation in the wave-length range of λ and $\lambda + d\lambda$ is given by

$$Q(\lambda, T) = N(\lambda)\ \eta\ (\lambda, T)\ A(\lambda, T) \qquad [1]$$

The number, $N(\lambda)$, of exciting quanta is of course not a function of temperature. The thermal behavior

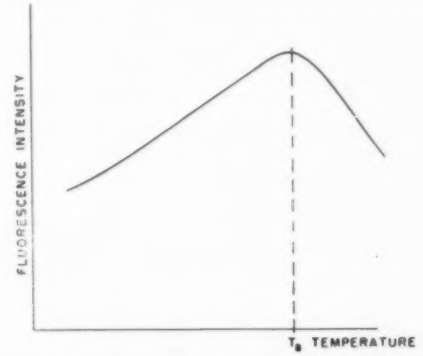

Fig. 1. Schematic representation of the temperature dependence of fluorescence intensity as observed for some phosphor systems.

of the quantum efficiency, $\eta(\lambda, T)$, can be expressed in the form

$$\eta = [1 + C \exp(-V_q/kT)]^{-1} \qquad [2]$$

where C is a constant and V_q is the quenching energy (2). Although in some cases this function is more complex (1, 7), for the present purpose its general trend is described adequately by Eq. [2]. If the phosphor is in powder form, the absorptance $A(\lambda, T)$, beside being dependent on λ and T, is a rather complex function of the sample thickness, s; the average particle diameter, d; the refractive index, n; and the absorptivity, ϵ, of the bulk material.

$$A = f(s, d, n, \epsilon)$$

No concise and accurate expression for the absorptance of phosphor powders is available. Schuster (8) derived a general equation for the absorption of radiation in plane scattering layers. This equation, with a slight modification, has been applied successfully to phosphor powder layers by several workers (9-13). The absorptance appears here as a function of an absorption coefficient, a, a scattering coefficient, r, and the layer thickness, s.

$$A(a, r, s) = \frac{\left(\sqrt{\left(\frac{a}{r}\right)^2 + 2\frac{a}{r}} + \frac{a}{r}\right)\left[\exp\left(rs\sqrt{\left(\frac{a}{r}\right)^2 + 2\frac{a}{r}}\right) - 1\right]}{\left(\sqrt{\left(\frac{a}{r}\right)^2 + 2\frac{a}{r}} + \frac{a}{r} + 1\right)\exp\left(rs\sqrt{\left(\frac{a}{r}\right)^2 + 2\frac{a}{r}}\right) + 1} \qquad [3]$$

The absorption coefficient, a, is approximately proportional to the bulk absorptivity, ϵ, and the scattering coefficient, r, is inversely proportional to the average particle diameter d (14). In addition both a and r are functions of the refractive index n (14).

$$a \approx \epsilon f_1(n)$$

$$r \approx \frac{1}{d} f_2(n)$$

Of course, neither s nor d are temperature dependent, and the temperature dependence of the refractive index is negligibly small in almost any case. Therefore, the temperature dependence of the absorptance, A, lies primarily in the absorption coefficient, a.

As far as the basic properties of the phosphor are concerned, the meaningful parameter is a. However, a given relationship $a(\lambda, T)$ does not have a unique effect on the measurable quantities $A(\lambda, T)$ and $Q(\lambda, T)$. If the phosphor layer is so thin that a considerable portion of the exciting radiation is transmitted, the argument of the exponential in Eq. [3] is small and a relatively small increase of a can result in a strong increase of A. On the other hand, if the layer is quasi-infinitely thick with reference to the exciting radiation, the exponential terms in Eq. [3] are much larger than unity and can be divided out. A small increase of a will, therefore, be concomitant with a relatively small increase of A. One thus expects the initial increase of fluorescence intensity to be steep for thin layers and flat for thick layers. Also since thermal quenching is not affected by the thickness of the sample, the competition of η and A should result in a lower temperature T_x of the fluorescence maximum for thick layers.

If, however, the initial rise of fluorescence intensity is due to reasons other than an increasing absorptivity, the described effect of the layer thickness does not exist. Dexter (15), for instance, mentioned the possibility of a temperature dependent energy transfer process in sensitized luminescence. As the temperature increases, both the emission band of the sensitizer and the absorption band of the emitter broaden and the transfer efficiency increases. This effect is confined to η in Eq. [1] and does not depend on the thickness of the phosphor sample considered.

The other external yet experimentally less accessible parameter is the average particle diameter, d, of the phosphor crystals. It is not immediately apparent from Eq. [3] in what manner the absorptance increase changes with temperature for given $a(T)$-dependencies, if the particle diameter is, say, diminished, *i.e.*, the scattering coefficient increased. A numerical discussion of Eq. [3] shows that such a change is negligibly small for very thin layers. However, for thick layers a smaller particle diameter, *i.e.*, an increased r, causes A and thus Q to increase at a slightly faster rate and the break point T_x, therefore, appears at a somewhat higher temperature.

There remain two practical questions to be answered. What is the correlation of the data measured on a plane layer and the phosphor performance in a lamp? If there is a definite correlation, what sample thickness should one choose to obtain a meaningful result?

For answering these questions one obviously needs an equation for the emission intensity of a phosphor layer in a lamp. For all practical purposes such a layer can be considered closed, *i.e.*, one can assume that any exciting radiation not transmitted or absorbed upon first incidence on the layer is reflected to other parts of the layer where it undergoes another chance of being transmitted or absorbed, and so forth. Again using the Schuster equation one can thus derive an expression for the effective absorptance (13) (Eq. [4], page 80).

There are now two cases of interest. Either the phosphor layer does not transmit the exciting radiation, a situation very nearly encountered in fluorescent lamps (16), or the phosphor layer transmits an appreciable portion of the exciting

$$\alpha(\lambda, T) = \frac{\left[\left(\sqrt{\left(\frac{a}{r}\right)^2 + 2\frac{a}{r}} + \frac{a}{r} + 1\right)\exp\left(rs\sqrt{\left(\frac{a}{r}\right)^2 + 2\frac{a}{r}}\right) - 1\right]\left[\exp\left(rs\sqrt{\left(\frac{a}{r}\right)^2 + 2\frac{a}{r}}\right) - 1\right]}{\left(\sqrt{\left(\frac{a}{r}\right)^2 + 2\frac{a}{r}} + \frac{a}{r} + 1\right)\exp\left(2rs\sqrt{\left(\frac{a}{r}\right)^2 + 2\frac{a}{r}}\right) + 1} \quad [4]$$

radiation. The latter is the case for certain exciting lines in high-pressure mercury-vapor lamps whose radiation is color-corrected by a thin layer of magnesium fluorogermanate (Mn) on the inside of the outer bulb. Here the phosphor layer transmits about 60% of the radiation at 365mμ (13). In the first case the effective absorptance, α, of the layer is independent of any variation of the absorption coefficient a. Since the exciting radiation cannot escape, the effective absorptance simply becomes unity. Even if some absorption in lamp parts other than the phosphor layer is taken into account, α will be very nearly constant. Thus whereas from measurements on an equally thick but plane phosphor layer one may obtain a plot as shown in Fig. 1, a closed layer of this phosphor in a lamp would emit with equal brightness at all temperatures almost up to T_s, at least as far as the phosphor is concerned, and then decrease. Therefore, in this case no significance can be derived from measurements of fluorescence intensity *vs.* temperature carried out on plane phosphor layers. If the shape of such a plot is similar to that shown in Fig. 1, even the temperature at which thermal quenching begins to appear can be appreciably lower for a closed layer since here the absorption coefficient a no longer competes with thermal quenching.

The situation is very much different for partly transmitting closed phosphor layers in lamps. Here the fluorescence intensity of a plane phosphor layer and that of the closed layer in the lamp may both exhibit a maximum which, however, need not necessarily lie at the same temperature. It is difficult to establish a general correlation between $A(T)$ and $\alpha(T)$. A numerical discussion, however, leads to the rule of thumb that one should choose for measurement a plane phosphor layer of the same thickness as that ultimately applied in the lamp. In this case sample measurements are significant in as much as the slope and the maximum, if existent at all, are approximately those one would observe in the closed lamp.

Experiment

For a factual discussion magnesium fluorogermanate activated with manganese was chosen. Values approximately proportional to $Q(T)$ were measured on plane phosphor samples between 20° and 450°C in a rarefied helium atmosphere (20 mm Hg). The phosphor, uniformly deposited on a glass disk, was excited by 365 mμ radiation from one side and viewed by a photomultiplier from the other side. A suitable filter prevented the exciting radiation from entering the photomultiplier, The resultant plots, normalized to their values at 20°C, are shown in Fig. 2 for a thin layer (s = 2 mg/cm^2) and a thick layer (s = 24 mg/cm^2). As expected neither the slope of the initial increase of fluorescence nor the temperature of the break point are intrinsic phosphor properties. From room temperature to the temperature of the break point the fluorescence intensity increases by 180% for s = 2 mg/cm^2 and by only 17% for s = 24 mg/cm^2. In the former case the temperature of the maximum is 360°C, in the latter case only 240°C, *i.e.*, 120°C lower.

No equipment is available at the present time for studying over the full temperature range the fluorescence intensity when both excitation and observation occur from the same side. Such measurements were made, however, between room temperature and +170°C. Although at +170°C the intensity maximum is not yet reached, the initial slope is much steeper for the thin layer (about 80% increase between room temperature and +170°C) than for the thick layer (about 20% increase between room temperature and +170°C). This would indicate that the side on which the observation is made does not influence the qualitative results.

Measurements of the effect of particle size on the shape of $Q(T)$ plots were unsuccessful for magnesium fluorogermanate since the average particle diameter, d, of this phosphor is rather small ($\simeq 3\mu$) and grinding did not reduce d much further. An additional difficulty is the necessity of measuring $Q(T)$ on thick phosphor layers. In such a case the maximum is not very pronounced (Fig. 2) and small changes can easily remain undetected. The measurements then were repeated on a related system, magnesium fluoroarsenate (Mn). Here the average particle size was about 15 μ with a very

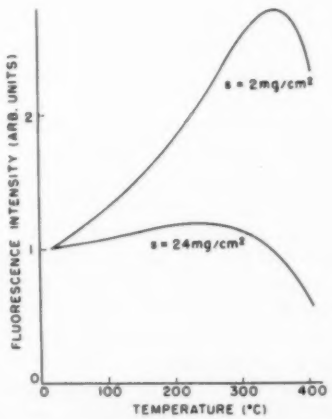

Fig. 2. Temperature dependence of fluorescence intensity of magnesium fluorogermanate (Mn) for two layer thicknesses: 2 mg/cm^2 and 24 mg/cm^2.

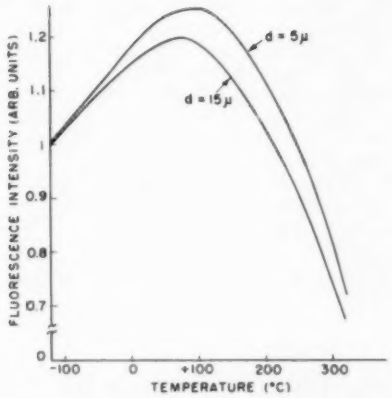

Fig. 3. Temperature dependence of fluorescence intensity of magnesium fluoroarsenate (Mn) for two average particle sizes: 5 μ and 15 μ.

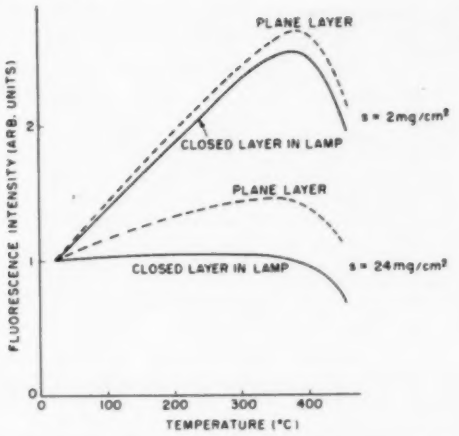

Fig. 4. Temperature dependence of fluorescence intensity computed for plane phosphor layers (dotted-lined curves) and for closed phosphor layers (solid-lined curves).

large standard deviation. After grinding the particle size was reduced to about 5 μ with a relatively small standard deviation. Samples of this phosphor were studied in a thickness of about 42 mg/cm^2. The result is shown in Fig. 3. Although the expected effect is not very pronounced, it can be seen that the sample with the small particles has its maximum about 20° higher than that for the large particle sample, and from −120°C to the temperature of the break point the fluorescence intensity increases by 25% for the small particles and by only 20% for the large particles.

It is of course not possible to measure the temperature dependence of fluorescence of a phosphor layer in a lamp since a forced change of the wall temperature will react on and thus change the discharge characteristics in the lamp. Therefore, a numerical example will be presented in which the data are nearly as practical as those of a magnesium fluorogermanate (Mn) phosphor for 365 mμ excitation. It is not known in what manner the absorption coefficient a increases with temperature, but for the purpose of the present study this is immaterial. One may, therefore, assume a simple linear relationship

$$a/r = a_o/r + \beta(T - T_o)$$

The coefficients a and r were determined at room temperature, T_o, for 365 mμ radiation. A thermal rate coefficient β and the constants C and V_q of Eq. [2] then were chosen such that a crude fit of the measured and computed values of fluorescence intensity for a thin plane phosphor layer was obtained:

$$a_o/r = 0.175 \qquad r = 0.24 \text{ cm}^2/\text{mg}$$

$$\beta = 1.02 \times 10^{-3} \text{ (degree)}^{-1} \qquad C = 10^5 \qquad V_q = 1.21 \text{ ev}$$

If these values are inserted in the equation for the absorptance A (Eq. [3]) and that for the effective absorptance, α, in a lamp (Eq. [4]), again for the two layer thicknesses $s = 2$ and 24 mg/cm^2, the four plots shown in Fig. 4 are obtained. For the thin layer with 2 mg/cm^2 there is not much difference between the plots. This then would imply that the lamp, if operated at the temperature of the break point as obtained from measurements on the plane layer, will exhibit maximum brightness as far as the phosphor is concerned. Even if the layer is thick, the maxima of the plots are not much displaced with respect to each other, and the rule of thumb mentioned earlier still holds.

Conclusion

It is insufficient to present the temperature dependence of fluorescence, if it shows a maximum, without at the same time specifying the thickness of the sample. The temperature of the fluorescence maximum originating from a competition of increasing absorption for the exciting radiation and decreasing efficiency of the emitted radiation depends very strongly on the thickness of the layer. Thick phosphor layers peak at temperatures much lower than those obtained for thin layers, and the slope of the initial fluorescence rise decreases with increasing thickness. A change of the average particle size also has an effect, although generally less pronounced, on the slope and the maximum. These changes, however, become discernible only for thick phosphor layers. A decreasing particle size, i.e., an increasing scattering coefficient, leads to a steeper slope and a higher temperature for the maximum.

If conclusions are to be drawn as to possible lamp performances of phosphor layers, a peak observed in the fluorescence-temperature plot is of no consequence in lamps using phosphor layers which do not or only to a minor degree transmit exciting radiation. This statement holds true only if the quantum efficiency does not increase with increasing temperature which, however, is rather unlikely. If the phosphor coating in the lamp is translucent for the exciting radiation, data obtained from plane phosphor layers are approximately representative of lamp performance only if the layer thickness is the same in both cases.

Manuscript received July 13, 1960. This paper was prepared for delivery before the Chicago Meeting, May 1-5, 1960.

Any discussion of this paper will appear in a Discussion Section to be published in the December 1961 JOURNAL.

REFERENCES

1. G. Kemeny and C. H. Haake, *J. Chem. Phys.*, **33**, 783 (1960).
2. H. A. Klasens, *Nature*, **158**, 306 (1946).
3. L. Thorington, *J. Opt. Soc. Am.*, **40**, 579 (1950).
4. C. W. Jerome, *This Journal*, **98**, 376 (1951).
5. R. W. Mooney, *ibid.*, **105**, 456 (1958).
6. G. F. J. Garlick, "Luminescent Materials," p. 105, Oxford University Press, (1949).
7. F. A. Kröger and J. van den Boomgaard, *This Journal*, **97**, 377 (1950).
8. A. Schuster, *Astrophys. J.*, **21**, 1 (1905).
9. H. C. Hamaker, *Philips Research Repts.*, **2**, 55 (1947).
10. J. W. Coltman, E. G. Ebbighausen, and W. Altar, *J. Appl. Phys.*, **18**, 530 (1947).
11. I. Broser, *Ann. Phys.*, **5**, 401 (1950).
12. K. H. Butler, M. J. B. Thomas, and H. H. Homer, The Electrochemical Society Meeting, Philadelphia, 1959.
13. C. H. Haake, *This Journal*, **106**, 866 (1959).
14. W. W. Antonov-Romanovski, *J. Exp. Theor. Phys.*, **26**, 459 (1954).
15. D. L. Dexter, *J. Chem. Phys.*, **21**, 836 (1953).
16. R. N. Thayer, *Trans. Electrochem. Soc*, **87**, 303 (1945).

Growth from the Vapor of Large Single Crystals of Lead Selenide of Controlled Composition

A. C. Prior

Royal Radar Establishment, Malvern, England

ABSTRACT

Lead selenide crystals have been grown by sublimation using a technique in which almost the whole charge of a few grams is frequently converted into only one single crystal. A substantial measure of control of the Pb:Se ratio of the resulting crystals is achieved by independent control of the partial vapor pressure of selenium during growth, giving carrier concentrations more than an order lower than has been achieved in crystals grown from the melt.

Single crystals of lead selenide have been grown from the melt by Lawson (1) and others. These crystals have in general had carrier concentrations of either electrons or holes in excess of 10^{18} cm^{-3}. Goldberg and Mitchell (2), from an experimental study of the phase diagram for the Pb-Se system, have shown that it is not possible to grow uniform stoichiometric crystals of PbSe from the melt, since the point at which the liquid and solid in equilibrium have the same composition occurs at a selenium excess of 0.005%. Crystals of this compound with carrier concentrations as high as 10^{18} cm^{-3} are unsuitable for the investigation of many properties, especially photosensitivity and optical properties. The present paper describes a method of crystal growth designed to produce crystals of adequate size for easy experimental investigation and with carrier concentrations controlled to substantially lower values than has been achieved in crystals grown from the melt.

The author's first attempt at composition control was to heat n-type crystals, grown from the melt, in an atmosphere of selenium, and p-type crystals in a vacuum, for periods of about 1 day and up to temperatures at which substantial loss of PbSe by evaporation occurred. No significant changes of carrier concentration attributable to the value of the selenium pressure during the baking were observed. Similar experiments carried out at the same time with natural lead sulfide crystals in sulfur atmospheres, however, did lead to changes indicating that the final composition was a function of the baking temperature and sulfur atmosphere, and independent of the initial carrier concentration. This method for PbS has been used successfully by Scanlon and Brebrick (3), and by Bloem, Kroger, and Vink (4,5). These experiments suggested that the equilibrium composition of these compounds is a sufficiently slow function of temperature and of S, and by analogy of Se, pressure, to make composition control by these means possible in principle, but that for PbSe the diffusion rate was too slow for practical composition control of an existing crystal. However, approximately the same conditions would be expected to apply to the near equilibrium system of a crystal growing slowly from a vapor atmosphere in which the partial selenium vapor pressure is controlled. This is the basis of the method to be described.

General Outline

The arrangement is shown schematically in Fig. 1. Small pieces of single-crystal PbSe grown from the melt are contained in a fused silica crucible at the point A. This material is sublimed, under the influence of a small temperature gradient (typically about 1°C at 775°C), to the end B where it redeposits in crystalline form. A reservoir of pure selenium is maintained at a carefully controlled temperature in a side arm D. The bore of capillary C is so chosen that the loss of PbSe during the growing time is only a few per cent of the initial charge, while being large enough to ensure that the excess or deficit of selenium in the starting material can be corrected as the material sublimes, without significant change of selenium pressure in the crucible. Capillary E allows impurity gases to be pumped away without significantly reducing the selenium

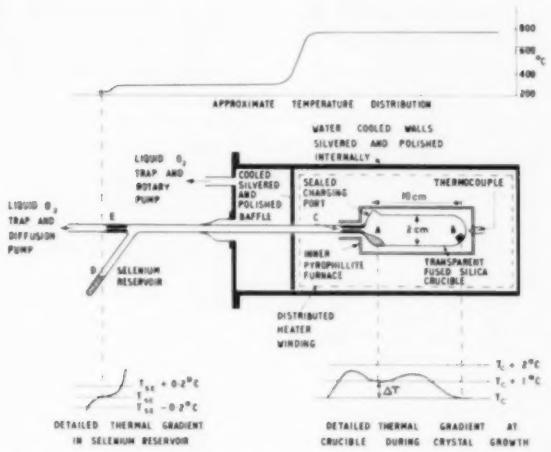
APPROXIMATE TEMPERATURE DISTRIBUTION
WATER COOLED WALLS SILVERED AND POLISHED INTERNALLY
LIQUID O2 TRAP AND ROTARY PUMP
COOLED SILVERED AND POLISHED BAFFLE
SEALED CHARGING PORT
THERMOCOUPLE
LIQUID O2 TRAP AND DIFFUSION PUMP
SELENIUM RESERVOIR
INNER PYROPHILLITE FURNACE
TRANSPARENT FUSED SILICA CRUCIBLE
DISTRIBUTED HEATER WINDING
DETAILED THERMAL GRADIENT IN SELENIUM RESERVOIR
DETAILED THERMAL GRADIENT AT CRUCIBLE DURING CRYSTAL GROWTH

Fig. 1. Schematic diagram of crystal growing arrangement

pressure. A typical run would last 2-3 days and yield crystals of the order of 0.2 cm^3 in volume.

Since thermal defects are formed more readily at higher temperatures, a low temperature seemed likely to favor the achievement of near stoichiometric composition without unduly stringent selenium pressure control. This tends to be supported by the work of Bloem, Kroger, and Vink (4,5) on PbS. Further, the lower the temperature of crystal growth the less should be the strains produced on cooling in contact with the crucible walls. The temperature chosen was therefore a compromise between these considerations and the achievement of a reasonable rate of crystal growth; the exact value of 775°C (cf. mp of 1060°C) actually used was arbitrary.

As shown in the next section the size and quality of the resultant crystals depend to a considerable extent on the use of small, easily controlled temperature gradients along the crucible. For this reason a special radiation furnace was designed. This will be described elsewhere but the main features may be seen in Fig. 1. A multi-tapped winding on the inner furnace gives detailed control of the gradient, which is measured by a system of multiple differential thermocouples (not shown), and which can be controlled to better than 1/10°C/cm. In order to control the resultant crystal composition, controllers are used for the absolute temperature T_c, measured by a thermocouple near the end B, and the temperature T_{se}, measured by a resistance thermometer, at the surface of the selenium in the reservoir. Auxiliary heaters are used to maintain the temperature of capillary E, and the connecting tubes on the crucible side of this, above the selenium temperature. The inner furnace includes a section to prevent blockage of capillary C by condensation of PbSe.

Control of Nucleation and Growth Conditions

If no special precautions are taken in the preparation and charging of the crucible and it is subjected to a temperature gradient of, say, 10°C or more between its ends, a typical result would be either a polycrystalline mass at the end or, depending on the shape of the temperature gradient, 10-100 small crystals scattered over the walls. Such a result is of little value, and the main difficulty in crystal growth from the vapor is to produce instead a small number of large crystals.

A variety of experiments was therefore performed to determine conditions which would favor the latter result. These experiments included a study of the effect of various methods of cleaning and processing the crucibles, the influence of the shape and magnitude of the temperature gradients used, and by processes of repeated growth and re-evaporation in single crucibles, a study of the properties of the nucleation centers at which crystals formed. It was clear from these experiments that nucleation occurred only at particular nucleation centers, which possessed some measure of permanency in that crystals would frequently grow on the same sites, and sometimes with the same orientation in the repeated growth and re-evaporation cycles.

The most effective process found for reducing the number of these centers was to clean the crucible carefully by any conventional wet process and to follow this, just before charging the crucible, by a very thorough flame treatment of the half of the crucible in which the crystals are to grow. In this the silica was worked in sections to the softening point in an oxy-propane flame for a total time of about 15 min. The action of this process seems likely to be either that of evaporating off the surface impurities from the growing end of the crucible, or to remove these from the surface by solution in the silica; it probably also reduces surface irregularities.

A precaution which was taken in charging the crucibles was to prevent the initial charge from coming into contact with the growing half of the crucible, since, even if any traces left at this end of the crucible are driven off by a reverse gradient before the growing gradient is applied, a significant probability of additional nucleation seems to remain.

The nucleation properties of a particular charged crucible could be assessed by counting the number of crystals formed after it had been maintained for a time under growing conditions at various temperature differences. The probability of nucleation increased only slowly with time at a given temperature difference, but rapidly with increasing temperature difference. Ideally the crucible properties could be described in terms of a distribution of nucleation centers, each characterized by a suitably defined temperature difference ΔT_c, below which the nucleation probability in the time of the experiment is small, and above which the probability rises very rapidly with ΔT.

The difference between a poor and a good crucible can be very considerable. With a good one nucleation has sometimes not occurred with 12°C temperature difference held for several days, and with differences as high as 40°C held for 15 min. On the other hand, a poor crucible will nucleate a considerable number of crystals at 1°C difference, and a very large number at 10°C difference. These extremes are exceptional, the normal number occurring in a reasonably carefully treated crucible being two or three, with up to 3°C difference. Sometimes a crucible which

has produced no nucleation at, say, 20°C or more in 15 min has nevertheless produced crystals when held with under 5°C difference for several days. The general trend of the bulk of the other experimental evidence, as well as very general considerations of the nature of nucleation processes, suggest, however, that the nucleation probability $-\Delta T$ characteristic for the center concerned would be much too steep to account for this. A more likely explanation is that new nucleation centers can arise during prolonged heating.

Under a high power optical microscope the centers can sometimes be correlated with visible imperfections on the walls, but this may be fortuitous as more often no correlation is apparent. The nature of these centers is a subject for speculation, but they seem likely to be on a scale of tens of Å or less; aggregates of impurities, particular chance configurations of the atoms of the silica glass surface, steps, or other irregularities could be responsible.

The impossibility of predicting the exact nucleation properties of a particular crucible is a serious difficulty. As a compromise between growth rate and considerations of crystal quality and composition control, the optimum temperature difference for growth appears to be about 1°C. The simplest method is to raise the furnace to its operating temperature with a reverse gradient of a few degrees in the crucible, and then to change to the growing gradient of 1°C and maintain this for the two or three days' duration of the run. This method often yields good crystals, usually about two but fairly frequently only one per run. However, if the crucibles are sufficiently carefully prepared to avoid the likelihood of a large number of small crystals, then no crystals form in about one third of the trials. In an attempt to overcome these difficulties a method for the control of nucleation was developed.

The principle is illustrated in Fig. 2 and 3. Figure 2(a) shows qualitatively that while the rate of growth of an existing crystal is roughly proportional to ΔT the probability of nucleation is vanishingly small for sufficiently small ΔT, but increases very rapidly for large ΔT. The object is to nucleate a single seed crystal, and then to continue its growth at a temperature difference ΔT_s at which the probability of further nucleation is very small.

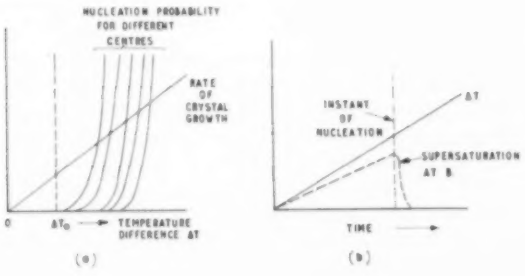

Fig. 2. Principle of controlled nucleation

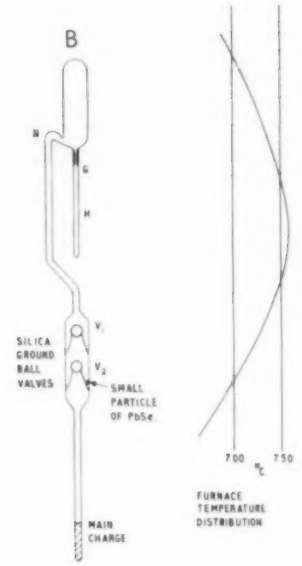

Fig. 3. Practical method for controller seeding of crucible

Figure 3 illustrates the apparatus used in the practical application of the method. The crucible assembly is placed initially in a subsidiary furnace in such a position that the end B is slightly hotter than the particle of PbSe trapped between the valves V_1 and V_2 (6); the latter valve prevents this particle from being lost by sublimation into the colder tube below. The whole assembly is then slowly raised over a period of about 1 hr so that the temperature difference ΔT between the PbSe particle and the end B increases as shown in Fig. 2(b), to a maximum usually about 20°C. Sufficient leakage through the valve V_1 occurs to allow the supersaturation at B to follow the value of ΔT until nucleation of a crystal takes place. When this happens, however, the supersaturation falls rapidly as the growing crystal absorbs vapor more rapidly than it can be replenished past the valve. Thus once one crystal is formed, the probability of further nucleation is very small. If microscopic examination after withdrawal from the furnace shows the seed to be of poor quality, or if, as happens very occasionally, more than one seed is obtained, the process can be repeated after re-evaporation with V_1 open.

When a satisfactory seed is obtained the charge is manipulated through V_1 and V_2 into the crucible, which is then sealed off at N. A small pellet of selenium is included with the charge and this is then manipulated by distillation to form a vacuum tight plug in the capillary at G.[1] The stem may then be broken at H and the crucible sealed into the growing furnace. The selenium plug distills into the reservoir D when the furnace is heated. As the temperature approaches the final value, care is taken to maintain a very small gradient in the growing direction to avoid re-evaporation of the seed but to keep the probability of further seed formation small.

A fair measure of success has been achieved by

[1] The use of selenium to form a vacuum seal was suggested by D. G. Coates.

this prenucleation process, the result frequently being one single crystal, though additional nucleation does sometimes occur.

Some crystals produced by these methods are shown in the figures: Fig. 4 shows a single crystal still on the walls of the crucible where it was grown; Fig. 5 shows four relatively small crystals which formed in one crucible without the use of the prenucleation technique; Fig. 6 shows a particularly well formed crystal; Fig. 7 shows a crystal of fairly typical quality.

Composition Control

In the earliest experiments no attempt was made to control the composition. The crucibles were baked out under vacuum overnight at about 1050°C, the charges introduced through a vacuum trap, and the crucibles sealed off after a further period of baking at about 300°C to achieve some measure of outgassing of the charge. No selenium reservoir or pumping stem was employed, and the crystals were grown directly with temperature differences of 2°-3°C. The initial charge consisted of small pieces cleaved from either n- or p-type single crystals grown from the melt and having carrier concentrations of 2-5 x 10^{18} cm^{-3}. The resulting crystals were found always to be of the same type as the initial charge and, as indicated by approximate measurements, to have the same value of conductivity. This is the result to be expected if the carrier concentration were determined principally by departures from stoichiometry; some loss of selenium equal to the contents of the crucible at the equilibrium vapor pressure must occur, but calculations show that the effect should be small compared with the initial carrier concentrations of over 10^{18} cm^{-3}.

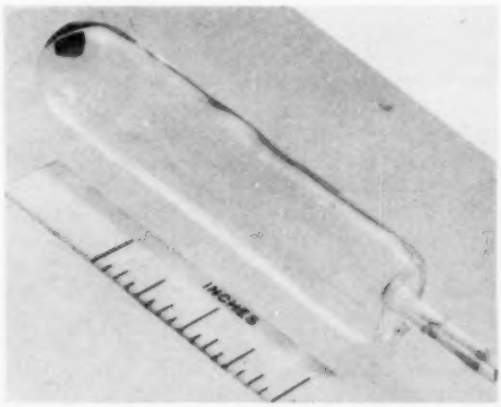

Fig. 4. Crucible with single crystal still attached to the wall where it grew.

Fig. 5. Four relatively small crystals which formed in one crucible without the use of the pre-seeding technique.

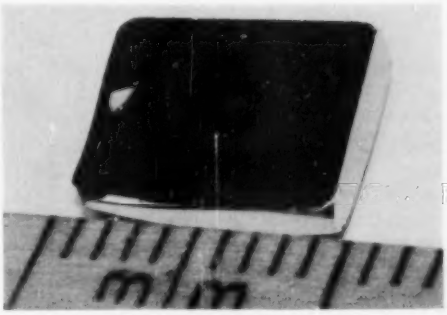

Fig. 6. A particularly well formed crystal

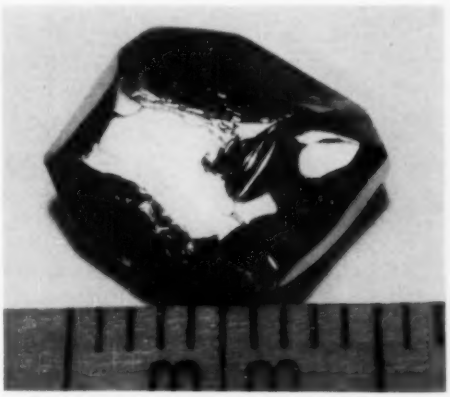

Fig. 7. A crystal of fairly typical quality

The next approach was to use a sealed-off crucible having a capillary, and a stem which, when in the furnace, terminated in a subsidiary temperature-controlled cavity situated beyond the baffle. A small pellet of selenium was included with the charge and distilled to the extremity of the stem. During crystal growth the temperature of the end of the crucible and of the stem were controlled. A substantial measure of composition control was achieved by these means and several crystals, both n- and p-type with carrier concentrations about 10^{17} cm^{-3}, were produced. The carrier concentrations were on the average about one order lower than those in crystals grown from the melt, but they showed a scatter of about $\pm$ 5 x 10^{17} cm^{-3} for apparently fixed growing conditions. There appeared to be no correlation between the carrier concentrations of the original and resultant crystals, indicating that the selenium vapor pressure control was effective, and that the scatter was due to other causes. Tests with a Tesla coil showed that the final pressure in the crucible after crystal growth was usually of the order of 0.1 mm Hg in spite of the vacuum baking procedure; presumably most of the gas came from the charge. The most likely cause of scatter seemed, therefore, to be associated with the presence of this gas, and accordingly the apparatus was modified to allow the continuous pumping method already described.

This resulted in a clear improvement, and a number of crystals with carrier concentrations below 10^{17} cm^{-3} were grown. Since the main interest at this time was the production of crystals with these low carrier concentrations for investigations of photoconductivity and optical absorption, a sufficiently wide range was not covered for a reliable plot to be obtained of the relation between carrier concentration and crystal and selenium reservoir temperatures. The consistency of the results appeared to be about $\pm$ 3 x 10^{16} cm^{-3}, and inadequacies of the temperature controller used seemed to be sufficient to account for this spread. A considerably better controller was therefore constructed; this employed a platinum resistance thermometer for the selenium reservoir, giving control to about $\pm$ 1/50°C, and a platinum-1% rhodium: platinum-13% rhodium thermocouple for the crystal temperature, controlled to about $\pm$ 1/10°C.

Figure 8 shows the results of measurements made on some crystals grown by D. G. Coates with this new system. The carrier concentrations were determined by E. H. Putley (7) from conductivity and Hall coefficient measurements at room temperature and 77°K. The crystals were grown in the order of the numbers, although the results for some intermediate runs are not shown where faults were known to have occurred during the process. A number of crystals were grown subsequent to 6 but these unfortunately showed a much wider scatter of the order of $\pm$ 2 x 10^{17} cm^{-3}. The cause for this was not apparent during the operation of the equipment, but when the apparatus was being dismantled at the termination of the program, a fault which seems likely to be the explanation came to light. This was associated with the heater around the capillary C, and it is probable that this capillary was liable to become blocked by PbSe for some time during each run. This would also explain why crystals grown during this period had typical inhomogeneity of the same order as the spread, whereas previous crystals measured appeared to be about ten times more uniform.

In addition to obtaining fuller data than shown in Fig. 8 it had been intended to measure the variation of composition with temperature of the growing crystal for fixed selenium reservoir temperature, but due to the difficulties mentioned this was not attempted. However earlier measurements suggested that the variation of composition with crystal temperature was about half as rapid as variation with selenium temperature.

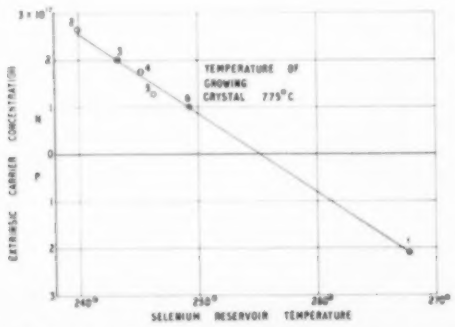

Fig. 8. Relation between crystal composition and selenium reservoir temperature.

Due to thermomolecular pressure effects the values of temperature given in Fig. 8 do not have any absolute significance, but only in relation to the particular apparatus used. This is because the partial pressure of selenium in the crucible will depend not only on the pressure in the selenium reservoir, but also on the diameter of the connecting tubes where these pass through a temperature gradient. If all the connecting tubes were small compared with the mean free path, the selenium pressure in the crucible would be some 50% greater than if all the tubes were large. Detailed practical calculations would be very difficult since the mean free path, for the selenium pressures used, is comparable with the diameters of the connecting tubes. Changes in the effective diameter of the connecting tube due to condensation of PbSe, as do occur on the cold side of the baffle in the furnace, could also affect the result, although no positive evidence of this was obtained in practice.

The potentialities for composition control of the system described appear from Fig. 8 to correspond to a carrier concentration spread of about $\pm$ 10^{16} cm^{-3}. Several factors could serve to limit the ultimate capabilities of such a system. The pressure difference of the selenium vapor between the ends of the capillary must cause some error, particularly for high growth rates, and for large differences in composition of the initial and final crystals; such errors could of course be reduced by repeating the process. For fundamental reasons perfect control could not be expected since a crystal can be in ideal equilibrium with the vapor only when the growth rate is zero. Some variation of composition with growth rate is therefore to be expected but may be negligible in practice. Early experiments suggested that crystals grown with temperature differences of 5-10°C did differ in composition from those grown more slowly, and this could not be explained satisfactorily on the basis of inadequate selenium flow through the capillary. For this reason, as well as to limit nucleation, differences of about 1°C were used subsequently. If there is a rate effect, the composition might also be expected to depend on the particular crystallographic face on which growth occurs, and this could cause inhomogeneity of the resultant crystal.

Due to departures from the appropriate relation between selenium pressure and crystal temperature, changes can take place near the surface of the crystals as the furnace cools. In practice such changes seem to be confined to layers less than 1/10 mm in depth. Use has been made of such effects in the preparation of p-n junctions very close to the surface, and measurements on the photovoltaic effect at such a junction will be described in another paper.

The purity of the PbSe used was improved during the project, but this did not seem to affect the crystal growing process, although some statistical correla-

tion was noted between the purity and the results of measurements on photo effects; these will be reported elsewhere. For the highest purity crystals the lead was first zone refined, then distilled in hydrogen, and the selenium was purified by a process described by Nielson and Heritage (8).

Summary and Conclusion

A new method of growing crystals of PbSe of a few grams in weight and good crystallographic quality has been described. The method appears to be potentially capable of producing crystals having carrier concentrations controlled to $\pm 10^{16}$ cm^{-3}. The full potentialities were not realized in practice due to instrumental failure and limitation of available effort, but a considerable number of crystals were produced having carrier concentrations between one and two orders lower than can be achieved in crystals grown from the melt. Many of these crystals had room temperature conductivities differing little from the value to be expected for intrinsic material.

One of the main problems in growing crystals from the vapor is to obtain a small number of large crystals rather than a large number of small ones. Different substances may differ widely in this respect, but this work has shown that, even with a substance such as PbSe which tends to form a very large number of very small crystals, successful results can be obtained. The importance of very careful preparation and pretreatment of the crucibles and the use of very small temperature gradients has been stressed.

Numerous measurements on these crystals have been made by the author and his colleagues in this laboratory, and will be the subject of separate papers. Photoconductivity has been studied, and Coates has developed a chemical etch with the aid of which he has been able to prepare, from the crystals, thin slices which show high sensitivity as infrared detectors. Measurements have been made also on the photovoltaic effect at a p-n junction. Jones (9) has made Hall coefficient and conductivity measurements from the liquid helium range up to 600°K on specimens with concentrations ranging from 3×10^{16} to 1.6×10^{17} cm^{-3}. From these he has deduced the intrinsic carrier concentration for temperatures down to 300°K, as compared with the previous lower limit of about 600°K. Optical absorption measurements show much reduced free carrier absorption, and this should enable a more detailed study of the structure of the absorption edge to be made.

The method, with changes of detail, should be applicable to some other substances which have adequate vapor pressures below their melting points. For reasonably rapid growth of a compound a necessary condition is that no component of the compound should be present in the vapor in very much greater concentration than any other component since, if it is, the rate of sublimation will be limited by the diffusion of the low concentration component through a relatively static and dense vapor. The vapor of mercury selenide, for example, contains a much greater quantity of mercury than of selenium. A few crystals up to about 6 x 6 x 2 mm of this compound were grown in sealed crucibles, without any attempt at composition control, at 400°C with about 1°C temperature difference, but the growth rate was much smaller than for the lead salt, and the avoidance of excessive nucleation more difficult.

Apart from lead sulphide and lead telluride, the group of compounds to which the process seems most likely to be applicable are the II-VI compounds; several of these have already been grown successfully from the vapor by Czyzak, *et al.* (10, 11), Hamilton (12), and others, although without systematic attempt at composition control.

Acknowledgments

The author is greatly indebted to Mr. D. G. Coates for his very able assistance throughout the greater part of the project. He is indebted also to many other of his colleagues for assistance or collaboration: to Mr. E. F. Good and Mr. J. D. R. McQuillin for the design and engineering of the improved temperature control system, to Mr. W. D. Lawson, Dr. S. Nielson, and Mr. J. G. Plant for the provision of the initial purified lead selenide crystals, to Dr. E. H. Putley for communication of the results of his Hall coefficient and conductivity measurements, and to Mr. C. Challacombe for his general assistance. This paper is published by permission of the Controller, H. M. Stationery Office.

Manuscript received May 31, 1960; revised manuscript received Sept. 9, 1960.

Any discussion of this paper will appear in a Discussion Section to be published in the December 1961 JOURNAL.

REFERENCES

1. W. D. Lawson, *J. Appl. Phys.*, **22**, 1444 (1951); **23**, 495 (1952).
2. A. E. Goldberg and G. R. Mitchell, *J. Chem. Phys.*, **22**, 220 (1954).
3. W. W. Scanlon and R. F. Brebrick, *Physica*, **20**, 1090 (1954).
4. J. Bloem, F. A. Kroger, and H. J. Vink, "Defects in Crystalline Solids," p. 273, The Physical Society, London (1955).
5. J. Bloem, *Philips Research Rpts.*, **2**, 273 (1956).
6. C. W. McCutchen, *Rev. Sci. Inst.*, **25**, 1220 (1954).
7. E. H. Putley, Private communication.
8. S. Nielson and R. J. Heritage, *This Journal*, **106**, 39 (1959).
9. R. H. Jones, to be published in *Proc. Phys. Soc.*
10. S. J. Czyzak, D. J. Craig, C. E. McCain, and D. C. Reynolds, *J. Appl. Phys.*, **23**, 932 (1952).
11. D. C. Reynolds, S. J. Czyzak, R. C. Allen, and C. C. Reynolds, *J. Opt. Soc. Am.*, **44**, 864 (1954); **45**, 136 (1955).
12. D. R. Hamilton, *Brit. J. Appl. Phys.*, **9**, 103 (1958).

Preparation of High-Purity Vanadium Metal by the Iodide Refining Process

O. N. Carlson and C. V. Owen

Institute for Atomic Research and Department of Chemistry, Iowa State University, Ames, Iowa

ABSTRACT

The preparation of vanadium of 99.95+% purity by the Van Arkel-deBoer iodide process is described. Conditions for optimum growth rate and maximum purity were determined. Data on impurity transfer from the feed to the hot filament are presented together with a discussion of contamination by the retort. The quality of vanadium obtained from feed material prepared by bomb reduction and by a sponge process is compared. Some physical properties of this metal are reported. An apparatus designed to prepare several pounds per batch is described.

The preparation of vanadium by the thermal decomposition of its iodide was first demonstrated by Van Arkel (1) in 1934. Crude vanadium was reacted with iodine in an evacuated quartz tube at 800°C and the volatilized iodide was decomposed on a tungsten filament at 1000°C. Shelton (2) has ascribed the limited applicability of the crystal bar process to vanadium to the relatively low volatility of the iodide.

A tendency to form a loose crystalline aggregate was observed by Nash, *et al.* (3) when the conventional Van Arkel technique was applied to vanadium; therefore they modified the process so that a coherent crystalline deposit could be obtained. This was accomplished by use of a "straight-flow" process in which vanadium iodide was passed over a hot filament and the liberated iodine was removed from the system. Crude vanadium was reacted with iodine vapors at 900°C to form the diiodide. When the iodination reaction was complete, the thermal decomposition of the iodide was carried out in a second step. The system was evacuated and heated slowly to 800°-900°C maintaining the filament at a temperature of 1400°C. This gave a dense, crystalline deposit of vanadium metal possessing a high degree of ductility and having a hardness of 64 VHN.

The investigation described in the present paper was undertaken in order to produce quantities of high-purity vanadium for use in research and development work. It included a comprehensive study of the conditions for obtaining the optimum growth rate and maximum purity. The ultimate objective was the development of a process capable of preparing iodide vanadium in 5-lb quantities, thus making high-purity metal available for use in vanadium research.

Experimental Apparatus and Procedure

All experiments were carried out in a sealed bulb apparatus. The early experiments were conducted in a Vycor vessel 3.5 in. in diameter by 12 in. long. The apparatus consisted of a lower section that held the crude vanadium, an upper section in which two tungsten electrodes were sealed, and a side tube for the iodine. The impure vanadium feed in the form of granules or chips was placed in the annulus between the wall of the Vycor tube and a molybdenum screen. A "hairpin-type" filament of vanadium wire was suspended from the tungsten electrodes, and the upper and lower sections of the retort were fused together. The bulb was evacuated to a pressure of 10^{-5} mm Hg, degassed by heating to 850°C, and sealed off. The side tube containing the iodine was immersed in a dry-ice bath during these operations. The filament was then brought to the decomposition temperature, and the iodine was sublimed into the retort to initiate the reaction. A normal run produced a 150-g bar in a 24-hr period.

Most of the experimental work was performed in an Inconel retort thus eliminating the troublesome closure step encountered with the Vycor system in which the head is fused to the lower section. The metal retort was equipped with a water-cooled vacuum head and electrode ports (see Fig. 1). The crude vanadium was loaded into the space between the molybdenum screen and liner, and the filament was attached to the molybdenum electrodes as shown in the figure. The system was closed, evacuated to a pressure of 10^{-5} mm Hg, and degassed at a temperature of 850°C. The filament was brought to the desired temperature, and iodine was admitted

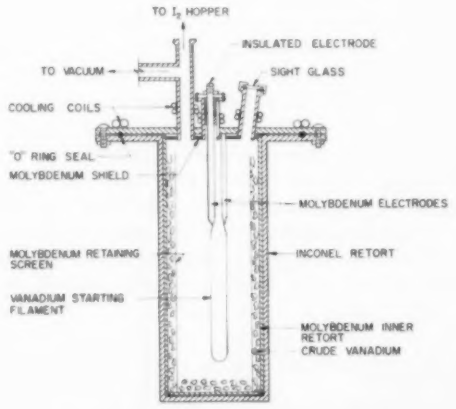

Fig. 1. Vanadium crystal bar apparatus

to the system by dropping the solid crystals from the hopper directly into the hot retort. At the conclusion of a run the pressure had increased to about 10^{-3} mm Hg probably due to a small amount of inleakage plus the partial pressure of the iodides. The condensation of vanadium iodide on the water-cooled head resulted in a lower efficiency for this apparatus, thus requiring 48 hr to produce a 150-g deposit.

In all experiments the apparent surface temperature of the filament was determined by an optical pyrometer prior to the admission of the iodine. No correction was made for the emissivity of the vanadium wire. The filament temperature remained nearly constant throughout the entire run so that no adjustment in voltage was necessary. This fortuitous condition eliminated the usual problems associated with the measurement and control of the filament temperature in crystal-bar processing.

The feed temperature was measured by a thermocouple placed on the external surface of the retort. This was calibrated by thermocouples placed in the feed during degassing, but no attempt was made to correct for the effect of heating by the filament during the run.

The retort was heated by a split-type resistance furnace capable of attaining temperatures of up to 1000°C. The filament was heated by internal resistance using a 15 kva stepdown transformer powered by an auto transformer.

Iodine attacked the Inconel retort at the high feed temperature contaminating the final product with iron and chromium. To minimize this contamination a molybdenum liner was employed as a vapor barrier. The liner was constructed from 20 mil molybdenum sheet and joined by inert gas welding. Molybdenum could be used without danger of cross-contamination because of its complete inertness toward iodine at the temperatures employed.

Monel, Monel K, nickel, and Inconel were tested as possible materials for metal retorts. Although all were relatively resistant to iodine attack, only Inconel withstood air oxidation above 800°C for a prolonged period of time.

Experimental Results

Several factors can affect the growth rate, physical nature, and chemical purity of the metallic deposit in a thermal decomposition process. Conditions for optimum growth rate and maximum purity are different for each metal and must be established experimentally.

Comparison of different types of feed material.—The crystal-bar refining technique requires use of a crude metallic feed material in the form of granules, chips, or porous particles. This assures adequate surface area to facilitate reaction with the iodine vapors. For this investigation two types of vanadium metal, hereafter referred to as "bomb-reduced" and "carbon-reduced" vanadium, were used as feed materials. The bomb-reduced metal was prepared by the metallothermic reduction of V_2O_5 with calcium in a sealed vessel using a method developed by Seybolt (4). The massive vanadium ingots, weighing approximately 20 lb apiece, were machined on a lathe or milled into small chips. These were heated in vacuo to 1200°C to remove the residual calcium.

Table I. Comparison of calcium-reduced and carbon-reduced vanadium feed

Element	Wt % in calcium-reduced feed	Wt % in carbon-reduced feed
V	99.0*	96.0*
Si	0.01-0.05	0.01-0.05
Fe	0.005-0.03	0.005-0.03
Mg	0.005	0.002
Cr	0.005	0.005
Cu	0.01	0.01
Ti	0.002	0.002
Ca	0.003	0.002
O	0.10-0.40	2.0-12.0
H	0.005	0.005
N	0.03-0.18	0.03-0.05
C	0.2	2.0-8.0

* Vanadium content determined by difference.

The carbon-reduced vanadium was prepared by a method developed by Wilhelm (5) utilizing the reaction of high-purity carbon with V_2O_5. The charge was heated under a stream of argon to approximately 800°C to reduce the V_2O_5 to a lower valent, more stable oxide. Heating was then continued *in vacuo* to 1600°C and this temperature was maintained for several hours. The resulting sponge was easily broken into small pieces and could be used directly in the iodide process. Chemical analysis showed appreciable amounts of carbon and oxygen present. The relative amounts of these impurities in the sponge were varied by controlling the ratio of oxide to carbon in the initial charge.

A comparison of the two types of feed is given in Table I. These data show that the bomb-reduced metal was generally lower in the nonmetallic impurities and of equivalent purity with respect to the metallic ones.

Effect of feed and filament temperatures on growth rate.—Morette (6) found that vanadium forms two compounds with iodine at low pressures. He identified these compounds as VI_2 and VI_3 but found that only the diiodide is volatile at the feed temperatures employed in this investigation. Morette reported that VI_3 sublimes at 750°C and that it undergoes some thermal decomposition at 800°C. To determine the optimum feed temperature a series of experiments was run maintaining the filament temperature constant at 1300°C while varying the temperature of the feed from 200° to 900°C. The growth rate, as determined from the amount of metal deposited in a 48-hr period, is plotted as a function of feed temperature in Fig. 2. It can be seen from the graph that the growth rate reaches a maximum at a feed temperature of approximately 850°C. This behavior is similar to that reported by Fast (7) for zirconium, although the optimum temperature is quite different.

To determine the optimum dissociation temperature of the iodide, the feed material was held at 800°C and the filament temperature was varied from 1000° to 1500°C. Although the optimum feed material temperature was later found to be 850°C

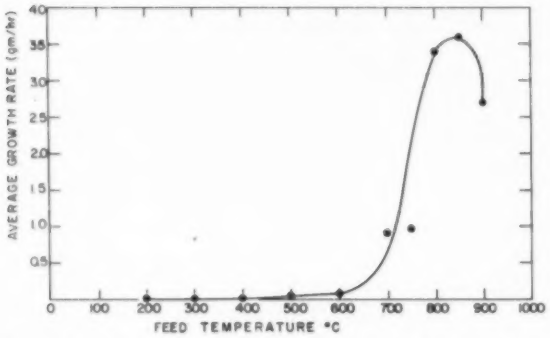

Fig. 2. Growth rate vs. feed temperature for iodide vanadium

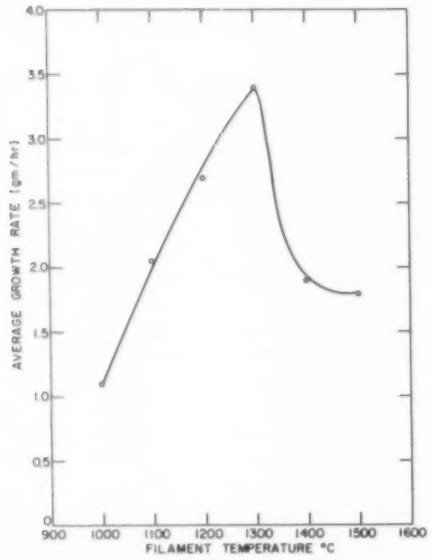

Fig. 3. Growth rate vs. filament temperature for iodide vanadium.

the series was not repeated at this temperature. Since the decomposition rate at a given filament temperature should be proportional to the partial pressure of the iodide over the feed, the over-all shape of the filament temperature *vs.* growth rate curve shown in Fig. 3 would not be expected to change. Each point on the curve represents the average growth rate of three or more runs as determined from the total weight of each bar divided by its time of growth. It is apparent that the deposition rate is dependent on filament temperature and that it reaches a maximum at about 1300°C. The curve shows a rise in deposition rate from 1000° to 1300°C. This is probably due to an increase in dissociation of vanadium iodide with increasing filament temperature. The decrease in growth rate at temperatures above 1300°C is similar to that observed for zirconium by Shapiro (8). He attributes this effect to the high concentration of free iodine in the vicinity of the filament, which interferes with the diffusion of iodide vapors toward the bar.

Transfer of nonmetallic impurities.—The principal benefit of iodide refining is generally considered to be the removal of nonmetallic or interstitial impurities. These impurities often interfere with the precise determination of structure-sensitive properties such as tensile strength, hardness, lattice parameter, and electrical resistivity. Therefore, extensive efforts were made to ascertain the source and to control the amounts of nonmetallic impurities in iodide vanadium.

There are two potential sources of these impurities in the iodide refining process. One is atmospheric contamination either from leaks in the reaction vessel or desorption of gases from the surface of the vessel or the feed material. In this investigation efforts were made to keep this source of contamination at a minimum by constant vigilance in detecting vacuum leaks and by thoroughly degassing the system and feed material at the start of each run.

The other source of nonmetallic impurities is the feed material itself. These impurities may be transferred to the filament either due to their inherent volatility or by the formation of a volatile intermediate such as an oxyiodide. The transfer of interstitials from feed to bar was investigated by varying the oxygen, carbon, and nitrogen content of the crude vanadium. These experiments were carried out at a feed temperature of 800°C and a filament temperature of 1300°C.

As was shown in Table I the crude vanadium employed in this investigation contained anywhere from 0.10 wt % oxygen up to 12.0 wt % oxygen depending on the reduction procedure. For the oxygen transfer experiments feed material containing 0.06 wt % oxygen was prepared by vacuum arc melting bomb-reduced vanadium. A comparison between the oxygen content of the initial and final metal for several runs is given in Table II. As indicated by the coefficient in the right hand column of the table, only 1% of the oxygen is transferred from the high-oxygen feed while about 8% carries over in the lower concentration range. Although the mechanism by which the oxygen is transferred was not determined, the authors believe that it is due to the formation of a volatile oxyiodide.

Crude vanadium containing from 0.11 to 8.3 wt % carbon was used in a series of runs. Analysis of the feed and the resulting bar is shown in Table III. A

Table II. Transfer of oxygen from feed to filament

Wt % oxygen in feed	Wt % oxygen in bar	Transfer* coefficient
0.06	0.004	0.07
0.4	0.033	0.08
0.60	0.020	0.03
2.6	0.027	0.01
3.7	0.031	0.008
4.0	0.050	0.01
4.9	0.052	0.01
5.9	0.062	0.01
7.5	0.039	0.005
9.5	0.047	0.005
10.0	0.038	0.004
10.0	0.130	0.01
11.3	0.180	0.02

* Fraction of the impurity in the feed carried over to the bar.

Table III. Transfer of carbon from feed to filament

Wt % carbon in feed	Wt % carbon in bar	Transfer* coefficient
0.11	0.020	0.18
0.12	0.009	0.08
0.14	0.007	0.05
0.15	0.020	0.13
0.17	0.012	0.07
0.21	0.006	0.03
0.23	0.003	0.01
0.25	0.018	0.07
1.0	0.034	0.03
2.8	0.013	0.005
3.6	0.015	0.004
4.9	0.016	0.003
6.2	0.020	0.003
7.2	0.016	0.002
8.3	0.010	0.001

* Fraction of the impurity in the feed carried over to the bar.

trend similar to that observed for oxygen was found to hold for carbon with a lower transfer coefficient occurring from feed containing the higher percentage of that impurity. Regardless of the carbon content of the starting material, the final metal generally contained 0.01-0.02 wt % carbon. While the most obvious source of this carbon is the crude vanadium, the mechanism by which it is transferred was not determined.

The nitrogen content of the feed metal used in this study varied from 0.08 to 0.18 wt %. With the exception of those runs in which leaks developed in the retort, the nitrogen content of the final bar was always below the detectable limit of the micro-Keldahl analytical method (less than 0.001 wt % nitrogen). Values obtained by a vacuum fusion method were generally below 0.0005 wt % and values of less than 1 ppm were frequently reported. The nitrogen results are shown in Table IV.

The hydrogen content was consistently lower in the crystal bar than in the feed (see Table IV). Since hydrogen is readily removed from vanadium by vacuum annealing, no systematic study was made of its transfer. Attempts were made to determine the iodine content of the metal, but no satisfactory analytical procedure has as yet been developed.

Table IV. Impurity transfer from the feed at 800° to the filament at 1300°C

Element	Wt % in feed	Wt % in bar	Transfer coefficient
Al	10.0	0.17	0.02
Cr	0.10	0.1	1.0
	0.08	0.1	1.2
Cu	0.12	0.020	0.16
	0.12	0.036	0.30
Fe	0.07	0.05	0.79
	0.06	0.07	1.35
H	0.005	0.001	0.2
N	0.18	0.0005	0.003
Ni	0.13	0.007	0.05
Si	0.13	0.017	0.13
Ti	0.05	0.006	0.12
	0.09	0.010	0.11
Y	0.50	Not detected	0

Metallic impurity transfer.—The two major sources of metallic impurities in crystal bar processing are the crude starting material and the reaction vessel. Elements whose iodides are volatile in the same temperature range as vanadium may be codeposited on the filament. Those metallic impurities often found in crystal-bar vanadium or the crude metal were intentionally added to the feed in the amounts of about 0.1 wt % of each. An arc-melted alloy containing various metallic additions was milled into chips for use in the metallic transfer experiments. As is seen from the data in Table IV, 5-15% of the nickel, silicon, and titanium present in the feed is transferred to the bar under the conditions employed. Copper carries over to a somewhat greater extent.

A 10 wt % Al alloy was included in this series. This experiment was of interest since this alloy is brittle and can be crushed readily into a form suitable for use as feed material. Although only 2% of the Al in the feed is transferred to the bar, the final aluminum concentration was too high to be of further interest in this investigation.

The experiments show that iron and chromium are quantitatively transferred from the feed to the final bar while nickel is left behind. This corroborated earlier observations that vanadium prepared in an Inconel retort prior to the introduction of a molybdenum liner contained iron and chromium in amounts of 0.3 to 0.5 wt % of each. The nickel content of this metal was consistently less than 0.01 wt %, even though Inconel contains 80 wt % Ni-5% Fe and 15% Cr. The use of a molybdenum liner lowered the iron and chromium contents consistent with their level in the feed.

The yttrium transfer value was obtained from several experiments employing a 0.5 wt % Y alloy as the feed. Since yttrium has a great affinity for oxygen it was expected that a stable yttrium oxide phase would be formed in the vanadium matrix and thus might reduce the transport of oxygen from the feed. Although there is no evidence that oxygen can be held back in this way, yttrium was found to have a very low transfer coefficient due to the stability of its iodide at the filament temperature.

Evaluation of iodide-refined vanadium.—Vanadium metal of 99.95+% purity was prepared by the iodide process. A typical analysis of metal refined by this procedure is shown in Table V. For many elements the value lies below the limit of analytical detection as designated in the table.

A compilation of some of the properties that were determined for metal of this quality is presented in

Table V. Typical analysis of iodide-refined vanadium*

Element	Wt %	Element	Wt %
Ca	<0.002	Mg	<0.002
C	0.015	Ni	0.002
Cr	0.007	N	<0.0005
Cu	0.003	O	0.004
H	0.001	Si	<0.005
Fe	0.015	Ti	<0.002

* Not detected: Al, Ag, As, Au, B, Be, Bi, Cd, Ge, Hf, Hg, Mn, Mo, Na, Nb, P, Pb, Pt, Sb, Sn, Ta, Te, Tl, W, Zn, Zr.

Table VI. Some properties of crystal bar vanadium

Property	Value obtained
Melting point	1890°C ± 10°
Lattice constant	3.026Å ± 0.001
Ultimate tensile strength	26,500 psi
Yield point	17,000 psi
Reduction in area	>99%
Hardness	57 DPH
	16 R_E
Resistivity 20°C	25.5 μohm-cm

Table VI. A comparison of the microstructures of vanadium before and after the refining treatment is seen from Fig. 4 and 5.

Scale Up of the Crystal Bar Process

An Inconel unit with the capacity to produce about 5 lb of crystal bar per run was built. This apparatus was similar to that of the laboratory unit described earlier. The Inconel retort was 3 ft in length and 1 ft in diameter with a wall thickness of 0.25 in. Attempts to fabricate a molybdenum can for the retort by conventional inert gas welding resulted in high stress levels within the weld area causing failure in the welded region upon cooling. The liner was fabricated from 25-mil molybdenum sheet using a nickel brazing technique developed for this application. Since a brittle intermediate phase occurs in the nickel-molybdenum system above 950°C, test specimens were subjected to repeated heating and cooling to determine the integrity of the brazed joint under simulated operating conditions. After these tests the specimens were found to possess an acceptable degree of ductility in the brazed region. Metal gaskets were employed as vacuum seals in order to overcome the condensation of iodide encountered on the water-cooled surfaces of the small apparatus. Platinum "O" rings were used to seal the retort flange to the head. This ring was extruded into a groove between these surfaces as the head bolts were tightened. A vacuum-tight closure was maintained at head temperatures above 600°C.

Fig. 4. Bomb-reduced vanadium, as arc-melted. Electrolytic etchant: C_2H_5OH-HCl. 250X.

Fig. 5. Iodide-refined vanadium, as arc-melted. Electrolytic etchant: C_2H_5OH-HCl. 250X.

A starting filament, 80 mils in diameter and 15 ft in length, was prepared by cold swaging arc-melted bars of iodide vanadium. This was bent into three hairpin loops and was suspended from a circular molybdenum plate using quartz insulators.

A high-temperature vacuum valve of a design similar to that used by Shapiro (9) in zirconium processing was employed in this apparatus. By means of this valve a vacuum seal can be effected at temperatures up to 850°C thus making it possible to maintain the entire reaction zone above the sublimation temperature of VI_2.

The optimum conditions already discussed in this paper were found to be applicable to the large iodide unit. Approximately 20 lb of vanadium chips were loaded around the periphery of the molybdenum liner. A column of feed was placed in the center so that both feed beds were equidistant from the filament. An increased growth rate was observed because of this favorable geometrical arrangement.

The largest bar produced to date was ⅜ in. in diameter and weighed about 4 lb. Although the bar was still growing after 24 hr, the run was terminated because of power limitations. Hardness values indicate that metal prepared in this unit is of equivalent purity to that obtained from the smaller retorts; however, a complete evaluation has not been made at this writing.

Summary

Massive vanadium metal of 99.95% purity was prepared by the iodide decomposition process. A detailed study was made of the effect of feed and filament temperatures on the deposition rate. The maximum growth was obtained at a feed temperature of 850°C and a filament temperature of 1300°C. Of the interstitial impurities commonly found in vanadium metal, nitrogen can be virtually eliminated and oxygen and carbon greatly reduced by

iodide refining. A significant decrease in most metallic impurities in vanadium can be achieved by iodide processing, iron and chromium being exceptions. Some of the properties most greatly affected by small amounts of impurities were determined on iodide vanadium.

A large Inconel apparatus was constructed to prepare larger quantities of crystal bar vanadium. Several runs were made in this apparatus and bars weighing up to 4 lb have been obtained.

Acknowledgments

The authors would like to express their thanks to E. DeKalb, V. Horrigan, and R. Bachman for the analytical results so important to this investigation. They would like to acknowledge the contributions of S. Bradford for the lattice parameter measurements and L. Reed for his assistance in performing the multitude of experiments described in this paper.

Manuscript received June 20, 1960. Contribution No. 901; work was performed in the Ames Laboratory of the U. S. Atomic Energy Commission. This paper was prepared for delivery before the Chicago Meeting, May 1-5, 1960.

Any discussion of this paper will appear in a Discussion Section to be published in the December 1961 JOURNAL.

REFERENCES

1. A. E. Van Arkel, *Metallwirtschaft*, **13**, 405 (1934).
2. R. A. J. Shelton, *Metallurgia*, **56**, 283 (1957).
3. J. W. Nash, H. R. Ogden, R. E. Durtschi, and I. E. Campbell, *This Journal*, **100**, 272 (1953).
4. R. K. McKechnie and A. U. Seybolt, *ibid.*, **97**, 311 (1950).
5. F. H. Spedding, *et al.*, Metallurgy Semi-Annual Research Report, ISC-903, Ames Laboratory USAEC, (Dec. 1957).
6. A. Morette, *Compt. rend.*, **207**, 1218 (1938).
7. J. D. Fast, *Z. anorg. u allgem. Chem.*, **239**, 145 (1938).
8. Z. M. Shapiro, "Metallurgy of Zirconium," p. 160, McGraw-Hill Book Co. Inc., New York (1955).
9. *Ibid.*, p. 199.

Thermodynamic Properties of Molten Mixtures of Cerium Chloride and Calcium Chloride

S. Senderoff, G. W. Mellors, and R. I. Bretz

Parma Research Laboratory, Union Carbide Corporation, Parma, Ohio

ABSTRACT

The thermodynamic properties of solutions of $CeCl_3$ in $CaCl_2$ were determined by emf measurements over the concentration range unity to 10^{-3} mole fraction and the temperature range 800° to 925°C. The solutions behaved nearly ideally under all conditions with small deviations, if any, in the positive direction. The solvent effect on the activity of the solute cation was found to depend on the "charge density" of the solvent cation in a manner consistent with previous work.

In a recent paper (1), an investigation of the thermodynamic properties of solutions of cerium chloride in molten potassium and sodium chlorides by means of emf measurements was described. Considerable evidence for the formation of complex compounds of cerium was found, and it was noted also that the complexes were apparently more stable thermodynamically in the potassium chloride than in the sodium chloride solvent.

Since the divalent calcium ion and monovalent sodium ion differ only slightly in radius (2), a similar series of emf measurements using calcium chloride as solvent should indicate unambiguously whether the differences in the solvent effect described in the earlier paper were the result of ion size alone or of some function of size and charge. A study of the cerium chloride-calcium chloride system was undertaken in an effort to establish the nature of the solvent effect on complex ion formation in molten halides. Aside from the theoretical interest, the presence and properties of complex compounds are of great practical interest in electrometallurgical, nuclear, and other applications of molten salt processes.

Experimental Procedures and Materials

The cell used for the emf measurements was the same as that used in the previous work (1) and already has been described in detail (3). The reversible electrodes for the measurements were the graphite-chlorine electrode (4) and the cerium-tin alloy electrode (1) containing approximately 15 mole % tin. Both have been described previously as have the evaluation of the potential of the alloy electrode with respect to pure cerium and the demonstration of its reversible behavior (1). Equilibrium potentials were measured at temperatures in the range 800°-925°C, the measurements at each temperature being made after the system had come to equilibrium such that for 15 min its emf and temperature were substantially constant. Measurements were made over three or four heating and cooling cycles during a period of 6-8 hr, and the average deviation from the mean was less than 1 mv. Details of the procedure may be found in previous papers (1, 3).

Cerium metal and cerium chloride were prepared as described earlier (1, 3). Calcium chloride was prepared as follows: "Baker analyzed reagent

$CaCO_3$, low in alkalies," was dissolved in HCl, the solution neutralized with ammonia, and calcium oxalate precipitated slowly by additions of oxalic acid and ammonia. The precipitate was filtered, dried, and charged into a previously chlorinated graphite crucible[1] contained in a quartz cylinder. The assembly was heated slowly in a resistance furnace under an atmosphere of flowing chlorine and argon. The gases were made to pass through the dry charge. At about 400°C a violent exothermic reaction occurred, external heating was interrupted, and the concentration of chlorine in the blanketing gas was reduced so that the temperature would not rise above 600°C. When the temperature became constant near 600°C, the furnace again was turned on, the chlorine concentration increased in the blanketing gas until the temperature of the charge rose to 900°C. Then this was held for 2 to 3 hr with almost pure chlorine (very little argon) bubbling through the melt. The melt was cooled under the chlorine and argon atmosphere, and a solid cylindrical ingot of about 500 g of $CaCl_2$ was obtained. This material was very soluble in water and in absolute alcohol with no perceptible turbidity at a concentration of 4 g/100 ml. Its analysis was:

	Found	Theoretical
Ca	36.10	36.11
Cl	63.10	63.89

It is interesting to note that charges which were not completely chlorinated could not be removed from the reactor as a solid ingot. Although at 900°C the charge was molten, a solid state transformation of the impure ingot during cooling resulted in its crumbling to powder. This powder gave a turbid solution in absolute alcohol but could be remelted and further chlorinated at 900°C to produce the pure material.

Details of charging and assembling the cell for emf measurements have been presented elsewhere (1).

Results

The cell which has been measured is

$$\text{Ce-Sn}\,|\,CeCl_3(N), CaCl_2(1-N)\,|\,Cl_2, \text{graphite} \quad \text{(I)}$$

where N, the mole fraction of $CeCl_3$, was varied from a value of unity to 10^{-2}. The appropriate value of the potential difference between the Ce-Sn alloy and pure cerium was taken from Fig. 1 and added to the measured emf of cell (I) to obtain the emf of cell (II)

$$\text{Ce}\,|\,CeCl_3(N), CaCl_2(1-N)\,|\,Cl_2, \text{graphite} \quad \text{(II)}$$

The emf, E, of cell (II) varied linearly with temperature at all compositions so that for any composition, N, one may write

$E = p + qT$, where $3\,\mathbf{F}E = -\Delta F$, $3\,\mathbf{F}p = -\Delta H$, and $3\,\mathbf{F}q = \Delta S$

for the formation reaction

$$Ce(l) + 3/2\,Cl_2(g) = CeCl_3(N) \text{ in } CaCl_2(l)$$

[1] National Carbon Company, Grade ATJ.

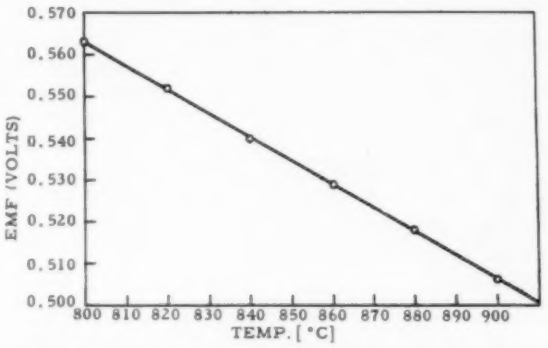

Fig. 1. Potential of Ce-Sn alloy electrode vs. pure cerium

where $\mathbf{F}$ is the Faraday constant, and q is the observed dE/dT of the cell. If the standard state is taken to be that of pure liquid $CeCl_3$, the difference between the value of ΔF, ΔH, or ΔS at $N = 1$ and that at another value of N represents the appropriate partial molar property at the latter value of N. The values of ΔH and ΔS obtained from the measured E and dE/dT at various compositions show considerable scatter because of the difficulty in measuring dE/dT accurately. Although the uncertainty in the values of the measured emf is less than 2 parts per 1000, the temperature coefficient is so small that the uncertainty in dE/dT may be as much as 10%.

A plot of ΔH $(-3\,\mathbf{F}p)$ obtained directly from the measured E and dE/dT against various functions of the concentration over the range 10^{-2} to unity (mole-fraction) showed no significant trend. The average of 10 values of ΔH (246.9 kcal/mole) over this range of concentration had a standard deviation of 1.7 kcal, or 0.7% of the measured value (245-250 kcal).

A least squares line, $\Delta H = -245.98 + 2.43 \log a$, for the same data had a very small slope (i.e., 2.4 kcal/mole) and a standard deviation of 1.0 kcal. The slightly smaller standard deviation of the least squares line as compared with that of the best horizontal line was not considered sufficiently meaningful to justify the assignment of values to $(\overline{H} - H^\circ)$ different from zero. In fact, had this assignment been made the values of $(\overline{H} - H^\circ)$ would have ranged from -0.1 to $+4.3$ kcal at 0.9 and 0.01 mole fraction, respectively, compared with ranges of 1-22 kcal for the $CeCl_3$-KCl system and 1-16 kcal for the $CeCl_3$-NaCl system (1) over approximately the same concentration range. In view of these considerations the mean value for the enthalpy of formation, 246.9 kcal/mole, was assigned to the solutions at each concentration, thus making $(\overline{H} - H^\circ) = 0$ at each concentration. The mean value of ΔH and measured values of E then were used to calculate ΔS and $(\overline{S} - S^\circ)$ at each concentration.

In Table I, the emf of cell (II), the activity coefficients for $CeCl_3$ and its partial molar free energy, enthalpy and entropy at 800°, 850°, and 900°C are listed for a number of concentrations of $CeCl_3$ dissolved in $CaCl_2$. The free energy of formation as a

Table I. EMF values and thermodynamic properties of the system $CeCl_3$-$CaCl_2$

N	emf (v)	800°C $-(F-F^\circ)$ kcal/mole	γ	emf (v)	850°C $-(F-F^\circ)$ kcal/mole	γ	emf (v)	900°C $-(F-F^\circ)$ kcal/mole	γ	$-\frac{dE}{dt}\left(\frac{mv}{deg\ C}\right)$	$-(H-H^\circ)$ kcal/mole	$(\bar{S}-S^\circ)$ cal / mole deg
1.0000	2.607$_0$	—	1.0000	2.563$_5$	—	1.0000	2.520$_0$	—	1.0000	0.870	—	—
0.9053*	2.602$_5$	−0.311	1.278	2.559$_0$	−0.311	1.232	2.516$_5$	−0.242	1.190	0.860	zero	−0.216
0.8020*	2.604$_0$	−0.207	1.374	2.558$_0$	−0.380	1.434	2.514$_0$	−0.415	1.446	0.900	zero	−0.277
0.6012	2.615$_0$	0.554	1.283	2.569$_5$	0.415	1.339	2.525$_0$	0.346	1.392	0.900	zero	0.431
0.5064	2.618$_0$	0.762	1.382	2.573$_0$	0.657	1.426	2.529$_5$	0.657	1.446	0.885	zero	0.647
0.4013	2.624$_5$	1.212	1.406	2.580$_0$	1.141	1.442	2.536$_0$	1.107	1.501	0.885	zero	1.078
0.3323	2.631$_5$	1.696	1.359	2.587$_0$	1.626	1.408	2.544$_0$	1.660	1.433	0.875	zero	1.509
0.2331	2.642$_5$	2.457	1.356	2.599$_5$	2.490	1.363	2.557$_0$	2.560	1.389	0.855	zero	2.279
0.1011	2.669$_0$	4.289	1.323	2.626$_0$	4.324	1.383	2.584$_0$	4.428	1.437	0.850	zero	3.911
0.01011	2.736$_0$	8.924	1.506	2.694$_0$	9.028	1.680	2.653$_5$	9.236	1.838	0.825	zero	8.100

* The uncertainty of emf is ±5 mv. The uncertainty in the activity can be calculated from the relationship

$$\frac{d(N\gamma)}{dE} = -\frac{nF}{RT}(N\gamma)\ \text{volt}^{-1}$$

In this temperature range this is approximately 30 $(N\gamma)$. Therefore with an uncertainty of 5 mv, the uncertainty in the activity $(N\gamma)$ for these concentrations is approximately 0.15, and the values of the activity are therefore not significantly greater than unity.

function of temperature and activity of $CeCl_3$ in solution is given by

$$\Delta F\,(\text{kcal/mole}) = -245.0 + 6.02 \times 10^{-2}\,T + 4.58 \times 10^{-4}\,T \log a$$

with a standard deviation of 0.06 kcal. The values for pure $CeCl_3$, from which the partial molar properties were calculated, were determined previously (1) and are given in Table II.

Discussion

In Fig. 2, the Nernst plots for solutions of $CeCl_3$ in KCl, NaCl, and $CaCl_2$ at 850°C show that the more nearly ideal behavior is approached in the order stated. In fact, in the case of the $CaCl_2$ solvent the theoretical slope is duplicated over practically the entire range of concentration studied.

It has been noted previously that the partial molar enthalpy of solution closely approximates zero in the $CaCl_2$ solvent, and examination of the values of the partial molar entropy in Table I shows that its variation with concentration is of the correct sign (except for the two most concentrated solutions in which the value is too small to be considered meaningful) though somewhat smaller than the theoretical value for the ideal solution, $\bar{S} - S^\circ = -R \ln N$. At $N = 0.5$ the measured value is about ½ the ideal, and at $N = -0.1$ and $N = 0.01$ the measured value is smaller than the ideal value by less than 10%. This departure from the theoretical cannot be considered as significant in view of the previously discussed uncertainty in the measured temperature coefficient of the emf. In any event, the departure from ideal behavior of both the enthalpy and entropy of solution in the KCl and NaCl solvents was very much greater (1). It appears then that solutions of $CeCl_3$ in $CaCl_2$ behave ideally with respect to the slope of the Nernst plot (although not the actual values of the emf) and the heat and entropy of solution.

The general solvent effect on the thermodynamic properties of $CeCl_3$ is in agreement with the findings of others in other molten salt systems. The results of the emf measurements by Lantratov and Alabyshev (5) on divalent metal chlorides in alkali and alkaline earth metal chlorides, and those of the spectroscopy studies of Gruen and McBeth (6) on

Table II. Thermodynamic properties of pure liquid $CeCl_3$

Temp, °C	emf (v)†	$-\Delta F^\circ$ (kcal/mole)†	$-\Delta H^\circ$ (kcal/mole)‡	$-\Delta S^\circ$ (cal/deg mole)†
800*	2.607$_0$	180.4$_5$	246.9	60.2
825	2.585$_0$	178.8$_5$		
850	2.563$_5$	177.3$_5$		
875	2.542$_0$	175.9$_0$		
900	2.520$_0$	174.2$_5$		
925	2.498$_0$	172.3$_5$		

* Extrapolated from lowest temperature of measurement, 820°C.

† Values taken from ref. (1).

‡ Mean of ten values of ΔH in $CeCl_3$-$CaCl_2$ system from $N = 1$ to $N = 10^{-2}$ mole fraction $CeCl_3$. The value obtained by measurement with pure $CeCl_3$ as electrolyte as given in ref. (1) is 245.0 kcal.

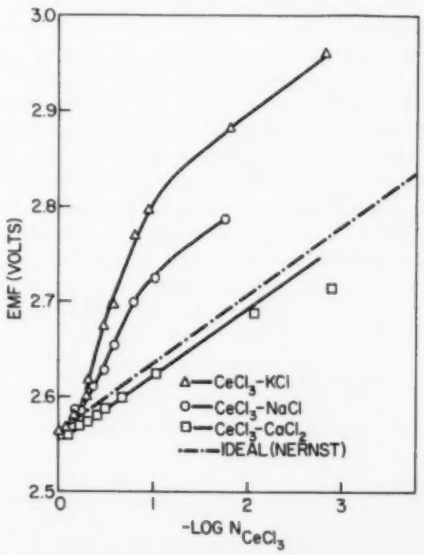

Fig. 2. Nernst plot (emf vs. log N_{CeCl_3}) for the systems $CeCl_3$-KCl, $CeCl_3$, and $CeCl_3$-$CaCl_2$ at 850°C.

nickel chloride in various solvents have been summarized by the latter authors with the statement that, "for the same solute, the smaller the size and the higher the charge of the solvent cation, the less will be the deviations from ideality of the solute cations." Results shown in Fig. 2 are clearly in agreement with this generalization. This behavior is probably the result of the competition among the cations for coordination with the chloride ions. Thus, the ion with the highest "charge density" (highest charge and smallest volume) will fill its coordination sphere most successfully leaving other cations uncomplexed, or associated with the chloride ligands by weaker bonds. These latter, therefore, would behave in a more nearly ideal manner.

However, if the pure chloride itself contains some clustering of chloride ions around metal ions to form structures approximating ions like $[CeCl_2]^+$ or $[CeCl_4]^-$ (as might be expected with higher valence metal ions like Ce^{3+}), then the effect of a small solvent cation of high charge might be to reduce the number or stability of such structures. To the extent that this occurs one would observe increasingly large positive deviations from ideal behavior. The generalization quoted above should probably be modified, therefore, to "the smaller the size and the higher the charge of the solvent cation, the smaller will be the negative or the greater will be the positive departures of the solute cation from ideality."

It will be noted in Fig. 2 that the data for the $CeCl_3$-$CaCl_2$ system fall below that of the ideal Nernst plot. This represents a positive deviation from ideality (i.e., activity greater than unity), albeit a small one. The size of the marked experimental points represents the over-all precision of the emf measurement (± 5 mv), and it will be noted that the displacement of the line for $CeCl_3$-$CaCl_2$ from the ideal line is about 10 mv. Since this displacement is only a little larger than the estimated precision of the measurement, one cannot with full confidence ascribe physical meaning to it. However, if the difference is real, it may be taken as evidence that some weak association or clustering exists in pure molten cerium chloride which is destroyed on adding $CaCl_2$. The initial addition of calcium chloride, about 10 mole %, resulted in an emf 5 mv below the ideal value, a departure of the order of the experimental uncertainty. The effect of "decomplexing" of $CeCl_3$ was essentially complete when about 20 mole % of $CaCl_2$ had been added.

In Table III are listed Pauling's crystal radii, r[3], and the quantity, z/r^2, where z is the valence on the ion. The quantity, z/r^2 is proportional to the "charge density," the charge per unit volume occupied by the ion. It is interesting to note that not only do the values of z/r^2 fall in the same order as the departures from ideality, but the change from negative to positive deviation between NaCl and $CaCl_2$ solvents, shown in Fig. 2, is also consistent with the values of z/r^2.[2]

Table III. "Charge density" of the ions K^+, Na^+, Ce^{+++}, Ca^{++}

Ion	Crystal radius, r (Å)	z/r^2
K^+	1.33	0.426
Na^+	0.95	1.17
Ce^{3+}	1.18*	1.83
Ca^{2+}	0.99	2.06

* Ref. (7).

Summary and Conclusions

The results of emf measurements on the system $CaCl_2$-$CeCl_3$ over the range of composition $N_{CeCl_3} = 10^{-3}$ to unity mole fraction between 800° and 925°C indicate nearly ideal behavior of the system over virtually the entire range of composition and temperature. Further confirmation was provided for generalizations regarding the solvent effect in molten salts, i.e., the larger is z/r^2 for the solvent cation, the smaller will be negative deviations or the greater will be positive deviations from ideality of the solute cations. Further evidence, although not conclusive, has been shown for the existence in pure $CeCl_3$ of ionic clusters, the extreme structures of which may be described by ions such as $[CeCl_2]^+$ or $[CeCl_4]^-$. The values of the partial molar thermodynamic quantities have been determined for this system.

Manuscript received May 16, 1960.

Any discussion of this paper will appear in a Discussion Section to be published in the December 1961 JOURNAL.

REFERENCES

1. S. Senderoff, G. W. Mellors, and R. I. Bretz, *Ann. N. Y. Acad. Sci.*, **79**, 878 (1960).
2. L. Pauling, "The Nature of the Chemical Bond," 2nd ed, p. 346, Cornell University Press, Ithaca, N. Y. (1940).
3. S. Senderoff and G. W. Mellors, *This Journal*, **105**, 224 (1958).
4. S. Senderoff and G. W. Mellors, *Rev. Sci. Instr.*, **29**, 151 (1958).
5. M. F. Lantratov and A. F. Alabyshev, *J. Appl. Chem. U.R.S.S.*, **26**, 235, 321 (1953); **27**, 685 (1954).
6. D. M. Gruen and R. L. McBeth, *J. Phys. Chem.*, **63**, 393 (1959).
7. T. Moeller, "Inorganic Chemistry," John Wiley & Sons, Inc., New York (1952).
8. D. H. Templeton and C. H. Dauben, *J. Am. Chem. Soc.*, **76**, 5237 (1954).

[2] The empirical crystal radius chosen for Ce^{3+}, 1.18A, is very close to the Pauling radius for La^{3+} (1.15Å). However, there are other empirical values for Ce^{3+} as low as 1.03Å (8). Use of the latter value would make $\frac{z}{r^2}$ M of Ce^{3+} larger than that of Ca^{2+}. It is believed that a set of values from a single source is probably most valid.

Transient Strain-Induced Electrode Potentials

Ken Nobe, Eric Baum, and Wm. F. Seyer

Department of Engineering, University of California, Los Angeles, California

ABSTRACT

Transient potentials produced when copper and zinc-plated copper wires are strained elastically in $CuSO_4$ and $ZnSO_4$ solutions, respectively, were investigated. The potential response on loading was almost instantaneous and decayed back to the original value within several seconds. The unloading response was similar to loading, but of opposite sign. The amplitude of response was approximately proportional to the load. Theoretical considerations of the electrical double layer predict the experimental results obtained.

The transient change in electrode potential of a cell consisting of two metal wires immersed in an electrolyte when one wire is stressed mechanically has been observed by several investigators (1, 2). The procedure followed by these investigators has been to measure the electrode potential response to loads large enough to deform the wire plastically. Transient potentials were observed with an amplitude of the order of 10 mv. There are certain advantages, however, in measuring the transient potential for stresses within the elastic range of the metal. The amplitudes in this range of load were of the order of 10-100 μv and therefore were harder to measure. The response to both loading and unloading can be observed repeatedly using the same load and wire, whereas elongation in the plastic range can be observed but once for a given wire and load. Since shock loading occurs during the loading process and results in poor reproducibility, there is also the advantage of being able to measure transients on removing the load, when the shock effect is negligible.

Theoretical.—According to the Stern model (3) of the electrical double layer at a metal-solution interface, there is a charge q_0 per unit area of the metal, and the corresponding charge in the solution is made up of two layers; a layer of adsorbed ions with a charge of $-q_1$ per unit area, and a diffuse layer of charge of magnitude $-q_2$, per unit area, where $q_1 + q_2 = q_0$. Then the electrostatic potential difference Ψ_0 across the double layer is made up of the potential difference across the adsorbed layer, Ψ_1, and the potential difference across the diffuse layer, Ψ_2.

At the instant a metal in contact with an electrolyte is elongated, the total charge in each of the layers is the same as it was before elongation. That is, qA is constant, where A is the area of the surface of the metal in contact with the electrolyte. Thus

$$\frac{dq}{q} = -\frac{dA}{A} \qquad [1]$$

For a wire

$$\frac{dA}{A} = \frac{d(2\pi rL)}{2\pi rL} = \frac{dL}{L} + \frac{dr}{r} \qquad [2]$$

where r is the radius and L the length. Poisson's ratio μ is defined by the relation

$$\frac{dr}{r} = -\mu\frac{dL}{L} \qquad [3]$$

From [1], [2], and [3]

$$\frac{dq}{q} = -(1-\mu)\frac{dL}{L} \qquad [4]$$

and therefore

$$L\frac{d\Psi}{dL} = -(1-\mu)\,q\frac{d\Psi}{dq} \qquad [5]$$

Since $\Psi_0 = \Psi_1 + \Psi_2$ and [5] applies to each of the layers separately as well as to the entire double layer

$$L\frac{d\Psi_0}{dL} = -(1-\mu)\left[q_1\frac{d\Psi_1}{dq_1} + q_2\frac{d\Psi_2}{dq_2}\right] \qquad [6]$$

If the radius of the metal wire is large compared with the thickness of the double layer, then the double layer can be considered to be planar and is so considered in the following calculations. Layer 1 consists of adsorbed ions whose effective distance from the metal surface is unaffected by the elongation of the metal. The potential across this layer is therefore the same as that across a capacitor with a charge density q_1. Thus

$$\Psi_1 \alpha\, q_1 \qquad [7]$$

and

$$q_1\frac{d\Psi_1}{dq_1} = \Psi_1 \qquad [8]$$

The relation between q_2 and the electrostatic potential change across the diffuse part of the electrical double layer, Ψ_2, has been calculated by balancing the effects of coulombic and diffusional forces within the double layer (4). This calculation gives

$$q_2 = \sqrt{\frac{DRTc}{2\pi}}\sqrt{\left[\exp\left(-\frac{Z^+e\Psi_2}{kT}\right)-1\right]+\left[\exp\left(+\frac{Z^-e\Psi_2}{kT}\right)-1\right]} \qquad [9]$$

where Ψ_2 is defined as the potential energy of a unit negative charge with respect to the bulk of the solution, D is the dielectric constant of electrolyte, c electrolyte concentration in moles per cc; Z valence of positive and negative ions, and e charge on an electron. When $Z^+ = Z^-$, Eq. [9] simplifies to

$$q_2 = 2\sqrt{\frac{DRTc}{2\pi}}\sinh\left(\frac{Ze\Psi_2}{2kT}\right) \qquad [10]$$

When the metal is elongated suddenly, charges in the double layer are immediately spread out over a larger area. If the charge density, q_2, is assumed to decrease instantaneously solely by the increase in surface area, the coulombic and diffusional forces are still in balance and Eq. [10] is valid immediately after elongating the wire. Thus, one can use Eq. [10] to show that

$$q_2 \frac{d\Psi_2}{dq_2} = \frac{2kT}{Ze} \tanh\left(\frac{Ze\Psi_2}{kT}\right) \qquad [11]$$

For small θ, $\tanh(\theta) \simeq \theta$, and for large θ, $\tanh(\theta) \simeq 1$. Now Eq. [6] can be written as

$$L\frac{d\Psi_0}{dL} = -(1-\mu)\left[\Psi_1 + \frac{2kT}{Ze}\tanh\left(\frac{Ze\Psi_2}{2kT}\right)\right] \qquad [12]$$

$$\simeq -(1-\mu)[\Psi_1 + \Psi_2] \text{ for small } \frac{Ze\Psi_2}{2kT} \qquad [13]$$

$$\simeq -(1-\mu)\left[\Psi_1 + \frac{2kT}{Ze}\right] \text{ for large } \frac{Ze\Psi_2}{2kT} \qquad [14]$$

When the elongation of the metal is very small compared with the length, as it is in this series of measurements, it is convenient to use the approximate integrated form

$$L\frac{d\Psi_0}{dL} = \frac{L}{\Delta L}\Delta\Psi_0 = \frac{1}{\epsilon}\Delta\Psi_0 \qquad [15]$$

where $\Delta L/L = \epsilon$ is the strain on the metal and $\Delta\Psi_0$ is the change in the measured emf on elongation due to the decrease in surface charge density in the electrical double layer. Thus

$$\Delta\Psi_0 \simeq -(1-\mu)\epsilon\Psi_0 \text{ for small } \frac{Ze\Psi_2}{2kT} \qquad [16]$$

$$\Delta\Psi_0 \simeq -(1-\mu)\epsilon\left[\Psi_1 + \frac{2kT}{Ze}\right] \text{ for large } \frac{Ze\Psi_2}{2kT} \qquad [17]$$

Thus far, only the potential at the instant of loading has been considered. If this does not coincide with the thermodynamic equilibrium potential between the two electrodes, then the potential will decay with time toward the equilibrium value. The difference between the equilibrium potentials before and after loading is just the difference in potential between two identical wires, one stressed and one unstressed. This value can be calculated readily by thermodynamic considerations. The equilibrium potential of the wire on stressing with respect to the unstressed wire is

$$E = -\frac{M\sigma^2}{2\,\mathrm{Y}n\rho\mathbf{F}} \qquad [18]$$

where σ is the stress, ρ the density, Y is Young's modulus, M is the atomic weight of the metal, n is the valence of ion, **F** is Faraday's constant.

Experimental

Two metal-electrolyte systems were investigated, copper in copper sulfate solutions and zinc-plated copper in zinc sulfate solutions. The electrolytic copper wires used in this investigation were annealed in an atmosphere of hydrogen at a temperature of 550°C for 2 hr. The entire surface of each wire except for an area 1 cm long where the wire came in contact with the electrolyte was covered with a thin Lucite film.

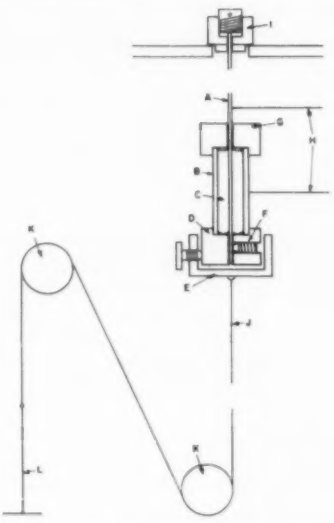

Fig. 1. Stress potential cell. A, copper wire; B, copper tube; C, electrolyte; D, plastic base of cell; E, steel chuck; F, set screw; G, plastic cap; H, electrical leads; I, plastic chuck; J, cord; K, low friction pulleys; L, weight pan.

An electrolytic cell was constructed as shown in Fig. 1. The metal tube served as both the container for the electrolyte and as the reference electrode. The wire in the center served as the test electrode.

The potential of the electrolytic cell was measured using the circuit shown in Fig. 2. The voltage dividers shown were used to oppose the large initial potential of the cell so that the transient potentials could be observed on a suitable voltage range of the amplifier. The initial potential of the cell was usually larger than 10 mv. A L&N d-c amplifier Model 9835A with scales of 0-50, 0-100, 0-200, 0-500, 0-1000 and 0-2000 μv and a maximum sensitivity of 0.3 μv was used to amplify the transient strain-induced potentials.

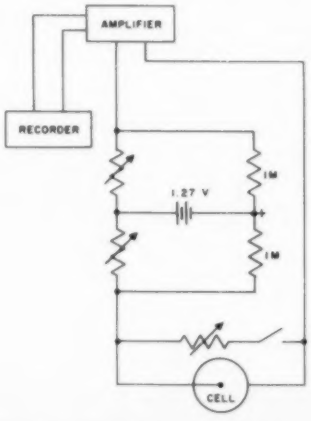

Fig. 2. Circuit diagram for stress potential measurements

The amplifier output then was recorded on a L&N Speedomex recorder. The maximum response time was found to be 1.5 sec full scale. On the 0-50 μv scale this required time of response to an input would be 30 m sec/μv.

At the start of a run, the copper cell was kept full of a solution of 1*N* NaCl, 1*N* $Cu(NO_3)_2$, 0.1*N* acetic acid for 1 hr. This solution was found to produce a clean metal surface. The cell then was flushed several times with distilled water and the electrolyte was added. Approximately 1 hr was required to stabilize the cell. The annealed B&S gauge No. 20 copper wires were strain-hardened by preloading to a stress of 5 x 10^8 dynes/cm^2 before readings were taken. The initial load then was removed. Weights were added to the weight pan by increments. At each incremental increase the weights were added and removed 4-10 times, and the transient potential responses were recorded. Elongation measurements were made with a cathetometer to ensure that the test loads did not exceed the elastic limit.

B&S No. 24 gauge copper wire was commercially zinc-plated to approximately one-thousandths inch thickness. The metal tube electrode was a zinc-plated copper sheet rolled into a cylindrical shape and placed in a ¼ in. polyethylene tube. The cell was filled with a sodium chloride and acetic acid solution for several minutes to clean the metal surfaces. The experimental procedure was similar to that for the copper cell. Solutions of 01.*N*, 0.01*N*, and 0.001*N* ZnSO, were studied with the zinc-plate cells.

Results

The load on the wires is reported in terms of elastic strain, calculated using a Young's modulus of 1.1 x 10^{12} dynes/cm^2 for copper. The response curves for a strain of 3.42 x 10^{-4} for the copper cell are shown in Fig. 3. The potential changes observed are of the wire with respect to the reference (metal tube) electrode. The response peaks of the 4 to 10 repetitions at each load were averaged. It was found that the amplitudes of the responses on loading and unloading were approximately the same, but the amplitudes on loading were always slightly higher than on unloading. This is probably due to shock loading, although great care was taken to apply the load smoothly. Since the deviation of readings from the average was smaller than on loading, only the unloading responses were used in Fig. 4, the plot of average peak potential *vs.* elastic strain for the copper cell. The mean deviation of readings from the average value was approximately 0.3 μv for all runs of the copper cells.

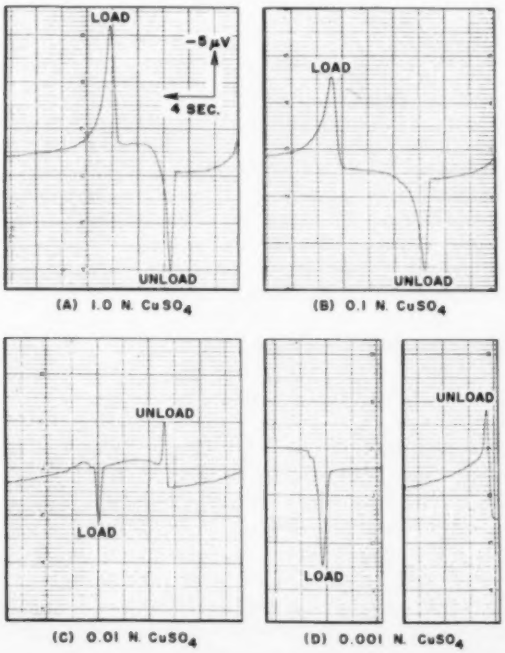

Fig. 3. Potential response, strain is 3.42 x 10^{-4}

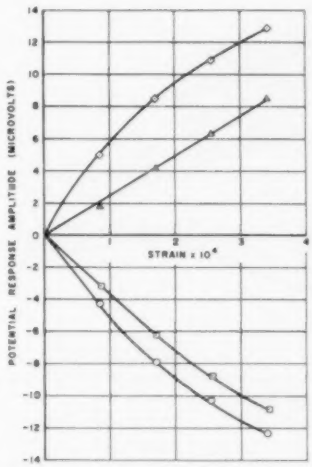

Fig. 4. Potential response amplitude vs. strain. Dotted circle 1N $CuSO_4$; dotted square 0.1N $CuSO_4$; dotted triangle 0.01N $CuSO_4$; dotted diamond 0.001N $CuSO_4$.

It should be noted that the observed initial rate of change of potential on loading or unloading before the peak has been reached (see Fig. 3) is not the true rate of change of potential, but is the maximum amplifier recorder response rate (1.5 sec full scale) which would be 30 m sec/μv on the 0-50 μv scale. Thus, the actual peak potentials are somewhat higher than those observed.

The plot of average peak potential *vs.* elastic strain for the zinc-plate cell is shown in Fig. 5.

Discussion

The model proposed leads to the prediction, from Eq. [12], that: (*A*) the amplitude of the response will be a linear function of strain; (*B*) the responses on loading and unloading will be equal but of opposite sign; and (*C*) the response per unit strain will change monotonically as the potential across the entire electrical double layer, Ψ_0, and will become a linear function of Ψ_0 at small Ψ_0.

The Nernst equation, when concentrations are small so that the activity of the ions can be approximated by concentration, gives the dependence of Ψ_0 on concentration.

$$\Psi_0 \simeq \Psi_0^\circ + \frac{RT}{2f} \ln C_{(M^{++})}$$

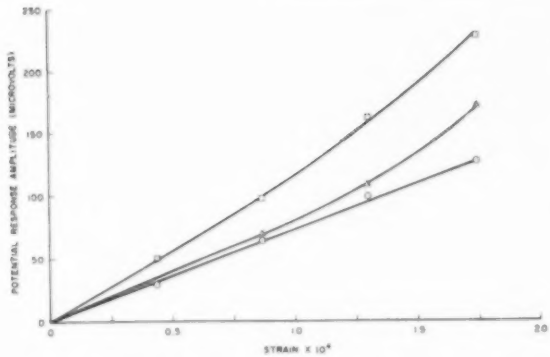

Fig. 5. Potential response amplitude vs. strain. Dotted circle 0.1N $ZnSO_4$; dotted triangle 0.01N $ZnSO_4$; dotted square 0.001N $ZnSO_4$.

Ψ_o° is the standard potential across the electrical double-layer. The assumption of a null potential at the electrocapillary maximum permits an estimate of the single electrode potential. (It is noted that the concept of an absolute electrode potential is a controversial one.) Ψ_o° would have a negative value for zinc and a positive value for copper. Thus, for the copper cell, Eq. [16] predicts that the amplitude of response per unit strain would be a negative value and would tend to zero and even become positive with decrease in concentration. On the other hand, the response per unit strain of the zinc-plate cell would be a positive value and would become increasingly positive with decrease in concentration. Figures 4 and 5 present the experimental data for the copper cell and the zinc-plate cell, respectively, and the behavior of the amplitude of response is as predicted by the model.

One would expect the potential to decay after loading to a value higher than that existing before loading by the amount given in Eq. [18]. The magnitude of this quantity is less than 1 μv for the largest loads applied in these experiments so that the potential should decay to essentially the same value it had before loading, within the sensitivity of the instruments.

The departure from linearity of some of the curves can be attributed to the errors introduced by the fact that the response time of the instruments was not fast enough to follow the initial rise or fall of potential on loading or unloading. Some of the response curves (see Fig. 3) do not decay to a potential as close to the value before loading as would be expected. The cause of this effect is not known. Otherwise, the experimental results agree reasonably well with those expected from the theoretical model.

Acknowledgment

The authors wish to express their appreciation to the Paper-Mate Company of the Gillette Corporation for their financial support of this project. A portion of this research was supported by funds from the University of California's Sea Water demineralization program.

Manuscript received Feb. 17, 1960. This paper was prepared for delivery before the Chicago Meeting, May 1-5, 1960.

Any discussion of this paper will appear in a Discussion Section to be published in the December 1961 JOURNAL.

REFERENCES

1. R. S. Dudley, R. Elliott, W. H. McFadden, and L. W. Shemitt, *J. Chem. Phys.*, **23**, 585 (1955).
2. A. G. Funk, J. C. Giddings, C. J. Christensen, and H. Eyring, *Proc. Nat. Acad. Sci*, May 1957; *J. Phy. Chem.*, **61**, 1179 (1957).
3. O. Stern, *Z. Electrochem.*, **30**, 508 (1924).
4. Cf. J. A. V. Butler, "Electrical Phenomena at Interfaces," p. 56, Methuen and Co., London (1951)

Technical Notes

Electrical Conduction in Thin Films of Silver Telluride

W. M. Kane and C. Wood

Research Division, Philco Corporation, Philadelphia, Pennsylvania

The conflict existing between the values of the forbidden energy gap in β-Ag_2Te (orthorhombic phase) obtained from optical transmission measurements on thin films (1) and Hall effect data on ingots (2) led to a further investigation of the properties of films of silver telluride. The purpose was to carry out Hall effect measurements on thin films of Ag_2Te in order to obtain the thermal activation energy. During the course of these investigations interesting time-dependent properties were observed which are reported below.

Initial attempts at producing films of Ag_2Te by vacuum evaporation and by sputtering onto a cooled substrate, in a reduced pressure of argon, were unsuccessful. X-ray analysis on these films showed that they were of the hexagonal $Ag_{2-x}Te$ structure (3). Subsequently the method reported by Weaver and Hill (4) was tried with success. Silver and tellurium were codeposited on adjacent regions of a substrate by vacuum evaporation. The silver was present in excess of stoichiometric proportions and was allowed to diffuse into the tellurium films by heating the substrate to 110°C, i.e., 20°C below the phase change of Ag_2Te, for 48 hr.

Electrical contact was made to the films by a pressure contact using a platinum wire, or by painting on an indium-gallium amalgam and making wire contact to the amalgam.

On applying a constant voltage to the contacts, the current through the film was found to vary with time, changing by a factor of 10 or more within minutes. The magnitude, direction, and rapidity of the variation depended on the area of the contacts and the past history of the film. This phenomenon was observed in both the $Ag_{2-x}Te$ and the Ag_2Te films with either pressure or amalgam contacts and prevented successful Hall effect measurements.

These experiments were repeated while observing the films by transmitted light under a Reichert metallurgical microscope. Two effects were observed to occur simultaneously on passage of current, the first causing a decrease in resistance near the negative contact, the second an increase in resistance near the positive contact. In Fig. 1a are seen tree-like structures extending out into on $Ag_{2-x}Te$ film from the negative terminal on the left of the photograph. While the dendrites were forming it was necessary to move the positive contact about on the film in order to prevent the current from dropping to an extremely low value. This contact motion caused the scratches seen near the contact. When finally the contact was left in one spot, the current decreased from ~100 μa to ~5 μa, dendrite formation essentially stopped, and the small circular light area seen at the positive contact appeared. This was found to be a region of high electrical resistance.

In Fig. 1b, the area of the positive contact was increased by applying In-Ga amalgam to the film, causing a lowering of the resistance and an increase

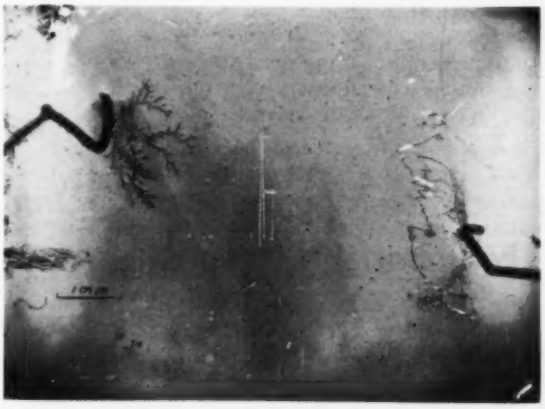

Fig. 1a. Dendrite formation in a film of $Ag_{2-x}Te$. Left contact negative (45 v).

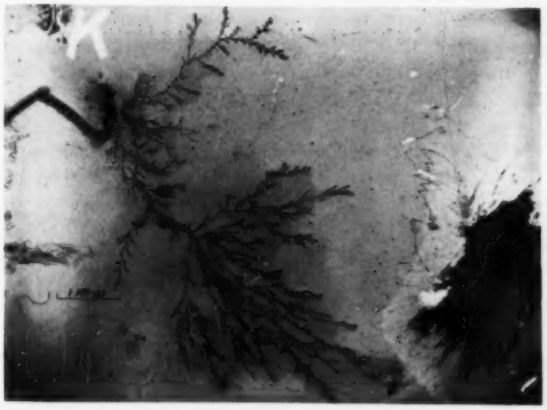

Fig. 1b. Dendrite formation in a film of $Ag_{2-x}Te$. Left contact negative (45 v).

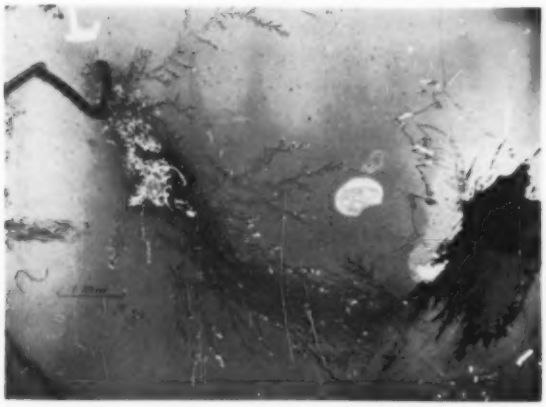

Fig. 1c. Dendrite formation in a film of $Ag_{2-x}Te$. Polarity reversed.

in dendrite formation until the high resistance barrier reformed.

Figure 1c shows the consequences of reversing the polarity of the applied potential difference. Dendrites forming at the large area contact have met and followed the paths of the other dendrites forming a very low resistance path which has essentially short circuited the film. The dendrites which had formed at the wire contact are now seen to have become less dense. The bright spots at the tips of the dendrites and near the wire contact are due to the material peeling off the substrate.

A similar experiment was performed on a β-Ag_2Te film and dendrite formation was observed.

In the above results the dendrites were found to present low resistance paths and these are probably silver-rich regions formed by silver ions migrating under the influence of the electric field. The light area of high resistance, which appeared near the positive contact, is believed to be silver deficient due to ionic motion (5). Silver is apparently very mobile in tellurium-rich compounds of silver telluride as illustrated by the method given by Weaver and Hill (4). Appreciable diffusion of silver into tellurium occurs for temperatures as low as room temperature, the diffusion constant being given by (4).

$$D = 5 \times 10^7 \text{ cm}^2/\text{day} \exp\left(-\frac{6910 \text{ deg}}{T}\right)$$

It is interesting to note that the activation energy in the exponential term is equal to 0.6 ev, a value corresponding to the optical activation energy measurements of Appel (1).

Attempts to determine the nature of the growth by x-ray methods were not successful due to the limitations in the resolution of the x-ray beam.

Manuscript received Aug. 22, 1960.

Any discussion of this paper will appear in a Discussion Section to be published in the December 1961 JOURNAL.

REFERENCES

1. J. Appel, *Z. Naturforsch.*, **10A**, 530 (1955).
2. Gottlieb, Kane, Walsh, and Wood, *J. Phys. Chem. Sol.*, **15**, Nos. 1/2 (1960).
3. Thompson, Peacock, Rowland, and Berry, *Am. Mineralogist*, **36**, 458 (1951).
4. C. Weaver and R. M. Hill, *Adv. Phys.*, **8**, (Oct. 1959).
5. S. Miyatani, *J. Phys. Soc. Japan*, **14**, 996 (1959).

Magnitude of IR-Drop Corrections in Electrode Polarization Measurements Made with a Luggin-Haber Capillary

Sidney Barnartt

Research Laboratories, Westinghouse Electric Corporation, Pittsburgh, Pennsylvania

A Luggin-Haber capillary (1) may be used for accurate measurements of electrode polarization, provided the capillary tip is sufficiently removed from the electrode surface so that it does not shield the latter (2-5). In practice a capillary tip of diameter d may be placed as close as $2d$ from the electrode surface with negligible shielding error. Because polarization measurements with a Luggin-Haber capillary are made while current is passing, the capillary will not measure directly the desired potential in the solution immediately adjacent to the electrode surface, but one at some distance δ from the surface. The difference in these two potentials represents an error in the polarization measurement and must be evaluated accurately. To minimize this correction a capillary of smallest convenient diameter is used and is positioned as close to the electrode as possible without introducing shielding errors.

Figure 1 shows a schematic diagram of the equipotentials in question for the case of a capillary of diameter d placed $2d$ from one of a pair of parallel plate electrodes. The capillary probe distorts the

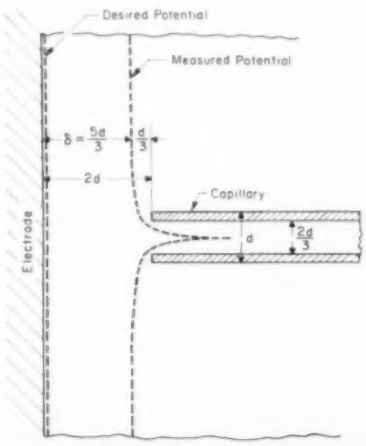

Fig. 1. Schematic diagram of IR drop in the electrolyte between capillary tip and electrode.

equipotential lines near it, and the potential inside it is that in the undistorted field a distance $d/3$ closer than the capillary-tip position. This result was found previously from potential-mapping studies in which a separation distance $2d$ and capillary bore $2d/3$ were used (3). Any larger separation, however, would be expected to yield the same $d/3$ displacement.

When the electrode being studied is connected as an anode, the potential measured by the probe will be too positive[1] and the *IR*-drop error must be subtracted from the measured potential. Similarly, when the electrode is a cathode the measured value is too negative and the *IR* correction is added.

The electrode geometry used for polarization measurements should yield uniform current distribution over the test electrode. When the distribution is nonuniform, the current density (c.d.) at the capillary-tip position will not be a constant and known fraction of the mean c.d. at all overpotential values (6,7). Instead of parallel plates other electrodes exhibiting uniform current distribution may be used, namely, coaxial cylinders or concentric spheres or shapes properly sectioned from these two systems (8). If coaxial cylinders or concentric spheres are used and the capillary tip is placed near an electrode of radius r_o, no change in the $d/3$ displacement of Fig. 1 is anticipated for $r_o >> d$. When r_o is small, however, this displacement might be expected to deviate from $d/3$, but the latter may be used as a first approximation until more precise values are developed.

In the design of practical cells for electrode polarization measurements the writer has found that Pyrex glass capillaries of outer diameter $d = 0.02$ cm (and bore diameter $= 2d/3$) are constructed readily, and are convenient to use with an electrometer voltmeter or a high-impedance potentiometer (9). When this capillary tip is placed at a distance $2d$ (0.04 cm) from the electrode surface, the magnitudes of the *IR*-drop voltage (V_{IR}) for parallel-plane, coaxial-cylinder, or concentric-sphere electrodes are as computed below. The assumption that the conductivity κ remains constant in the region δ is implicit.[2]

[1] IUPAC-Stockholm sign convention.

[2] Under conditions of natural or forced convection the capillary tip itself may alter the hydrodynamic flow locally. This must be considered in determining the c.d. at which appreciable changes occur in κ or in solution concentration.

Parallel planes.—The *IR*-drop corrections are given by

$$V_{IR} = i_o \delta/\kappa \qquad [1]$$

and are tabulated in Table I for various values of the current density (i_o) and solution conductivity. The ranges of i_o and κ over which polarization measurements are corrected readily with an accuracy of $\pm$ 1 mv are those below the stepped line. Thus even in a solution of relatively high conductivity, $\kappa = 0.1$, the largest useful c.d. for accurate polarization measurements is only 3×10^{-2} amp cm^{-2}.

Coaxial cylinders.—If the electrode shown in Fig. 1[3] represents the inner cylinder, radius r_o, over which the c.d. is uniformly i_o, the *IR*-drop over the distance δ is given by

$$V_{IR} = \frac{i_o r_o}{\kappa} \ln\left(1 + \frac{\delta}{r_o}\right) \qquad [2]$$

which is obtained by integrating Ohm's law in the form $i = -\kappa(\partial V/\partial r)$. For large cylinders such that $r_o >> d$, one may expect the relation $\delta = 5d/3$ of Fig. 1 to hold, and furthermore $\ln(1 + \delta/r_o)$ may be replaced by δ/r_o. Equation [2] then reduces to [1] and the *IR* corrections are those given in Table I. When r_o is small one might expect some change in the displacement length $d/3$, but the magnitude of this change has not been determined. As a first approximation, therefore, numerical values of the *IR* correction were calculated from Eq. [2] by retaining $\delta = 5d/3$, and these are presented in Table II for an electrolyte of conductivity $\kappa = 0.1$. A cylindrical electrode of 10 cm radius yields the same *IR* drops as those in Table I. As the cylinder is made smaller the *IR* correction decreases. The corresponding correction for any other value of κ is obtained readily from the value in Table II, since it is inversely proportional to conductivity.

Concentric spheres.—Where the electrode of Fig. 1 represents the inner sphere, radius r_o, the *IR* voltages over the distance δ are given by

$$V_{IR} = \frac{i_o \delta}{\kappa}\left(\frac{r_o}{r_o + \delta}\right) \qquad [3]$$

When the sphere is large, $r_o >> d$, this equation reduces to [1] and the results in Table I apply. For smaller spheres the value $\delta = 5d/3$ may be substituted in [3] as a first approximation, following

[3] Breiter and Guggenberger (10) have described a closed-end capillary probe placed parallel to a wire electrode, the probe containing a tiny hole facing the electrode. They showed that this arrangement produces negligible distortion of the current distribution at the electrode if the separation between probe and electrode axes is 1.5 probe diameters or more.

Table I. *IR* correction in mv for a capillary tip of diameter 0.02 cm situated 0.04 cm from a plane electrode

i_o (amp cm^{-2}) \ κ (ohm cm)$^{-1}$	1	10^{-1}	10^{-2}	10^{-3}
3×10^{-1}	10	100	1000	10,000
3×10^{-2}	1	10	100	1,000
3×10^{-3}	0.1	1	10	100
3×10^{-4}	0.01	0.1	1	10
3×10^{-5}	0.001	0.01	0.1	1

Table II. *IR* correction in mv for a capillary tip of diameter 0.02 cm situated 0.04 cm from a cylindrical electrode, radius r_o, $\kappa = 0.1$ (ohm cm)$^{-1}$

i_o (amp cm^{-2}) \ r_o (cm)	10	1	0.1	0.01
3×10^{-1}	100	98	86	44
3×10^{-2}	10	9.8	8.6	4.4
3×10^{-3}	1	0.98	0.86	0.44
3×10^{-4}	0.1	0.098	0.086	0.044

Table III. *IR* correction in mv for a capillary tip of diameter 0.02 cm situated 0.04 cm from a spherical electrode, radius r_o, $\kappa = 0.1$ (ohm cm)$^{-1}$

i_o (amp cm^{-2}) \ r_o (cm)	10	1	0.1	0.01
3×10^{-1}	100	97	75	23
3×10^{-2}	10	9.7	7.5	2.3
3×10^{-3}	1	0.97	0.75	0.23
3×10^{-4}	0.1	0.097	0.075	0.023

the above procedure for cylindrical electrodes. This yields the numerical values listed in Table III for $\kappa = 0.1$. The *IR* correction decreases as the electrode radius is decreased and does so more rapidly than in the cylindrical-electrode case.

Although there is some doubt as to the validity of the approximation $\delta = 5d/3$ for small spherical or cylindrical electrodes, it would be expected that δ would decrease rather than increase as r_o is made smaller. Any refinement of the numerical values listed in Tables II and III is expected to yield even smaller values. Thus the general result that a decrease in electrode radius can cause an appreciably lower *IR* correction is evidently real.

The following conclusions may be drawn in summary.

1. Large capillaries (diameter > 0.1 cm) are useful only at relatively low current densities in solutions of high conductivity.

2. Even with the smallest convenient capillary (0.02 cm diameter) placed as close to the electrode as possible without incurring shielding errors, the *IR* corrections greatly limit the maximum c.d. for accurate polarization measurements, especially in solutions of relatively low conductivity.

3. Small cylinders (wires) or spheres may be used advantageously as test electrodes in polarization studies, since the *IR* correction decreases as the electrode is made smaller.

Manuscript received May 18, 1960.

Any discussion of this paper will appear in a Discussion Section to be published in the December 1961 JOURNAL.

REFERENCES

1. F. Haber, *Z. physik. Chem.*, **32**, 208 (1900).
2. R. Piontelli and G. Bianchi, *Gazz. chim. ital.*, **80**, 581 (1950).
3. S. Barnartt, *This Journal*, **99**, 549 (1952).
4. R. Piontelli, G. Bianchi, and R. Aletti, *Z. Elektrochem.*, **56**, 86 (1952).
5. R. Piontelli, G. Bianchi, U. Bertocci, C. Guerci, and B. Rivolta, *ibid.*, **58**, 54 (1954).
6. C. Kasper, *Trans. Electrochem. Soc.*, **78**, 131, 147 (1940).
7. C. Wagner, *This Journal*, **98**, 116 ((1951).
8. C. Kasper, *Trans. Electrochem. Soc.*, **77**, 353 (1940).
9. S. Barnartt, *This Journal*, **106**, 722 (1959).
10. M. Breiter and T. Guggenberger, *Z. Elektrochem.*, **60**, 594 (1956).

Electrolytic Polish for Lead Telluride

P. H. Schmidt

Bell Telephone Laboratories, Incorporated, Murray Hill, New Jersey

Previous attempts to polish-etch PbTe chemically or electrolytically have been relatively unsuccessful. Several dislocation and material removal etches are described in the literature (1,2), but they are unsatisfactory as polishes. Laboratory experiments using standard chemical polish etches for Pb[3] and Te[4] have been performed without successful results on PbTe. The usual result of using such etches is the formation of a black, gray, or white film (usually an oxide) which could not be removed from the sample surface easily. One attempt to electropolish PbTe using the "Jacquet solution" (5,6), a rather universal aqueous electrolyte, produced a minor explosion. The composition of the electrolyte was 75 cc glacial acetic acid of sp gr 1.05 and 25 cc perchloric acid of sp gr 1.67. Some encouraging polish-etch effects were observed when the author used a chromic-phosphoric electropolish described by Walker, Williams, and Bozorth (7), which originally was designed for electropolishing Fe, Ni, Co, and their mutual alloys. The purpose of this note is to describe a modification of this electropolish which produces an excellent polish-etch on all crystallographic planes in lead telluride.

Method

The specimen is prepared by first abrading the surface to be electropolished with 600 grit silicon carbide paper lubricated with water. After thoroughly cleaning off any traces of the abrasive from the sample with benzene, the sample is then preheated at 70°C in a drying oven. Preheating the sample helps to reduce the possibility of thermal shock during the electropolish. Electropolishing is performed immediately upon removing the sample from the drying oven, the sample being continuously agitated while current is permitted to flow.

The electrolyte consists of a mixture of 100 ml of reagent grade 85% phosphoric acid (H_3PO_4) and 10 g reagent grade chromic acid (CrO_3). The temperature of the electrolyte is important; it must be held at 90°-105°C. The specimen to be polished is made anodic while a tantalum strip serves as the cathode.

Electropolishing is carried out at a current density of about 3 amp/cm^2. To maintain this high current density, a cell voltage of 6-12 v is required. A warm water (70°C) rinse removes the electrolyte and an air jet is used to dry the sample. The etch rate, using a current density of 3 amp/cm^2, is about

2.5×10^{-3} cm (1×10^{-3} in.)/min. This method produces "mirror-like" polished surfaces having no macroscopic defects or waves on specimens of PbTe.

Acknowledgment

The author would like to thank B. B. Houston of the Naval Ordnance Laboratory, White Oak, Silver Spring, Maryland, and J. H. Wernick of Bell Telephone Laboratories for samples and W. M. Walsh of Bell Telephone Laboratories for helpful discussions.

Manuscript received July 27, 1960.

Any discussion of this paper will appear in a Discussion Section to be published in the December 1961 JOURNAL.

REFERENCES

1. B. B. Houston and M. K. Norr, *J. Appl. Phys.*, **2**, [3], 615 (March 1960).
2. U.S. Pat. 2,822,250, Material Removal From Semiconductive Metal Telluride, (Feb. 4, 1958).
3. D. F. Gibbons, Personal communication.
4. L. C. Lovell, J. H. Wernick, K. E. Benson, *Acta Met.*, **6**, [11], 716 (1958).
5. P. A. Jacquet, *Met. Rev.*, Vol. **1**, Part 2, 157 (1956).
6. W. J. McG. Tegart, "The Electrolytic and Chemical Polishing of Metals in Research and Industry," pp. 45-50, Pergamon Press, N. Y. (1956).
7. J. G. Walker, H. J. Williams, and R. M. Bozorth, *Rev. Sci. Instr.*, **20**, [12], 947 (1949).

Digital Programming Unit for Automatic Temperature Control during Pyrosynthesis of Inorganic Compounds

Norman L. Hozak, J. Stanley Cook, and Donald R. Mason

Department of Chemical and Metallurgical Engineering, The University of Michigan, Ann Arbor, Michigan

The first step in studying the electronic properties of inorganic compounds is the preparation of homogeneous high-purity samples.

Many investigators (1,2) have found that the direct fusion of stoichiometric amounts of highly purified elements remains as one of the simplest and best preparational procedures. A clean fused silica tube can serve as the nonreactive container which may be evacuated after the elemental constituents have been loaded, and an inert atmosphere may be introduced if desired. During fusion, the samples often explode. The explosion limit is, among other things, a function of the heat of formation of the compound from the elements, the vapor pressure over the reaction mixture, the reactor geometry, and the reaction kinetics. The furnace fusion cycle must be adjusted so that the influence of these factors is mitigated. Our experience indicates that a nonlinear heating cycle gives best results. The heating cycle must be determined for each individual type of sample, so that a means for automatically adjusting and controlling fusion cycles becomes necessary for efficient and successful operation.

Digital programming unit for automatic temperature control.—A digital programming temperature control unit capable of providing temperature control points which can be changed every 15 min by increments of 25°C has been made from readily available components and used successfully. A schematic diagram of the equipment is shown in Fig. 1. The potentiometer-type temperature controller is set to control at a fixed emf input which normally would be provided by a thermocouple inside the fusion furnace. However, in order to obtain programming action, an emf generator is placed in series with the control thermocouple. A patchboard between the emf generator and a time-sequence selector circuit is used to vary the magnitude of the emf inserted in series with the control thermocouple.

The emf generator.—The emf generator utilizes a 1.5 v dry cell and a series of resistors which will not change their characteristics with time. The current flow in the circuit is adjusted so that the voltage drop across each resistor is equivalent to 25°C. For chromel-alumel thermocouples, this is equivalent to about 1 mv, and a maximum emf equivalent to 1000°C is obtained with 40 resistors.

Furnace temperatures above the set point on the controller can be obtained by introducing the positive lead of the furnace thermocouple into a jack on the emf generator other than the "output" jack. Since this operating condition tends to be unstable, only limited temperature excursions should be made in this way.

The selector circuit.—The time variations in the furnace temperature are controlled by the selector circuit which is shown in Fig. 2. The central component of this circuit is a rotary stepping switch (Model RVF, North Electric Company). A cam-operated microswitch is used to generate a pulse of about 1 sec in duration once each 15 min in order

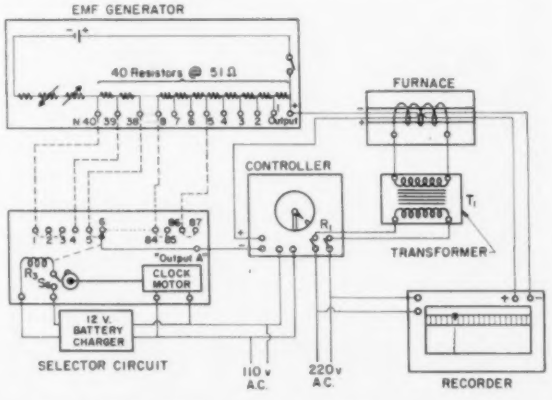

Fig. 1. Block diagram circuit of digital program control unit for fusion furnace.

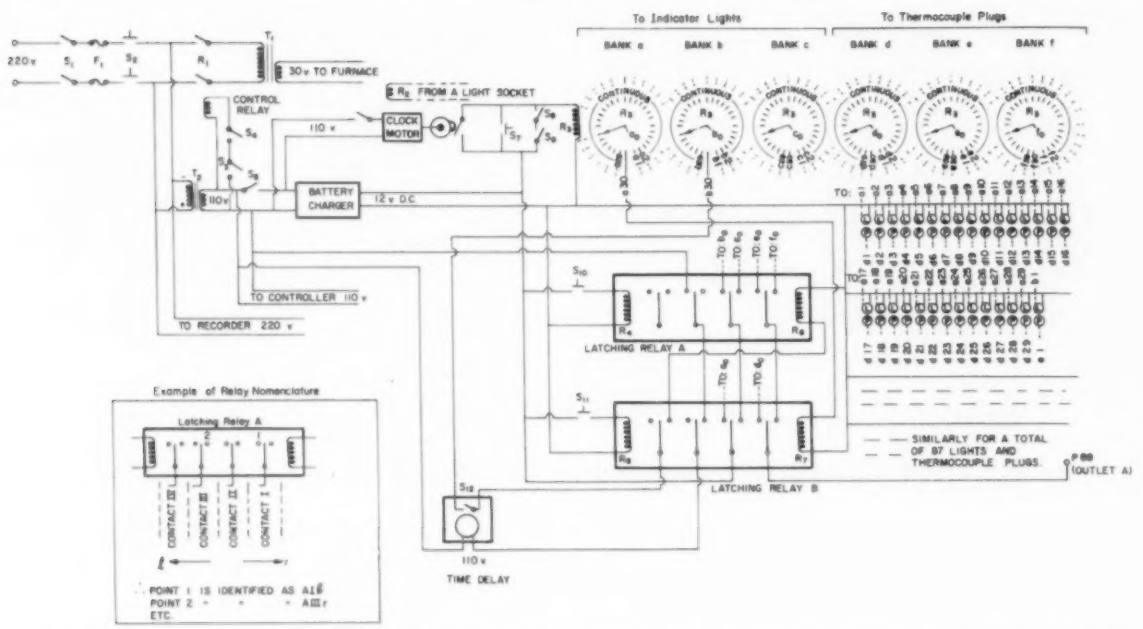

Fig. 2. Wiring diagram for stepping switch selector circuit and control circuits. F_1 main power fuses; R_1 power control relay; R_2 "hold" relay; R_3 stepping relay coil on North Electric Company Model RVF rotary stepping switch; R_4, R_5, R_6, R_7 latching coils on Potter and Brumfield Model KB17D latching relays; S_1 main power switch; S_2 circuit breaker; S_3 power control contact, high level turn-off, in controller; S_4 power control contact, low level turn-on, in controller; S_5 selector power switch; S_6 pulse generator microswitch, on clock motor timer; S_7 stepping relay actuator switch, on side panel; S_8, S_9 interrupter contacts on RVF rotary stepping switch; S_{10}, S_{11} reset push-button switches for latching relays, on top panel; S_{12} time delay switch; T_1 main furnace power stepdown transformer; T_2 auxiliary control stepdown transformer.

to move the stepping switch successively through 87 different positions during the course of the 21¾-hr cycle. The stepping switch has six banks of gold-plated contacts, each bank containing 30 positions around its circumference. Three banks are utilized to switch the thermocouple circuit as described above, and the other three banks are used in a pilot lamp indicator circuit. The first 29 positions on each bank of contacts are utilized to perform the switching functions. Position 30 is used to control the position of two 4 PDT latching relays (Potter and Brumfield Type K B 17D) which switch the thermocouple and indicator circuits onto the appropriate banks of contacts on the stepping switch for the second and third revolutions of the switch.

The cycle can be terminated at any specified time and temperature by removing the indicator lamp adjacent to the appropriate emf plug and replacing it with contacts which can energize the coil of Relay R-2. This relay opens the 110-v circuit operating the pulse generator. It thereby becomes possible to run a complete 21¾-hr cycle followed by automatic shut-off or to maintain the control point at the particular temperature designated by the programmer until the "Hold" is removed by the operator.

With this equipment, heating rates, cooling rates, and holding times and levels, can be selected easily, readily and reproducibly. Wide fluctuations in furnace temperature can be obtained if desired, limited only by the time constant of the furnace. The time increment could be changed easily by changing the cycle time of the clock motor, and the temperature increment could be changed by varying the size of the precision resistors or the current drain through the emf generator. At the same time the advantages of simplicity, low cost, compactness, and flexibility are obtained.

It should be evident that a device of this kind should not find its usefulness limited to temperature fusion cycles. Any process where a variable time-emf program is required could benefit from the application of a digital programmer as described.

Acknowledgment

The authors would like to express their appreciation for discussions and assistance given by their colleagues in the design and construction of this system.

Manuscript received May 31, 1960. This paper was prepared for delivery before the Chicago Meeting, May 1-5, 1960. Contribution No. 3 from The Semiconductor Materials Research Laboratory, the College of Engineering, The University of Michigan, Ann Arbor, Michigan. This work was supported in part by grant NSF-G4127 from the National Science Foundation, and in part by Project MICHIGAN, under Department of the Army Contract (DA-36-039-SC-78801), administered by the U. S. Army Signal Corps.

Any discussion of this paper will appear in a Discussion Section to be published in the December 1961 JOURNAL.

REFERENCES

1. G. Busch and U. Winkler, *Helv. Phys. Acta*, **26**, 395 (1953).
2. H. J. Hrostowski and M. Tanenbaum, *Physica*, **20**, 1065 (1954).
3. L. Thomassen and D. R. Mason, Paper presented at the Columbus Meeting of the Society, October 1959.

Preparation of Nickel Polyhedra by Reduction in Fused Salt Systems

Robert A. Lefever[1]

Virginia Institute for Scientific Research, Richmond, Virginia

Considerable interest currently exists in the influence of particle symmetry on the magnetic properties of metal powders, and several procedures designed to produce asymmetric particles have been described recently in the literature (1). The demonstrated influence of surface orientation on such properties as catalytic activity and oxidation rates (2) indicates that the surface orientations of particles comprising metal powders also may be of considerable importance in these and related areas. A convenient experimental procedure that can be employed to prepare nickel powders containing uniform polyhedra is described below, with a summary of exploratory studies designed to evaluate the influence of experimental conditions on particle size, symmetry, and surface orientation. Limited work with iron and cobalt indicates that the method also is applicable to these metals.

Experimental

The powders were prepared by adding a reducing agent to a binary melt composed of the transition metal halide and the corresponding alkali halide. Optimum conditions for the preparation of nickel polyhedra were the reduction of nickel chloride in potassium chloride at 800°-1000°C. In a typical experiment, 10 g each of analytical reagent grades of $NiCl_2 \cdot 6H_2O$ and KCl were placed in a vertical fused silica reaction tube and dried for several hours at 550° under a continuous flow of argon. After heating to 1000° and holding at this temperature for 1 hr, reduction was effected by adding six pellets, weighing approximately 30 mg each, of aluminum to the melt. (Reducing agents were added in relatively small amounts in order to avoid influencing particle characteristics by significant changes in concentration.) After addition of the reducing agent, the melt was held at 1000° for a specific length of time, normally between 1 and 24 hr, and then allowed to cool to room temperature. The metal polyhedra were recovered by dissolving the halides in distilled water, magnetically collecting the powder at the bottom of the container, and pouring off the solution. After repeated washing, a wet sample of the polyhedra was transferred to a microscope slide. The water then was allowed to evaporate after agitating the slide to provide a uniform particle distribution.

Photomicrographs were made with a metallographic microscope. The metallic products were identified by analysis of x-ray powder patterns. Surface orientations were established by chemical etching and comparing etch pit orientation and geometry with pits produced under identical conditions on oriented surfaces of large nickel single crystals.

Results and Discussion

Most of the powders prepared contained a high percentage of particles that were uniform in size and crystal habit. Figure 1 is a photomicrograph of cubic nickel polyhedra that resulted from a typical experiment. The surfaces of these particles were shown to be parallel to {100} crystal planes by etch pit studies. The majority of the particles ranged in size from about 1-10 μ for reaction times of 5 min to 1 hr after addition of the reducing agent. Although cubic polyhedra were observed most frequently, several lots of nickel chloride gave polyhedra with surfaces parallel to {111} crystal planes (Fig. 2). Certain of the metal ions likely to be present as impurities in the nickel chloride appeared to favor the formation of cubes. For example, the addition of ferrous, cobaltous, or cupric chloride in low concentrations to melts that normally gave particles exhibiting {111} surfaces altered the habit to cubic.

An exploratory study of the influence of various experimental parameters on polyhedron size, surface quality, and habit was conducted. The nature of

[1] Present address, Hughes Research Laboratories, Malibu, California.

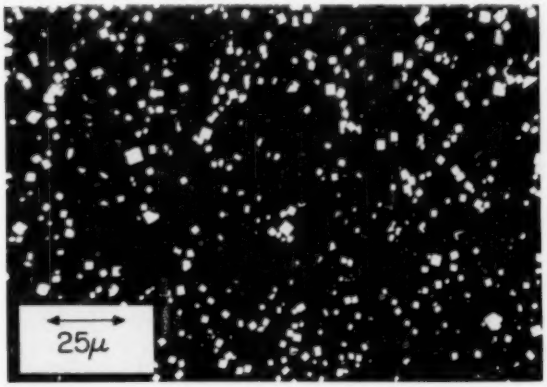

Fig. 1. Cubic nickel polyhedra

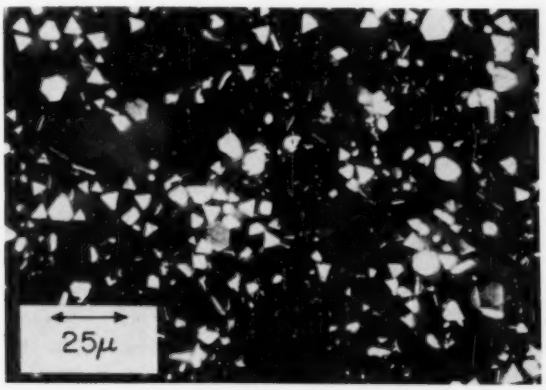

Fig. 2. Triangular and hexagonal nickel platelets

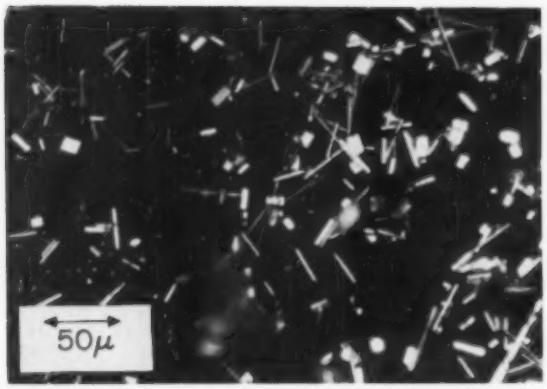

Fig. 3. Nickel rods and rectangular platelets

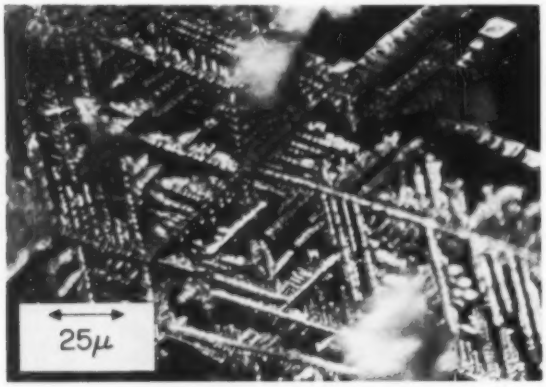

Fig. 4. Branched nickel dendrites

the final product was not influenced appreciably by variations in procedures used for drying the halides (including sublimation under vacuum), reaction temperature (between 700° and 1200°C), or concentration of the nickel chloride in the range of about 10-80 wt % (as the hydrate). Changing the melt anion to bromide or iodide had no observable influence on crystal size or habit. Surface quality, however, was somewhat reduced. With the bromide and iodide systems, polyhedra also resulted from thermal decomposition alone.

Particle morphology was influenced by the nature of the reducing agent, concentration of the nickel chloride (although only at relatively high and low concentrations), and reaction time subsequent to addition of the reducing agent. Nickel rods of the type shown in Fig. 3 normally resulted when hydrogen (at low partial pressures in argon and low flow rates) was used as the reducing agent and nickel chloride concentrations in the melts were below about 1 mole %. Rods also frequently resulted with

Fig. 5. Rectangular nickel platelets

low nickel chloride concentrations when aluminum was used as the reducing agent. The rods prepared in this manner were normally 100-200 μ in length, with cross sections of about 1 μ. The use of magnesium as a reducing agent with melts of normal nickel chloride concentrations resulted in highly branched nickel dendrites (Fig. 4).

The effect of short reaction times on the product was determined by periodically sampling the melt immediately after addition of the reducing agent. Samples removed within the first few minutes (from melts that subsequently gave cubes) normally contained large numbers of rods and rectangular platelets. Rods, with long dimensions of approximately 0.1-1 μ, were predominant when reaction times were less than a minute. After several minutes, platelets of the type shown in Fig. 5 were observed frequently. The long dimensions of the platelets were normally about 1-10 μ, or about ½ the size of those shown in Fig. 5 (selected for optimum reproduction).

Acknowledgment

The author wishes to express appreciation to Dr. Henry Leidheiser, Jr., for many helpful discussions and Mr. Forrest Hettinger for assistance with the experimental work. This study was supported by a grant from Texaco, Inc.

Manuscript received May 31, 1960; revised manuscript received Aug. 18, 1960.

Any discussion of this paper will appear in a Discussion Section to be published in the December 1961 JOURNAL.

REFERENCES

1. For a summary of the preparation and magnetic properties of metal powders see E. P. Wohlfarth, *Advances in Phys.*, **8**, 87 (1959).
2. See for example the work of A. T. Gwathmey and associates, *J. Chem. Phys.*, **8**, 569 (1949); *J. Phys. Chem.*, **44**, 35 (1940); *J. Am. Chem. Soc.*, **70**, 1200, 1206 (1948); *Acta Met.*, **4**, 145 (1956); *J. Appl. Phys.*, **31**, 225 (1960).

Twin Structures in Silver Dendrites

J. W. Faust, Jr. and H. F. John

Research Laboratories, Westinghouse Electric Corporation, Pittsburgh, Pennsylvania

Dendrites of metals and compounds can, under the proper conditions, be obtained during electrodeposition, solidification from a melt, vapor deposition, or growth from a solution. Until recently, dendrites were assumed or shown to be single crystals. Silver dendrites, and other face centered cubic metals, grown during solidification of a melt have a growth direction of <100> and are single crystals (1). In 1952, Dawson (2) showed that dendrites of paraffin grow by a twin plane supplying an indestructible re-entrant groove. Dendrites of germanium, grown by pulling from a supercooled melt, were reported to be single crystals as a result of x-ray examination (3); however, it was later shown by metallographic techniques that these dendrites actually contained two twin planes parallel to their flat faces (4). It has now been shown that dendrites of the diamond and zinc blende lattice must have at least two twin planes to maintain an indestructible re-entrant groove (5, 6).

Wranglen (7) reported that silver dendrites grown by electrodeposition from a silver nitrate solution were single crystal and grew in the <110> direction. Yang, Chien, and Hudson (8) grew silver dendrites by electrodeposition from a molten LiCl-KCl eutectic mixture containing AgCl. Microscopic and x-ray examination of the dendrites showed that (*a*) the main stem runs in the <211> direction, (*b*) the branches on one side are in the <211> direction, (*c*) the branches on the other side are in the <110> direction, and (*d*) the dendrites are faceted by {111} planes. Since the twin composition plane of silver is the {111}, the above findings suggested to us that the silver dendrites may be growing by a twinning mechanism similar to that found for germanium, silicon (6), and the III-V intermetallic compounds (9, 10).

Hudson supplied us with some of the silver dendrites reported in their paper (8). The dendrites were examined microscopically, and cross sections were examined for twin structure after potting, polishing, and etching in $NH_4OH:H_2O_2$ (5:1) for 2 sec. Figure 1 is a photomicrograph of a silver dendrite showing that it is indeed highly faceted. It is strikingly similar to the tip ends of dendrites of Ge, Si, and InSb, even to the pits running down the center. Microscopic investigation of a number of dendrites showed that many of them had <211> side branches on both sides, while others had the asymmetric branching mentioned by Yang, *et al.* (8).

Figures 2 and 3 show some examples of etched cross sections. At least one twin lamella can be seen in each dendrite. Detailed metallographic examination has shown that the line which appears to be a single twin plane in the photomicrographs is actually in most cases a twin lamella consisting of two very closely spaced twin planes. Thus Fig. 2a and b have two twin planes and Fig. 3a contains four twin planes. The thin piece at the side in Fig. 2b belongs to another dendrite that was bent toward the larger one during potting.

Fig. 1. Silver dendrite, direction of growth <112>, shows flat {111} face, side faceting, and pipes. Magnification 200X before reduction for publication.

It is beyond the scope of this communication to discuss the growth in much detail; however, a few things should be mentioned in explanation of the photomicrographs. Wranglen (7) stated that at high current densities growth proceeded at the corners and edges while at lower current densities growth proceeded from the "interior" of the faces. Since the current density is highest at corners and edges, one would expect that growth would occur easily at these places without the need of twinning; from Wranglen's statement this must indeed be true at high current densities. At the lower current densities used in the work of Yang, *et al.* (8), it appears that twin lamellae contribute to the directional propagation of the dendrites. We believe that the <110> dendrites of Pb, Ag, and Cu grown by Wranglen may also have grown by a twinning mechanism. The widening and thickening of the silver dendrites appear, from Fig. 2, to take place by growth at corners and edges. Growth then proceeds inward to complete the faces. This thickening mechanism makes it unnecessary to postulate a screw dislocation mechanism. Incomplete growing together probably accounts for the pipes and pits found in

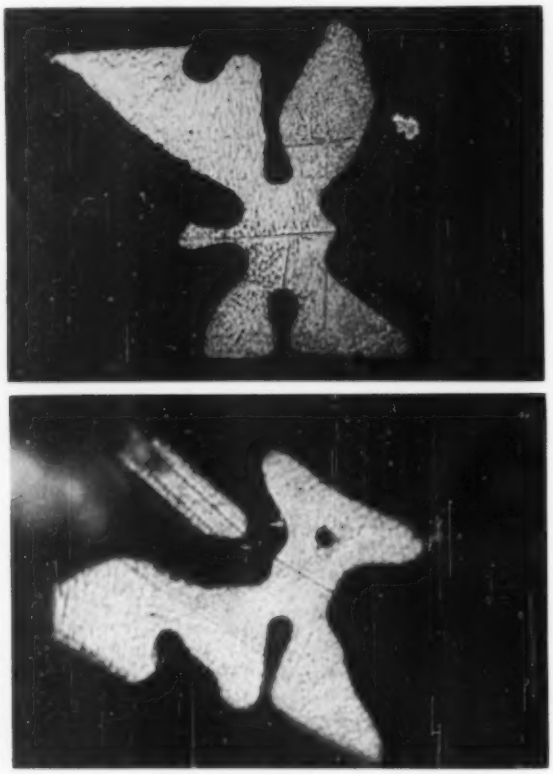

Fig. 2. Cross sections of silver dendrites showing a twin lamella and pipes. Fig. 2B (bottom) has an entrapped pocket. Magnification before reduction for publication, a (top) 1000X, b (bottom) 500X.

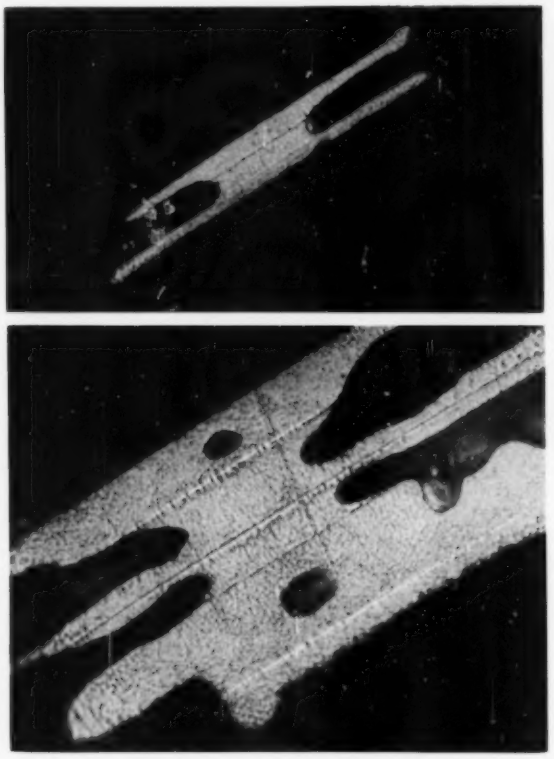

Fig. 3. Cross sections of silver dendrites showing twin lamellae and entrapped pickets. Magnification 1000X before reduction for publication.

these dendrites rather than impurity segregation and etching mentioned by Yang, *et al.* (8). NH_4OH used by them to remove the electrolyte will not etch silver.[1] Figure 2a shows a pipe on either side of the twin lamella. Figure 2b shows a pipe on one side of the twin lamella, while on the other side, the face has been completed, leaving an entrapped pocket reminiscent of those found in dendrites of Ge, Si, and the III-V intermetallic compounds (11).

Figure 3 shows two other cross sections of dendrites. The dendrite in Fig. 3b contains seven twin planes; the pocket between the twin planes has not been observed in dendrites of semiconductors and may have been formed by two lateral arms growing together in the earlier stages of growth of this dendrite.

From this investigation, which shows that a twin mechanism can contribute to the growth of dendrites during electrodeposition, and from the work on dendrites of semiconductors and face-centered cubic metals grown from melts, it appears likely that dendrites of these materials grown by any method will contain two or more twin planes if their direction of propagation is either the <211> or <110>.

[1] Oxygen in NH_4OH would cause some etch attack; however, our experience indicates that the etch would be too slow to account for the pipes and pits.

Manuscript received Aug. 4, 1960.

Any discussion of this paper will appear in a Discussion Section to be published in the December 1961 JOURNAL.

REFERENCES

1. W. A. Tiller, Private communication.
2. I. M. Dawson, *Proc. Roy. Soc.*, **214A**, 72 (1952).
3. E. Billig, *ibid.*, **A229**, 346 (1955); E. Billig and P. J. Holmes, *Acta Cryst.*, **8**, 353 (1955).
4. E. Billig and P. J. Holmes, *Acta Met.*, **5**, 53 (1957).
5. D. R. Hamilton and R. G. Seidensticker, *J. Appl. Phys.*, **31**, 1165 (1960); R. S. Wagner, *Acta Met.*, **8**, 57 (1960).
6. J. W. Faust, Jr., and H. F. John, Electronics Division Abstracts, E.C.S., **9**, 145 (1960).
7. G. Wranglen, *Acta Polytechnica*, **4**, 182 (1955).
8. L. Yang, C. Chien, and R. G. Hudson, *This Journal*, **106**, 632 (1959).
9. J. W. Faust, Jr., H. Nicholson, and R. Moss, Electronics Division Abstracts, E.C.S., **9**, 165 (1960).
10. R. Moss and H. Nicholson, To be published.
11. J. W. Faust, Jr., and H. F. John, *Bull. Am. Phys. Soc.*, Ser. II, **5**, 165 (1960).

Ferroelectric Properties of the System $(NH_2CH_2COOH)_3 \cdot H_2(SO_4, PO_3F)$

T. G. Dunne and M. L. Wang

Research Laboratory, International Business Machines Corporation, Poughkeepsie, New York

A partial substitution of $PO_3F^=$ for $SO_4^=$ has been effected in the room temperature ferroelectric $(NH_2CH_2COOH)_3 \cdot H_2SO_4$ (1). It has not been possible to date to obtain single crystals of pure $(NH_2CH_2COOH)_3 \cdot H_2PO_3F$.

Single crystals were prepared by slow evaporation from aqueous solutions containing m moles of C. P. NH_2CH_2COOH, x moles reagent grade H_2SO_4, and $m/3 - x$ moles of H_2PO_3F (Ozark-Mahoning 85%). In order to minimize solid solution inhomogeneities caused by hydrolysis of H_2PO_3F (2) as well as the usual anion segregation, as soon as crystals had grown to usable size they were removed from solution. Crystals were analyzed for fluorine and phosphorus by standard techniques. It was necessary to use aqueous solutions with a nominal mole ratio $N_c = mH_2PO_3F/(mH_2SO_4 + mH_2PO_3F) > 0.5$ in order to obtain crystals with $N_c = mH_2PO_3F/(mH_2SO_4 + mH_2PO_3F) > 3 \times 10^{-2}$. Solutions with $N_c > 0.9$ precipitated γ-glycine (3) instead of $(NH_2CH_2COOH)_3 \cdot H_2(SO_4, PO_3F)$.

The N_c calculated from fluoride analysis of the crystals always agreed within 7% with the N_c calculated from phosphorus analysis. These variations in N_c can be accounted for by errors in analysis, so it is assumed that $PO_3F^=$ is present in the crystals rather than products of hydrolysis. A check on the homogeneity of the $PO_3F^=$ concentration of a large crystal grown from a solution with $N_c = 0.50$ was made by dissolving part of the weighed crystal, analyzing the resulting solution for fluoride, and repeating the cycle. Three solutions resulting from the successive dissolution of about equal amounts of the crystal gave N_c's within 5% of the average N_c for the entire crystal. X-ray powder patterns for all crystals showing ferroelectric behavior were identical with the $(NH_2CH_2COOH)_3 \cdot H_2SO_4$ pattern, as would be expected for solid solutions so dilute in $(NH_2CH_2COOH)_3 \cdot H_2PO_3F$.

Hysteresis loops and dielectric constants were measured on platelets cleaved perpendicular to the ferroelectric monoclinic b axis. Evaporated silver or 'dag' dispersion No. 154 electrodes were both found to be satisfactory. The apparatus used to measure the capacitance *vs.* temperature was similar to that described by Triebwasser (4). The spontaneous polarization was measured using a Sawyer-Tower circuit (5).

For a given sample the uncertainty in measurement of temperature was less than 1°C and that of the spontaneous polarization and dielectric constant was less than 10%.

Table I. Crystal growth solution mole fraction, crystal mole fraction, transition temperature, and spontaneous polarization of $(NH_2CH_2COOH)_3 \cdot H_2(SO_4, PO_3F)$ single crystals

N_s	N_c	T_c °C	P' (μ/coul/cm^2)
0	0	48.7	1.75
0.50	0.031	49.5	0.48
0.50	0.031	50.0	1.3
0.50	0.031	49.1	1.5
0.62	0.062	44.9	
0.62	0.062	44.1	0.36
0.62	0.104	43.0	1.84
0.62	0.104	43.5	2.75
0.89	0.135	33.0	0.536

Table I lists the chemical and electrical results for the mixed systems. The temperature of maximum capacitance was taken to be the transition temperature T_c. In some crystals more concentrated $PO_3F^=$ (see Fig. 1) the peak in dielectric constant was considerably broadened, and hysteresis loops of greatly diminished spontaneous polarization were seen at temperatures as high as 2°C above T_c. This broadening may be caused by inhomogeneity of the $PO_3F^=$ concentration. The dielectric constant peaks were also lowered compared to those for $(NH_2CH_2COOH)_3 \cdot H_2SO_4$. Crystal inhomogeneity again may be the major cause for the decrease in the peak dielectric constant.

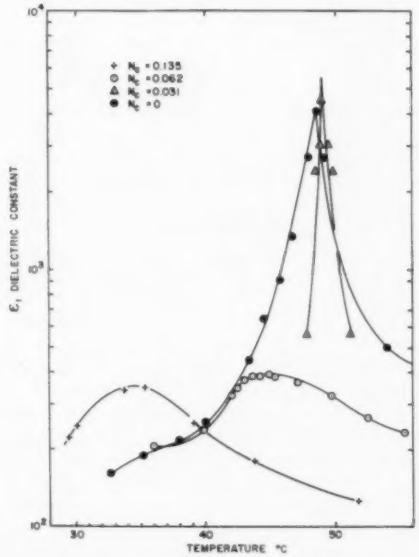

Fig. 1. Dielectric constant of $(NH_2CH_2COOH)_3 \cdot H_2(SO_4, PO_3F)$ single crystals as a function of temperature.

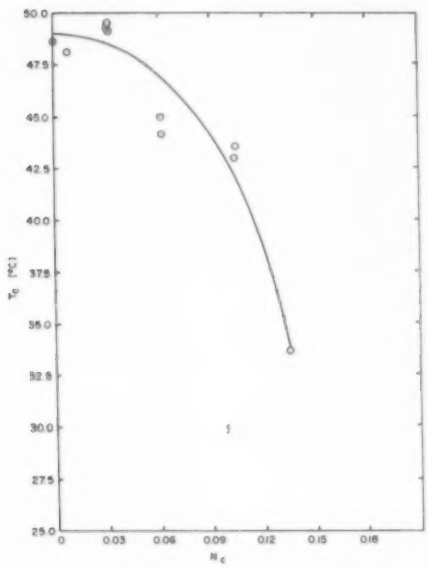

Fig. 2. Transition temperature of $(NH_2CH_2COOH)_3 \cdot H_2(SO_4, PO_3F)$ single crystals as a function of the mole fraction of $(NH_2CH_2COOH)_3 \cdot H_2PO_3F$.

For the purposes of comparison, the spontaneous polarization, P'_s was taken at a temperature 7° below T_c. It would have been more desirable to use a lower temperature in order to be in a temperature range where the spontaneous polarization was less temperature dependent (6). This was not possible because the very large increase of coercive field did not permit the observation of saturated hysteresis loops at a temperature 10°C below T_c in some cases. As can be seen from Table I, $PO_3F^=$ substitution has a small effect on the spontaneous polarization.

The concentration dependence of T_c seen in Fig. 2 is quite large. It is seen that T_c decreases by 16.5°C when N_c is increased from 0 to 0.135.

In general, a small change in lattice constants might be expected when $PO_3F^=$ is substituted for $SO_4^=$ because both ions are found to be of about the same size (7) in the K_2SO_4 lattice. Since this substitution in the $(NH_2CH_2COOH)_3 \cdot H_2SO_4$ results in a large decrease in T_c, it is indicated that the asymmetry of hydrogen bonding of the anion (8) is playing a more important role than the change in the unit cell volume (9) upon isomorphous substitution in determining ferroelectric properties in $(NH_2CH_2COOH)_3 \cdot H_2SO_4$ isomorphs.

Further understanding of ferroelectric mechanisms may be gained by coupling a study of the substitution by asymmetric anions with that of the substitution by more symmetric ions in various ferroelectric systems.

Acknowledgment

The authors wish to thank Mr. N. Stemple for doing the x-ray analyses and Mr. S. Phillips for some of the chemical analyses.

REFERENCES

1. B. T. Matthias, R. C. Miller, and J. P. Remeika, *Phys. Rev.*, **104**, 849 (1956).
2. W. Lange, "Fluorine Chemistry," J. H. Simons, Editor, Vol. 1, p. 141, Academic Press Inc., New York (1950).
3. Y. Iitaka, *Acta Cryst.*, **11**, 225 (1958).
4. S. Triebwasser, *Phys. Rev.*, **101**, 993 (1956).
5. C. B. Sawyer and C. H. Tower, *ibid.*, **35**, 269 (1930).
6. S. Triebwasser, *IBM Jour. Res. and Dev.*, **3**, 212 (1958).
7. M. T. Robinson, *J. Chem. Phys.*, **62**, 925 (1958).
8. S. Hoshino, Y. Okaya, and R. Pepinsky, *Phys. Rev.*, **115**, 323 (1959).
9. T. Dunne and G. Burns, To be published.

Henry B. Linford—The Acheson Medalist[1]

L. I. Gilbertson

I am honored to have the privilege of speaking to you tonight of the life and activities of our very good friend and fellow member who is the 16th to be awarded the Acheson Medal of our Society. He is widely known among our membership and in educational circles for his great devotion to electrochemistry and for his untiring labors in behalf of its advancement. Surely there are few who have been officers of a Division or of a Section of our Society in the past 15 years who have not felt, in some way or other, tangible evidence of his interest in the affairs of the Society.

Our medalist is a man of many accomplishments and wide interests. Born in Logan, Utah, the seventh child and sixth son of Professor and Mrs. James Henry Linford, he was, in early childhood, oriented toward science and education. His father, a biologist and professor at Utah State University, provided him with an example of diligence, inquiry, and an uncompromising attitude toward right and wrong. His mother, now in her 90's, is still active in genealogical research. She taught him order and logical thinking and seasoned this with tolerance and humanitarianism. Three brothers before him set high standards of scholarship in physical science. These became targets for his endeavors. So it is little wonder that he received the Bachelor's degree in chemistry from Utah State University only a few weeks after his 20th birthday.

In 1931, he was awarded a graduate fellowship at Washington State University. He elected to pursue electrochemistry as a major, and chose to work with the late Professor Wilbur E. Bradt, a member of our Society, who subsequently became head of the chemistry department in the University of Maine. This association was instrumental in determining many later events. Our medalist began his electrochemical research career in electro-organic chemistry. His researches in several areas of electrochemistry have been continuous since 1931. In 1933, he received the M.S. degree from Washington State University, presenting a thesis on electro-organic reduction. He was an outstanding graduate student and a hard-working assistant, and he was rewarded with a second graduate fellowship to continue his studies at Washington State. Again, he chose to work with Dr. Bradt but now he turned his attention to inorganic electrochemistry. His doctorate dissertation among other things demonstrated the successful electrodeposition of zirconium. Our medalist continued to distinguish himself as a scholar. In graduate courses, which I taught for many years, I had no other student who could match him in brilliance, comprehension, and in diligence. We did not always agree, and, as others here present can testify, he is courageous and persistent in defending his beliefs, but always fair.

At Washington State University, he established much of the pattern for years to come. Electrochemistry was definitely his field in science. He also had received an opportunity to experience the trials and tribulations of teaching and to savor its joys. He was then, and I am assured he still is, a stern taskmaster making short shrift of shirkers but patient with those who would learn. His students testify to this fervently and loyally.

Additionally, Dr. Bradt had sowed the seed of interest in our Society. Sometime in 1935, he had spoken to Professor Colin G. Fink at Columbia University about this brilliant young student and had suggested him as a candidate for the Weston Fellowship established a few years previously. Almost simultaneously with the award of his Ph.D. degree from Washington State, our medalist became the seventh Weston Fellow of The Electrochemical Society. He elected to study with Dr. Fink.

Turning now to physical chemistry, he studied electrokinetic phenomena at Columbia University in 1936 and 1937. Later in 1937, he joined the research staff of the American Smelting and Refining Co. in Perth Amboy, N. J. Again, he worked with rare metals, developing processes for electrowinning and thermal recovery of indium, and patenting electrorefining and electroplating processes for the same metal. He also developed and supervised the installation of a palladium control process used in electrorefining silver. These activities gave him first-hand experience in industrial research and engineering.

However intriguing the research may be, a teacher needs students and so he returned again to the classroom in 1941 as instructor in chemical engineering in Columbia University. Advancing successively to assistant professor in 1946 and associate professor in 1949, he became professor in 1952. Also, since 1947, he has been in charge of the Columbia Chemical Engineering Camp in Connecticut and, as director of Project 12 of the American Electroplaters' Society since 1949, he has been responsible for the publication of 14 papers related to the cleaning and preparation of metals for electrodeposition. With his students, he has published in the fields of electrodeposition and corrosion and also has contributed to our Society's monograph, "Modern Electroplating." Currently, his research interests are in electrode kinetics and fuel cells.

Always interested in education at all levels, he has been active for many years in the school life of his home town, and, in 1951, he found time to be president of the Leonia, N. J., Home and School Association. His interest in civic affairs has been expressed by his activity in the Civic Conference of his home town. Active in his church, he has found another outlet for his industry as a member of the building committee. Closely allied to these activities has been his interest in scouting. About ten years ago, seeing need for unit expansion in his home town, he commandeered some friends one evening and founded a boy scout troop with which he has been associated actively ever since.

Affiliating with the New York Metropolitan Section of the Society in 1941, five years after he joined as a student, he has worked in various Section offices. He was Chairman of the New York Section in 1943. His interest in the Electrodeposition Division led him to the Chairmanship of that Division in 1948. In 1949, he became National Secretary and served in this capacity for ten years, acting as Interim Secretary during his first term as Vice-President in 1958-1959. The decade during which our medalist held the office of Secretary was a period of substantial growth and change. He participated in nearly every change of this period, acting as the binding element when necessary and spearing us into activity when we lagged.

[1] Introductory remarks by L. I. Gilbertson on the occasion of the Acheson Medal Award to H. B. Linford on October 11, 1960.

The JOURNAL was first published in 1948. The Monograph Series was established about the same time. These involved many considerations of policy regarding publishing, advertising, and the means whereby the policies could be implemented. In all of these matters, the Secretary was a substantial contributor and, in somewhat lesser matters, such as office staff, location, how much rent to pay, and so on, the Secretary usually was expected to make the recommendation and carry out the decision. Back in 1949, the Secretary also prepared and defended the budget—and it was hard to stay in the black in some of those years. When he took office as Secretary, our membership was not over 1800. In the decade of which I speak, we grew to more than 3000. It would take a very long time, indeed, to detail the many important matters which our Secretary influenced in this ten-year period. As I said earlier, he did not always agree with all of us but he constantly pressed with courage and persistence for those actions which he believed were in the best interests of the Society. Upon his retirement as Secretary in May 1959, he was presented with a Certificate of Appreciation recognizing his many years of dedicated service. It read:

"In grateful recognition of many years of faithful and distinguished service and unselfish devotion to the interests and welfare of The Electrochemical Society, this scroll is hereby presented to Dr. Henry B. Linford as a token of our genuine appreciation of his outstanding contributions to the progress and building of the Society during his tenure of office as Secretary."

From his devotion to the cause of electrochemistry, our Society has gained much. His energy and zeal came to us in a decade of transition when it was most needed and in no small measure contributed to making our Society what it is today. It is now my very great honor to present to you the seventh Weston Fellow and 16th Acheson Medalist . . . Professor Henry Blood Linford.

The Education of Electrochemists[2]

Henry B. Linford

Mr. President, ladies, and gentlemen: For many years, I have had association with The Electrochemical Society in one capacity or another, and to have it culminate this evening with the presentation of the Edward Goodrich Acheson Medal and Award is really beyond all expectations. I am greatly honored. Or rather, I should say, we are greatly honored, since I am sure most of you will realize that I would not have been capable of more than a small fraction of what I have accomplished without the help and encouragement of my wonderful wife, Rebecca.

My early association with this Society began in the 1930's when I was a graduate student at Washington State University in Pullman. I was doing my research under the direction of a man for whom I have the highest regard, Professor Wilber E. Bradt. At the time of World War II, he went into the Service and did not return; therefore, most of you present tonight did not have the opportunity to know this fine man. In the fall of 1935, Professor Bradt returned from a trip to New York after a meeting with Professor Colin G. Fink; he told me I should apply for the Weston Fellowship, feeling that a year's postdoctoral study would be very much to my advantage. I was also counseled by Dr. Lyle I. Gilbertson, then an instructor in the same department, and to him I owe a great debt of gratitude for all of his advice and friendship, and also to his wife, Ruth. I did receive the award and elected to study under Professor Fink at Columbia University the following year. This, I believe, was one of the most fortunate choices that I have made. I have felt through the intervening years a great obligation to The Electrochemical Society for granting that fellowship to me in 1936. This has made all the difference in the world in my career, and I would be very remiss if I did not in every way possible make such assistance available to other young people. It was with this sense of debt that I accepted the nomination for Secretary of the Society in 1949. It now seems that it is impossible to pay back a debt to this organization. I can truthfully say that for all the work I have done for the Society I have been repaid manyfold.

For the last 19½ years, I have been teaching and, as a result, I have, through the years, made a study of scientific education. I have therefore decided, in the light of the need for a nontechnical talk, to develop some thoughts along these lines. My real interest in education was a natural result of my own home life, since my father was an educator. All through my childhood, I had a desire to teach and I am grateful for the chance to fulfill this desire. In fact, while I was attending a small country high school in Utah, I received my first stimulus in science. This, coupled with the home background, led me into my present profession. In this small high school, I was fortunate to have a chemistry teacher, N. W. Christiansen, who during his own college training had studied and understood chemistry. As a result, he was competent to teach the subject. In addition, he was enthusiastic, the complete antithesis of the general situation I will describe later.

Upon leaving high school and entering Utah State University, I studied under Professor Sherwin Maeser[3] whom I believe to be one of the best freshman chemistry teachers I have ever known. The final boost along this path was given to me by Professor Fink and The Electrochemical Society.

This evening, we are interested in the education of electrochemists. The starting point is, therefore, to determine what an electrochemist is. Our Society has, wisely I believe, indicated many times that we do not consider electrochemistry a profession. Electrochemists are chemists, chemical engineers, metallurgists, or physicists, for the most part, who have a common interest in the field we know as electrochemistry. Therefore, to discuss the education of an electrochemist, we must discuss the education of scientists and engineers since it is from these groups that electrochemists are derived.

One thing about engineering education is causing a lot of concern; while total college enrollment is increasing, engineering schools are experiencing a decline in enrollment. However, enrollment in the sciences is increasing. I do not have the complete answer to this but, as far as the Society is concerned, it may not be vital since we draw from both engineering and the sciences. Our only need for concern would come if the balance between pure science and engineering were to get out of control. This is not too serious a problem since the law of supply and demand will keep a damper on the radical swings. The point of interest here is the declining registration in engineering schools in the face of supposed shortages. These shortages may or may not be

[2] Acheson Medal Address delivered October 11, 1960 at the Houston Meeting of The Electrochemical Society.

[3] *Chemical & Engineering News*, May 23, 1960.

real when you consider both engineers and technicians, but I am sure there is a shortage of competent engineers. We must distinguish clearly between these two categories in this discussion. The good engineer is trained in a manner not too dissimilar from that of the pure scientist, but he is given the slant of practicality that the scientist does not receive. It is in my opinion very important that we maintain a proper balance between the two groups.

There are several reasons for this declining engineering enrollment, and I believe the following factors deserve consideration. In the first place, engineers have not received the favorable press that the scientists have of late. There is a joke that has been going around on that very point: "When a missile fails to function it is the engineers who have made an error, but, on the other hand when a shot goes off as expected, it is the scientist who gets the credit." The second reason is that the term engineer is used in two ways in this country. It can mean the engineer in a railroad locomotive or the engineer in the radio station on the one hand, or it can mean the competent engineer scientist that we, as technical people, think of as engineers. This distinction between the engineer and technician can be brought into focus by example. For years, it was considered the job of a civil engineer to survey new highways, etc., but the modern civil engineer considers this to be the job of a technician. The lack of knowledge by the general public as to the true work of an engineer is a result of poor public relations by the engineering societies. The need for better publicity is great because in the average community in this country the child growing up knows what the medical doctor does, he knows what the lawyer does, he has some contact, even if it is second hand, with what the scientist does since he will have one or more teachers who have had some courses in science, but his contact with engineers is usually nonexistent.

The problems of science and engineering education are not confined to the number of students enrolled; as you will remember, earlier I made mention of the difference between the engineer and the technician. Oftentimes, this difference appears to be a fine line; it is more a matter of quality than anything else. What are we doing about the quality of our raw material? Our colleges and universities get their raw material from our high schools. Even though the prep school has much more flexibility in its teacher recruitment and, in many cases, salary schedule, science teaching there is not ideal. In our public schools it is not ideal; in fact, in many cases it is downright disgraceful. In a recent survey conducted by the U. S. Office of Education and reported in *Chemical & Engineering News* (May 2, 1960), 594 science teachers in New Jersey, Maryland, and Virginia were surveyed. Of this number, 13% had had no college chemistry, 22% had had no college biology, and 28% had had no college physics. Only one in 20 reported having taken a science course since 1950. This is alarming in the face of all the publicity about summer education of teachers, raising their pay every time they take another course. Too many times, the courses are taken in administration or something else that is meaningless in relation to what they are trying to teach; these are courses so devoid of solid content that they can obtain good grades with a minimum of effort. The result is that the teachers get the increased salary, but they go on handing out the same set of diluted half-truths. Even more startling is the situation with respect to the training in mathematics. Of the high school teachers surveyed, 41% reported no college training in mathematics and 83% reported that they had not studied calculus or more advanced mathematics. This means that, of the teachers surveyed, 83% were incompetent to discuss rate problems. How much real science can be taught without an understanding of rate? I think the situation is shocking.

Why does it come about? It comes about because our laws are set up to allow anyone to teach, providing he has had enough courses in psychology, theory of education, education administration, etc. Very few states worry about the material a teacher is to teach. In most states, so long as he can get a license, he can teach any subject whether he knows the material or not.

I am very happy to report that, since this speech was prepared, New York State has moved in the right direction. As reported in *The New York Times* (August 27, 1960) and *Chemical & Engineering News* (September 19, 1960), New York State has raised the number of credits required in the subject to be taught and lowered the requirements in methodology courses. Thus, in science the new teachers must have 42 semester hours, an increase of 21, and in mathematics 18 semester hours, an increase of 9. This is a step in the right direction, but care must be exercised to insure that these courses in science and mathematics are taken in recognized liberal arts colleges, since many of our teachers colleges teach "science courses" that are not up to college level as far as content is concerned.

It is about time that our parents' groups get together and put a little pressure on the other state legislatures to change the laws. In this way, we have a chance to make sure that the people teaching our children are competent in the field they are trying to teach. I believe that, as a student grows older, his teacher's need for teaching methods decreases while need for knowledge of the subject taught increases. In kindergarten, for instance, the problem of knowledge of the subject does not exist for the teacher; her success or failure depends on her teaching methods. However, a high school physics teacher who knows but little physics and no calculus is, in my opinion, incompetent to teach the subject.

There are several things that make rapid improvement in this area impossible. One of them is an insidious problem, namely, the single salary schedule. Even though the teachers do not like to think of it that way, they are using union methods; as a result, they lose their professional status as soon as they fight for and get such a schedule adopted. Under this system, every teacher with the same amount of education, measured in degrees and extra courses without regard to content, and with the same number of years experience is paid the same amount. There is no reward for excellence! I wonder how many in this audience would be satisfied to work under these conditions. Then, you say, why should the teachers be satisfied? And I am afraid I must reply that too many of those going into teaching in our elementary and secondary schools are not capable of doing anything else. This was exemplified by the draft examination given to college students soon after the war to see which ones should be deferred to complete their education. The teacher college students were at the bottom of the list.

What does all this add up to? It leads to courses that are geared to our poor students. One might ask, "Can anything be gained by gearing courses otherwise?" I can now quote from first-hand experience. Since the beginning of the spring semester of 1959, I have worked with three different groups of high school students. Our engineering school has sponsored a Science Honors program which has been underwritten by the Hebrew Technical Institute, The Fund for the Advancement of Education which is a Ford Foundation subsidiary, and the National Science Foundation. During the spring of 1959 and again in 1960, I gave classes to these high school

students on Saturdays. The success of the work in the spring of 1959 led me to undertake a much more extensive program in the summer of 1959. Columbia has a good process inorganic laboratory at its Summer Engineering Camp located in the town of Morris, Conn., about 95 miles from our main campus. It was to this location that I took 24 high school boys for a six weeks' course. They received instruction, lectures, laboratory, and recitation, about six and one half hours each day, five days a week, with home work assigned each day. In this group, the most advanced students had completed their junior year in high school. Some had had chemistry, some had had physics, some had had neither chemistry nor physics. To this class, I gave a course in thermodynamics using as my text "Introduction to Chemical Engineering Thermodynamics" by Smith and Van Ness. The first day I asked how many had had calculus, and two hands went up rather timidly. Then I asked how many had studied it on the side. Over half of the hands went up. In fact, later on, one of the boys told me that he had belonged to a club in his high school; the objective of the members of the club was to teach themselves differential equations. With a class of this background, I proceeded to teach thermodynamics based on the calculus, spending a little extra time with those who had difficulty with the mathematical concepts. At the conclusion of this course, I gave an examination which I consider equivalent to the one I give my junior chemical engineering students. The boys did not average quite as high as our regular chemical engineering students, but they did do a very creditable job. Just remember, these boys were taking the course when they were many years younger than our college students; they had had no college chemistry nor physics, while our regular students had had very extensive training in elementary chemistry, physics, and mathematics. It should be remembered that these high school boys were unusually intelligent. This example shows what can be done with the very good students. It shows that we should make provision to conserve one of our most valuable natural resources, the brilliant mind. Many people have expressed this opinion; I want to add my voice. Unless we conserve our technical man power, we are threatened with extinction.

I would be very remiss if I left the situation at this point and did not outline what I believe could be done to alleviate this condition. In the first place, I feel that our secondary schools should have a complete rebirth. I think we should gear our courses to the bright student and let the average absorb what he can, rather than gear our courses to the mediocre thus allowing mediocrity to prevail. This can be done if we are willing to spend sufficient money to hire men and women capable of teaching science and mathematics at a considerably higher level than it is now being taught. You may be interested in a conversation I had with some of my high school boys a few months after we had completed our summer work. These boys were seniors at one of New York City's high schools that has limited admission, granted on the basis of ability and interest in science. They reported that the science teachers at that school fall into two categories: first, those who do not know any modern science, and, second, those who know the material but are completely indifferent to teaching. The type of slovenly administration and teaching that leads to this situation should never be permitted but, all too frequently, it is the rule rather than the exception. We must see to it that the single salary scale is dropped so that the individual teachers can be paid what they are worth. We should have high school teachers who are not only capable of understanding the application of mathematics to the physical sciences but are able to teach mathematics since many of our high school students are capable of grasping this material. We, as teachers, are remiss when we withhold from students material they can understand. It is by this procedure that we are prolonging the formal education period in our children's lives.

Parents are the only ones who can bring about such a change. Most of our school administrators, I am sorry to say, will never of their own free will do anything about it. Why? Because most of the "educators" are indifferent to the problem as is shown by their actions, or lack thereof, to date. Their incompetence stems from their own inadequate training. However, school boards are sensitive to public opinion and, since our public schools are controlled by elected boards, parents' groups working through the school boards can bring about changes.

I do not believe that we should encourage students to enter college at a younger age, but we should prepare the bright youngster so that he may enter with advanced standing. This is the system whereby the entering student takes examinations administrated by the College Board and, as a result of these exams, is placed in his proper level in the various sequences. Thus, an entering freshman may be excused from first year chemistry and be found ready for quantitative analysis and organic chemistry. The student need not substitute courses but can complete the requirements for the bachelors degree in less than four years. It is interesting to note that most of our leading universities today are making extensive use of this idea. One must never forget that maturity is important and, therefore, it is in my opinion wrong to send youngsters to college when they are too immature. It is for this reason that I believe that the advanced placement principle is our better solution.

By way of contrast, a by-product of gearing our schools to the mediocre students showed up at Columbia last fall. In the fall of 1959, we admitted our first class of freshmen engineers since 1914. It was a class of 92 very superior students. Their average College Board Achievement tests in mathematics placed them in the top 10% in comparison to those taking the College Board tests and within the top 2% nationally. Many of them were bright enough so that they had not had to learn to study to obtain very good grades in high school. The net result was a frightful mortality in freshman mathematics. Failure to learn how to study was shown to be one of the major reasons for this mortality; during the second semester, the failing students were given extra instruction in how to study mathematics with the result that a good percentage were able to make up the failure and complete the second term's work.

In my opinion, the schools are failing when they do not teach students how to study. Therefore, we must bring our schools up to a level which forces even our very bright students to study. I believe that it is only by this high level of performance that we can achieve our goal, namely, the flow of scientists and engineers from the liberal arts and technical schools into our graduate schools and on into teaching and industrial pursuits, thereby maintaining our lead in the scientific development of this world.

Current Affairs

C. L. Faust Appointed Publication Committee Chairman

Charles L. Faust was appointed Chairman of the Publication Committee by the Board of Directors of The Electrochemical Society at its meeting held in Houston, Texas, on October 9, 1960.

Dr. Faust has been active in Society affairs since 1938. He was President in 1950-1951 and Vice-President during 1947-1949. He also served as Chairman of the Electrodeposition Division in 1942; member of the Board of Directors as Manager, 1943-1945; member of the Publication Committee in 1944; member of the Ways and Means Committee, 1946-1959 (Chairman, 1951); Acheson Award Committee; Nominating Committee (Chairman, 1946 and 1958); and Honors and Awards Committee (Chairman, 1960). He was General Chairman of the Columbus Conventions of 1948 and 1959.

He received his B.S. degree in chemical engineering in 1930 and the M.S. degree in chemistry in 1931 from Washington University, and the Ph.D. degree in chemical engineering in 1934 from the University of Minnesota. He joined Battelle Memorial Institute as a research engineer in 1934 and has been head of the Electrochemical Engineering Division since 1945. His industrial research and development activities are in the fields of metal finishing; electrorefining; electrowinning; electrolysis; electroforming; electroplating; electropolishing and electroshaping; battery technology; aqueous, fused, and organic electrolytes; and other electroprocesses. He has led pioneering development work on commercial processes for the electrodeposition of alloys, electropolishing, and electroshaping.

C. L. Faust

Dr. Faust is an associate editor of "Modern Electroplating" (1953) and its new edition; of "Electroplating Engineering Handbook" (1955); and of the *Monthly Review* of the American Electroplaters' Society (later *Plating*), 1942-1949. At present, he is Section Editor for *Chemical Abstracts*, Electrochemistry, Section 4. He is the author or coauthor of over 80 papers, 130 patents, and chapters in eight books.

During World War II, he served on a subcommittee of the War Metallurgy Committee and was associated with special research and development for the war effort. He has served on committees of the Materials Advisory Board of the National Academy of Science and is a registered professional engineer. He also is a member of the American Chemical Society, American Electroplaters' Society, and The Institute of Metal Finishing, London. He has been named to receive the Scientific Achievement Award in June 1961, the highest award of the American Electroplaters' Society.

Manuscripts and Abstracts for Fall 1961 Meeting

Papers are now being solicited for the Fall Meeting of the Society, to be held at the Statler Hotel in Detroit, Mich., October 1, 2, 3, 4, and 5, 1961. Technical sessions probably will be scheduled on Batteries, Corrosion, Electrodeposition (including symposia on Addition Agents and on Electrodeposited Magnetic Films), Electronics (Semiconductors), Electro-Organics, and Electrothermics and Metallurgy.

To be considered for this meeting, triplicate copies of abstracts (*not exceeding 75 words in length*) must be received at Society Headquarters, 1860 Broadway, New York 23, N. Y., *not later than May 15, 1961. Please indicate on abstract for which Division's symposium the paper is to be scheduled and underline the name of the author who will present the paper.* No paper will be placed on the program unless one of the authors, or a qualified person designated by the authors, has agreed to present it in person. Complete manuscripts should be sent in triplicate to the Managing Editor of the JOURNAL at the above address.

Presentation of a paper at a technical meeting of the Society does not guarantee publication in the JOURNAL. However, all papers so presented become the property of The Electrochemical Society, and may not be published elsewhere, either in whole or in part, unless permission for release is requested of and granted by the Editor. Papers already published elsewhere, or submitted for publication elsewhere, are not acceptable for oral presentation except on invitation by a Divisional program Chairman.

Ralph A. Schaefer Named Director of Research of The Electric Storage Battery Co.

E. J. Dwyer, president of The Electric Storage Battery Co., recently announced the appointment of Ralph A. Schaefer as director of research of the company, effective December 15, 1960.

In his new post, Dr. Schaefer will make his headquarters at the Carl F. Norberg Research Center in Yardley, Pa., where he will direct the expanding research activities of the company. Since 1958, he had been director of engineering and research of Bunting Brass and Bronze Co., Toledo, Ohio.

A native of Grafton, Ohio, Dr. Schaefer graduated in 1935 as a chemistry major from Western Reserve University, Cleveland, and was elected to Sigma Xi. A year later, he received a master's degree in physical chemistry and, in 1941, Western Reserve awarded him the degree of doctor of philosophy in physical chemistry.

In 1936, he joined Cleveland Graphite Bronze Co., Cleveland, a division of the Clevite Corp., as a research chemist. In the next 22 years, he worked successively as supervisor of chemical development, director of research, and technical advisor to the president. For two years, he was vice-president of the

R. A. Schaefer

Clevite Brush Development Co., another Clevite division.

During the last 15 years, Dr. Schaefer has been responsible for initiating, planning, and administering research and development programs in electrochemistry and metallurgy. His career has been highlighted by important contributions to electroplating processes, the improvement of bearing alloys, the agglomeration process in casting, sintering, and plating, and by other significant metallurgical and chemical developments.

Numerous chemical and metallurgical patents have been issued to him, and others are pending. He has written many technical papers for publication in scientific journals and for presentation before technical societies.

In addition to serving as President of The Electrochemical Society in 1960-1961, Dr. Schaefer's activities have included the national Vice-Presidency, Chairmanship of the Cleveland Section and the Electrodeposition Division, Directorship in the national Society, and membership in various policy-making committees.

In the American Electroplaters' Society, Dr. Schaefer served as national president in 1954-1955 and held various other positions of responsibility. He also is a member of the American Society for Testing Materials, American Institute of Mining and Metallurgical Engineers, American Chemical Society, Society of Automotive Engineers, Institute of Metal Finishing, and American Society of Metals.

Electrochemistry Enters a New Field

Precision removal of metal is now done by an electrolytic process originated in research at Battelle Memorial Institute and being developed industrially by The Steel Improvement and Forge Co. This process of electroshaping is potentially capable of duplicating all stock removal needs common to metal shaping today. Electroshaping is particularly well suited to the difficult-to-machine nuclear and "space-age" metals such as tungsten, molybdenum, uranium, thorium, super alloys, and cemented carbides. The process is equally suited to the commonly used metals.

The work piece to be shaped is made the anode in a specially designed fixture with a cathode and means for flowing electrolyte between the work and the cathode. The contour design of the cathode causes essentially "directed electropolishing" to take place. The shaping action is accomplished with no need for first "roughing-out" the shape and contour. In contrast to other methods, the best surface results at the greatest stock removal rate.

Anodic dissolution in electroplating and electropolishing takes place at rates limited by diffusion and simple stirring. Current flow is limited to an upper limit of about 7 amp per sq in., which corresponds to metal removal of about 0.0009 in. per min per sq in. Generally, the rates are around 0.0004 in. or less. Of course, the electrochemical equivalent weight of the anode will determine the rate figure for different materials. These rates are much too slow for practical processes of electrolytically cutting off a billet, or for grinding off 0.030 in. or more of metal for shaping, or for trepanning, or hole drilling, or die cavity sinking, or milling. These operations can be performed by the new electroshaping process for which penetration rates of up to 0.170 in. per min are being achieved in production. Current densities up to 1500 amp per sq in. have been used, and 50 to 500 are most general.

Electroshaping proceeds in accordance with Faraday's Law. There is no physical contact between the work piece and the cathode or "tool." Hence, there is no pressure on the work piece. There is no disturbed or stressed surface "skin" of weakened distorted metal. There is no mechanical or physical damage. The process depends on electrochemical properties only. Because there is no pressure, there are no burrs at cut edges, and hardness, *per se*, of a metal is not a problem. The tools do not wear, nor, therefore, is compensation for wear needed. Because there is no

Fig. 1. Before and after electroshaping is shown dramatically by this pair of Waspalloy 11½ in. by 4 in. chord turbine blades. Blade on the left is in "as forged" condition; blade at right has been electroshaped by new Steel Improvement and Forge Co. process. Leading and trailing edges of airfoils have been electroshaped successfully as thin as 0.005 in.

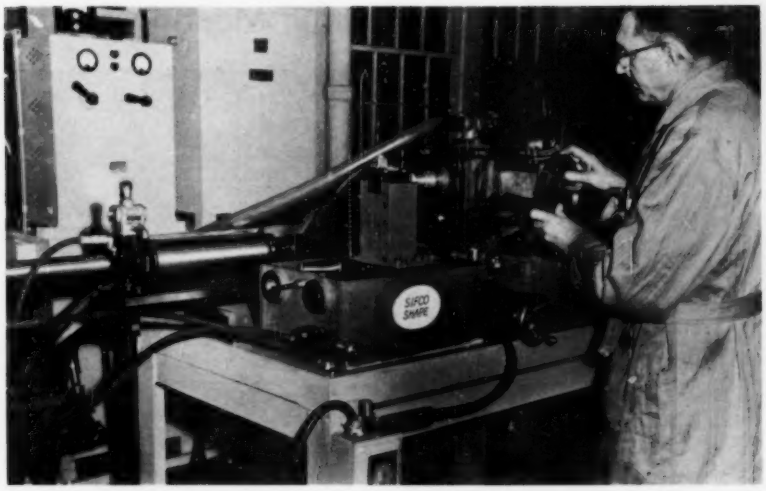

Fig. 2. Operator is shown loading one of smaller SIFCO-shape machines with a forged blade. The blade is held in a special fixture which is inserted into the machine's plastic-walled shaping chamber. An electric current, passed from work piece to electrodes through a rapidly flowing chemical solution, does the metal removing.

contact and no pressure, electrolytic stock removal is quiet: no sparks, no arcs, no scraping, no dust.

Once fixturing and tooling are designed, electroshaping is simple to operate. This was demonstrated at a press conference at The Steel Improvement and Forge Co. in Cleveland on October 26, 1960. Charles H. Smith, Jr., president; Aubrey H. Milnes, executive vice-president; Cloyd A. Snavely, general manager of SIFCO Metachemical, Inc.; and Charles L. Faust, Battelle Memorial Institute, explained company plans, process demonstration, and process principles. The work at Battelle was directed by Dr. Faust assisted by John E. Clifford and John A. Gurklis, and at SIFCO by Mr. Milnes and Dr. Snavely.

The new process for various machining operations is to be known as SIFCO-shape, SIFCO-sink, SIFCO-cut, etc. It is in production use for shaping turbine blades as shown in Fig. 1 and 2; for multiple hole drilling simultaneously—for example: a multiple of 3 holes 5/16 in. diameter by 3/4 in. deep simultaneously in tungsten in 10 min with no scrap relative to 10 to 15 hr by other means and 25% scrap of $300 each work piece; and sinking die cavities in 50 min in soft or hard steel relative to 7 hr in *soft* steel only.

Electroshaping gives designers a new degree of freedom in choice of materials to be used and shapes which can be made economically.

Division News

Battery Division

The annual luncheon and business meeting of the Battery Division was held at the Shamrock-Hilton Hotel in Houston, Texas, on October 11, 1960.

The following were elected officers of the Division for two-year terms (fall 1960-1962):

Chairman—E. J. Ritchie, Research Labs., Eagle-Picher Co., Joplin, Mo.
Vice-Chairman—Arthur Fleischer, 466 Centre St., Orange, N. J.
Secretary-Treasurer—C. H. Clark, 34 Pleasant Place, Deal, N. J.
Members-at-Large—Jeanne B. Burbank and E. B. Yeager.

C. H. Clark, *Secretary-Treasurer*

Corrosion Division

The Corrosion Division luncheon and business meeting was held at the Shamrock-Hilton Hotel in Houston, Texas, on Wednesday, October 12, 1960.

The Nominating Committee provided a double slate of nominees. No additional nominations were made from the floor. The following were elected officers of the Division for two-year terms (fall 1960-1962):

Chairman—R. T. Foley, General Electric Co., Schenectady, N. Y.
Vice-Chairman—H. C. Gatos, Lincoln Lab., Massachusetts Institute of Technology, Lexington, Mass.
Secretary-Treasurer—E. L. Koehler, Central Research and Engineering Div., Continental Can Co., Chicago, Ill.

Dr. A. C. Riddiford of the University of Southhampton, England, was our guest at luncheon and spoke on his work and interests.

An announcement was made that a new edition of the "Corrosion Handbook" would have to sell at about $40.00 per copy, which is prohibitive. Issuing of a new handbook in this area is currently planned in Great Britain. No immediate action is contemplated.

Announcements were made of various coming meetings in the field of corrosion.

Dr. Hackerman announced that of 29 corrosion manuscripts submitted to the JOURNAL, 5 have been found acceptable, 3 unsuitable, and the rest are in the hands of the reviewers. It was stated that this ratio of acceptable to unsuitable papers is about normal.

The Division cash balance remains at $21.68. This will be decreased by an expenditure of $3.50 for a luncheon ticket, and increased by $100.00 which has been voted by the Society for the work of the Corrosion Division.

The meeting closed on a vote of thanks for the retiring officers and a motion of appreciation for the Corrosion Division Newsletter.

E. L. Koehler,
Secretary-Treasurer

(Continued on page 15C)

Houston Meeting Flashbacks

Photographs by W. D. Murdy

Row A—L. I. Gilbertson, H. B. Linford receiving Acheson Medal from President R. A. Schaefer, and H. A. Acheson; Mrs. Osborn (Chairman Houston Ladies' Committee) and Oliver Osborn (General Chairman Houston Meeting); Dr. and Mrs. E. J. Williams (Houston Committee—Plant Trips); Dr. and Mrs. I. E. Campbell. **Row B**—Mrs. H. B. Linford and Mrs. H. A. Acheson; J. J. Motley and R. M. Fowler; Mrs. L. I. Gilbertson, Mrs. R. M. Hurd (Houston Ladies' Committee), and Mrs. Norman Hackerman. **Row C**—Maurice Indig, R. M. Wilson, and S. W. Smith; D. R. Hoffman; Dr. and Mrs. E. F. Kiefer; B. W. Neher, M. F. Quaely, Mrs. L. O. Case, and C. A. Snavely. **Row D**—N. J. Johnson, N. C. Cahoon, G. C. Allen, Mrs. Cahoon, and Mrs.

Allen; R. M. Hurd (Houston Committee—College Relations) and L. O. Case; E. G. Enck, J. M. Booe, and Dr. and Mrs. C. L. Faust. **Row E**—Arthur Fleischer, Dr. and Mrs. H. H. Uhlig, Hans Neumark, and J. E. Draley; R. G. Post (Houston Committee—Membership) and J. E. Loeffler (Houston Committee—Hotel Arrangements); B. D. Cahan, P. C. Douglass, and A. C. Riddiford. **Row F**—Sherlock Swann, Jr.; E. F. Foley, Mrs. Foley, H. B. Linford, and D. O. Feder; Acheson Medal Banquet Receiving Line; Lottie Fink and F. W. Fink. **Row G**—Names withheld to protect the innocent; S. W. Scott and E. M. Sherwood; W. C. Gardiner (back to camera), F. L. LaQue, and W. J. Hamer.

Division News

(Continued from page 13C)

Electrodeposition Division

The annual luncheon meeting of the Electrodeposition Division was held at the Shamrock-Hilton Hotel, Houston, Texas, on October 12, 1960.

The Treasurer reported that the total assets of the Division held by the National Society, as of August 31, 1960, were $2,595.49. In addition, the petty cash account contains $107.68.

Fred Lowenheim reported on the status of the revised edition of "Modern Electroplating." Due to delays in receiving some chapters, the new estimated publication date is about the end of 1961.

The following Division officers were elected for two-year terms (fall 1960-1962):

Chairman—D. G. Foulke, Sel-Rex Corp., Nutley, N. J.
Vice-Chairman—D. R. Turner, Bell Telephone Labs., Inc., Murray Hill, N. J.
Secretary-Treasurer—Dan Trivich, Wayne State University, Detroit 2, Mich.
Members-at-Large—F. A. Lowenheim and L. O. Case.

Plans for the Addition Agent Symposium scheduled for the Detroit Meeting in 1961 were revealed by the program Chairman, Dan Trivich. A group of invited speakers will be asked to talk on specific topics to review the status of our present knowledge of addition agents. The second part of the symposium will be contributed papers dealing with current work. The Division has the approval of the Board of Directors of the Society and its membership for the expenditure of up to $500.00 to aid in securing one or more guest speakers from outside the United States for the special symposium. Some help from one of the government agencies may be sought so that more than one guest can be invited.

Herman Koretzy thought it desirable to have a planned Symposium on Electrodeposited Magnetic Films at the Detroit Meeting. He already was aware of several papers which could be presented then. Koretzy assumed the responsibility of organizing such a symposium for 1961.

The time allotted for discussion of papers is too short according to Ed Saubestre. He suggested having an evening round table session for additional discussion. Dan Trivich said that a round-table discussion was being considered for the Detroit Meeting.

D. R. Turner, *Secretary-Treasurer*

Notice to Members and Subscribers
(Re Changes of Address)

To insure receipt of each issue of the JOURNAL, please be sure to give us your old address, as well as your new one, when you move. Our records are filed by states and cities, not by individual names. The Post Office does not forward magazines.

Section News

Washington-Baltimore Section

The October 20, 1960 meeting of the Washington-Baltimore Section was held at the Industrial Lecture Hall, National Bureau of Standards, Washington, D. C.

Guest speakers were Dr. Gilbert W. Castellan and Brother Richard LaPietra of the Catholic University of America. The topic for the evening, "The Transmission of Electrolytically Deposited Hydrogen through A Palladium Diaphragm," was presented in three parts: "Part I. Experimental"—Brother LaPietra, "Part II. Theoretical Aspects"—Dr. Castellan, "Part III. Interpretation of Data"—Brother LaPietra.

The speakers discussed some of their current research at the Catholic University. They electrolytically deposited hydrogen on one side of a palladium foil. The amount of hydrogen transmitted through the foil as well as the overpotential on both sides of the foil was measured as a function of the deposition current density and the thickness of the foil. A kinetic analysis of the data yielded the diffusion coefficient of hydrogen in palladium as well as the rate of combination of hydrogen atoms on the surface.

The paper was followed by a lively question period.

S. Schuldiner, *Secretary*

New Members

In November 1960, the following were elected to membership in The Electrochemical Society by the Admissions Committee:

Active Members

J. F. Bates, Applied Research Lab., U. S. Steel Corp.; Mail add: 210 Dawkins Dr., Monroeville, Pa. (Corrosion)

P. W. Bolner, Socony Mobil Oil Co., Field Research Lab., Box 900, Dallas 21, Texas (Corrosion)

R. N. Boyd, Dept. of Chemistry, New York University, Washington Square, New York 3, N. Y. (Electro-Organic)

A. P. Briganti, Chemolean Products Corp.; Mail add: 275 N. Syracuse Ave., North Massapequa, N. Y. (Electrodeposition)

W. J. Brisk, Semiconductor Products Div., General Electric Co.; Mail add: 131 Pine Tree Dr., North Syracuse, N. Y. (Electronics–Semiconductors)

Electronics Division Enlarged Abstracts

Copies of past issues of the Electronics Division Enlarged Abstracts booklets are available as follows:

1956—Vol. 5, No. 1, at $2.50
1959—Vol. 8, No. 1, at $3.00
1960—Vol. 9, No. 1, at $3.50

Please send order and check directly to:

Austin E. Hardy
Secretary-Treasurer
Electronics Division
Electrochemical Society
c/o RCA
Lancaster, Pa.

By action of the Board of Directors of the Society, all prospective members must include first year's dues with their applications for membership.

Also, please note that, if sponsors sign the application form itself, processing can be expedited considerably.

D. B. Colbeck, Gould National Batteries, Inc.; Mail add: 9319 Columbus Ave. S., Minneapolis 20, Minn. (Battery)

Daniel Curie, Laboratoire de Luminescence, Faculté des Sciences, 12 rue Cuvier, Paris 5, France (Electronics)

G. A. DiBari, Research Lab., International Nickel Co., Inc., 30 Oak St., Bayonne, N. J. (Electrodeposition)

S. S. Flaschen, Motorola Inc., 5005 McDowell, Phoenix, Ariz. (Electronics)

I. B. Giron, National Bureau of Standards, Guest Worker; Mail add: Hotel Jumin, La Oroya, Peru (Electrodeposition, Electrothermics & Metallurgy, Industrial Electrolytic)

D. N. Goens, American Potash & Chemical Co.; Mail add: 548-7th St., Boulder City, Nev. (Industrial Electrolytic, Theoretical Electrochemistry)

Howard Gong, Electro-Optical Systems, Inc.; Mail add: 2290 W. Brightwood St., Monterey Park, Calif. (Electronics)

J. C. Harris, Jr., Heat & Control, Inc., 1615 Cortland Ave., San Francisco 10, Calif. (Electrothermics & Metallurgy)

J. K. Higgins, Atomic Energy Research Authority; Mail add: 33 Upthorpe Dr., Wantage, Berks., Great Britain (Corrosion)

H. D. Kaiser, I.B.M. Corp.; Mail add: RFD 5, Box 172A, Kingston, N. Y. (Electrodeposition, Electronics)

P. C. Karr, I.B.M. Corp.; Mail add: 1 Knox Rd., Red Hook, N. Y. (Corrosion, Electronics–Semiconductors, Electrothermics & Metallurgy)

D. K. Kauppi, Dow Corning Corp.; Mail add: 2416 Manor Dr., Midland, Mich. (Electronics–Semiconductors)

L. J. Kotnik, Applied Research Lab., U. S. Steel Corp., Monroeville, Pa. (Corrosion)

G. M. Krembs, Research Div., Philco Corp.; Mail add: 7011 N. 15 St., Philadelphia 26, Pa. (Corrosion, Electrodeposition, Electronics-Semiconductors, Electrothermics & Metallurgy)

B. F. Larrick, U. S. Naval Ordnance Lab.; Mail add: 1910 Longmead Rd., Silver Spring, Md. (Battery)

W. R. D. Leigh, C. S. R. Chemicals Pty. Ltd., 1 Mary St., Rhodes, Sydney, Australia (Industrial Electrolytic)

D. J. Manus, Texas Instruments Inc.; Mail add: 1303 Cloverdale Dr., Richardson, Texas (Electronics-Semiconductors)

W. A. Mueller, Pulp & Paper Research Institute of Canada: Mail add: 3420 University St., Montreal, Que., Canada (Corrosion, Theoretical Electrochemistry)

P. B. Myers, Motorola, Inc., 5005 E. McDowell Rd., Phoenix, Ariz. (Electronics)

T. G. McWilliams, Jr., Dept. of Chemical Engineering, University of Maryland, College Park, Md. (Electrodeposition, Electrothermics & Metallurgy)

G. E. Pellissier, Jr., Applied Research Lab., U. S. Steel Corp.; Mail add: Woodland Dr., Box 785, R.D. 3, Murrysville, Pa. (Corrosion)

F. J. Ross, Jr., Carborundum Co. 1-2, Niagara Falls, N. Y. (Electrothermics & Metallurgy)

C. L. Rulfs, Dept. of Chemistry, University of Michigan, Ann Arbor, Mich. (Theoretical Electrochemistry)

S. G. Schroter, Raytheon Co.; Mail add: 18 Harrington St., Newtonville, Mass. (Electric Insulation)

R. G. Seed, Semicon, Inc., Box 328, Bedford, Mass. (Electronics-Semiconductors and Luminescence)

Bernice A. Smith, Missile & Space Vehicle, General Electric Co.; Mail add: 112 Wentz Ave., Woodbury, N. J. (Battery)

H. W. Sternberg, U. S. Bureau of Mines; Mail add: 130 Sylvania Dr., Pittsburgh 36, Pa. (Electro-Organic)

Takehiko Takahashi, Dept. of Applied Chemistry, Faculty of Engineering, Nagoya University, Chikusa-Ku Nagoya, Japan (Battery, Theoretical Electrochemistry)

M. L. Thorpe, Thermal Dynamics Corp., Lebanon, N. H. (Corrosion, Electrothermics & Metallurgy)

G. M. Towns, Texas Instruments, Inc.; Mail add: 3623 Binkley Ave., Dallas 5, Texas (Electronics-Semiconductors)

F. A. Trumbore, Bell Telephone Labs., Inc., Murray Hill, N. J. (Electronics)

L. F. Wallace, Westinghouse Electric Corp.; Mail add: 6511-A Brownsville Rd., Pittsburgh 36, Pa. (Electronics)

P. T. Wrotenbery, Texas Research Association; Mail add: 4907 Creekwood Rd., Austin, Texas (Electronics)

R. A. Wynveen, Allis-Chalmers Mfg. Co.; Mail add: 3926 N. Farwell Ave., Milwaukee 11, Wis. (Battery, Electrodeposition, Theoretical Electrochemistry)

Associate Members

H. D. Shepherd, P. R. Mallory & Co.; Mail add: 6186 Commodore Dr., Indianapolis, Ind. (Electric Insulation, Electro-Organic)

Student Associate Member

W. H. Ferguson, Jr., Massachusetts Institute of Technology, Rm. 4-133, Cambridge 39, Mass. (Corrosion)

Reinstatements

M. C. Forbes, Aquatrol, Inc., Box 12345, Houston, Texas (Corrosion)

E. V. Raymond, Sprague Electric Co.; Mail add: 93 Pillsbury St., Concord, N. H. (Electronics-Semiconductors)

D. K. Roe, Shell Development Co.,

(Continued on page 19C)

June 1961 Discussion Section

A Discussion Section, covering papers published in the July–December 1960 JOURNALS, is scheduled for publication in the June 1961 issue. Any discussion which did not reach the Editor in time for inclusion in the December 1960 Discussion Section will be included in the June 1961 issue.

Those who plan to contribute remarks for this Discussion Section should submit their comments or questions in triplicate to the Managing Editor of the JOURNAL, 1860 Broadway, New York 23, N. Y., *not later than March 1, 1961*. All discussion will be forwarded to the author(s) for reply before being printed in the JOURNAL.

Officers of Local Sections of The Electrochemical Society

Council of Local Sections (1960-1961)
A. J. Cornish, Chairman
Westinghouse Electric Corp., Beulah Rd., Churchill Boro., Pittsburgh 35, Pa.
J. C. White, Vice-Chairman
R. F. Bechtold, Secretary
N. C. Cahoon† (1960-1962)
M. F. Quaely† (1959-1961)

Boston (Spring 1960-1961)
Horace Homer, Chairman
Sylvania Electric Products Inc., Salem, Mass.
Paul Woodberry, Vice-Chairman
E. H. Newton, Secretary
Harold Creamer, Treasurer
H. C. Gatos* (1960-1962)
Charles Levy* (1960-1962)

Chicago (Spring 1960-1961)
Jacob Miller, Chairman
Armour Research Foundation, 10 W. 35 St., Chicago, Ill.
Ralph Wehrmann, Vice-Chairman
J. J. Daly, Jr., Secretary
R. G. Chelton, Treasurer
C. A. Hampel* (1960-1962)

Cleveland (Spring 1960-1961)
R. A. Powers, Chairman
Union Carbide Consumer Products Co., P. O. Box 6116, Cleveland 1, Ohio
J. F. Yeager, Vice-Chairman
R. C. Griffis, Secretary
F. C. Keller, Treasurer
N. C. Cahoon*
K. S. Willson*

Columbus (Fall 1960-1961)
L. D. McGraw, Chairman
Battelle Memorial Institute, Columbus 1, Ohio
R. W. Hale, Vice-Chairman
J. G. Beach, Sec.-Treas.
J. M. Blocher, Jr.*
F. W. Fink*

Detroit (Spring 1960-1961)
J. P. Hoare, Chairman
Ford Motor Co., P. O. Box 2053, Dearborn, Mich.
S. E. Beacom, 1st Vice-Chairman
A. A. Johnson, 2nd Vice-Chairman
Ann Piken, Sec.-Treas.
Frank Passal* (1960-1961)
Henry Brown* (1959-1961)

† Council Representative on Board of Directors.

* Representative on Council of Local Sections.

India (Elected Spring 1959)
M. S. Thacker, Chairman
Council of Scientific & Industrial Research, Old Mill Rd., New Delhi 2, India
A. Jogarao, Vice-Chairman
N. R. Srinivasan, Vice-Chairman
S. Krishnamurthy, Sec.-Treas.
H. V. K. Udupa*
J. Balachandra*

Indianapolis (Spring 1960-1961)
Bernard Agruss, Chairman
Allison Div., General Motors Corp., Indianapolis, Ind.
R. R. Haberecht, Vice-Chairman
T. C. O'Nan, Sec.-Treas.
F. C. Mathers* (1960-1961)
Ernest Paskell* (1960-1962)

Midland (Spring 1960-1961)
M. R. Bothwell, Chairman
13 Erie Court, Midland, Mich.
Donald Chapin, Vice-Chairman
C. K. Bon, Sec.-Treas.
P. F. George* (1959-1961)
R. S. Karpiuk* (1960-1962)

Mohawk-Hudson (Spring 1960-1961)
D. A. Vermilyea, Chairman
General Electric Co., P. O. Box 1088, Schenectady, N. Y.
N. D. Greene, Vice-Chairman
R. J. Stamets, Sec.-Treas.
W. H. Smith* (1960-1961)

New York Metropolitan (Spring 1960-1961)
P. L. Howard, Chairman
Yardney Electric Corp., 40-50 Leonard St., New York 13, N. Y.
Richard Glicksman, Vice-Chairman
Philip Crispino, Sec.-Treas.
M. F. Quaely* (1960-1961)
G. D. Stendahl* (1960-1961)

Niagara Falls (Spring 1960-1961)
S. W. Scott, Chairman
Union Carbide Metals Co., P. O. Box 580, Niagara Falls, N. Y.
D. J. Hansen, Vice-Chairman
J. A. Peterson, Sec.-Treas.
S. W. Scott* (1960-1961)
A. C. Haskell* (1960-1961)

Ontario-Quebec (Spring 1960-1961)
L. G. Henry, Chairman
Canadian Industries Ltd., P. O. Box 10, Montreal, Que., Canada
R. A. Ritchie, Vice-Chairman (Program)
R. P. Bailey, Vice-Chairman (Membership)
R. A. Campbell, Sec.-Treas.
R. P. Bailey* (1960-1961)
R. R. Rogers* (1960-1961)

Pacific Northwest (Elected June 1958)
H. J. Wittrock, Chairman
Kaiser Aluminum & Chemical Corp., Spokane 69, Wash.
G. C. Ware, Vice-Chairman
Lawrence Young, Sec.-Treas.

Philadelphia (Spring 1960-1961)
K. A. Krieger, Chairman
University of Pennsylvania, 34th & Spruce Sts., Philadelphia, Pa.
H. C. Mandell, Jr., Vice-Chairman
E. C. Evers, Secretary
A. A. Ware, Treasurer
(Councilor to be chosen)

Pittsburgh (Spring 1960-1961)
J. W. Faust, Jr., Chairman
Westinghouse Electric Corp., Beulah Rd., Churchill Boro., Pittsburgh 35, Pa.
W. E. Haupin, Vice-Chairman
E. J. Smith, Sec.-Treas.
A. J. Cornish* (1960-1961)
E. H. Phelps* (1960-1962)

San Francisco (Spring 1960-1961)
R. E. De La Rue, Jr., Chairman
Stanford Research Institute, Menlo Park, Calif.
Worden Waring, Vice-Chairman
H. F. Stout, Secretary
J. E. Chelton, Treasurer
R. F. Bechtold* (1959-1961)
R. A. Lewis* (1960-1962)

Southern California-Nevada (Spring 1960-1961)
M. E. Carlisle, Chairman
Norair Div., Northrop Corp., Hawthorne, Calif.
G. A. Larchian, Vice-Chairman
Lahmer Lynds, Sec.-Treas.
W. M. Hetherington* (1959-1961)
W. F. Seyer* (1960-1962)

Texas (Spring 1959-1961)
R. G. Post, Chairman
P. O. Box 535, Richardson, Texas
L. G. Dean, Vice-Chairman
R. M. Hurd, Sec-Treas.
T. C. Franklin,* Dallas (1959-1960)
C. S. Templeton,* Houston (1959-1961)

Washington-Baltimore (Spring 1960-1961)
Jerome Kruger, Chairman
National Bureau of Standards, 101 N.W. Bldg., Washington 25, D. C.
R. J. Brodd, Vice-Chairman
Sigmund Schuldiner, Secretary
V. A. Lamb, Treasurer
David Schlain* (1960-1962)
J. C. White* (1959-1961)

Officers of Divisions of the Society

Battery (Fall 1960-1962)

E. J. Ritchie, Chairman
Research Labs., Eagle-Picher Co., Joplin, Mo.
Arthur Fleischer, Vice-Chairman
C. H. Clark, Sec.-Treas.

Corrosion (Fall 1960-1962)

R. T. Foley, Chairman
Bldg. 37, General Electric Co., Schenectady, N. Y.
H. C. Gatos, Vice-Chairman
E. L. Koehler, Sec.-Treas.

Electric Insulation (Spring 1960-1961)

A. J. Sherburne, Chairman
1770 Wendell Ave., Schenectady, N. Y.
T. D. Callinan, Vice-Chairman
C. C. Houtz, Sec.-Treas.

Electrodeposition (Fall 1960-1962)

D. G. Foulke, Chairman
Sel-Rex Corp., Nutley, N. J.
D. R. Turner, Vice-Chairman
Dan Trivich, Sec.-Treas.

Electronics (Spring 1959-1961)

M. F. Quaely, Chairman
88 Mt. Hebron Rd., Montclair, N. J.
J. S. Prener, Vice-Chairman (Luminescence)
P. H. Keck, Vice-Chairman (Semiconductors)
A. E. Martin, Vice-Chairman (General Electronics)
A. E. Hardy, Sec.-Treas.

Electro-Organic (Fall 1960-1962)

M. J. Allen, Chairman
Electro-Optical Systems, Inc., 125 N. Vinedo Ave., Pasadena, Calif.
R. A. Day, Jr., Vice-Chairman
E. C. Olson, Sec.-Treas.

Electrothermics and Metallurgy (Spring 1959-1961)

E. M. Sherwood, Chairman
Battelle Memorial Institute, Columbus 1, Ohio
J. H. Westbrook, 1st Vice-Chairman
W. E. Kuhn, 2nd Vice-Chairman
L. H. Juel, Sec.-Treas.

Industrial Electrolytic (Spring 1960-1962)

W. D. Sherrow, Chairman
Electrode Div., Great Lakes Carbon Corp., Niagara Falls, N. Y.
R. F. Bechtold, Vice-Chairman
J. E. Currey, Sec.-Treas.

Theoretical Electrochemistry (Spring 1960-1961)

C. W. Tobias, Chairman
Dept. of Chemistry & Chemical Engineering, University of California, Berkeley, Calif.
L. G. Longsworth, Vice-Chairman
Paul Rüetschi, Sec.-Treas.

Committees of The Electrochemical Society, Inc., 1960-1961

Admissions Committee

	Term Expires
Louis Weisberg, Chairman	Spring 1961
L. I. Gilbertson	Spring 1962
M. F. Quaely	Spring 1963

F. M. Becket Memorial Award

	Term Expires
E. M. Sherwood, Chairman	Spring 1962
L. H. Juel	Spring 1961
R. R. Rogers	Spring 1961
J. H. Westbrook	Spring 1962
G. M. Butler	Spring 1963
I. E. Campbell	Spring 1963

Finance Committee

	Term Expires
L. I. Gilbertson, Chairman	Treas.'s term
I. E. Campbell	Secy.'s term
E. G. Enck	Spring 1961
H. B. Linford	Spring 1961
F. P. Peters	Spring 1961

Honors and Awards Committee

	Term Expires
C. L. Faust, Chairman	Fall 1963
J. R. Musgrave	Fall 1961
Abner Brenner	Fall 1961
H. C. Froelich	Fall 1962
W. J. Hamer	Fall 1962
L. O. Case	Fall 1963
E. F. Kiefer	Fall 1964
A. U. Seybolt	Fall 1964

Investment Advisory Panel

	Term Expires
R. M. Hunter, Chairman	Spring 1961
Hans Thurnauer	Spring 1962
George Heise	Spring 1963
E. G. Enck	Spring 1964
N. M. Winslow	Spring 1965

Membership Committee (Contributing)

J. C. Schumacher, Chairman—Term expires Spring 1961

Membership Committee (Personal)

F. W. Koerker, Chairman—Term expires Spring 1961

Nominating Committee

	Term Expires
W. C. Gardiner, Chairman	Spring 1961
F. W. Fink	Spring 1961
C. W. Tobias	Spring 1961
R. R. Rogers	Spring 1961
Arthur Middleton	Spring 1961

Palladium Medal Award Committee

	Term Expires
R. B. Mears, Chairman	Spring 1964
H. A. Liebhafsky	Spring 1962
A. L. Ferguson	Spring 1962
C. W. Tobias	Spring 1964
A. T. Gwathmey	Spring 1964

Perkin Medal Award Committee

	Term Expires
W. C. Gardiner, Chairman	Year ending 1960
Sherlock Swann, Jr.	Year ending 1960
L. I. Gilbertson, Alternate	Year ending 1960
C. V. King, Alternate	Year ending 1960

Publication Committee

	Term Expires
C. L. Faust, Chairman	Spring 1961
C. V. King	Spring 1961
H. A. Laitinen	Spring 1962
Norman Hackerman	Spring 1963
I. E. Campbell	Secy.'s term

Resolutions Committee

	Term Expires
H. B. Linford, Chairman	Spring 1961
H. R. Copson	Spring 1961
William Blum	Spring 1961

Special Committee on Preparation of Model Division Bylaws

N. C. Cahoon—Term expires Spring 1961

Committee on Protocol

	Term Expires
L. O. Case, Chairman	Spring 1961
Sherlock Swann, Jr.	Spring 1961
Paul Delahay	Spring 1961

Convention Advisory Committee

	Term Expires
E. G. Enck, Chairman	Spring 1961
C. L. Faust	Spring 1961
E. L. Koehler	Spring 1961
I. E. Campbell	Spring 1961
L. I. Gilbertson	Spring 1961

Ways and Means Committee

	Term Expires
H. B. Linford, Chairman	Spring 1961
F. L. LaQue	Spring 1961
W. J. Hamer	Spring 1961
W. C. Gardiner	Spring 1961
M. F. Quaely	Spring 1961
A. C. Haskell	Spring 1961
C. A. Snavely	Spring 1961

Tellers Committee

F. P. Peters, Chairman
C. B. Sanborn
A. C. Loonam
H. R. Neumark, Alternate
D. S. Carr, Alternate
P. L. Howard, Alternate

Committee for Administration of the Corrosion Handbook Fund

R. T. Foley, Chairman—Corrosion Division Chairman
R. M. Burns—Representative of Editorial Advisory Board of Corrosion Handbook
F. L. LaQue—Board Representative
H. H. Uhlig—Editor of Corrosion Handbook

Representatives of The ECS to Other Societies

American Association for the Advancement of Science

Harry Alsentzer—Term expires Spring 1961
G. W. Heise—Term expires Spring 1962

American Standards Association

	Term Expires
C-18—C. K. Morehouse	Spring 1961
Y-10 and Y-32—L. O. Case	Spring 1961
C-42—W. C. Vosburgh	Spring 1961
C-67—U. B. Thomas	Spring 1961
C-40—Eugene Willihnganz and R. C. Shair, Alternate	Spring 1961

Inter-Society Corrosion Committee

F. W. Fink—Term expires Spring 1961
K. C. Compton—Term expires Spring 1961

National Academy of Sciences—National Research Council—Advisory Board for the Office of Critical Tables

E. B. Yeager—Term expires June 30, 1961

National Research Council—Division of Chemistry and Chemical Technology

Norman Hackerman—Term expires June 30, 1961

American Society for Testing Materials

C-25—A. Gunzenhauser—Term expires Spring 1961

Instrument Society of America

C-96—Thermocouple Sectional Committee, American Standards Association, organized by Instrument Society
E. M. Sherwood—For duration of project, estimated completion end of 1961

American Electroplaters Society—Representative to Electrodeposition Division

D. G. Foulke—Term expires June 1961

New Members

(Continued from page 16C)

Emeryville, Calif. (Corrosion, Theoretical Electrochemistry)

Deceased

Norman Bauer, Logan, Utah
C. A. Crowley, Phoenix, Ariz.
H. K. Ihrig, Milwaukee, Wis.

Personals

A. Ausderau has been appointed director of Electrona Ltd., lead and alkaline batteries, Boudry/Neuchâtel, Switzerland. Formerly, he was vice-director.

J. Howard Brown has been named manager of research in a realignment of the corporate research and development department of Hooker Chemical Corp., Niagara Falls, N. Y. Dr. Brown, who has been with the company since 1937, had been manager of chemical research.

Eldridge K. Camp, formerly with the IBM Corp. in Poughkeepsie, N. Y., has joined the American Chemical & Refining Co., Waterbury, Conn., as director of research and development.

Peter P. Grad recently took a position as chief chemical engineer with Rotron Manufacturing Co., Inc., Woodstock, N. Y. Previously, he was associated with the Research Dept. of Aerovox Corp., New Bedford, Mass., as technical director.

Clarence K. Morehouse has been appointed vice-president of engineering for the Globe Battery Division of Globe-Union Inc., Milwaukee, Wis. Before joining Globe-Union, Dr. Morehouse was manager of component development of the RCA Microelectronics Dept. at Somerville, N. J.

Edward A. Parker, formerly research director, has been promoted to the newly created post of technical director of Technic, Inc., Providence, R. I. Dr. Parker has been with the firm, one of the nation's largest producers of solutions for electro-

plating with gold, platinum, rhodium, and palladium, since 1945.

Stanley Wawzonek, professor of organic chemistry at the State University of Iowa, recently was the recipient of the 1960 Iowa Chemistry Medal of the Iowa Section of the American Chemical Society. The gold medal is given annually for "meritorious achievement in teaching, research, or industry." Dr. Wawzonek currently is directing research in organic chemistry and organic polarography, particularly as applied to endocrinology and chemotherapy in medicine. He is a Divisional Editor on the ECS JOURNAL.

Norman Bauer

Norman Bauer, professor of chemistry at Utah State University, Logan, Utah, died on September 9, 1960. He was 45 years old.

Dr. Bauer was active in both research and writing, his most important area of research being the physical-chemical study of the process of nitrogen fixation.

He had been a member of The Electrochemical Society since January 1950.

News Items

New ECS Sustaining Member

The Kawecki Chemical Co., Boyertown, Pa., recently became a Sustaining Member of The Electrochemical Society.

1960 Annual Index

The Annual Index for Vol. 107 (1960) of the JOURNAL will appear in the February 1961 issue. Reprints of the Index can be obtained about the middle of March by writing to The Electrochemical Society, 1860 Broadway, New York 23, N. Y.

1960 Cryogenic Engineering Conference

More than 750 scientists and engineers, representing industry, government, and universities, attended the 1960 Cryogenic Engineering Conference held August 23, 24, and 25, 1960 at Boulder, Colo., under the joint sponsorship of the Boulder Laboratories of the National Bureau of Standards and Colorado University at Boulder. The nine technical sessions, at which 45 papers were presented and two guest speakers were heard, approached the subject of extreme low-temperature engineering from the aspects of both research and application, including processes, equipment, transfer, physical equilibria and other properties, semiconductivity, and the relationship of the field to space technology.

Twelve additional papers were accepted by the Conference Committee and, with the papers delivered at the Conference, will be included in the published proceedings, "Advances in Cryogenic Engineering," Vol. 6, which will be available from Plenum Press, Inc., early this year.

International Rectifier Launches Large-Scale Manufacturing in Italy

International Rectifier Corp., El Segundo, Calif., semiconductor manufacturers, and Piemontese Sviluppo Industriale S.P.A. (Piedmont Industrial Development Co.), one of Italy's largest industrial holding companies, have combined forces to launch a projected multimillion-dollar semiconductor manufacturing facility on the European continent.

Eric Lidow, president of International Rectifier, who made the announcement, stated that the company's Italian subsidiary, International Rectifier Corp. Italiana, S.P.A., has become the corporate structure for the joint venture.

A complete range of semiconductor rectifiers and automotive diodes will be produced in Italy to supply industry in the European common market.

Hooker Expands Sodium Chlorate Production at Columbus, Miss.

Hooker Chemical Corp. is substantially expanding capacity for making Oldbury-brand sodium chlorate at the Columbus, Miss., plant of its Eastern Chemical Division. With more chlorate cells and electrical equipment required, the expansion program is utilizing space provided earlier in existing buildings, and is employing finishing equipment now on hand.

Construction was well underway in the fall of 1960 and the new production is expected early in 1961. Although Hooker does not disclose present and anticipated sodium chlorate production capacities, this marks the fourth expansion since the original 12,000-ton-per-year Columbus plant began production in late 1954, the most recent expansion having been completed early in 1959. Hooker also makes sodium chlorate at Niagara Falls, N. Y.

Announcements from Publishers

"A High-Temperature Vacuum Extensometer," July 1960. AEC Report IS-167,* 24 pages; 50 cents.

"Analysis of Current Distribution in Electrolytic Cells with Flowing Mercury Cathodes," July 1960. AEC Report UCRL-9187,* 78 pages; $2.00.

"Scientific Conference on the Metallurgy, Chemistry, and Electrochemistry of Titanium," S. V. Ogurtsov, Akademiya Nauk SSSR, *Ordeleniye Tekhnicheskikh Nauk,*

* Order from Office of Technical Services, U.S. Dept. of Commerce, Washington 25, D.C.

Brief Communications

The JOURNAL accepts short technical reports having unusual importance or timely interest, where speed of publication is a consideration. The communication may summarize results of important research justifying announcement before such time as a more detailed manuscript can be published. Consideration also will be given to reports of significant unfinished research which the author cannot pursue further, but the results of which are of potential use to others. Comments on papers already published in the JOURNAL should be reserved for the Discussion Section published biannually.

Submit communications in triplicate, typewritten double-spaced, to the Editor, Journal of The Electrochemical Society, 1860 Broadway, New York 23, N. Y.

Izvestiye: Metallurgiya i Toplovo, July 1960. Translation 60-11939,* 2 pages; 50 cents.

"On the Mechanics of Hydrogen Exchange in Solutions," A. I. Shatenshteya, *Ukrainskiy Khimicheskiy Zhurnal USSR, 1956*, May 1960. Translation 60-31201,* 11 pages; 50 cents.

"Kinetics of Dissolution of Zirconium in Molten Uranium," May 1960. AEC Report ANL-6167,* 38 pages; $1.00.

"Corrosion Control of Copper and Steel by Vacuum Deaeration," May 1960. AEC Report GAT-296,* 14 pages; 50 cents.

"Hydrides of Metals and Metalloids. A Literature Search," July 1960. AEC Report TID-3902,* 164 pages; $2.75.

"Accurate Micrometer for Corrosion Samples," June 1960. AEC Report DP-488,* 10 pages; 50 cents.

* Order from Office of Technical Services, U.S. Dept. of Commerce, Washington 25, D.C.

New Products

Glass for Calibrating Spectrophotometers. A new type glass provides a method for quick and precise calibration of recording spectrophotometers for wave length accuracy. To produce the filters, Corning research scientists successfully combined holmium and a special glass that transmits radiant energy in the ultraviolet region of the spectrum between 200 and 300 mμ. The new glass, identified as Corning Code No. 3130, is available in the form of flat plates. It is stable, nonvolatile, noncorrosive, and nontoxic.

For further information, write to Optical Sales Dept., Corning Glass Works, Corning, N. Y.

Automatic Silver-Zinc Battery. When reliable reserve electrical power is needed in America's missiles, satellites, and weapons, batteries now can supply plenty of it, almost instantaneously, despite subzero temperatures in space. The Missile Battery Division of the Electric Storage Battery Co. has developed a new silver-zinc battery that is the first of its type of automatically activated unit to incorporate successfully an internal chemical heating device. The battery needs no preheating from external electrical sources, yet it heats up to full-power temperature several critical minutes faster than conventionally heated batteries.

Further information on the chemically heated battery models can be obtained from the Missile Battery Div., Electric Storage Battery Co., P. O. Box 11301, Raleigh, N. C.

Miniature High-Voltage Silicon Rectifiers. Two new high-voltage silicon plug-in rectifiers manufactured by International Rectifier Corp. are equipped with tube bases to allow direct replacement of electronic tube types 6X4, 12X4, OZ4, and 6X5. The St-8, which measures 1.10 x 1.40 in. (dia.), is rated at 1250 v peak reverse voltage at 80 ma d-c output. The miniature 1N570, rated at 1500 PRV at 75 ma d-c output, measures only 0.845 x 0.710 in. (dia.). Both units have an operating temperature range from −65° to +75°C.

For detailed data on both rectifiers, request Bulletin SR-209B from International Rectifier Corp., 1521 E. Grand Ave., El Segundo, Calif.

Miniature 1N429 Zener Reference Element. Hermetically sealed 1N429 silicon zener reference elements for military and civilian land, sea, and airborne power supplies will provide voltage stability of ±1% or better over the temperature range from −55° to +100°C. Rated at 200 mw power dissipation at 25°C, the 1N429 has a maximum dynamic impedance of 20 ohms at 7.5 ma, and a power derating factor of 1 mw/°C.

For detailed data, request Bulletin XSR-256 from International Rectifier Corp., 1521 E. Grand Ave., El Segundo, Calif.

Penton Spray-Coating Technique. Pfaudler 301, a new sprayable coating of Penton in water-suspension, has been introduced by the

EXCEPTIONAL OPPORTUNITIES *NOW* AVAILABLE

As a result of its expanding research and development activities, Electro-Optical Systems, Inc., *now* has rewarding openings on its technical staff for M.S. or Ph.D. Physical Chemists or Physicists. Area of work requires experimental background and capability in surface physics, surface chemistry, alkali metal adsorption and desorption studies, and thermionics.

Write or phone in confidence

D. L. Smelser
Professional Placement Coordinator
ELECTRO-OPTICAL SYSTEMS, INC.
125 North Vinedo Avenue
Pasadena, California
MUrray 1-4671

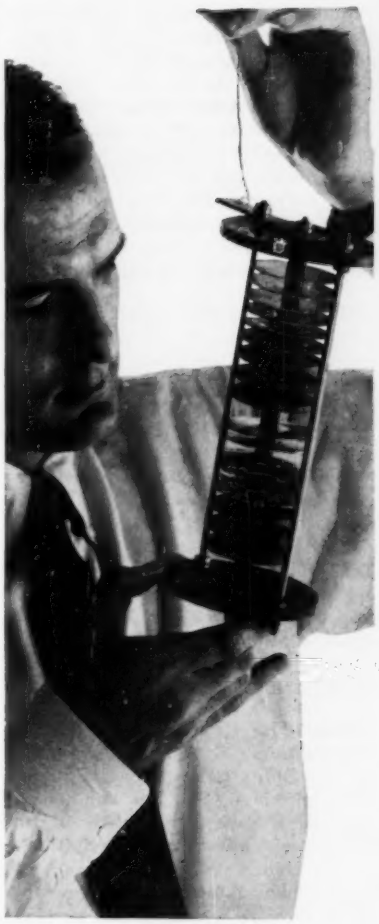

Career opportunities in corrosion research

* * *

Are you qualified for the opportunities that INCO's Laboratory offers to three additional scientists who are able to plan and conduct programs in corrosion research?

Requirements: Ph.D. or Sc.D. Also M.S. degree with research experience is acceptable.

More information is given in the current report of INCO activities, "Metals Plus Research." Do you want to review a copy?

Director of Research
The International Nickel Company, Inc.
67 Wall Street, New York 5, N. Y.

Pfaudler Co., a division of Pfaudler Permutit Inc., Rochester, N. Y. The coating can be appplied to desired thickness (20 to 40 mils) with as few as two applications. Also (*a*) parts do not require preheating, as in dry-coating techniques; (*b*) complex shapes can be covered easily, and surfaces not requiring the coating can be excluded easily; (*c*) a superior bond is obtained between the metal surface and the resin.

Gallium Arsenide Single Crystals. Crys-Tech Inc. is offering single crystals of gallium arsenide for sale. Current stock includes both n- and p-type material in crystal sizes ranging from 30 to 75 g. Undoped material typically has a carrier mobility of 3000 $cm^2/v\text{-}sec$ and 10^{18} net carriers/cm^3. Zinc doped p-type material is available in a variety of resistivities from 0.06-0.07 down to 0.003-0.005 ohm-cm.

Product information can be obtained from Crys-Tech Inc., 1534 E. Chestnut St., Santa Ana, Calif., or from Crys-Tech Sales, P. O. Box 85, Cochituate, Mass.

Micro-Fine Precipitated Silicas. Philadelphia Quartz Co., Public Ledger Bldg., Independence Square, Philadelphia 6, Pa., has announced the commercial manufacture of its family of micro-fine precipitated silicas under the trade name of Quso. Two different products currently available have a high surface area of 280 square meters per gram. They are soft white micro-fine particles sized from 9 to 15 mμ. The one called Quso F 20 is slightly acid (pH 6.4); the other, Quso G 30, is on the alkaline side with a pH of 8.2. Both are hydrophilic and insoluble, with a high oil absorbency.

Advertiser's Index

Bell Telephone Laboratories, Inc. 5C

Electric Boat, Division of General Dynamics 22C

Electro-Optical Systems, Inc. 21C

General Motors Research Laboratories 2C

Great Lakes Carbon Corp., Electrode Division ..... Cover 2

International Nickel Company, Inc. 21C

E. H. Sargent & Company 6C

Literature from Industry

Electropolishing Processes Bulletin. Two-color, 24-page bulletin gives a brief description of 18 Hanson-Van Winkle-Munning processes, including the new conversion coating processes Chem-Rite A-22, a conversion coating for aluminum, and Chem-Rite Z-33, a clear conversion coating for zinc. An illustrated description of the H-VW-M laboratory, and testing and field services available, is included.

For a copy, write to Hanson-Van Winkle-Munning Co., Church St., Matawan, N. J.

Employment Situations

Positions Available

Four challenging research positions for experienced surface chemists, in fully-equipped laboratory devoted to research and development on aluminum and copper alloys, involving: A. Electrochemical kinetics, adsorption, and oxide film structure investigations related to finishing processes. B. Studies of interfacial surface reactions between polymeric resins and metal oxide surfaces relating to strength and permanence of joints in the adhesive bonding of metals. C. Mechanisms relating to surface phenomena, associated with liquid metal-solid metal inter-action as applied to soldering and brazing. D. Surface and electrochemical reactions effecting the kinetics of general, localized, and stress corrosion processes. Pleasant living, with access to major university. Send reply to R. H. Endriss, Personnel Manager, Olin Mathieson Chemical Corp., 125 Munson St., New Haven, Conn.

Position Wanted

Chemical Engineer—B.S., registered professional engineer, 17 years of electrolytic background including development and production of tantalum capacitors, development in electrodeposition processes, corrosion. Desires responsible position in development or production work. *Reply to Box No. 371, c/o The Electrochemical Society, 1860 Broadway, New York 23, N. Y.*

Research Chemist

Immediate opportunity in the Chemistry and Metallurgical Section of the Research and Development Department at Electric Boat, leading designer and builder of America's nuclear submarines. Requires BS or MS in Chemistry with at least 2 years of radio-chemical experience.

Principal duties will be radiochemical work on submarine technical service projects such as determination of relative corrosion and/or erosion of rotating shafts and bearings in various solutions, and radiochemical analysis of submarine primary coolant water during power plant start-up, and many other problems which can be analyzed more effectively by radio-isotope trace techniques. Will also involve the direction of chemical analysis work in the fields of materials analysis and water chemistry .

The expanding and diversifying research effort at Electric Boat provides a variety of interesting assignments for qualified scientists. Please send resume to Mr. Peter Carpenter.

ELECTRIC BOAT
A DIVISION OF **GENERAL DYNAMICS**
Groton, Connecticut

The Electrochemical Society

INSTRUCTIONS TO AUTHORS OF PAPERS

(Revised as of 1/1/61)

Address all correspondence to the Editor, JOURNAL OF THE ELECTROCHEMICAL SOCIETY, 1860 BROADWAY, NEW YORK 23, N. Y.

GENERAL

Manuscripts must be submitted in triplicate to expedite review. They should be typewritten, double-spaced, with 2½-4 cm margins.

Title should be brief, followed by the author's name and business or university connection. Authors should be as brief as is consistent with clarity and should omit introductory or explanatory material which may be regarded as familiar to specialists in the particular field. Proprietary and trade names should be avoided if possible; if used, they should be capitalized to protect the owners' rights.

Authors may suggest qualified reviewers for their papers, but the JOURNAL reserves the right of final choice.

TYPES OF ARTICLES

Technical Articles must describe original research of basic nature and must have adequate scientific depth. Articles of wide diversity of interest are appropriate, but subjects primarily covered in other specialized journals (*e.g.*, analytical or nuclear chemistry) are not considered appropriate. An ***Abstract*** of about 100 words should state the scope of the paper and summarize its results. Suitable headings and subheadings should be included, but sections should not be numbered. Articles in recent issues of the JOURNAL should be consulted for current style.

Technical Notes are used for reporting briefer research, developmental work, process technology; new or improved devices, materials, techniques, or processes which do not involve more basic scientific study. No abstract is required.

Brief Communications are used only to report new information of scientific or technological importance which warrants rapid dissemination.

ILLUSTRATIONS

Drawings and ***Graphs*** ordinarily will be reduced to column width, 8.3 cm, and after such reduction should have lettering no less than 0.15 cm high. Lettering must be of letter-guide quality. India ink on tracing cloth or paper is preferred, but India ink on coordinate paper with blue ruling is acceptable. The sample graph shown on the reverse page conforms to suggestions of the American Standards Association (ASA Report Y15.1-1959).

Photographs should be used sparingly, must be glossy prints, and should be mailed with protection against folding. ***Micrographs*** should have a labeled length unit drawn or pasted on the picture

Captions for figures (including photographs) must be included on a separate sheet. Captions and figure numbers must *not* appear in the body of the figure; they will be removed if they do.

Numerical Data should not be duplicated in tables and figures.

EQUATIONS

Mathematical Equations should be written on a single line if possible, and parentheses, brackets, the solidus (/), negative exponents, etc., may be used freely for this purpose. Authors are urged to consult Chapter VI of the "Style Manual" of the American Institute of Physics (available for $1.00 at American Institute of Physics, 57 East 55 St., New York 22, N. Y.) and to follow the patterns described there.

SYMBOLS

If more than a few ***Symbols*** are used, they should be defined in a list at the end of the paper, with units given. For example:

$a, b \ldots =$ empirical constants of Brown equation

$f_i^* =$ fugacity of pure ith component, atm

$D_v =$ volume diffusion coefficient, cm^2/sec

ABBREVIATIONS

The AIP "Style Manual" referred to here gives a suitable list of common ***Abbreviations.*** Units usually will be abbreviated without periods throughout the text, as sec, min, hr, cm, mm, etc.

UNITS

Metric Units should be used throughout, unless English units are clearly more appropriate in the area of discussion.

POTENTIAL SIGNS

Electrode Potentials: Authors are urged to state and make use of the polarity of test electrodes with respect to the reference electrode used, *i.e.*, Zn is normally negative, Cu normally positive with respect to the standard hydrogen electrode. The sign for the emf of a cell should conform to the free energy change of the chemical reaction as written or implied, in accordance with the definition $\Delta G = nFE$. These suggestions agree with the IUPAC conventions adopted in 1953. If any other convention is used, it should be stated clearly and used consistently throughout the manuscript.

REFERENCES

Literature References should be listed on a separate sheet at the end of the paper in the order in which they are cited in the text. Authors' initials must be given, and the style and abbreviations adopted by *Chemical Abstracts* should be used. Any recent issue of the JOURNAL may be consulted.

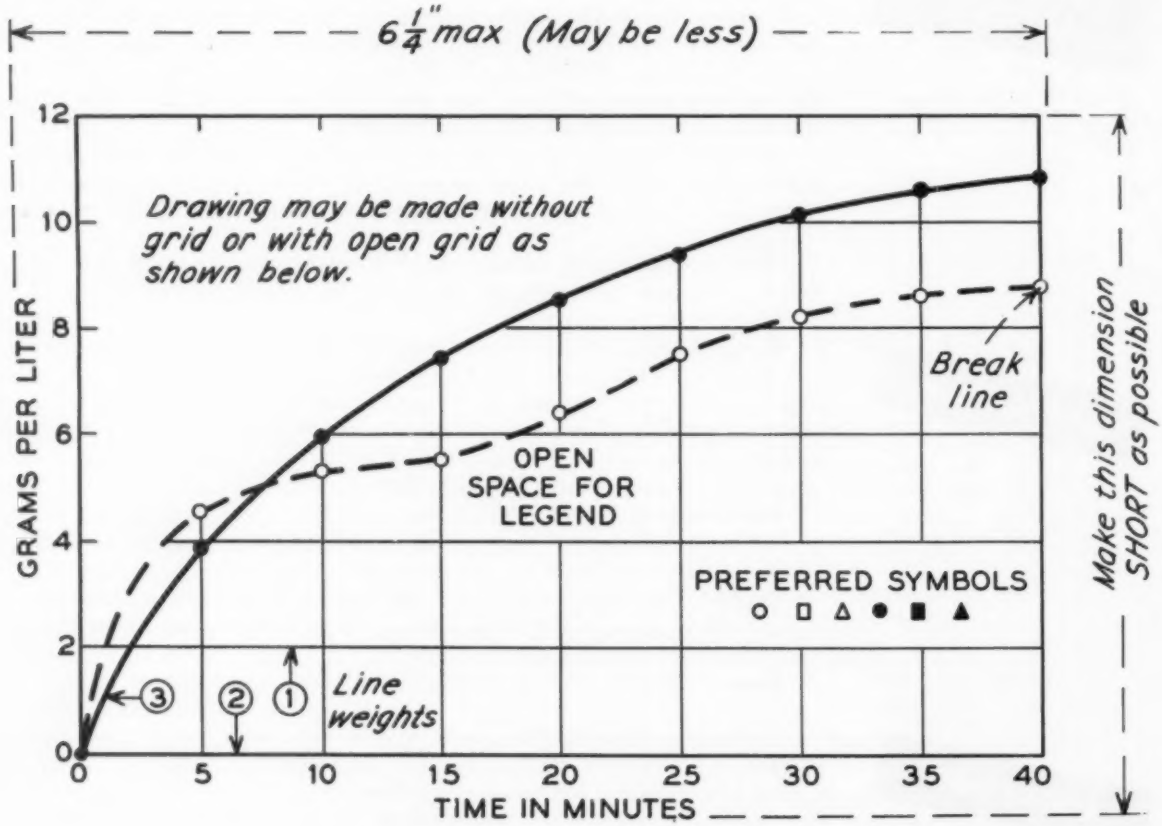

Remarks: Line weight 2 is used for borders and zero lines. When several curves are shown, each may be numbered and described in the caption. Lettering shown is approximately ⅛ in. In plotting current or potential as ordinate, increasing negative values should go down.

SAMPLE CURVE DRAWING FOR REDUCTION TO $\frac{1}{2}$ SIZE

The Electrochemical Society

Patron Members

Aluminum Co. of Canada, Ltd., Montreal, Que., Canada

International Nickel Co., Inc., New York, N. Y.

Olin Mathieson Chemical Corp., Chemicals Div., Industrial Chemicals Development Dept., Niagara Falls, N. Y.

Union Carbide Corp.
Divisions:
Union Carbide Metals Co., New York, N. Y.
National Carbon Co., New York, N. Y.

Westinghouse Electric Corp., Pittsburgh, Pa.

Sustaining Members

Air Reduction Co., Inc., New York, N. Y.

Ajax Electro Metallurgical Corp., Philadelphia, Pa.

Allen-Bradley Co., Milwaukee, Wis.

Allied Chemical & Dye Corp.
General Chemical Div., Morristown, N. J.
Solvay Process Div., Syracuse, N. Y. (3 memberships)

Allied Research Products, Inc., Detroit, Mich.

Alloy Steel Products Co., Inc., Linden, N. J.

Aluminum Co. of America, New Kensington, Pa.

American Metal Climax, Inc., New York, N. Y.

American Potash & Chemical Corp., Los Angeles, Calif. (2 memberships)

American Smelting and Refining Co., South Plainfield, N. J.

American Zinc Co. of Illinois, East St. Louis, Ill.

American Zinc, Lead & Smelting Co., St. Louis, Mo.

American Zinc Oxide Co., Columbus, Ohio

M. Ames Chemical Works, Inc., Glens Falls, N. Y.

Armco Steel Corp., Middletown, Ohio

Basic Inc., Maple Grove, Ohio

Bell Telephone Laboratories, Inc., New York, N. Y. (2 memberships)

Bethlehem Steel Co., Bethlehem, Pa. (2 memberships)

Boeing Airplane Co., Seattle, Wash.

Burgess Battery Co., Freeport, Ill. (4 memberships)

Canadian Industries Ltd., Montreal, Que., Canada

Carborundum Co., Niagara Falls, N. Y.

Catalyst Research Corp., Baltimore, Md.

Ciba Pharmaceutical Products, Inc., Summit, N. J.

Columbian Carbon Co., New York, N. Y.

Columbia-Southern Chemical Corp., Pittsburgh, Pa.

Consolidated Mining & Smelting Co. of Canada, Ltd., Trail, B. C., Canada (2 memberships)

Continental Can Co., Inc., Chicago, Ill.

Cooper Metallurgical Associates, Cleveland, Ohio

Corning Glass Works, Corning, N. Y.

Diamond Alkali Co., Painesville, Ohio (2 memberships)

Dow Chemical Co., Midland, Mich.

Wilbur B. Driver Co., Newark, N. J. (2 memberships)

E. I. du Pont de Nemours & Co., Inc., Wilmington, Del.

Eagle-Picher Co., Chemical Div., Joplin, Mo.

Eastman Kodak Co., Rochester, N. Y.

Thomas A. Edison Research Laboratory, Div. of McGraw-Edison Co., West Orange, N. J.

Electric Auto-Lite Co., Toledo, Ohio
C & D Division, Conshohocken, Pa.

Electric Storage Battery Co., Yardley, Pa.

Englehard Industries, Inc., Newark, N. J. (2 memberships)

The Eppley Laboratory, Inc., Newport, R. I. (2 memberships)

Erie Resistor Corp., Erie, Pa.

Exmet Corp., Tuckahoe, N. Y.

Fairchild Semiconductor Corp., Palo Alto, Calif.

Food Machinery & Chemical Corp.
Becco Chemical Div., Buffalo, N. Y.
Westvaco Chlor-Alkali Div., South Charleston, W. Va.

Foote Mineral Co., Paoli, Pa.

Ford Motor Co., Dearborn, Mich.

General Electric Co., Schenectady, N. Y.
Chemistry & Chemical Engineering Component, General Engineering Laboratory
Chemistry Research Dept.
General Physics Research Dept.
Metallurgy & Ceramics Research Dept.
Aircraft Accessory Turbine Dept., West Lynn, Mass.

General Instrument Corp., Newark, N. J.

(Sustaining Members cont'd)

General Motors Corp.
Delco-Remy Div., Anderson, Ind.
Guide Lamp Div., Anderson, Ind.
Research Laboratories Div., Detroit, Mich.
General Transistor Corp., Jamaica, N. Y.
Gillette Safety Razor Co., Boston, Mass.
Globe-Union, Inc., Milwaukee, Wis.
Gould-National Batteries, Inc., Minneapolis, Minn.
Grace Electronic Chemicals, Inc., Baltimore, Md.
Great Lakes Carbon Corp., New York, N. Y.
Hanson-Van Winkle-Munning Co., Matawan, N. J. (2 memberships)
Harshaw Chemical Co., Cleveland, Ohio (2 memberships)
Hercules Powder Co., Wilmington, Del.
Hill Cross Co., Inc., New York, N. Y.
Hoffman Electronics Corp., El Monte, Calif.
Hooker Chemical Corp., Niagara Falls, N. Y. (3 memberships)
Hughes Aircraft Co., Culver City, Calif.
Industro Transistor Corp., Long Island City, N. Y.
International Business Machines Corp., Poughkeepsie, N. Y.
International Minerals & Chemical Corp., Skokie, Ill.
ITT Laboratories, Nutley, N. J.
Jones & Laughlin Steel Corp., Pittsburgh, Pa.
K. W. Battery Co., Skokie, Ill.
Kaiser Aluminum & Chemical Corp.
Div. of Chemical Research, Permanente, Calif.
Div. of Metallurgical Research, Spokane, Wash.
Kawecki Chemical Co., Boyertown, Pa.
Kennecott Copper Corp., New York, N. Y.
Keokuk Electro-Metals Co., Keokuk, Iowa
Libbey-Owens-Ford Glass Co., Toledo, Ohio
M. & C. Nuclear, Inc., Attleboro, Mass.
Mallinckrodt Chemical Works, St. Louis, Mo.
P. R. Mallory & Co., Indianapolis, Ind.
McGean Chemical Co., Cleveland, Ohio
Merck & Co., Inc., Rahway, N. J.
Metal & Thermit Corp., Detroit, Mich.
Minnesota Mining & Manufacturing Co., St. Paul, Minn.
Monsanto Chemical Co., St. Louis, Mo.
Motorola, Inc., Chicago, Ill.
National Cash Register Co., Dayton, Ohio
National Lead Co., New York, N. Y.
National Research Corp., Cambridge, Mass.
National Steel Corp., Weirton, W. Va.
New York Air Brake Co., Kinney Vacuum Div., Boston, Mass.
Northern Electric Co., Montreal, Que., Canada
Norton Co., Worcester, Mass.
Olin Mathieson Chemical Corp., Research & Engineering Operations, Energy Div., New Haven, Conn.
Ovitron Corp., Long Island City, N. Y.
Peerless Roll Leaf Co., Inc., Union City, N. J.
Pennsalt Chemicals Corp., Philadelphia, Pa.
Phelps Dodge Refining Corp., Maspeth, N. Y.
Philco Corp., Philadelphia, Pa.
Philips Laboratories, Inc., Irvington-on-Hudson, N. Y.
Pittsburgh Metallurgical Co., Inc., Niagara Falls, N. Y.
Poor & Co., Promat Div., Waukegan, Ill.
Potash Co. of America, Carlsbad, N. Mex.
Radio Corp. of America
Tube Div., Harrison, N. J.
RCA Victor Record Div., Indianapolis, Ind.
Ray-O-Vac Co., Madison, Wis.
Raytheon Manufacturing Co., Waltham, Mass.
Reynolds Metals Co., Richmond, Va. (2 memberships)
Rheem Semiconductor Corp., Mountain View, Calif.
Schering Corporation, Bloomfield, N. J.
Shawinigan Chemicals Ltd., Montreal, Que., Canada
Speer Carbon Co.
International Graphite & Electrode Div., St. Marys, Pa. (2 memberships)
Sprague Electric Co., North Adams, Mass.
Stackpole Carbon Co., St. Marys, Pa.
Stauffer Chemical Co., New York, N. Y.
Sumner Chemical Co., Div. of Miles Laboratories, Inc., Elkhart, Ind.
Sylvania Electric Products Inc., Bayside, N. Y. (2 memberships)
Tennessee Products & Chemical Corp., Nashville, Tenn.
Texas Instruments, Inc., Dallas, Texas
Three Point Four Corp., Yonkers, N. Y.
Titanium Metals Corp. of America, Henderson, Nev.
Tung-Sol Electric Inc., Newark, N. J.
Udylite Corp., Detroit, Mich. (4 memberships)
Universal-Cyclops Steel Corp., Bridgeville, Pa.
Upjohn Co., Kalamazoo, Mich.
Victor Chemical Works, Chicago, Ill.
Western Electric Co., Inc., Chicago, Ill.
Wyandotte Chemicals Corp., Wyandotte, Mich.
Yardney Electric Corp., New York, N. Y.